

TECTONICS AND SEDIMENT GEOCHEMISTRY OF TUZO WILSON SEAMOUNTS, NORTHEAST  
PACIFIC OCEAN

by

ALEXANDER W. S. DENTON

B.Sc. (Honours), University of Calgary, 1978

A THESIS SUBMITTED IN PARTIAL FULFILMENT OF  
THE REQUIREMENTS FOR THE DEGREE OF  
MASTER OF SCIENCE

in

THE FACULTY OF GRADUATE STUDIES  
(Department of Geological Sciences)

We accept this thesis as conforming  
to the required standard

THE UNIVERSITY OF BRITISH COLUMBIA

September, 1986

© Alexander W. S. Denton, 1986

In presenting this thesis in partial fulfilment of the requirements for an advanced degree at the University of British Columbia, I agree that the Library shall make it freely available for reference and study. I further agree that permission for extensive copying of this thesis for scholarly purposes may be granted by the head of my department or by his or her representatives. It is understood that copying or publication of this thesis for financial gain shall not be allowed without my written permission.

Department of Geological Sciences

The University of British Columbia  
1956 Main Mall  
Vancouver, Canada  
V6T 1Y3

Date October 1, 1986

## ABSTRACT

The Tuzo Wilson Seamounts are two submarine volcanic edifices that are located 50 km southwest of the Queen Charlotte Islands, offshore British Columbia. These geologically-recent features have formed on the boundary between the Pacific and Explorer plates in the vicinity of their triple junction with the North American plate. Seafloor photographs, acoustic images and conductivity-temperature surveys have been used to elucidate tectonic relationships and to detect hydrothermal activity. Seventy-five samples from seven short (<1.5 m) cores have been analyzed to characterize the sediments. Major elements, trace elements and halogens (I, Br, Cl) were analyzed by X-ray fluorescence spectrometry (XRF). Carbon and nitrogen were determined with a CHN analyzer and carbonate carbon with a coulometer. Components of selected samples have been examined by scanning electron microscopy (SEM). X-ray diffraction (XRD) has been used to study the mineralogy of some samples with unusual geochemistry.

The seamounts occur at the foot of the narrow continental slope, 30 km from the edge of the shelf, and consequently sedimentation is dominated by terrigenous input. The cores are located along a fault scarp which runs southwest from the shelf. Conductivity-temperature measurements indicate that discharge of hydrothermal fluids is occurring along this scarp. However, the geochemistry of the sediments does not reveal any evidence of hydrothermal activity, probably due to terrigenous dilution.

Accelerator  $^{14}\text{C}$  dates indicate that core 3 penetrated the Pleistocene-Holocene transition. Abrupt changes in the depth distribution of Fe, Mg, Mn and the Rb/Zr ratio occur exclusively in this core, coincident with a shift in quartz/amphibole XRD peak-height ratios. These changes are attributed to a change in provenance and depositional conditions which occurred in response to climatic change and consequent rise in sealevel during deglaciation.

A lower Holocene sedimentation rate for this core, suggested by its iodine distribution, explains why similar geochemical and mineralogical changes are absent in the other cores, which apparently have higher sedimentation rates. The distribution of iodine and bromine is closely related to that of organic carbon and the distribution of certain trace metals (Cu, Ni and Zn) may be influenced by biogenic productivity.

Although evidence of hydrothermal activity was not detected in the sediments examined in this study, the Tuzo Wilson Seamounts are still considered a promising location for discovery of hydrothermal activity. Further research on the tectonic setting of the area and exploration for hydrothermal vent sites is strongly recommended.

## Table of Contents

List of Figures .....	viii
List of Tables .....	xi
Acknowledgements .....	xii
1. INTRODUCTION .....	1
2. TECTONICS AND PHYSICAL CHARACTERISTICS OF THE TUZO WILSON SEAMOUNTS AND SURROUNDING AREA .....	8
2.1 Introduction .....	8
2.2 Regional Physiography .....	10
2.2.1 Tuzo Wilson Seamounts .....	10
2.2.2 Continental Shelf and Slope .....	11
2.2.3 Queen Charlotte Fault .....	13
2.2.4 Abyssal Plain .....	14
2.3 Tectonic Setting .....	15
2.3.1 Historical Summary .....	15
2.3.2 Discovery of Tuzo Wilson Seamounts .....	18
2.3.3 Explorer Plate .....	20
2.3.4 Age and Petrology of Basalts from Tuzo Wilson Seamounts .....	22
2.3.5 Recent Seafloor Mapping .....	23
2.3.6 Heat Flow and Hydrothermal Activity .....	24
2.4 Hydrography .....	27
2.5 Other Studies Pertaining to the Tuzo Wilson Area .....	28
3. SEAFLOOR MAPPING .....	29
3.1 Introduction .....	29
3.2 SEABEAM .....	29
3.3 SeaMARC II .....	30
3.4 Underwater Photography .....	33

3.4.1	Methods .....	33
3.4.2	Results .....	34
3.4.3	Discussion .....	36
3.5	Echo-Sounding .....	42
3.6	Conductivity-Temperature-Depth Surveys .....	43
3.6.1	Methods .....	43
3.6.2	Results .....	43
3.6.3	Discussion .....	43
4.	SEDIMENT CHARACTER AND SEDIMENTATION .....	53
4.1	Introduction .....	53
4.1.1	Pleistocene Sedimentation .....	54
4.1.2	Lysocline .....	57
4.2	Sediment Description .....	57
4.2.1	X-Radiography .....	60
4.2.2	Smear-Slide Descriptions .....	60
4.2.2.1	Quartz .....	66
4.2.2.2	Chlorite .....	67
4.3	Age Dates and Sedimentation Rates .....	68
4.3.1	Introduction .....	68
4.3.2	Results and Discussion .....	69
4.4	Scanning Electron Microscopy .....	71
4.4.1	Introduction .....	71
4.4.2	Results and Discussion .....	71
4.4.2.1	Framboidal Pyrite .....	71
4.4.2.2	Heavy Minerals .....	72
4.4.2.3	Segmented Bone .....	73

5.	MAJOR ELEMENT AND HALOGEN DISTRIBUTION .....	75
5.1	Introduction .....	75
5.2	Results and Discussion .....	76
5.2.1	Silicon .....	76
5.2.2	Aluminum .....	78
5.2.3	Iron and Magnesium .....	78
5.2.4	Potassium and Titanium .....	83
5.2.4.1	Mineralogy of low K-Al intervals .....	86
5.2.5	Calcium and Carbonate .....	86
5.2.6	Phosphorus .....	92
5.2.7	Organic Carbon, Iodine and Bromine .....	94
5.2.8	Nitrogen .....	100
6.	TRACE ELEMENT DISTRIBUTION AND THE EFFECT OF DEGLACIATION ON SEDIMENT GEOCHEMISTRY .....	105
6.1	Introduction .....	105
6.2	Results and Discussion .....	105
6.2.1	Rubidium and Zirconium .....	105
6.2.2	Barium and Strontium .....	108
6.2.3	Zinc, Vanadium, Chromium, Cobalt, Nickel and Copper .....	111
6.2.4	Manganese .....	118
6.3	The Effect of Deglaciation on Sediment Geochemistry .....	121
	SUMMARY AND CONCLUSIONS .....	125
	BIBLIOGRAPHY .....	128
	APPENDIX 1 – SAMPLING AND ANALYTICAL PROCEDURES .....	145
6.1	Coring and Sampling Procedures .....	146
6.2	Analytical Procedures .....	148
6.2.1	<sup>14</sup> C Dating .....	148

6.2.2 Scanning Electron Microscopy .....	148
6.2.3 X-Ray Diffraction .....	149
6.2.4 Major Elements .....	150
6.2.5 Minor Elements and Halogens .....	151
APPENDIX 2 — RAW XRF, CHN AND COULOMETER DATA .....	153
APPENDIX 3 — SALT-CORRECTION PROGRAM .....	158
APPENDIX 4 — SALT-CORRECTED XRF, CHN AND COULOMETER DATA .....	162

List of Figures

Figure	Page
1. Location of study area. ....	2
2. SEABEAM bathymetry. ....	5
3. SeaMARC II acoustic imagery mosaic. ....	6
4. Tectonic elements of Explorer plate. ....	9
5. Seismic profile through Tuzo Wilson Seamounts. ....	11
6. Bathymetry of Tuzo Wilson area. ....	12
7. Tectonic elements of Northeast Pacific (1965). ....	17
8. Heat flow in vicinity of Tuzo Wilson Seamounts. ....	26
9. Locations of underwater camera tows. ....	37
10. Photogeology, northeast sheet. ....	38
11. Photogeology, southwest sheet. ....	39
12. Sedimented seafloor, tow 10. ....	40
13. Sedimented seafloor, tow 6. ....	40
14. Pillow lavas, tow 8. ....	41
15. Sedimented talus, tow 9. ....	41
16. Echo-sounding profile across fault scarp. ....	42
17. Conductivity-temperature anomalies, northeast sheet. ....	46
18. Conductivity-temperature anomalies, southwest sheet. ....	47
19. Conductivity-temperature plot, camera tow 1. ....	48
20. Conductivity-temperature plot, camera tow 2. ....	48
21. Conductivity-temperature plot, camera tow 3. ....	49
22. Conductivity-temperature plot, camera tow 5. ....	49
23. Conductivity-temperature plot, camera tow 6. ....	50
24. Conductivity-temperature plot, camera tow 7. ....	50
25. Conductivity-temperature plot, camera tow 9. ....	51
26. Conductivity-temperature plot, camera tow 10. ....	51
27. Conductivity-temperature plot, camera tow 11. ....	52

28. Conductivity-temperature plot, camera tow 12. ....	52
29. X-radiograph of sediment cores. ....	61
30. X-radiograph of sediment cores. ....	62
31. X-radiograph of sediment cores. ....	63
32. X-radiograph of sediment cores. ....	64
33. Smear-slide photomicrograph. ....	66
34. Age versus depth profile, core 3 ....	70
35. SEM photomicrograph of bone from core 3. ....	74
36. SEM photomicrograph of internal structure of bone. ....	74
37. Si distribution in sediment cores. ....	77
38. Al distribution in sediment cores. ....	79
39. Si/Al ratio in sediment cores. ....	80
40. Fe distribution in sediment cores. ....	81
41. Mg distribution in sediment cores. ....	82
42. K distribution in sediment cores. ....	84
43. Ti distribution in sediment cores. ....	85
44. K/Al ratio in sediment cores. ....	87
45. XRD peak-height ratios, core 3. ....	88
46. Ca distribution in sediment cores. ....	89
47. Carbonate carbon distribution in sediment cores. ....	90
48. Ca vs carbonate plot. ....	91
49. CaCO <sub>3</sub> vs depth plot. ....	92
50. P distribution in sediment cores. ....	93
51. C <sub>Org</sub> distribution in sediment cores. ....	95
52. I distribution in sediment cores. ....	96
53. I/C <sub>Org</sub> ratio in sediment cores. ....	98
54. Br distribution in sediment cores. ....	99
55. Br/C <sub>Org</sub> ratio in sediment cores. ....	101

56. N distribution in sediment cores. ....	102
57. C <sub>Org</sub> vs Total N plot. ....	103
58. C <sub>Org</sub> /N ratios in sediment cores. ....	104
59. Rb distribution in sediment cores. ....	106
60. Zr distribution in sediment cores. ....	107
61. Ba distribution in sediment cores. ....	109
62. Sr distribution in sediment cores. ....	110
63. Sr vs Ca plot. ....	111
64. Zn distribution in sediment cores. ....	112
65. V distribution in sediment cores. ....	113
66. Cr distribution in sediment cores. ....	114
67. Co distribution in sediment cores. ....	115
68. Ni distribution in sediment cores. ....	116
69. Cu distribution in sediment cores. ....	117
70. Plots of C <sub>Org</sub> /N vs Cu, Ni, and Zn. ....	119
71. Mn distribution in sediment cores. ....	120
72. Rb/Zr ratio vs depth in core 3. ....	121
73. XRD Diffractogram, core 3. ....	123
74. XRD peak-height ratios, core 3. ....	123

List of Tables

Table	Page
1. Sediment core locations. ....	7
2. Summary of camera tows. ....	35
3. Summary of CTD anomalies. ....	44
4. Description of sediment cores. ....	59
5. Components visible in smear-slides. ....	65
6. <sup>14</sup> C ages and sedimentation rates for core 3. ....	69

## ACKNOWLEDGEMENTS

The author would like to thank Dr. R.L. Chase for supervising this study and for providing the opportunity to participate in the CASM 3, 5 and 6, and Paclärk research cruises. I am also grateful to Dr. S.D. Scott (University of Toronto) for his support and encouragement, to Dr. T.J. Barrett (also of the University of Toronto) for assistance with coring and for sharing the sediment cores with me. Acquiring these sediment cores would not have been possible without the skilled assistance of Captain Brian McKenzie and the crew of the CFAV *Endeavour*.

I am indebted to Dr. W.C. Barnes (Geological Sciences, UBC) and Dr. T.F. Pedersen (Oceanography, UBC) for reviewing this thesis and for their many helpful comments. I am particularly indebted to Dr. Pedersen who, during periods when other demands on his time were overwhelming, provided cheerful and inspiring assistance, especially with the analytical work. Maureen Soon of Oceanography also provided considerable assistance with the laboratory work.

I am grateful to Dr. Al Lewis of the Department of Oceanography for identifying some bones found in one of the cores, to Greg Shea, a fellow graduate student, for reducing and plotting the CTD data, to Suzanne Carbotte for providing a seismic-reflection profile, and to Terry McLean of Industrial Nondestructive Testing Ltd. of Vancouver for X-radiography of the cores. John Knight of the Geological Sciences Department helped perform the Scanning Electron Microscope work. Ed Montgomery photographed and printed some of the figures.

The study was funded by the Natural Sciences and Engineering Research Council of Canada through a Strategic Research Grant to Drs. Chase and Scott. Financial assistance in the form of a generous scholarship to the author from the Canadian Society of Petroleum Geologists is gratefully acknowledged.

This work would not have been possible without the support and unfailing patience of my wife, Carol, and the inspiration of my son, David, who was born during the early stages of this research, and whose grandfather studied under Tuzo Wilson.

## Chapter 1

### INTRODUCTION

The Tuzo Wilson Seamounts (TWS), are two prominent submarine volcanic edifices adjacent to the base of the continental slope which rise to depths of 1400 m and 1700 m below sealevel approximately 65 km south-southeast of Cape St. James, the southerly tip of the Queen Charlotte Islands offshore Western Canada (Fig. 1). The seamounts are 180 km northwest of Cape Scott at the northern tip of Vancouver Island and 175 km southwest of the closest point on the Canadian mainland. Little is known about the depositional history or geochemical nature of the sediments in this area. The purpose of this study was to:

1. characterize the sediment around the seamounts;
2. determine whether the sediment revealed any evidence of hydrothermal activity which would be expected to be associated with the young oceanic crust;
3. determine whether the high heat flow in the area has produced any detectable accelerated diagenesis;
4. evaluate to what extent the seamounts and small active tectonic features have influenced the nature of sedimentation by deflecting and controlling terrigenous input; and
5. determine to what extent the transition from a cold continental climate to a moist temperate climate at the Pleistocene-Holocene boundary had on deep-water sedimentation.

A suite of sediment cores was collected in the vicinity of Tuzo Wilson Seamounts during the CASM 5 (Canadian-American Seamount Expedition) research cruise in the Northeast Pacific in May, 1985 aboard the Canadian Forces Auxiliary Vessel (CFAV) *Endeavour*. This study incorporates several different types of data in addition to analysis of the cores themselves to elucidate the history of sedimentation around Tuzo Wilson Seamounts. Black and white seafloor photography, 3.5 kHz echo sounding profiles and CTD

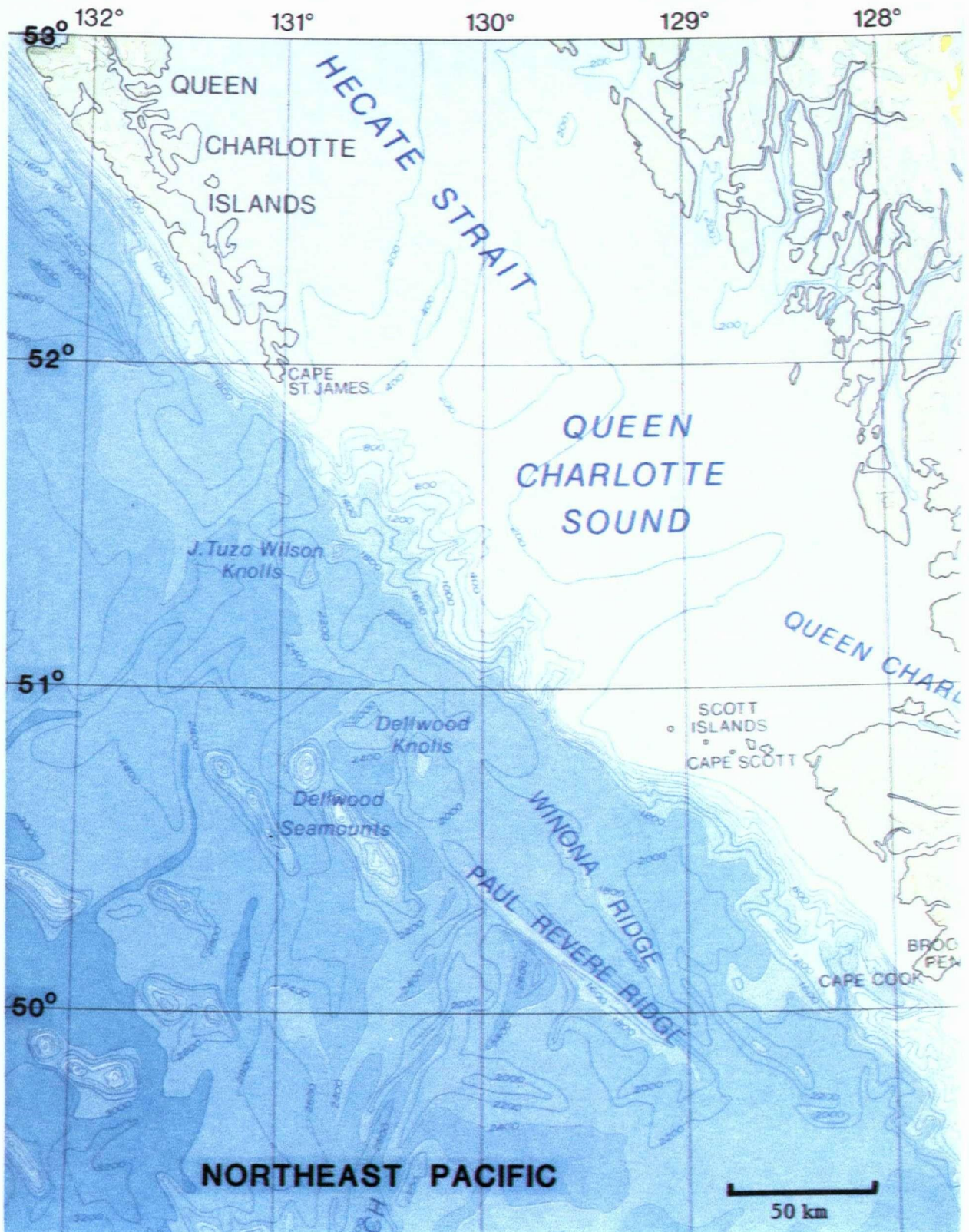


**Figure 1:** Location of study area in Northeast Pacific showing Tuzo Wilson Seamounts (Knolls) (from Juan de Fuca Plate Map series).

(Conductivity-Temperature-Depth) measurements carried out during the CASM 5 cruise provide important information on the amount of sediment cover, bioturbation, basalt flow morphology, small tectonic features and hydrothermal activity. In addition, previously published SEABEAM bathymetric maps, with 10 m contour intervals, and SeaMARC II acoustic seafloor imagery provided data for tectonic interpretation and for selection of core locations.

The sediment itself has been characterized by measuring major element (Si, Ti, Al, Fe, Mg, Ca, Na, K, P, and S), trace element (Ba, Co, Cr, Cu, Mn, Nb, Ni, Pb, Rb, Sr, V, Y, Zn, Zr), organic carbon, carbonate carbon, nitrogen and halogen (I, Br, Cl) concentrations as well with smear-slide descriptions. The cores were X-radiographed to reveal internal structure and evidence of bioturbation. Certain components of the sediments have been examined by Scanning Electron Microscopy (SEM). The date of a suspected hydrothermal event and sediment accumulation rates have been determined using two accelerator  $^{14}\text{C}$  dates obtained from one of the cores. X-ray diffraction (XRD) has been used to study mineralogical variation through this event and through another interval of abrupt geochemical variation.

The cores were obtained on the CASM 5 cruise during a six day period (May 16–21, 1985) spent at Tuzo Wilson Seamounts prior to conducting similar work at Explorer ridge for the remainder of the cruise. Dredging for volcanic rock was the only other work attempted at Tuzo Wilson Seamounts, apart from the previously mentioned underwater photography, CTD and echo sounding surveys. Dredging was unsuccessful due to winch failure but some chips of basalt glass were recovered from the plywood fin of the deep-tow camera frame where they had become embedded as a result of occasional impact of the camera frame with the seafloor. Analysis of these basalt samples will form part of a separate study (P.J. Michael, oral comm., 1986). A study of hydrothermal plumes by T.F. McConachy of the University of Toronto is underway and will incorporate water samples collected on the CASM 6 cruise in 1986. A geophysical study of the Tuzo Wilson Seamounts area (Carbotte, 1986) is the only other recent investigation known.

Recovery of sediment cores at was attempted at eight locations. Core 5 had no recovery, but core 6 was taken close to the site of core 5 and was successful. Core 7 recovered only 15 cm of sediment and contained several chips of glassy basalt up to 4 mm in diameter. This core was probably from an area of very thin sediment cover and the core barrel may have hit the underlying basaltic bedrock. A summary of the cores is given in Table 1 and their locations are plotted in Fig. 2.

All positioning on CASM 5 was conducted using a LORAN-C navigation system (5990-X and 5990-Y chains). Testing of the LORAN-C system with respect to the SEABEAM maps (satellite-navigated) by running echo-sounding traverses over prominent bathymetric features such as the Tuzo Wilson Seamounts revealed a discrepancy which was compensated for by recording the LORAN-C positions on a grid that had been shifted by 0.2' north and 0.8' east so that the underlying bathymetric features aligned correctly.

The core locations were chosen using SEABEAM bathymetric map NTS 102 O/6,7 (Malahoff *et al.*, 1984) (Fig. 2), and a SeaMARC II acoustic mosaic (Fig. 3) prepared by Davis *et al.* (1985). Cores 1–4 and 8 were positioned close to a northeasterly trending fault scarp, readily identifiable on the SeaMARC mosaic. Based on heat flow data, Hyndman *et al.* (1978) suggested that venting of hydrothermal fluids would be expected near these seamounts. The fault scarp could be the locus of such activity. Cores 6 and 7 were located farther from the base of the continental slope, close to the southwest seamount and close to a possible southwesterly extension of the linear feature. The tectonic significance of this feature is not yet fully understood but is discussed in more detail in the section on SeaMARC II acoustic imagery in Chapter 3.

The maximum distance between two adjacent cores is 8.25 km and the closest two are only 850 m apart. The total distance from the most shelfward core (1) to the most seaward (6) is 18.5 km. Except for core 3, the cores are of insufficient length to penetrate the Pleistocene-Holocene boundary, even at core 6 where turbidite input would be expected to

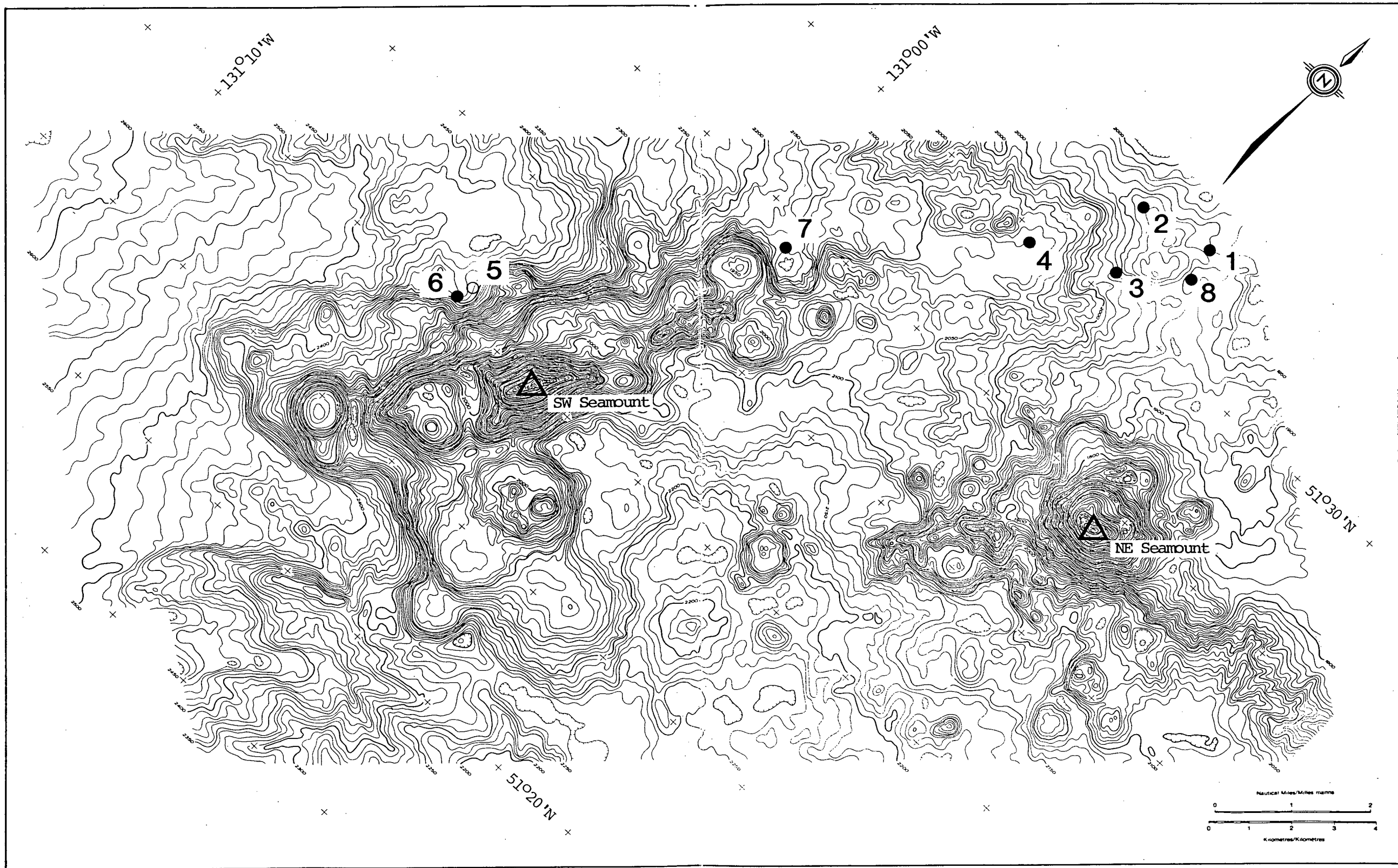
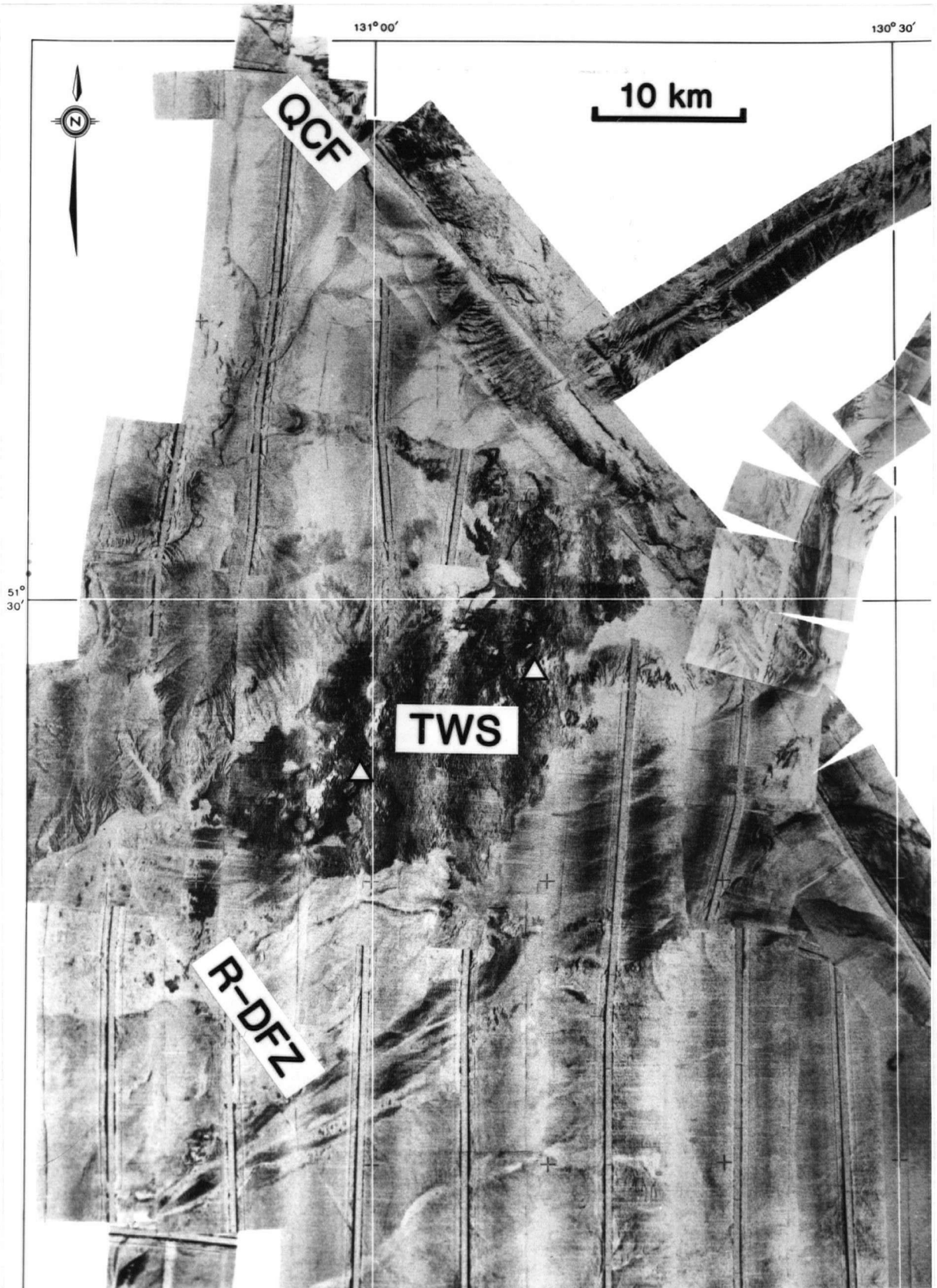


Figure 2: SEABEAM bathymetry of Tuzo Wilson Seamounts showing sediment core locations (from Malahoff et al., 1984).



**Figure 3:** SeaMARC II acoustic imagery mosaic of Tuzo Wilson area (from Davis *et al.*, 1985).

**TABLE 1: Sediment core locations and recovery.**

Core	Latitude <sup>1</sup> (N)	Longitude <sup>1</sup> (W)	Water Depth (m)	Length Recovered (cm)
1	51° 31' 13"	130° 53' 27"	1950	97
2	51° 31' 00"	130° 55' 06"	1935	140
3	51° 30' 07"	130° 54' 38"	1970	85
4	51° 29' 37"	130° 56' 25"	2080	96
5	51° 24' 12"	131° 04' 07"	2415	NO RECOVERY
6	51° 24' 01"	131° 04' 17"	2415	113
7	51° 27' 27"	130° 59' 55"	2160	15
8	51° 30' 44"	130° 53' 23"	1950	82

<sup>1</sup> LORAN-C navigated position. To plot on SEABEAM map, shift 0.2'N and 0.8'E.

be lowest. Also, due to lack of cores from the seaward side of the seamounts, it has not been possible to determine whether the seamounts have had any shadowing effect on sedimentation. Deep-sea channels are readily distinguishable on SeaMARC mosaics and these likely dominate sediment-dispersal. These channels are discussed in more detail in Chapter 2.

## Chapter 2

# TECTONICS AND PHYSICAL CHARACTERISTICS OF THE TUZO WILSON SEAMOUNTS AND SURROUNDING AREA

### 2.1 INTRODUCTION

In this chapter the current state of knowledge of the physiography, tectonics, geophysics and hydrography of the Tuzo Wilson Seamounts and surrounding area is presented in order to provide a firm basis for the interpretation of geochemical data that is presented in later chapters. A brief tectonic summary is followed by a survey of historical developments that led to the present state of knowledge. An excellent compilation of plate tectonics in the Northeast Pacific can be found in Cox (1973) and an overview of early developments in plate tectonics in Bullard (1975), and Vine (1977). A review of the geological history of the Juan de Fuca plate system over the past 100 Ma can be found in Riddihough (1982b), and a study of its recent movements in Riddihough (1984).

The Tuzo Wilson Seamounts are situated at the extreme northern end of Explorer plate (Fig. 4), near the triple junction between North America, Explorer, and the northwestward-moving Pacific Plate ( $55 \text{ mm a}^{-1}$  relative to North America). The Explorer plate, originally part of the Juan de Fuca plate, appears to have become coupled to North America due to the difficulty of subducting its young, hot buoyant crust. Relative motion between the Explorer and the still-subducting Juan de Fuca plates is accommodated by the left lateral Nootka fault. The Tuzo Wilson Seamounts are aligned perpendicular to the relative motion of the Pacific and North American plates suggesting that they are a locus of spreading that is accommodating extension in this area. They do not display classic rift morphology although they appear to have formed in a depression. The seamounts are young ( $<1 \text{ Ma}$ ) and may represent an immature spreading zone resulting from a recent northward shift of the triple junction although the chemistry of the basalts capping these seamounts does not unequivocally

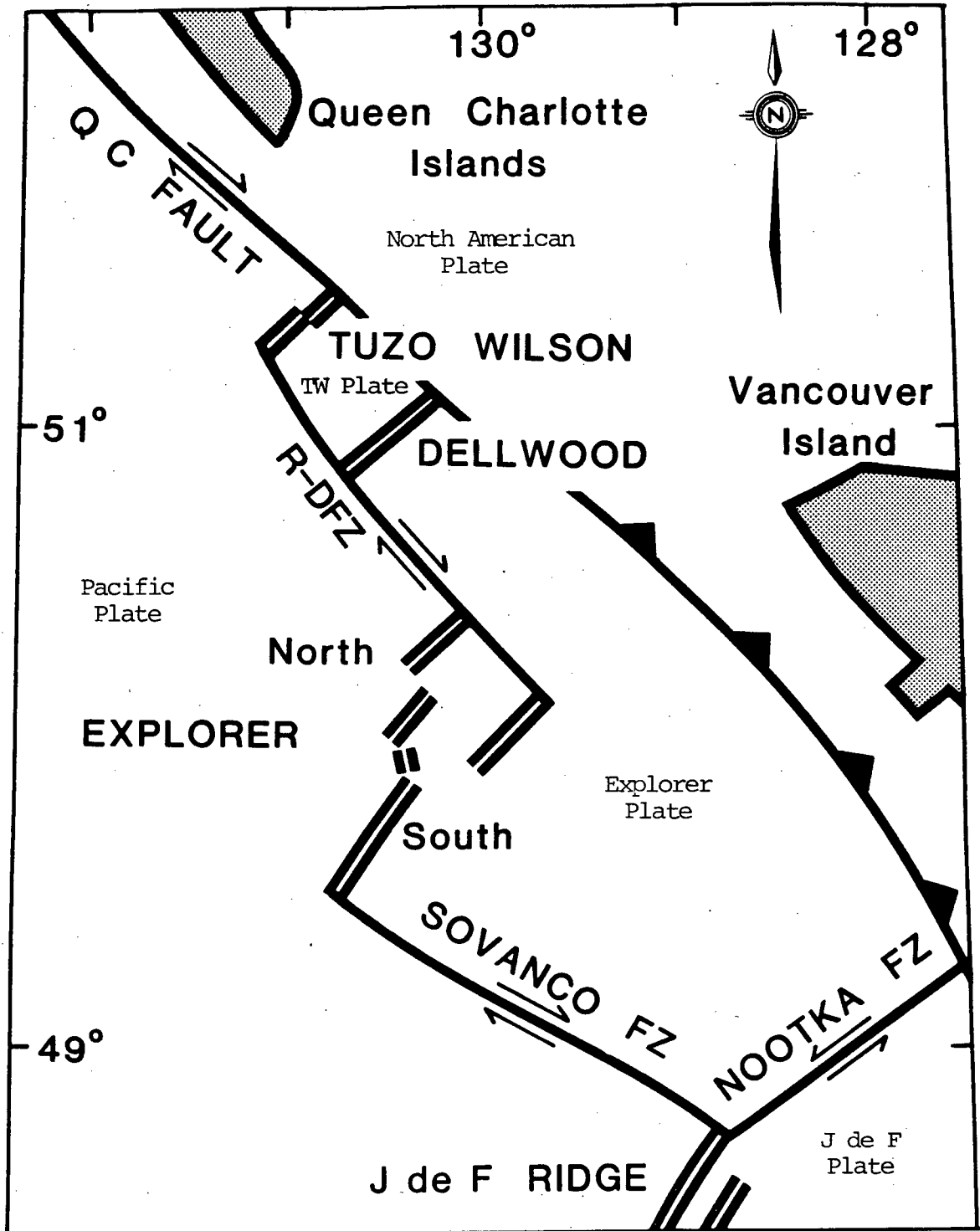


**Figure 4:** Tectonic elements in the vicinity of Explorer plate. The short Tuzo Wilson spreading segment comprises the two Tuzo Wilson Seamounts.

support the spreading hypothesis. Spreading may be occurring simultaneously at Tuzo Wilson Seamounts and Dellwood Knolls to the south. The young age of the Tuzo Wilson Seamounts and the high rate of sedimentation at the base of the continental slope may account for the absence of features typically associated with active spreading centres.

## 2.2 REGIONAL PHYSIOGRAPHY

### 2.2.1 TUZO WILSON SEAMOUNTS

The Tuzo Wilson Seamounts are two prominent submarine volcanic cones located 20 and 10 km from the base of the continental slope (Figs. 2 and 6), at 51°24'N, 131°00'W and 51°28'N, 130°50'W. They rise to depths of 1640 and 1370 m below sealevel respectively from base levels at 2200 and 1800 m below sealevel according to SEABEAM mapping (Malahoff *et al.*, 1984). They pierce through a thick sequence of hemipelagic and turbiditic sediment (Chase *et al.*, 1975). Numerous satellite cones rise from the flanks of the seamounts, some of which are aligned along trends perpendicular to the spreading direction. Slopes as steep as 25° occur near the peaks of the two main seamounts. Cliffs and fault scarps occur locally.

The seamounts occupy a southwest-northeast trending valley. This feature is evident on the continuous seismic-reflection profile (CSP) in Fig. 5 (from Carbotte, 1986). Using this and other CSP lines, Carbotte suggested that the Tuzo Wilson Seamounts have formed in a rift valley that has faulted sides with throws of 400 m on the northwest side and 50–100 m on the southeast side. Although the seamounts do not display classic rift morphology, a discontinuous chain of central volcanoes is characteristic of segments with slow spreading rates (Macdonald, 1982). Sedimentary strata overlying acoustic basement in Fig. 5 thicken and fan away from the seamounts, suggesting deposition concurrent with rifting.

Both CSP and gravity modelling suggest that the flanks of the seamounts must be composed of both basalt and sediment (Carbotte, 1986). Interbedding of sedimentary strata

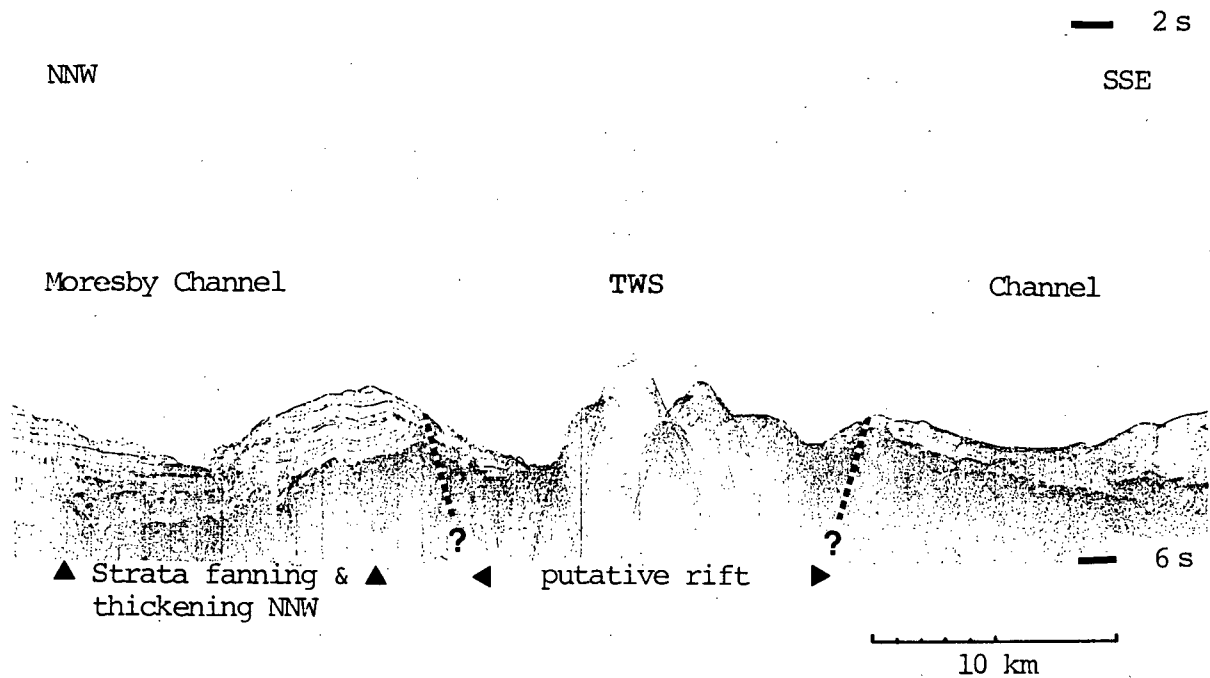


**Figure 5:** CSP line 73-19, oriented perpendicular to the trend of the seamounts (from Carbotte, 1986), showing them lying in a rift (?) valley.

and basalt has also been suggested for Dellwood Knolls (Riddihough *et al.*, 1980).

SeaMARC II acoustic imaging (Davis *et al.*, 1985) revealed numerous lava flows from the seamounts, some of which flowed down deep-sea sediment channels. Moresby channel, northwest of the seamounts, and another channel to the southeast are visible in Fig. 5.

Seafloor photography conducted from CASM 5 has revealed pillows, talus covered slopes and large areas covered by sediment. Interpretation of SeaMARC II images and seafloor photographs is discussed in further detail in Chapter 3.

### 2.2.2 CONTINENTAL SHELF AND SLOPE

A continental shelf, in some places 150 km wide, borders the west coast beneath Queen Charlotte Sound (Fig. 1). The continental slope is narrow (18-25 km) and a rise is essentially absent (Chase and Tiffin, 1972). Three broad channels cut Queen Charlotte Sound (Luternauer, 1972), converging downslope as canyons (Fig. 6). Moresby trough (the

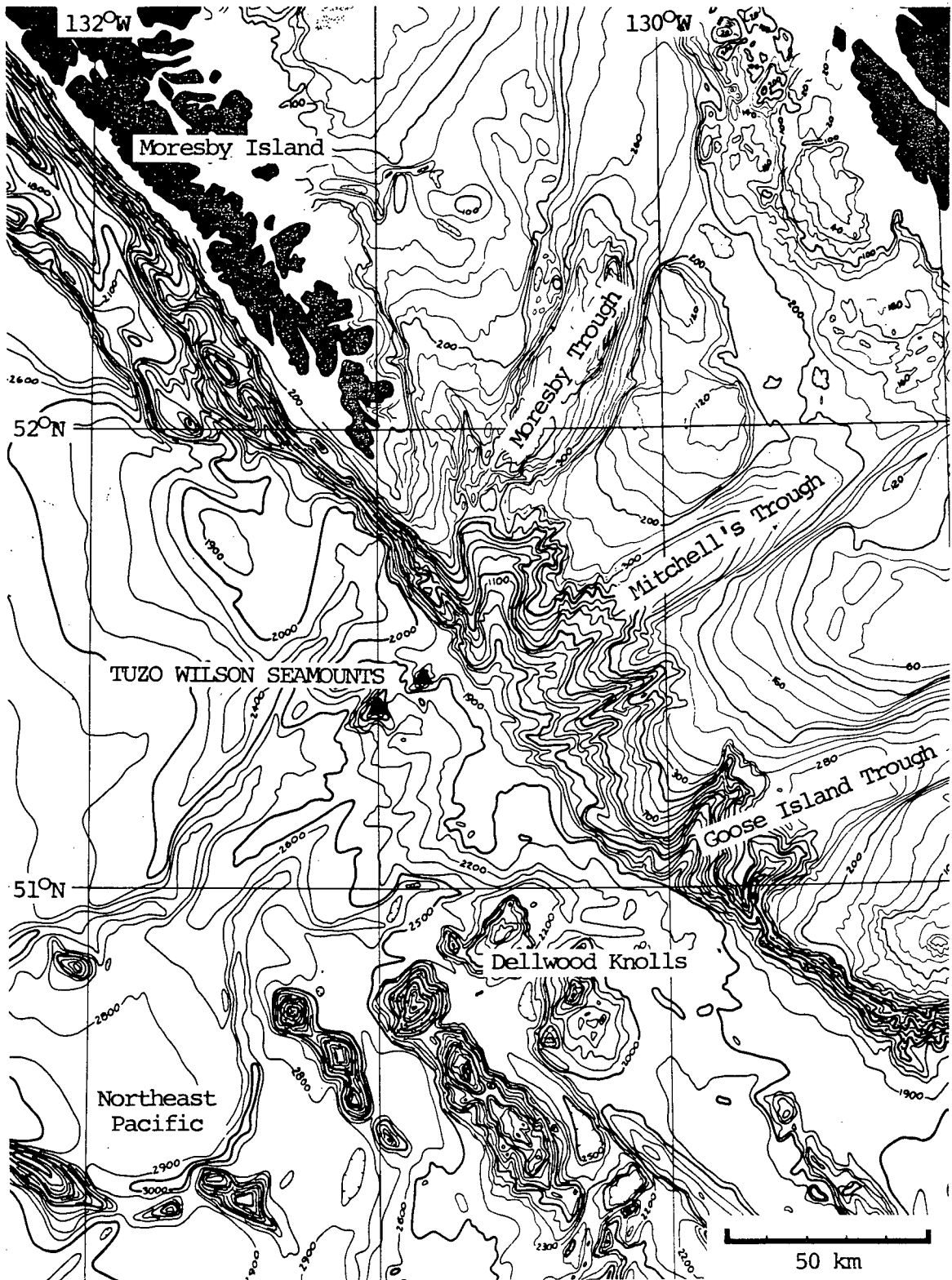


**Figure 6:** Bathymetry of Tuzo Wilson area showing southern Moresby Island, Queen Charlotte Sound, the continental shelf and the seamounts lying at the base of the slope (from Seemann, 1982).

northernmost) and Mitchell's trough join on the slope immediately above Tuzo Wilson Seamounts and funnel sediment onto a poorly developed deep-sea fan (see Nelson and Kulm, 1973). To the south, Goose Island trough feeds the area of Dellwood Knolls. Moresby trough has an irregular relief characteristic of a glacially excavated valley (Luternauer, 1972). All three channels have ice-deepened depressions, and are silled by recessional moraines (Chase *et al.*, 1975). Other features such as infilled erosional channels, stream profiles and scour features visible on CSP are indicative of extensive glacial and postglacial modification of the shelf and slope (Young, 1981).

The shelf is now a large sediment trap (Thomson, 1981) and sediment transport across it is virtually non-existent (Davis and Riddihough, 1982). Bypassing of the shelf during periods of lower sealevel combined with intense erosion during glaciation would have allowed transport of an enormous volume of sediment to the continental slope and beyond resulting in very high rates of sedimentation at the foot of the slope in the vicinity of the seamounts. The effects of glaciation on sedimentation are discussed further in Chapter 4.

### 2.2.3 QUEEN CHARLOTTE FAULT

The physiography along the western margin of the Queen Charlotte Islands and along the Queen Charlotte fault (Fig. 8) differs dramatically from that of Queen Charlotte Sound. Here the continental shelf is virtually nonexistent (Chase and Tiffin, 1972), and movement of the Pacific plate northwards past the Queen Charlotte Islands has carried sediment away to the Aleutian trench and prevented formation of a continental rise (Chase *et al.*, 1975). In addition, the Queen Charlotte Islands protected the adjacent seafloor and much Pleistocene sediment was intercepted by a trough between the Islands and the mainland and diverted south through Moresby trough (Chase and Tiffin, 1972; von Huene *et al.*, 1979). An irregular slope extends from the 1100 m high Insular Belt mountains of the Queen Charlotte Islands on the east side of the Queen Charlotte fault to the seafloor at the Queen Charlotte trough at a depth of 3000 m on the west side of the fault (Chase *et al.*, 1975). The fault zone itself has

two steep, parallel slopes separated by a 30 km wide irregular terrace at depth of 2000 m (Hyndman *et al.*, 1982). The present active fault is probably nearly vertical and lies very near the coast under the landward, shallower of the two steep slopes (Hyndman and Ellis, 1981).

#### 2.2.4 ABYSSAL PLAIN

The seafloor slopes very gently west from the base of the continental slope to the Tufts abyssal plain, interrupted only by occasional seamounts. Hamilton (1967) asserted that the abyssal plain, which is dominated by Pleistocene turbiditic sediment, is a relict feature produced by a previous depositional regime. Two submarine channels, Moresby and Scott channels, visible on SeaMARC II images (Seemann, 1983) and even on early bathymetric charts (e.g., Mammerickx and Taylor, 1971), extend west from the mouths of the canyons that cut the slope, and have been observed as far west as Tufts abyssal plain (Hamilton, 1967), a distance of several hundred kilometres. Their existence extends the area dominated by terrigenous sedimentation well out into the Northeast Pacific (Horn *et al.*, 1970; Davies and Gorsline, 1976). Moresby Channel is leveed, with the northwest levee about twice as high as the opposite one (Srivastava *et al.*, 1971). This is in agreement with the Coriolis effect which produces higher levees on the right hand side of channels causing them to bend to the left (Kennett, 1982). This effect has also been observed in the Cascadia channel off the Oregon coast where the right levee is consistently 30 m higher than the left one (Griggs and Kulm, 1970). Disturbed reflectors beneath the channel may indicate southeasterly migration (Srivastava, 1971), possibly in response to their relative northward movement with the Pacific plate while their sediment source area on North America remained stationary. Chase *et al.* (1975) suggested that Moresby trough would once have fed Moresby channel, but that due to the relative motion of the underlying plates, Moresby channel has been displaced 40 km north. Despite this movement, the southeasterly migration of the channel as mentioned above and the existence of feeder channels on both sides of Tuzo Wilson Seamounts (visible on SeaMARC II mosaic in Fig. 3) suggest that Moresby channel will continue to be fed by

Moresby trough although, as stated previously, sediment transport across the shelf during the present interglacial is minimal. Any sediment dispersal occurring today is probably confined to the channels (Horn *et al.*, 1970).

## 2.3 TECTONIC SETTING

### 2.3.1 HISTORICAL SUMMARY

The understanding of the tectonic setting of the Tuzo Wilson Seamounts has evolved hand in hand with plate tectonic theory. In fact much of the early work conducted in the Northeast Pacific formed the basis for some of the concepts that are central to plate tectonic theory.

The marine magnetic surveys conducted by Mason (1958), Raff and Mason (1961) and Mason and Raff (1961) aboard the U.S. Coast Guard and Geodetic Survey Vessel *Pioneer* off the west coast of Canada and the United States provided the first data from the then unknown Juan de Fuca plate. Raff and Mason did not provide a satisfactory explanation for the configuration of the magnetic anomalies. Subsequent studies (Vine and Matthews, 1963; Wilson, 1965a, b; Vine and Wilson, 1965; and Vine, 1966) attributed the magnetic stripes to seafloor spreading, a theory originally proposed by Holmes (1929) and Hess (1962) but largely ignored until resurrected to explain the seafloor magnetic anomalies. Interestingly, Vine and Wilson (1965, p. 485) state that

"These anomalies are not obviously parallel to any active oceanic ridge ...".

At that time the Mid-Atlantic Ridge and the East Pacific Rise were becoming recognized as continuous submarine topographic features, largely due to careful mapping done during the 1950's (Cox, 1973) which resulted in the first reliable global seafloor maps (e.g., Heezen and Tharp, 1959; Heezen, 1962; Heezen *et al.*, 1965; Mammerickx and Taylor, 1971). Both Menard (1964) and Hess (1965) proposed a ridge in the area of the magnetic anomalies but Wilson (1965a) was the first to tie the magnetic data, the proposed spreading ridge off the

coast of Vancouver Island, and his new theory of transform faults into a global system of rigid interacting plates. In another paper that year, Wilson (1965b) attempted to reconcile his tectonic interpretation with the magnetic data of Raff and Mason (1961). He named the Queen Charlotte fault (Fig. 7), the presence of which had been previously suggested by St. Amand (1957) and Benioff (1962), but misplaced it slightly to the southwest and extended it much farther to the southeast than is presently thought. The dextral nature of the fault was indicated previously (Hodgson and Milne, 1951) and corroborated by Tobin and Sykes (1968) through first motion studies. The Tuzo Wilson Seamounts were still unknown in 1965 and the Juan de Fuca plate, separated from North America by a subduction zone along the western margin of the continent, had not yet been recognized. The Juan de Fuca ridge was named by Wilson (1965b) but was also named the Cobb Rise by McManus (1967) although the latter name did not become accepted and is now attached only to Cobb Seamount.

Knowledge about the tectonics of the Northeast Pacific continued to evolve rapidly with the recognition by Vine (1966) of Explorer ridge, and with the introduction of spherical geometry to account for the motions of plates on the spherical surface of the Earth (McKenzie and Parker, 1967; Morgan, 1968). McKenzie and Parker (1967) were the first to suggest the need for a convergent margin north of Cape Mendocino and cited earthquake epicentres and the presence of the Cascade volcanoes as evidence for consumption of oceanic crust beneath North America.

Research in the late 1960's into seismicity (e.g., Isacks *et al.*, 1968; Tobin and Sykes, 1968) helped delineate plate boundaries but the tectonics of the Juan de Fuca - North America - Pacific triple junction were poorly understood. In fact Morgan (1968) was the first to conclude that the Juan de Fuca "block" had a motion separate from the North America and Pacific plates. This is probably the first recognition of Juan de Fuca as a separate plate, although McKenzie and Parker (1967) alluded to it by invoking a convergent margin off Washington and Oregon as mentioned previously. This concept was expanded on further by

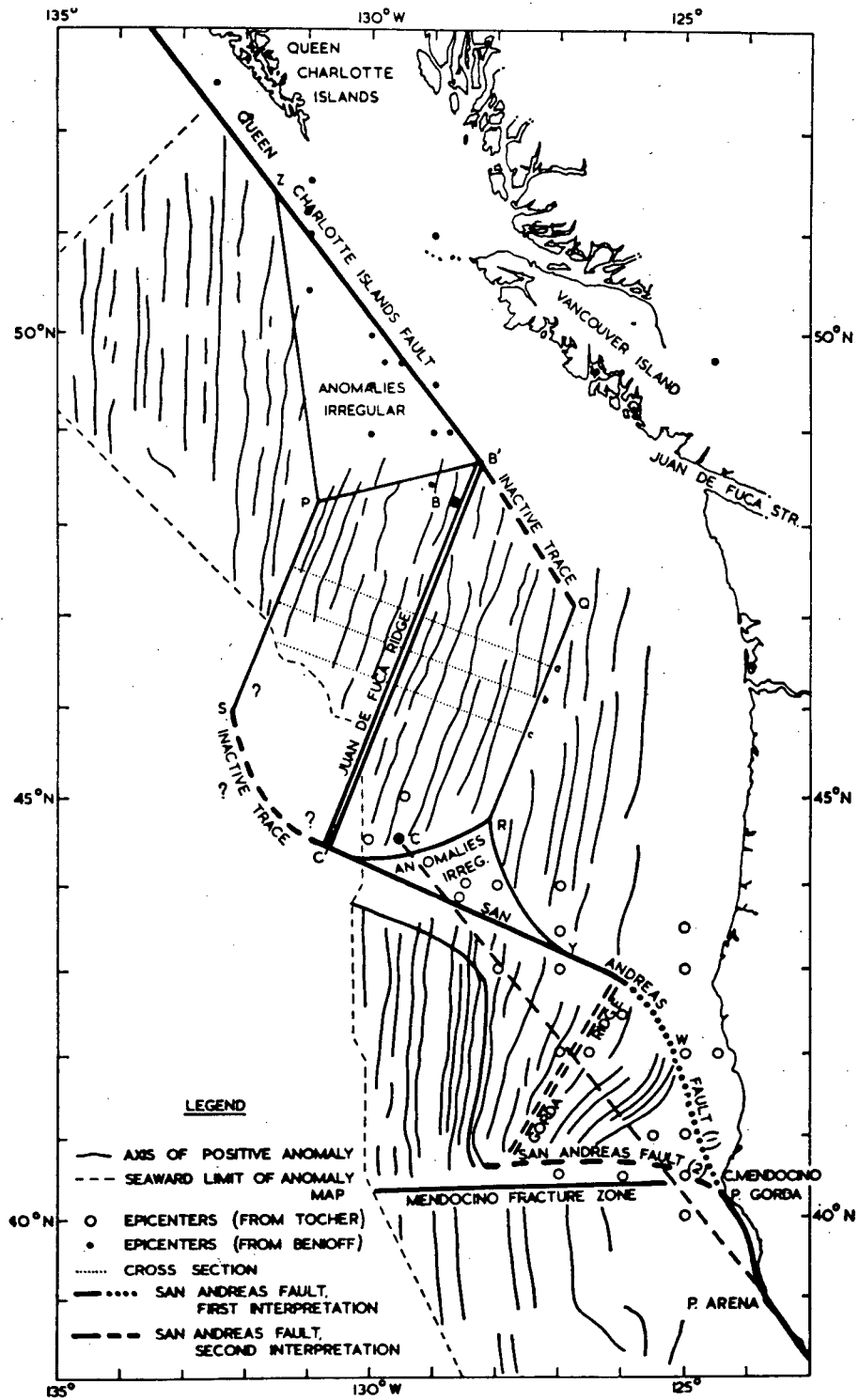


Figure 7: Tuzo Wilson's 1965 interpretation of the tectonics of the Northeast Pacific (from Wilson, 1965b).

McKenzie and Morgan (1969) with their recognition of the Mendocino triple junction.

Morgan (1968) also recognized that the dextral displacement on the San Andreas fault of  $\sim 6 \text{ cm a}^{-1}$  represented relative motion between the North America and Pacific plates and that such motion would also have to be accommodated by the Queen Charlotte fault.

In the late 1960's and early 1970's detailed research work began to focus on the tectonics of the Juan de Fuca plate which was named after the Strait of Juan de Fuca which separates Vancouver Island from the Olympic Peninsula of Washington. The Strait in turn was named in 1787 by Captain Charles Barkley of the trading ship *Imperial Eagle* after a Greek pilot in the Spanish Navy who sailed these waters in 1592 whose real name was Apostolos Valerianus of Cephalonia (Akrigg and Akrigg, 1986).

Most tectonic interpretations in the early 1970's (e.g., Srivastava *et al.*, 1971; Barr, 1972; Bertrand, 1972) connected the Queen Charlotte fault to the Dellwood spreading segment or the Revere-Dellwood fracture zone, named by Srivastava *et al.* (1971) after the adjacent Dellwood Knolls. Bathymetric compilations such as Mammerickx and Taylor (1971) do not indicate the Tuzo Wilson Seamounts. Barr (1974) and Barr and Chase (1974), based on analysis of poorly located earthquake epicentres, suggested that the Queen Charlotte fault connected directly to the north end of the Juan de Fuca ridge in a manner similar to that suggested by Wilson (1965) and Tobin and Sykes (1968).

### 2.3.2 DISCOVERY OF TUZO WILSON SEAMOUNTS

The two Tuzo Wilson Seamounts were not discovered until 1972-3, although their presence is detectable as areas of shallow water at the base of the continental slope in maps and profiles in Gibson (1960) and Dehlinger *et al.* (1970). They were discovered separately by seismic profiling supported by gravity and magnetic highs and later confirmed by dredging and seafloor photography (for magnetics see Tiffin and Currie, 1977). The photography revealed fresh lava flows, tensional cooling fractures and negligible sediment cover (Tiffin,

1974). The southwest seamount was discovered in 1972 and the northeast seamount in 1973 (Tiffin, 1973, 1974). The seamounts were named by Chase and Tiffin in 1972 after the eminent Canadian earth scientist, J. Tuzo Wilson who contributed so much to the understanding of plate tectonics (R.L. Chase, oral comm., 1986). Since their discovery their role in the tectonics of the Northeast Pacific has been controversial, and is still uncertain.

Tiffin (1973) suggested that the southwest seamount might represent a spreading centre and drew an analogy with the Gulf of California. He later speculated (1974) that the Tuzo Wilson Seamounts might be manifestations of a hot spot close to the continent at Queen Charlotte Sound and might be the youngest part of the Kodiak-Bowie seamount chain described by Silver *et al.* (1974). In 1977 the Tuzo Wilson Seamounts were officially named the J. Tuzo Wilson Knolls. Chase (1977) argued in favour of the hot spot origin for the seamounts and also named the hot spot after Tuzo Wilson, the originator of the hot spot hypothesis. Chase (1977) used the global plate movement calculations of Minster *et al.* (1974) to demonstrate that the Kodiak-Bowie seamount chain represented a hot spot scar across the northwestward-moving Pacific plate. Although Chase (1977) suggested other possible locations for the active end of the seamount chain such as the Dellwood Knolls, he did not suggest that the Tuzo Wilson Seamounts are a spreading segment but instead reasserted (Chase *et al.*, 1975) that the triple junction is located near the Dellwood Knolls to the south (Fig. 4). The Dellwood Knolls are two small submarine volcanoes 70 km southeast of Tuzo Wilson Seamounts that rise 800-1000 m above the surrounding seafloor. They were named in the 1940's after the cable ship *Dellwood* and later identified as being a possible segment of the East Pacific Rise by Ewing *et al.* (1968) from evidence of shallow basement (Riddihough *et al.*, 1980).

### 2.3.3 EXPLORER PLATE

Until the mid-1970's there was some skepticism in the geological community about whether the Juan de Fuca plate was subducting below North America as originally suggested by McKenzie and Parker (1967) and Morgan (1968). Some workers (e.g., Bostrom *in* Moen, 1971) suggested that subduction was incipient and that some of the features normally associated with subduction had not yet developed. Certainly the presence of the active Cascade volcanoes supported the concept but the bend in the western coastline of North America between Washington and Vancouver Island and the corresponding lack of andesitic volcanoes north of Mt. Baker in Washington made it difficult to argue in favour of subduction along Canada's western continental margin. Other features such as the lack of a well developed trench and absence of a clearly defined Benioff zone (Riddihough and Hyndman, 1976) and lack of fault plane solutions showing underthrusting (Milne *et al.*, 1978; Rogers, 1979) detracted from the subduction hypothesis.

Riddihough and Hyndman (1976), in a study drawing data from an array of ocean bottom seismometers and from other sources, argued that a portion of the Juan de Fuca plate which they named the Explorer plate, originally suggested as a sub-plate by Barr (1972) and McManus *et al.* (1972), has moved independently for at least 8 Ma. They showed that the Juan de Fuca-North America convergence rate has been decreasing, from  $55 \text{ mm a}^{-1}$  at 9 Ma to  $36 \text{ mm a}^{-1}$  over the last 1 Ma and that the convergence of Explorer plate has in the same period decreased from 55 to  $20 \text{ mm a}^{-1}$ . The implied left-lateral fault between these two plates, first suggested by Barr and Chase (1974), was named the Nootka fault by Hyndman *et al.* (1979) and is shown in Fig. 4. Its presence is supported by offset magnetic anomalies (Riddihough, 1977) and by seismological studies (Milne *et al.*, 1978).

A number of locations for the North America - Explorer - Pacific triple junction have been suggested, some of which were discussed previously. Although Tiffin (1973) suggested that the Tuzo Wilson Seamounts might represent the locus of the triple junction, the

Dellwood Knolls were the preferred location and Tuzo Wilson was not suggested again until 1978 (Hyndman *et al.*, 1978; Keen and Hyndman, 1979). Riddihough *et al.* (1980) suggested three possible scenarios for plate interaction in this area: (1) a triple junction at Dellwood; (2) a triple junction at Tuzo Wilson Seamounts, with Tuzo Wilson Seamounts as a spreading segment; and (3) a diagonal fault connecting the south end of the Queen Charlotte fault to the northeasterly end of the Explorer spreading segment. They argued that the orientation of the diagonal fault would be very close to the Pacific - North America motion vector of Minster and Jordan (1978). This would make the motion on it purely strike slip and it would have a slightly different orientation from the Queen Charlotte fault which has a small component of underthrusting (Hodgson and Milne, 1951; Davis and Riddihough, 1982; Yorath and Hyndman, 1983; Dehler *et al.*, 1986). Volcanism at Dellwood and Tuzo Wilson Seamounts could then be considered indicative of a leaky transform, a concept first suggested by Menard and Atwater (1969). The volcanism might also be analogous to the enigmatic volcano, Mt. Edgecumbe, which occurs on the Chichagof-Baranof fault, an extension of the Queen Charlotte fault, near Baranof Island in the Alaska panhandle (von Huene *et al.*, 1979). In later studies, (Riddihough and Davis, 1982; Hyndman *et al.*, 1982) the model incorporating the triple junction at Tuzo Wilson Seamounts was favoured and this seems to be the most likely explanation today although it is not undisputed. The Tuzo Wilson Seamounts and Dellwood Knolls may have a shared role as spreading centres implying that the area between them is a separate plate, which would be most appropriately named the Tuzo Wilson microplate. The Tuzo Wilson Seamounts will probably become the dominant spreading segment.

There is some evidence to suggest that part of the Explorer plate is now attached to the North American plate. Davis and Riddihough (1982) suggested that a fracture has occurred along a preexisting structural weakness in the oceanic crust beneath Winona Basin, which is located between the Revere-Dellwood fracture zone and the northern tip of Vancouver Island. They argued that the break occurred at about 1 Ma, forming Paul Revere ridge, and that this occurred contemporaneously with initiation of spreading on the Dellwood

segment. The break probably occurred due to resistance to underthrusting and sinking of the young buoyant oceanic crust. Deformation is seen in sediments as young as Pleistocene indicating that compressional tectonic activity may still be occurring (Tiffin, 1974). The rearrangements of plate boundaries necessitated by the welding of portions of Explorer plate onto North America are complex. Reorganizations of the type that have occurred in the past 4Ma as described by Davis and Riddihough (1981, 1982) and Riddihough *et al.* (1983) will likely continue as long as small plates such as Explorer and Tuzo Wilson are sandwiched between, and therefore dominated by, very large plates along the transform boundary that separates them. The actual location of the triple junction may not be accurately locatable until after the next few Ma of tectonic movement have occurred.

#### 2.3.4 AGE AND PETROLOGY OF BASALTS FROM TUZO WILSON SEAMOUNTS

The first rock dredged from Tuzo Wilson Seamounts (in 1973) was fresh glassy basalt from near the summit, compositionally a hawaiite (Chase, 1977). A whole-rock K-Ar date of  $55,000 \pm 100\%$  years (Cousens *et al.*, 1985) confirmed the youth suggested by underwater photography, SeaMARC II imagery and lack of manganese encrustation on dredged basalts. The strong positive magnetic anomaly also suggests a young age ( $<0.7$  Ma) (Carbotte *et al.*, 1986), and gravity data suggest a shallow body with no appreciable root, indicative of a recently formed feature. Riddihough *et al.* (1980) assigned, on the basis of extrapolated magnetic anomalies, an age of 4.5–5.3 Ma to the underlying crust, and suggested that spreading at Tuzo Wilson Seamounts and Dellwood was initiated simultaneously, at about 0.5–1.0 Ma.

Chase (1977) suggested that the Tuzo Wilson Seamounts were the most recent manifestations of a hot spot that produced the Kodiak-Bowie seamount chain, whereas Turner *et al.* (1980), using new radiometric ages for the seamount chain, contradicted this and suggested that the hot spot is located 40–130 m south of Bowie Seamount, or about 150 m due west of the southern Queen Charlotte Islands. Cousens *et al.* (1985) suggested that the

petrochemistry of the basalts does not clearly resolve this problem. Hawaiiites are usually characteristic of late-stage volcanism on oceanic islands associated with mantle plumes but they may also be present in the early stage of volcanic activity that precedes the tholeiitic stage (Cousens *et al.*, 1985). The REE patterns of these hawaiiites are not indicative of a hot spot origin although Cousens *et al.* (1985) indicated that a metasomatic event affecting either the source region or the parental magma may have altered the REE pattern. Using a partial melting model, they also demonstrated that the hawaiiites could not have been generated from the same source as the Explorer and Juan de Fuca ridge tholeiites. In addition  $^{87}\text{Sr}/^{86}\text{Sr}$  and  $^3\text{He}/^4\text{He}$  ratios in Tuzo Wilson basalts suggest a source that has a large component of depleted mantle. Thus the Tuzo Wilson Seamounts are enigmatic. Their chemistry and isotopic ratios indicated that they are neither spreading ridge nor hot spot. Cousens *et al.* (1985) concluded that it is possible that spreading has "jumped" to the Tuzo Wilson area because the Pratt-Welker (alias Kodiak-Bowie) hot spot has created a weak spot in the lithosphere and is providing a readily tapped magma source. Carbotte (1986) pointed out that the seamounts are situated within a rift valley (Fig. 5 and section on physiography). Preliminary work on samples acquired in 1985 confirms the unusual petrochemistry (P.J. Michael, oral comm., 1986).

### 2.3.5 RECENT SEAFLOOR MAPPING

Recently developed seafloor mapping techniques have contributed significantly to the understanding of tectonics in world oceans (Detrick, 1986). The Tuzo Wilson Seamounts and much of the Juan de Fuca - Explorer ridge system is covered by SEABEAM maps (Fig. 2) that give detailed (10 m contour interval) bathymetry and SeaMARC II (Fig. 3) mosaics that give an acoustic image of large areas of the seafloor. Clearly visible in Fig. 3 are features such as the Revere-Dellwood fracture zone which appears as a distinct linear break in the seafloor, lava flows (darker areas) flowing off Tuzo Wilson Seamounts and Dellwood Knolls, and large sediment distributary channels down which some lava has flowed. Evidence for extensive lava

flows is also seen on seismic reflection profiles (Davis, 1982). The prominence of the Revere-Dellwood fracture zone and its apparent termination adjacent to Tuzo Wilson Seamounts gives support to the hypothesis that Tuzo Wilson Seamounts is a spreading centre and that the northeast end of this spreading segment, where it meets the Queen Charlotte fault, is a triple plate junction. As mentioned previously, spreading is probably occurring at Dellwood Knolls simultaneously. Seafloor mapping is discussed in greater detail in Chapter 3.

### 2.3.6 HEAT FLOW AND HYDROTHERMAL ACTIVITY

Numerous studies of heat flow have been made on the Explorer plate and adjacent areas and several of these include measurements in the Tuzo Wilson Seamounts area (Srivastava *et al.*, 1971; Hyndman *et al.*, 1978, 1981, 1982; Davis and Riddihough, 1982). Hyndman *et al.* (1978) reported heat flow measurements close to Tuzo Wilson Seamounts, and a series of multipenetration measurements at two stations on the Queen Charlotte abyssal fan, ~230 km due west of Tuzo Wilson Seamounts. Their 46 abyssal fan measurements averaged  $56.8 \text{ mW m}^{-2}$  with a range of 21.0–102.2  $\text{mW m}^{-2}$  compared with values as low as  $8.4 \text{ mW m}^{-2}$  200 km west of Juan de Fuca ridge on the Tufts abyssal plain measured by Lister (1970). Five measurements of heat flow near Tuzo Wilson Seamounts ranged between 159.2 and 347.8  $\text{mW m}^{-2}$ , with an average of 216.2  $\text{mW m}^{-2}$  (Hyndman *et al.*, 1978). These values are consistent with the lithospheric age of <5 Ma reported by Davis and Lister (1977a). A thick cover of sediment where the measurements were taken would reduce hydrothermal cooling but Hyndman *et al.*, (1978) suggested that hydrothermal fluids may be vented at the outcropping seamounts. In a similar study on the Winona Basin, Davis and Riddihough (1982) attributed reduced heat flows to venting of hydrothermal fluid through basement outcrops at the Paul Revere ridge fault scarp. Davis (1981, and see also Davis and Clowes, 1986) suggested that lithification of sediments as young 0.5 Ma in the Winona Basin may be the result of porewater circulation driven by the regional heat flux. Hydrothermal activity has not yet been detected at this location, probably because recent work has concentrated on areas

where SEABEAM coverage exists. In a study incorporating detailed heat flow measurements on the Juan de Fuca ridge system, Davis *et al.* (1980) concluded that seamounts are extremely effective in localizing hydrothermal discharge and often have low heat flow values. This effectiveness may be due to a number of reasons including the fact that seamounts are physiographically high-standing features and because they are often free of sediment cover. Observations on the East Pacific Rise have indicated that high standing portions of ridge segments are the most likely sites for hydrothermal activity (Ballard and Francheteau, 1983; Francheteau, 1983; Crane, 1985; Crane *et al.*, 1985). Hydrothermal activity has been observed in the caldera on Axial seamount on Juan de Fuca ridge (CASM, 1985; Hannington, 1986).

In areas of hydrothermal circulation, conductive heat flow is reduced. Heat is convectively removed at sites of venting of hot fluid onto the seafloor (Hyndman *et al.*, 1982). A thick sediment cover tends to act as an insulating blanket (Chase *et al.*, 1975) because it reduces permeability and inhibits hydrothermal circulation, resulting in more accurate conductive heat flow values (Anderson and Hobart, 1976; Sclater *et al.*, 1976). However on the sedimented northern Juan de Fuca ridge lateral heat transport beneath an extensive impermeable sediment cover has been observed up to 20 km away from basement outcrop (Davis and Villinger, 1986) and, at a recently discovered site of active venting through sediments, heat flow values are commonly  $1-5 \text{ W m}^{-2}$  and in places reach  $25 \text{ W m}^{-2}$  (not  $\text{mW m}^{-2}$ !), (W. Goodfellow, oral comm., 1986). Rapid sedimentation, which probably took place around Tuzo Wilson Seamounts during the Pleistocene due to intense glacial erosion action (Hamilton, 1967; Horn *et al.*, 1970), also tends to reduce measured heat flow values significantly (Lister, 1972). Davis and Riddihough (1982) pointed out that heat flow values measured in turbiditic sediments may be in error by 10–20% due to large conductivity variations both laterally and with depth.

A further series of measurements reported by Hyndman *et al.* (1982), and summarized on Juan de Fuca plate map series JFP-10 (Hyndman, 1983), was made in the vicinity of Tuzo

Wilson Seamounts and to the northwest along the Queen Charlotte fault zone. Values on the continental slope east of the seamounts and to the northeast of the extrapolation of the Queen Charlotte fault to the southeast past the Tuzo Wilson Seamounts (Fig. 8) are higher than those estimated from wells in Queen Charlotte Sound (Yorath and Hyndman, 1983). Hyndman *et al.* (1982) attributed this to underthrusting of the Tuzo Wilson Seamounts spreading segment which, if the spreading was initiated at 0.5–1.0 Ma as suggested by Riddihough *et al.* (1980), would have progressed a maximum of 20 km to the northeast.

The heat flow data, tectonic setting, dredging of hydrothermal crusts (Piper *et al.*, 1975; Grill *et al.*, 1981) and discovery of hot springs along Explorer ridge, Juan de Fuca ridge and on Axial seamount (CASM, 1985; Hannington, 1986; Scott, in press) all suggest that hydrothermal activity and polymetallic sulphides may be present at Tuzo Wilson Seamounts (Scott, in press). The hydrothermal systems and related sulphide deposits on Explorer and

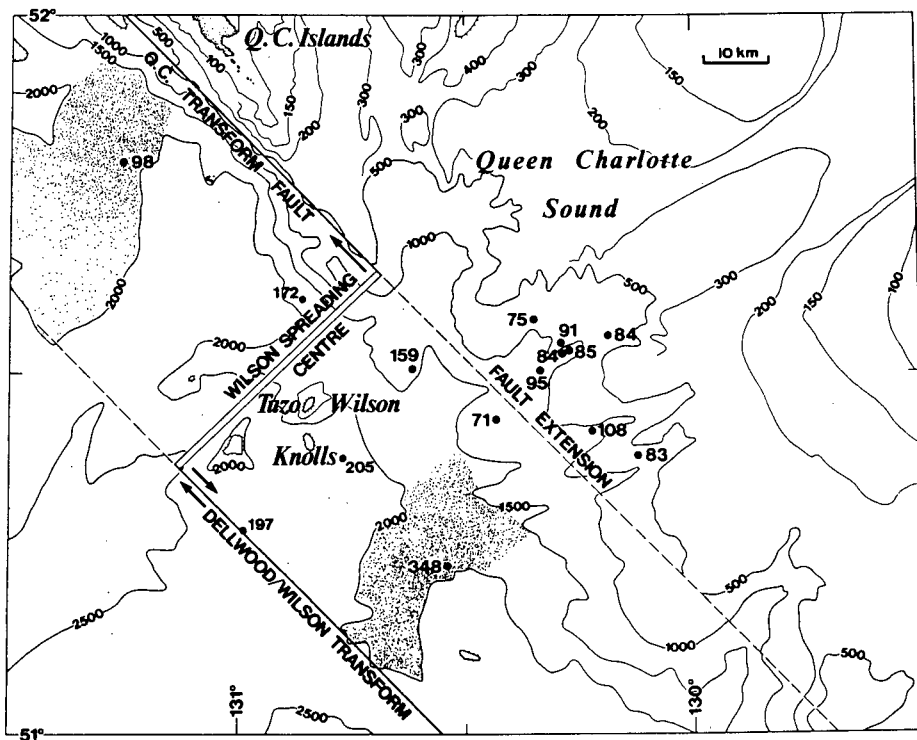


**Figure 8:** Heat flow (in  $\text{mW m}^{-2}$ ) in vicinity of Tuzo Wilson Seamounts (from Hyndman *et al.*, 1982).

Juan de Fuca ridges occur in young unsedimented portions of these ridge crests.

Hydrothermal mounds in sediments at Galapagos 18–25 km south of the axis of the spreading centre (e.g., Corliss *et al.*, 1978, 1979), in the Guaymas basin (e.g., Lonsdale *et al.*, 1980; Simoneit and Lonsdale, 1982), and 25 km east of the spreading axis of Juan de Fuca ridge over a fault in sedimented Middle Valley (Villinger and Davis, 1984; Adshead *et al.*, 1986) support the possibility of sediment-hosted hydrothermal activity at Tuzo Wilson Seamounts. However it has not yet been observed there although recent research, described below, gives some indication of its existence.

## 2.4 HYDROGRAPHY

Surface currents in the Northeast Pacific south of the Queen Charlotte Islands are dominated by the weak poleward drift of the Alaska current which swings to the north as it approaches the British Columbia coast. In winter this northerly flow is supplemented by the Davidson current to give an average speed of  $35 \text{ cm s}^{-1}$  (0.7 knots) and up to  $75 \text{ cm s}^{-1}$  (1.5 knots) in winter storms (Thomson, 1981). The north-flowing Haida current also occurs during the winter and hugs the west coast of the Queen Charlottes (Thomson and Emery, 1986). In summer the easterly-flowing Subarctic current diverges into the north-flowing Alaska current and the south-flowing California current as it approaches the coast, leaving a triangular area off the Queen Charlotte Islands and Vancouver Island with confused and variable currents (Thomson, 1981). The currents of the west coast are also described in detail by Freeland *et al.* (1984).

Little information seems to be available on deep sea currents in the area. Diurnal tidal currents are superimposed on the local drift along parts of the Juan de Fuca ridge (R.E. Thomson, oral comm., 1986), but no research has been done on tidal currents in the Tuzo Wilson Seamounts area. Analysis of bottom photography (see Chapter 3) indicates a gentle northwesterly flow at the base of the continental slope at a depth of  $\sim 2000 \text{ m}$ .

## 2.5 OTHER STUDIES PERTAINING TO THE TUZO WILSON AREA

Numerous other studies have been made covering many facets of the geology and geophysics of the Tuzo Wilson Seamounts area including: detailed studies of plate motions of the whole Juan de Fuca system during the last 100 Ma (Riddihough, 1982c); recent movements of the Juan de Fuca plate (Riddihough *et al.*, 1983; Riddihough, 1984); basalt geochemistry (Cousens, 1982; Cousens *et al.*, 1984, 1985; Michael and Chase, 1985; Michael *et al.*, 1986); crustal structure (Malacek and Clowes, 1978; Clowes and Knize, 1979; Cheung and Clowes, 1981; Clowes *et al.*, 1981; Au and Clowes, 1982; Ellis *et al.*, 1983; Clowes and Gens-Lenartowicz, 1985; Sutherland Brown and Yorath, 1985); geophysics of Western Canada continental margin (Riddihough, 1979; Keen and Hyndman, 1979; Riddihough and Seeman, 1982); structure of Queen Charlotte Basin (Young, 1977, 1981; Yorath and Chase, 1981; Carbotte, 1986); petroleum geology of Queen Charlotte Basin (Shouldice, 1971, 1973; Stacey, 1974; Haimila and Proctor, 1982; Yorath and Chase, 1982; Yorath and Hyndman, 1983); geology of the continental shelf (Luternauer, 1972; Tiffin *et al.*, 1972; Herzer and Bornhold, 1982; Currie and Bornhold, 1983; Luternauer and Murray, 1983; Bornhold and Yorath, 1984; Conway and Luternauer, 1984, 1985); seismicity (Milne, 1978; Hyndman *et al.*, 1978; Keen and Hyndman, 1979; Yorath *et al.*, 1979; Hyndman and Rogers, 1981); Queen Charlotte fault (Srivastava, 1973; Currie *et al.*, 1980; Horn *et al.*, 1981, 1984; Riddihough, 1981; Hyndman and Ellis, 1981a, b; Hyndman *et al.*, 1981, 1982; Hyndman and Weichert, 1983, 1986; Dehler *et al.*, 1986); DSDP Hole 177 (drilled on northern Paul Revere ridge in 1971) (Couch and Chase, 1973; Kulm, von Huene *et al.*, 1973); and vertical tectonics (Riddihough, 1982a, b).

## Chapter 3

### SEAFLOOR MAPPING

#### 3.1 INTRODUCTION

A variety of different techniques used to map the seafloor are described in this chapter. SEABEAM and SeaMARC II surveys conducted by other organizations and their published results are described herein and used to complement the data collected on the CASM 5 cruise. Results of underwater photography, 3.5 kHz echo sounding and conductivity-temperature-depth (CTD) surveys provide the most information when used in conjunction with each other. Individually they often provide inconclusive results. Unfortunately these surveys are often hampered by equipment failure, a problem common to most oceanographic operations.

#### 3.2 SEABEAM

SEABEAM is a seafloor mapping system that uses an array of 12kHz narrow beam transducers mounted on the hull of a ship. It produces real-time contoured maps of the seafloor with a contour interval of 10 m at a rate of 1200 km<sup>2</sup> per day under good conditions (Detrick, 1986). This system is described in detail by de Moustier and Kleinrock (1986).

Twenty-eight 1:50,000 scale sheets have been produced for the Juan de Fuca Ridge Atlas series published jointly by the Pacific Geoscience Centre (Canada) and the National Oceans and Atmosphere Administration (U.S.A.). The 102 O/6,7 sheet (Malahoff *et al.*, 1984) has been used extensively in this study as a bathymetric base map. A reduced version is shown in Fig. 2.

Features visible in the SEABEAM maps include:

1. The two volcanic edifices of the Tuzo Wilson Seamounts.

2. Numerous smaller satellite cones.
3. What appears to be a linear trend of the locations of these eruptive centres, oriented perpendicular to the relative motion of the North American and Pacific plates.
4. Deep-sea sediment channels.
5. Smooth, sediment-mantled areas; and
6. Bathymetric features consistent with the scarp discussed in more detail later in this chapter.

### 3.3 SEAMARC II

SeaMARC II acoustic imagery as it relates to tectonic interpretation and physiography has already been discussed briefly in section 2.3.5.

The SeaMARC (**S**ea **M**apping **A**nd **R**emote **C**haracterization) system is an acoustic analogue of side-scanning radar. It uses the amplitude of sound reflected off the seafloor to give a sound-illuminated image. Two systems exist: SeaMARC I is towed a few hundred metres above the seafloor, uses a frequency of 30 kHz and provides good resolution for mapping small areas; SeaMARC II is a coarse resolution, long range (10 km swath) system using a frequency of 12 kHz which is towed near the surface (~100 m depth). It can be towed at speeds of up to 18 km hr<sup>-1</sup> and is capable of insonifying 3500 km<sup>2</sup> of seafloor per day (Detrick, 1986). The system is described in detail by Davis *et al.* (1984).

The SeaMARC II images recorded for the Juan de Fuca Ridge Atlas series have been published by Davis *et al.* (1984). Five mosaics have also been published at a scale of 1:250,000 by Davis *et al.* (1985). The northernmost mosaic covers the Tuzo Wilson Seamounts and Dellwood Knolls area and provides a wealth of tectonic and geologic information. It was described by Currie *et al.* (1984), and has been analysed in detail by Carbotte (1986). Fiducial marks on the mosaics should be used with caution as their locations are inexact in some cases (N. Massey, oral comm., 1986). Numerous features can

be seen in this mosaic, most of which are visible on the northern portion shown in Fig. 3:

1. The Revere-Dellwood fracture zone, a single continuous fault trace running 70 km from Tuzo Wilson Seamounts to Dellwood Knolls.
2. A southwest-northeast trending "scarp" (referred to by Carbotte (1986) as the Seamarc fault) cutting across the Tuzo Wilson Seamounts area, bifurcating in two locations north of the northeast seamount, in an area hereinafter referred to as the "scarp area".
3. Volcanic edifices of Tuzo Wilson Seamounts and Dellwood Knolls.
4. Extensive lava flows coming off Tuzo Wilson Seamounts and Dellwood Knolls, in some cases extending up to 60 km from their sources (Davis, 1982), but usually <5 km at Tuzo Wilson Seamounts (Carbotte, 1986).
5. Deep-sea sediment distributary channels.
6. Offset of two channels across the Revere-Dellwood fracture zone.
7. Channels adopted by lavas as flow paths; in some cases flows are obscured by sediment indicating subsequent use of channel by turbidity currents.
8. Lava flows "spilling over" the Revere-Dellwood fracture zone, indicating a small vertical offset.
9. Canyons incising the continental margin; and
10. Slope failure along the Queen Charlotte fault.

The scarp (2, above) is of particular interest as it appears to cut both sedimented and basalt-covered seafloor and is generally oriented parallel to a linear trend of eruptive centres associated with the southwest seamount. It is probably an extensional feature produced by the same stress field which localizes volcanism. In the scarp area it appears to curve counter-clockwise into the Queen Charlotte fault. At its southwest end it may also curve in the same sense into the Revere-Dellwood fracture zone. Such curvature of normal faults into bounding transform faults has been noted by Morgan and Parmentier (1984) on slow spreading ridges. The scarp also appears on echo-sounding profiles and possibly on seafloor photographs, and has associated temperature and conductivity anomalies. These

characteristics will be discussed further in later sections.

According to CSP data examined by Carbotte (1986), a buried basement ridge trends roughly parallel to the Revere-Dellwood fracture zone to the south of Tuzo Wilson Seamounts. This ridge may exist to the north of the seamounts as well. Near Dellwood Knolls, Scott channel has been eroded through to the basement ridge which is visible on the SeaMARC II mosaic as an acoustically hard floor of the channel. Sediment overlying basement is 400-500 m thicker on the southwest side and gravity modelling requires an even larger vertical offset of basement to account for the gravity low coincident with the buried ridge (Carbotte, 1986). This ridge could be a former extension of the Queen Charlotte fault.

Carbotte *et al.* (1986) suggest that Tuzo Wilson Seamounts may be the result of a recent northwestward relocation of the triple junction. However, evidence from acoustic imagery of recent volcanism at Tuzo Wilson Seamounts and Dellwood Knolls and of recent movement along the Revere-Dellwood fracture zone supports the argument that Tuzo Wilson Seamounts and Dellwood Knolls are paired spreading centres, although Tuzo Wilson Seamounts may be younger and will probably become the dominant spreader. Currie and Davis (1986) note that the volume of young lavas seen at Tuzo Wilson Seamounts is far greater than that at Dellwood Knolls and that Dellwood has features indicative of an older, more established spreading centre. If these two areas are paired spreading centres, then an extension of the Queen Charlotte fault south of Tuzo Wilson to Dellwood would be required to accommodate motion relative to North America, implying that the area between the two spreading centres constitutes a separate plate (Tuzo Wilson microplate). Ocean bottom seismograph studies (Hyndman and Rogers, 1981) do not give any indication that such a fault, if it exists, is active, and earthquake epicentres located by the land station network are too uncertain to define a discrete fault zone. However, the very short deployment period of the ocean bottom seismographs, in some cases as short as five days, and the fact that only one small earthquake was recorded along the Queen Charlotte fault north of Tuzo Wilson

Seamounts suggests that activity along the postulated southward extension of the Queen Charlotte fault could easily go undetected. Carbotte (1986) noted that the lack of sediment deformation observed on CSP lines across the southward extension of the Queen Charlotte fault indicates that the fault has probably not been active in the past 200,000 years; however, as she pointed out, Pleistocene sedimentation rates were probably sufficiently high that the undeformed sediment is young enough to lack deformation without refuting recent fault movement.

### 3.4 UNDERWATER PHOTOGRAPHY

#### 3.4.1 METHODS

Photography of features on the seafloor at depths of 1500–2500 m was carried out using the University of British Columbia Deep-tow Camera System, which consists of an underwater camera, high power (100 W s) strobe and battery pack mounted on a metal frame that is towed along three metres above the seafloor. A 12 kHz pinger mounted in the frame allows the person aboard the ship who is flying the camera to control the height of the camera above the seafloor by sending voice commands to the winch operator. A timer is set to delay the start of photography until the system has been lowered to the seafloor. Once photography has started the flash discharges and the film advances every 12–15 seconds (depending on battery state). No shutter is required for use so far below the photic zone. A data frame is included in each photograph giving time, depth and information such as date, *f*-stop and film speed. The camera is loaded with a 100 foot (30 m) roll of film which lasts about 110 minutes and produces 500 exposures. Under normal conditions, the system is towed at 1 knot ( $1.8 \text{ km h}^{-1}$  or  $0.5 \text{ m s}^{-1}$ ) resulting in a spacing of 6–7.5 m between the centres of frames. More detailed information on the system can be found in Denton (1986).

The paths of camera tows were chosen after examination of the SEABEAM map and SeaMARC II acoustic images. The former was used principally for selecting tow sites on the

volcanic edifices and the latter for those in the scarp area.

### 3.4.2 RESULTS

The results of the camera tows are summarized in Table 2. The locations of the 12 camera tow tracks are shown in Fig. 9 and results are summarized in two photogeologic maps (Figs. 10 and 11). Only those portions of tows that actually yielded interpretable results are shown in these two figures, whereas all attempted tows are shown in Fig. 9. All photography was done using black-and-white film which was developed on board ship. As is evident from the comments in Table 2, attempts at bottom photography were fraught with problems. Out of a total of 22 hours (on-bottom time) of camera tows, a total of only 5.8 hours of usable photographs were obtained, for an average success rate of only 26%. However the photographs that did turn out provide a wealth of valuable information. Photographs illustrating some of the features seen on the seafloor are shown in Figs. 12–15.

The bottom photographs indicate that:

1. Pillows are the dominant flow morphology, although most non-sediment photographs are of talus.
2. Parts of the seamount flanks are old, as indicated by sediment covering pillow lavas and talus, although other evidence (e.g., dredging, SeaMARC II imagery) indicates that recent volcanism has occurred.
3. The sedimented "scarp area" north of the northeast seamount, which may comprise part of a submarine fan at the base of the continental slope, is interrupted by frequent areas of rubble and gravel, probably indicative of small-scale vertical tectonics.
4. There is no visible evidence of hydrothermal activity.
5. Bottom fauna in sedimented areas consist almost exclusively of brittle stars (Ophiuroidea), although burrows and evidence of other activity such as grazing and resting trails are often visible (Figs. 12 and 13). Such activity has important implications for sediment geochemistry.

**Table 2: Summary of camera tows.**

Camera Tow #	Location <sup>1</sup>	Features <sup>2</sup>	Percentage of film usable <sup>3</sup>	Comments
1	Scarp area	-	0	fogged during developing
2	Scarp area	-	0	camera jammed
3	Scarp area	-	0	camera jammed
4	Scarp area	-	0	flown 750 m off bottom
5	SW side of SW seamount	blocky talus and pillow talus	23	camera jammed, strobe failed <sup>4</sup>
6	Scarp area <sup>5</sup>	smooth sediment with occasional rubble/gravel	40	camera started prior to reaching bottom; many internal gaps
7	SE side of SW seamount	talus with abundant coral	5	strobe failed early in run
8	NE side of SW seamount	sediment and sedimented talus	77	strobe failure late in run
9	NW side of NE seamount	talus and sedimented talus	65	camera started prior to reaching bottom
10	Scarp area <sup>6</sup>	smooth sediment with occasional rubble/gravel	86	
11	SW side of NE seamount	sedimented talus and sediment	53	camera failure late in run
12	on small knoll N of SW seamount	-	0	film did not go through camera

<sup>1</sup>See Figure 9.<sup>2</sup>See Figures 10 and 11.<sup>3</sup>Assumes maximum run time of 110 minutes.<sup>4</sup>Camera was anchored for part of tow. Fin and strobe coated in clear bacterial (?) gel.<sup>5</sup>Transits area where cores 1 and 3 were taken.<sup>6</sup>Transits area where core 8 was taken.

6. Bottom fauna on talus are varied in types and numbers of animals and includes corals (Fig. 14), crabs, sea cucumbers, and fish (Figs. 13 and 15).
7. Evidence of bottom currents is limited to a few leaning corals that suggest a flow to the northwest, (i.e. parallel to the continental margin).
8. Bedforms such as ripples and scouring were not observed, suggesting that bottom currents are gentle.

#### 3.4.3 DISCUSSION

The lack of photographic evidence must not be considered to preclude hydrothermal activity, especially in the scarp area. The scarp was probably not crossed by either of the successful camera tows in the area (6, 10), although 6 did come close to it, and 10 may have crossed it. It is important to note that numerous gaps in coverage exist in both of these tows. What appears to be a small scarp is visible in some photographs in tow 10 (Fig. 10). Its location is about 300 m from the trace of the scarp as determined from SeaMARC II images and echo-sounding profiles. It may represent a small local feature or a bifurcation of the main scarp. Alternatively the photograph could be of the main scarp itself given that the absolute accuracy for the SEABEAM map which was used as the navigation base map is  $\pm 300$  m (Malahoff *et al.*, 1984).

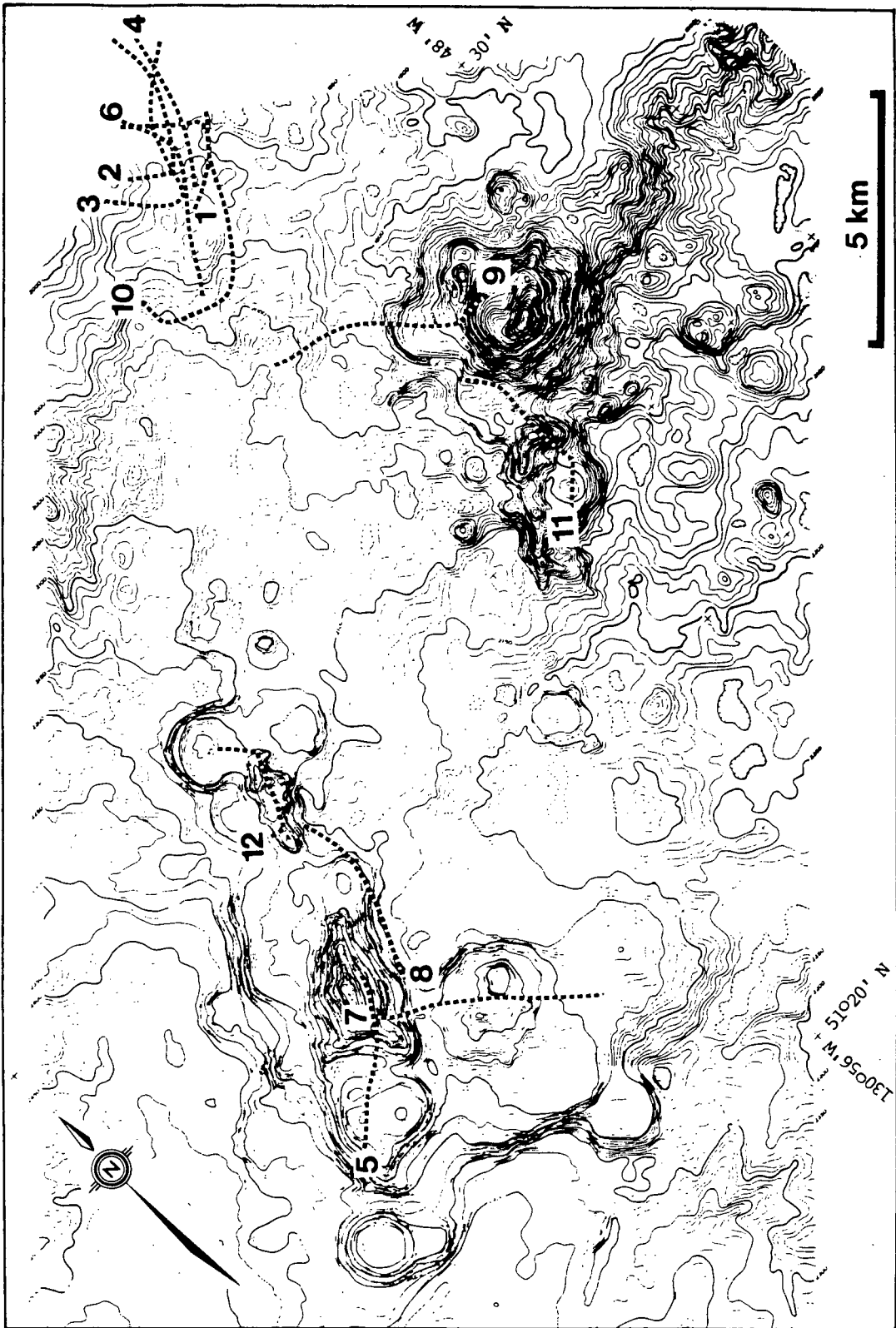


Figure 9: Locations of underwater camera tows.

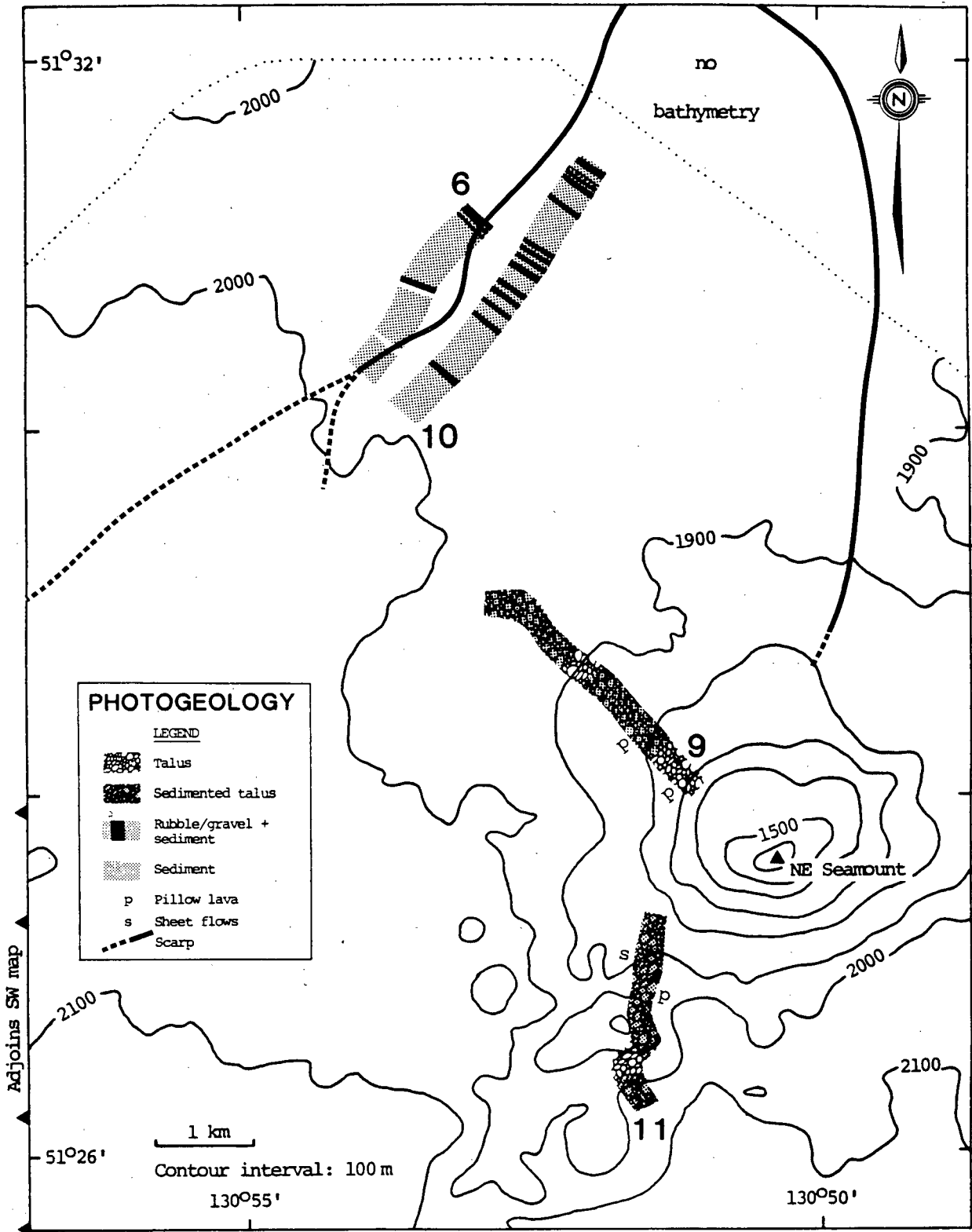


Figure 10: Photogeology, northeast sheet. Swath width exaggerated for clarity.

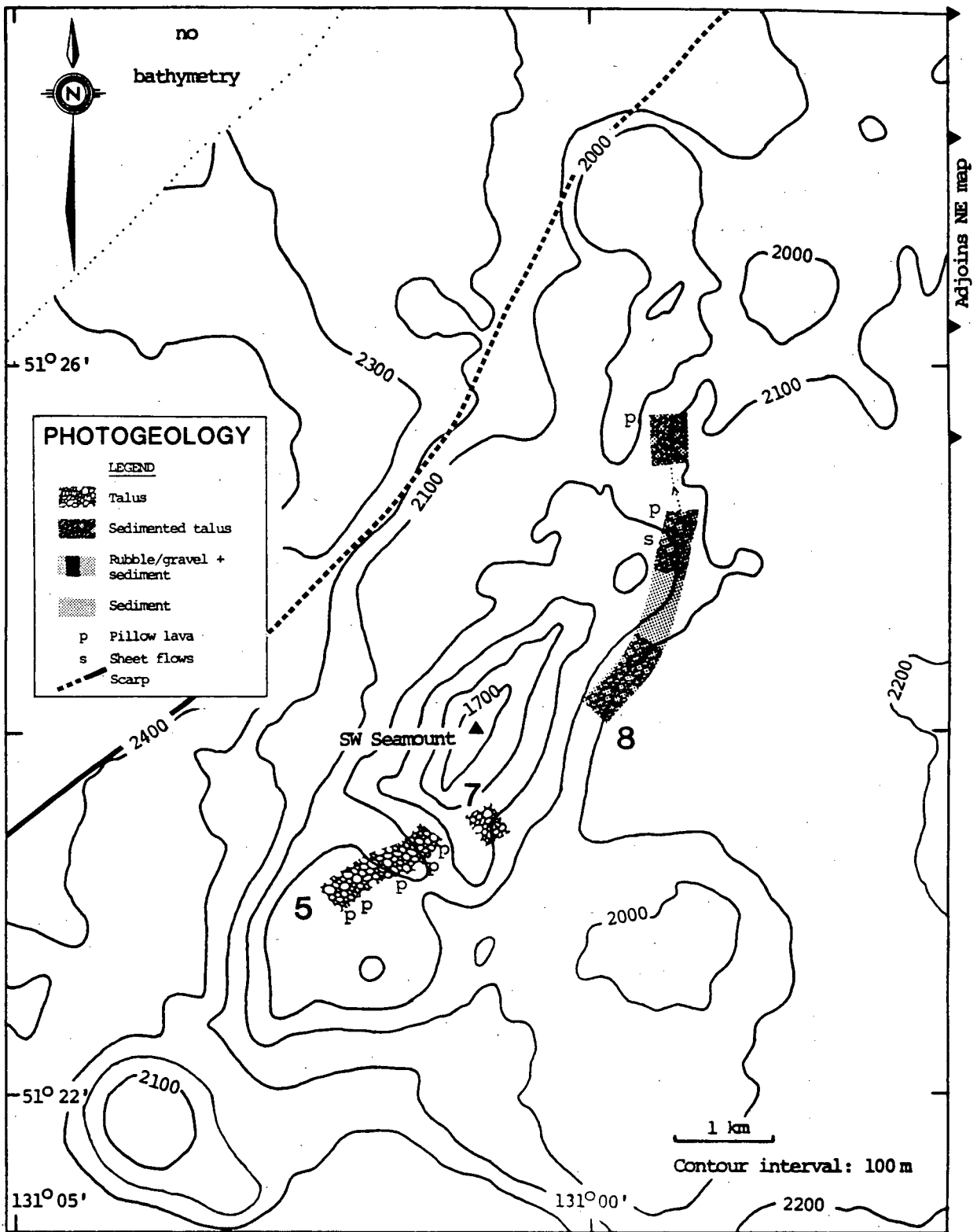


Figure 11: Photogeology, southwest sheet. Swath width exaggerated for clarity.



**Figure 12:** Smooth sediment with brittle stars (Ophiuroidea) and burrows; scarp area 1945 m depth, tow 10.



**Figure 13:** Smooth sediment with rat-tail fish, vertical "straw" and ubiquitous brittle stars; scarp area at 1970 m depth, tow 6.



**Figure 14:** Pillow lavas with fan corals; northeast side of southwest seamount at 2080 m depth, tow 8.



**Figure 15:** Sedimented talus with stingray; northwest side of northeast seamount at 1825 m depth, tow 9.

### 3.5 ECHO-SOUNDING

Echo-sounding traverses were made over the scarp using the ship's 3.5 kHz system to attempt to locate and characterize this feature. It appears as a down-to-the-southeast scarp on each of three lines that run perpendicular to it, with a throw of up to 40 m. The scarp is illustrated by the 3.5 kHz profile in Fig. 16. Loran-C location: 51°30'21"N, 130°54'05"W. Such echo-sounding profiles confirm the existence of this feature which was first noticed on the SeaMARC II images. The echo-sounding bathymetry is in very close agreement with the SEABEAM bathymetry. The location of the scarp is shown in Figs. 17 and 18.

The 12 kHz pinger records obtained concurrently with the bottom photographs do not provide any positive indication of the presence of the scarp, probably because none of the tows crossed the scarp at a high angle.

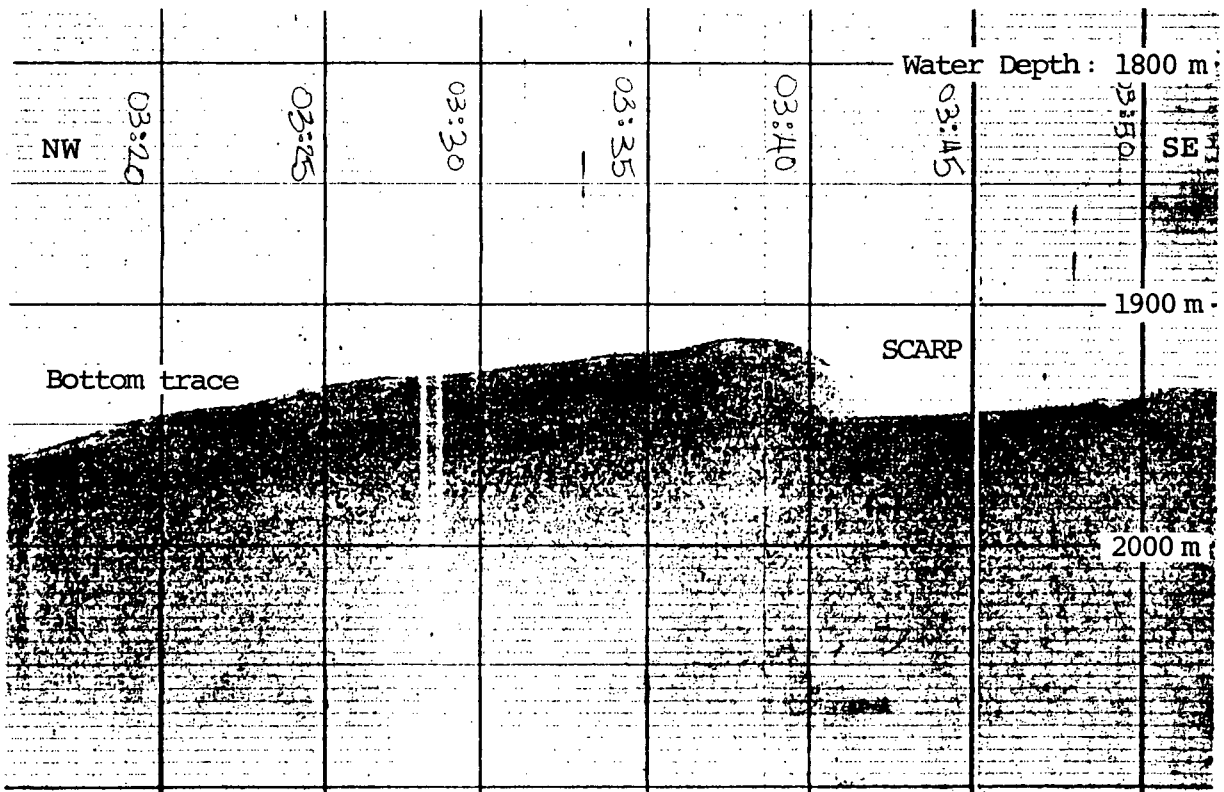


**Figure 16:** 3.5 kHz profile across fault scarp showing 40 m throw (down-to-southeast, 1910–1950 m).

## 3.6 CONDUCTIVITY-TEMPERATURE-DEPTH SURVEYS

### 3.6.1 METHODS

CTD measurements were taken on all camera tows using an Aanderaa current meter adapted to record conductivity and temperature attached to the camera frame. The system recorded data every 30 seconds, or every 15 m assuming a camera tow speed of  $0.5 \text{ m s}^{-1}$ . The temperature response time was undesirably long as it was capable of detecting only 66% of a given temperature change in 12 seconds. The implications of this are that a small area of discharge could easily go undetected and also that any anomaly that actually did get detected is probably much more significant than the data indicate.

### 3.6.2 RESULTS

The results are summarized in Table 3 and locations of CTD anomalies shown in Figs. 17 and 18. Salinity and temperature are plotted against time for each camera lowering except 4 and 8 which did not yield results due to instrument malfunction. These plots comprise Figs. 19 through 28.

### 3.6.3 DISCUSSION

Only two temperature anomalies were recorded, both of which are significant. The anomaly on camera tow 1 occurs in the immediate vicinity of the scarp (Fig. 17) and has corresponding conductivity anomalies which oscillate both above and below the background level (Fig. 19). Unfortunately no corresponding photographs exist due to problems developing the film for this tow. However the coexistence of temperature and conductivity anomalies is good evidence for the existence of hydrothermal activity along the scarp. Sediment core 8 was recovered 800 m southeast of this anomaly.

A large temperature anomaly of  $+0.98^\circ\text{C}$  occurred on tow 7 on the southeast flank of the southwest seamount (Fig. 18). This is accompanied by a decrease in salinity (Fig. 24).

**Table 3: Summary of CTD Anomalies.**

Camera Tow <sup>1</sup>	Temperature	Conductivity <sup>2</sup> (Salinity)	Comments
1	+0.26°C	+ and -	
2	no change	-	
3	no change	-	
4	no data	no data	instrument malfunction
5	no change	+	spurious anomaly (camera anchored)
6	no change	-	
7	+0.98°C	-	
8	no data	no data	instrument malfunction
9			no anomalies recorded
10			no anomalies recorded
11	no change	+	prior to reaching bottom
12			no anomalies recorded

<sup>1</sup>See Figures 17 and 18 for locations.

<sup>2</sup>+ and - mean positive and negative excursions from background conductivity levels.

Unfortunately no photographs are available for this part of the tow due to failure of the flash system early in the run.

The other anomalies involve only salinity and not temperature. Both positive and negative anomalies occur, and three of these are located on or close to the scarp trace. In every case (tows 2, 3, 5 and 6) corresponding photographs are unavailable due to equipment failure. The positive anomaly in tow 11 was recorded prior to reaching the bottom.

Both positive and negative conductivity anomalies can be attributed to hydrothermal activity. Chlorinities of vent waters in the Pacific range from 0.6 to 2.0 times that of seawater (Scott, in press). Increased salinities can be explained if water is lost to the hydration of minerals in basalt. However until recently, lower-than-seawater salinities have not been adequately explained. Seyfried *et al.* (1986) suggest, on the basis of experimental basalt alteration studies, that chloride is removed from solution at high temperatures (400–425°C) into an as yet unidentified phase, possibly an Fe-hydroxy chloride. Their experiments also suggest that the Cl-bearing phase is characterized by retrograde solubility. Therefore as hydrothermal vent systems age and cool down, Cl<sup>-</sup> concentrations would increase. Both positive and negative anomalies can therefore be used as indicators of hydrothermal activity.

The near superimposition of the positive and negative anomalies in camera tow 1 is enigmatic. One possible explanation is that fluids could be discharging from two separate systems with vents that are very close together, although this does not seem likely.

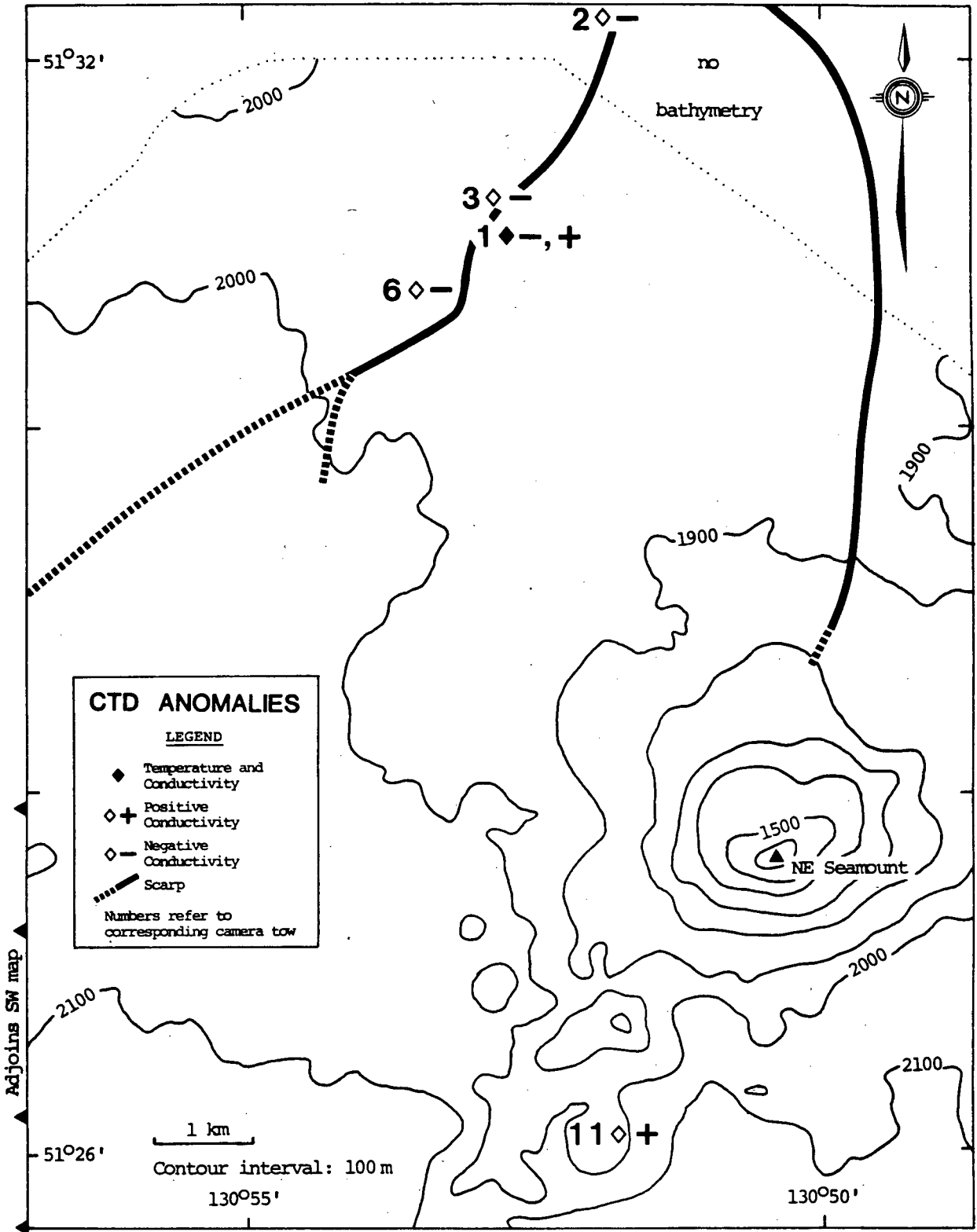
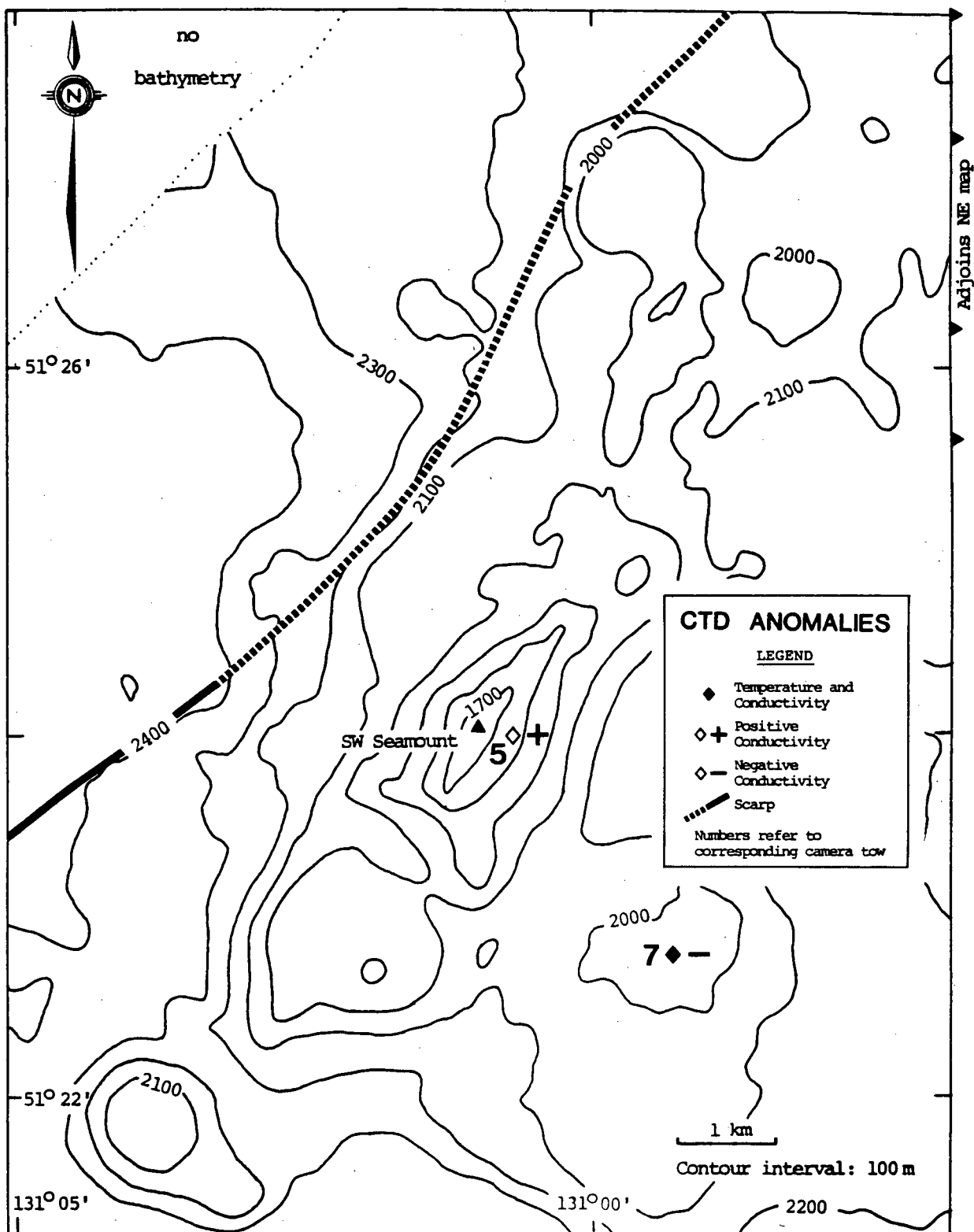


Figure 17: Conductivity-temperature anomalies, northeast sheet. See Table 3 for summary.



**Figure 18:** Conductivity-temperature anomalies, southwest sheet. See Table 3 for summary.

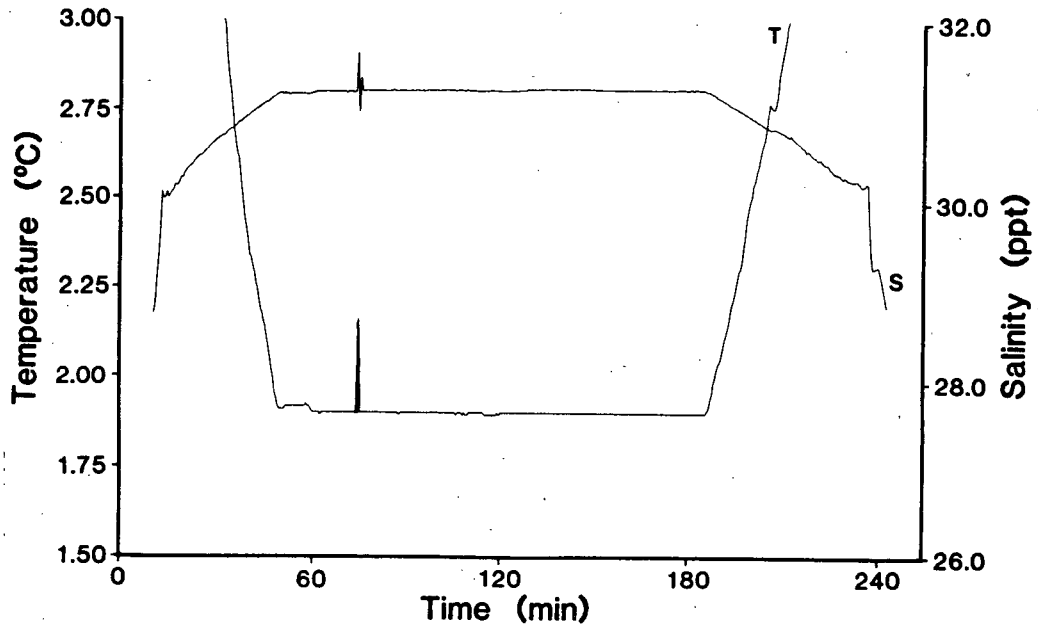


Figure 19: Conductivity (salinity) and Temperature plot for camera tow 1.

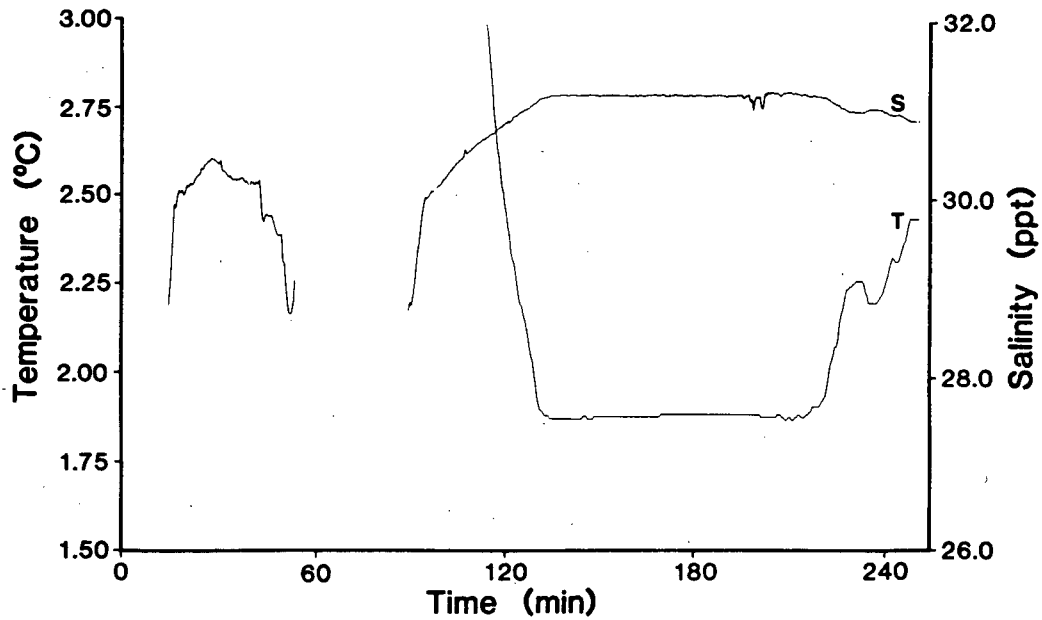


Figure 20: Conductivity (salinity) and Temperature plot for camera tow 2.

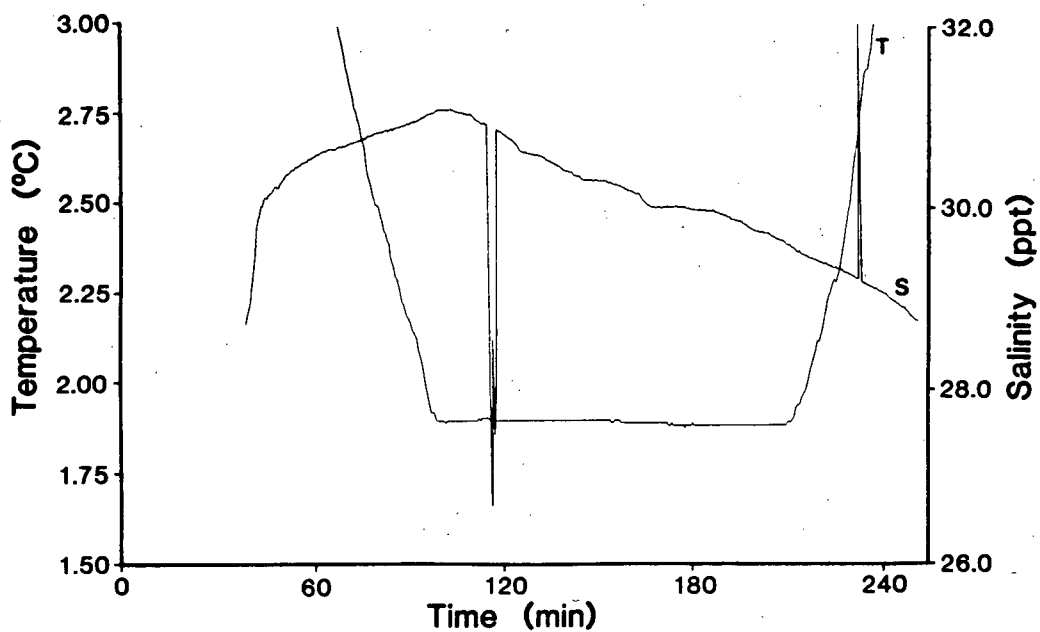


Figure 21: Conductivity (salinity) and Temperature plot for camera tow 3.

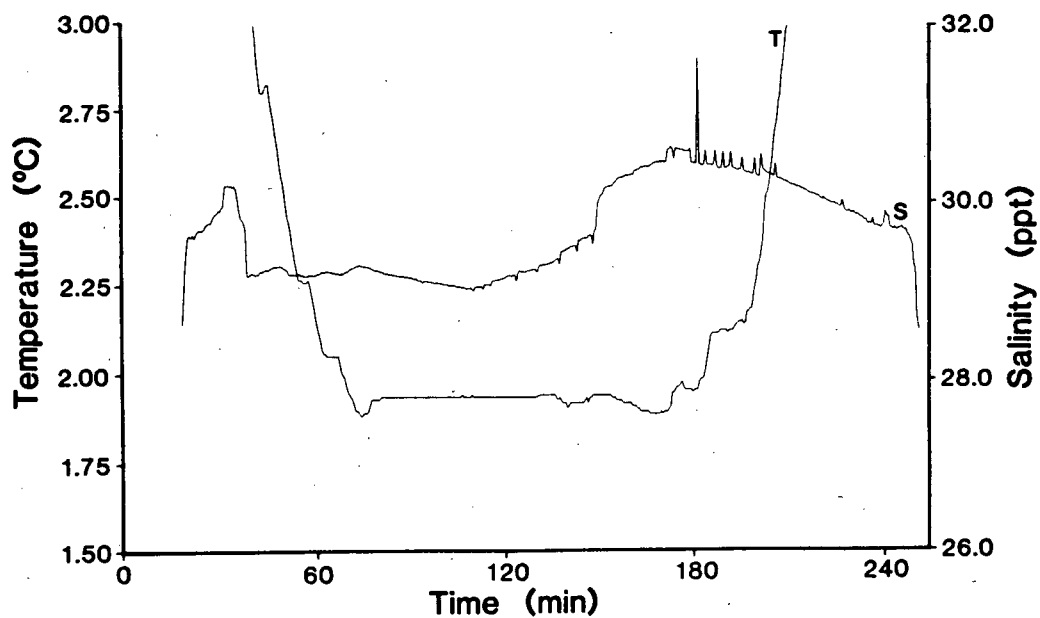


Figure 22: Conductivity (salinity) and Temperature plot for camera tow 5.

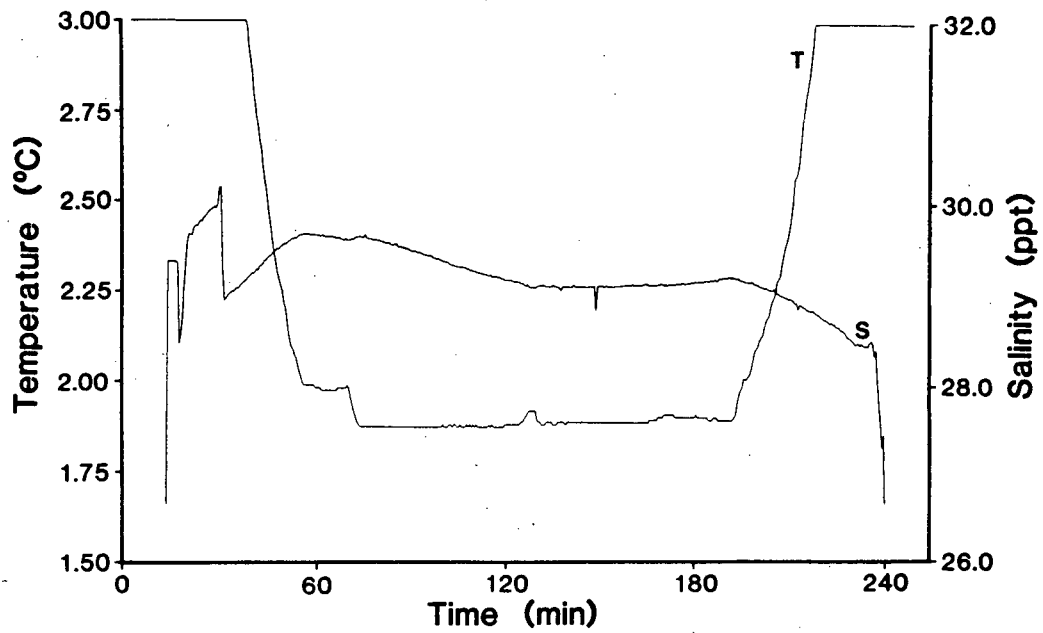


Figure 23: Conductivity (salinity) and Temperature plot for camera tow 6.

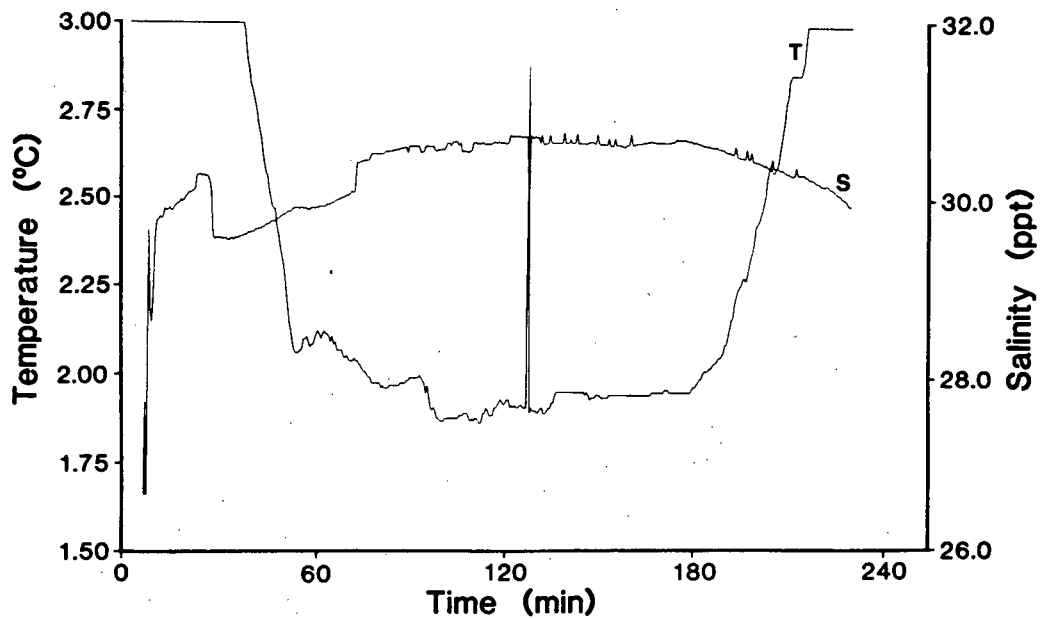


Figure 24: Conductivity (salinity) and Temperature plot for camera tow 7.

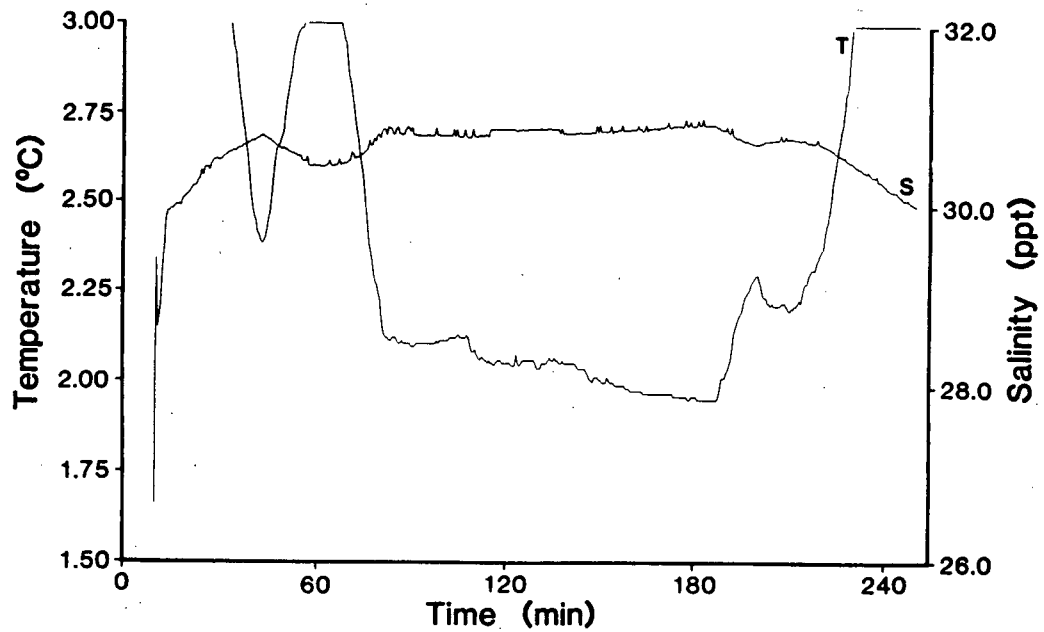


Figure 25: Conductivity (salinity) and Temperature plot for camera tow 9.

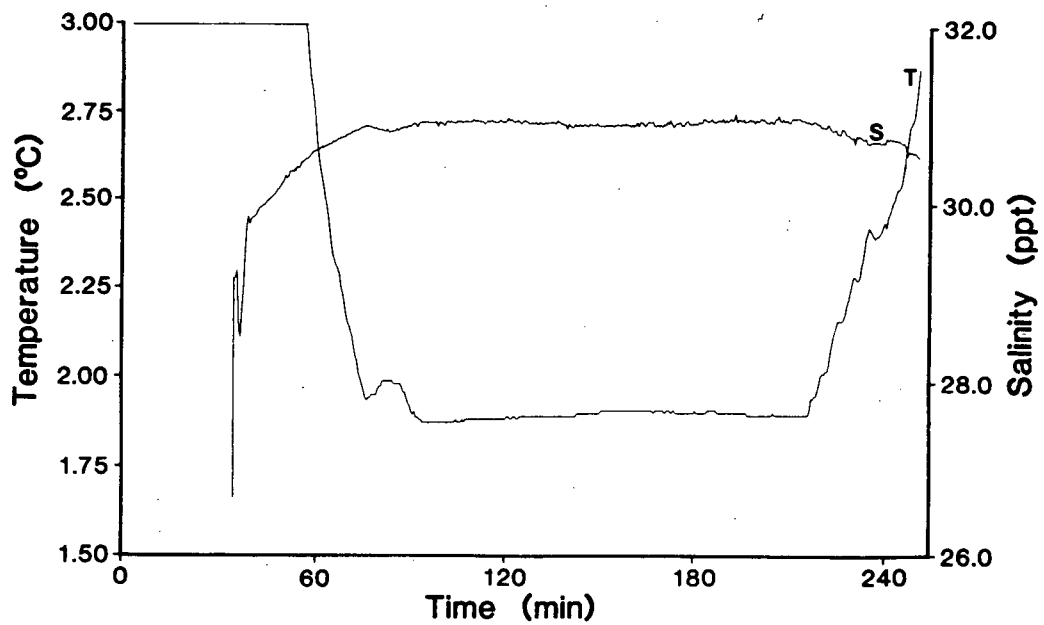


Figure 26: Conductivity (salinity) and Temperature plot for camera tow 10.

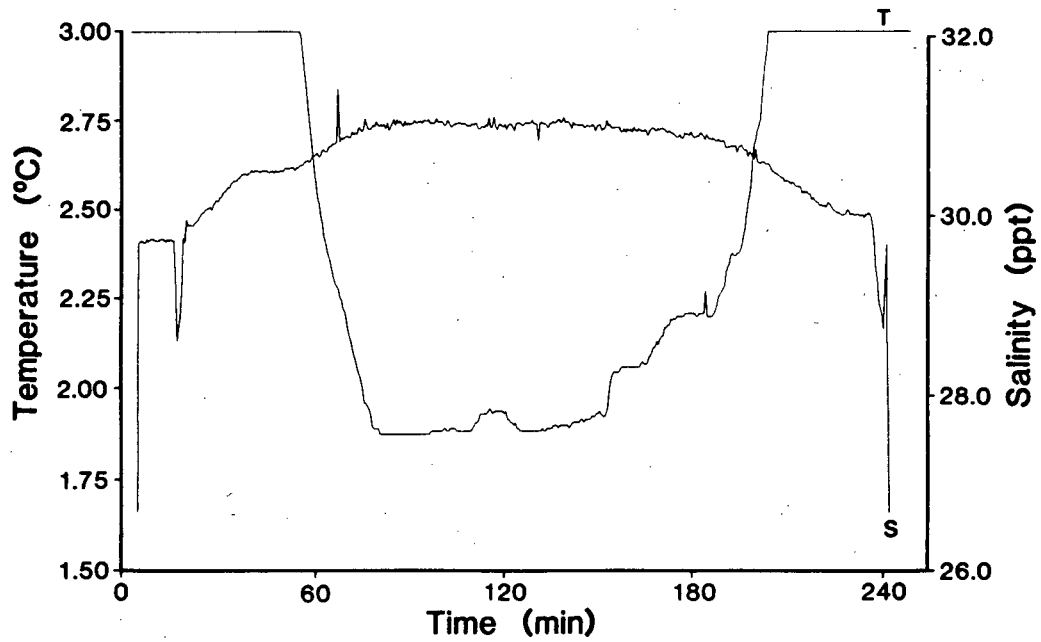


Figure 27: Conductivity (salinity) and Temperature plot for camera tow 11.

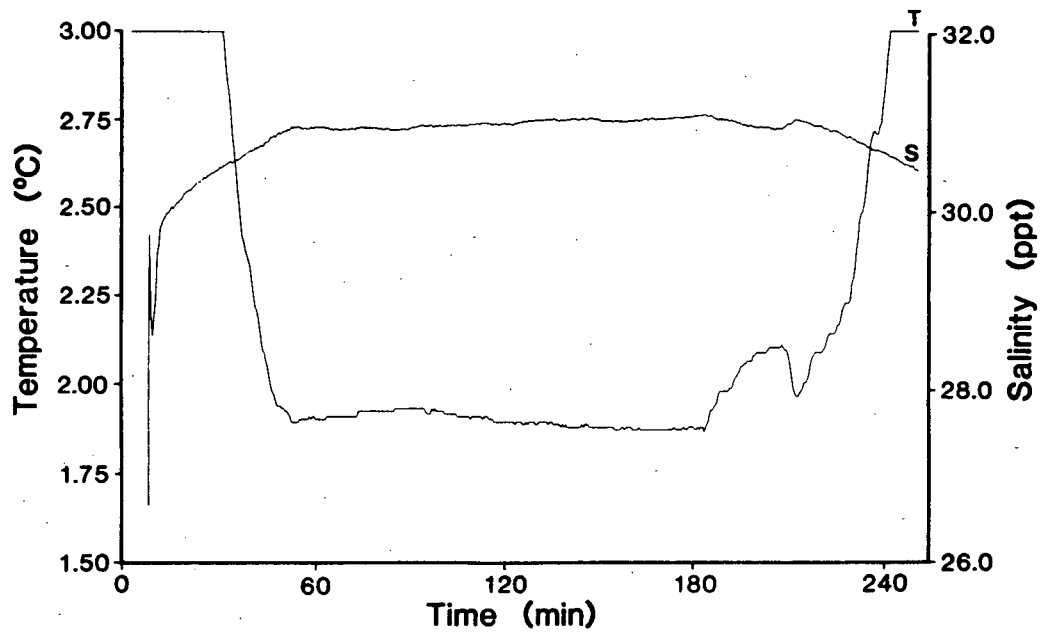


Figure 28: Conductivity (salinity) and Temperature plot for camera tow 12.

## Chapter 4

### SEDIMENT CHARACTER AND SEDIMENTATION

#### 4.1 INTRODUCTION

The effects of tectonic activity and physiography on sedimentation and the use of seafloor mapping techniques to understand sedimentary processes on the deep-sea fan around Tuzo Wilson Seamounts have been discussed in previous sections. Important factors controlling sedimentation include:

1. proximity of Tuzo Wilson Seamounts to the base of the continental slope resulting in dominance by terrigenous and hemipelagic sediments;
2. the presence of deep-sea channels which control and localize turbidite deposition;
3. local small tectonic features such as the southwest-northeast trending scarp along which most of the cores were taken;
4. seismicity of the nearby Queen Charlotte fault, which would produce thinner, more frequent turbidite deposition (e.g., Pilkey *et al.*, 1980); and,
5. lack of sediment transport across the shelf since deglaciation.

The last point could be disputed. In relative terms present sediment transport across the shelf is probably negligible compared to that which occurred during the Pleistocene.

However, even if transport across the shelf is minimal, removal of sediment that is already on the shelf must be occurring. Yorath *et al.* (1979) have shown that coarse sands and carbonate shell hash can be transported by storms in water as deep as 105 m on the shelf off northern Vancouver Island. Sediment trap studies off the Washington coast also indicate that shelf sediments are re-suspended and transported offshore during storms (Carson and Baker, 1983). In addition, extensive recent research (e.g., Walker, 1984) emphasizes the importance of storm-induced sediment transport. In fact, in terms of volume of sediment transported and redeposited it may represent the dominant process even though very large storms are only (in human terms, at least) occasional events.

Sediment deposition on the shelf was discussed in detail by Luternauer and Murray (1983). No major rivers drain into Queen Charlotte Sound. Minor rivers empty into deep glacially-excavated fiords which act as sediment sinks. The Skeena, which drains into Hecate Strait near Prince Rupert, is the closest major river to the north of Queen Charlotte Sound.

The fact that the seamounts protrude through and stand high above the sediment allows reworking of sediment deposited on the seamount. Redeposited sediment which originated high on Great Meteor Seamount in the North Atlantic has been noted on its flanks. Sedimentation there is strongly influenced by bottom currents which results in an asymmetric sediment distribution (von Stackleberg *et al.*, 1979; Verhoef, 1985).

Sedimentation on other parts of the Juan de Fuca ridge system, where terrigenous influence is less, though not absent, has been studied by several researchers (e.g., Barr, 1972; Bertrand, 1972; McManus *et al.*, 1972; Davis and Lister, 1977; Tiffin *et al.*, 1978; Bornhold *et al.*, 1981; Cook, 1981; Malott, 1981; Price, 1981; Hansen, 1984; Bornhold, 1986; and Blaise *et al.*, in press).

#### 4.1.1 PLEISTOCENE SEDIMENTATION

Most of southern British Columbia was covered by the thick glacial ice of the Cordilleran Ice Sheet during the Pleistocene. The climax of the most recent major glacial event, the Fraser Glaciation, was reached about 15,000–14,000 years BP (before present) (Clague, 1983) although 18,000 years BP is normally considered to be the Wisconsin maximum for the Laurentide Ice Sheet in the northeastern United States (Clague *et al.*, 1980). The Fraser ice sheet probably covered all of Vancouver Island, the Queen Charlotte Islands and most of Queen Charlotte Sound at the peak of the Wisconsin glaciation, although there is some evidence for ice-free conditions on parts of the Queen Charlotte Islands (Clague *et al.*, 1982b; Mathewes and Clague, 1982; Warner *et al.*, 1982; and Mathewes *et al.*, 1985). The western edge of the sheet was probably close to Tuzo Wilson Seamounts at times during the

Pleistocene (Clague, 1983), although Luternauer and Murray (1983) present evidence to suggest that during the Fraser Glaciation, grounded ice may only have extended part-way across the shelf due at least in part to the rising sealevel. However this does not preclude the existence of a floating ice shelf extending farther offshore. Glaciation of Queen Charlotte Sound is discussed by Luternauer and Murray (1983) and the late Quaternary climate of the North Pacific coast by Heusser *et al.* (1985).

On the mainland adjacent to Queen Charlotte Sound ice is estimated to have reached elevations of 2300 m and thicknesses of 2500 m in the Interior (Clague, 1983). Isostatic depression of  $\sim 300$  m was combined with a drop in sealevel of  $\sim 140$  m (Luternauer, 1972) at the peak of glaciation. Relict shorelines at elevations up to 200 m above present sealevel are known (Clague, 1983). Isostatic effects are least pronounced near the margins of the ice sheet to the extent that relative sealevels were below present sealevel even at the Wisconsin glacial maximum (Clague, 1975; Clague *et al.*, 1982). A forebulge effect may also have contributed to this uplift or apparent lack of depression. Isostatic equilibrium was probably reestablished as early as 8000 years BP (Mathews *et al.*, 1970), after a deglaciation period of only 4500 years (14,000–9,500 BP; Clague *et al.*, 1982a). Uplift occurring at present on the Queen Charlotte Islands at rates of  $1 \text{ mm a}^{-1}$  is probably purely tectonic, associated with the small component of underthrusting on the Queen Charlotte fault (Riddihough, 1982a).

The depositional regime on the Tufts abyssal plain changed from one of rapid deposition of turbidites during the Pleistocene, to one dominated by slow pelagic sedimentation at the Pleistocene-Holocene transition (Hamilton, 1967; Horn *et al.*, 1970, 1971). Exposure to the open sea probably allowed deglaciation of the shelf before protected areas such as fiords (Clague, 1985), and significant erosion and transport of sediments across the shelf probably occurred prior to the eustatic sealevel rise caused by dwindling ice volume could prevent bypassing of the shelf. Pleistocene sedimentation at Tuzo Wilson Seamounts would therefore be expected to be dominated by abundant coarse turbidites and ice-rafted

glacial detritus.

On the Juan de Fuca ridge the Pleistocene-Holocene transition is accompanied by a marked decrease in sedimentation rate and a change in clay content (Cook, 1981), changes in terrigenous and biogenic accumulation rates (Heath *et al.*, 1976), compositional changes (Price, 1981), a change in the foraminiferan-radiolarian ratio in the Cascadia Basin and Juan de Fuca ridge (Griggs *et al.*, 1969; Barnard and McManus, 1973; Malott, 1981), changes in frequency, distribution and grain size of turbidite deposits in the Cascadia deep-sea channel (Griggs and Kulm, 1970) and Astoria Fan (Nelson, 1976), and colour changes from gray (Pleistocene) to olive-grey (Holocene) on Astoria Fan (Nelson, 1976; Howell and Normark, 1982). Analysis of glacial components such as ice-rafted detritus has been used in palaeoceanographic studies (e.g., Conolly and Ewing, 1970; von Huene *et al.*, 1973, 1976) and ice-rafted detritus has been dredged (Bertrand, 1972), and noted in cores (Blaise *et al.*, 1984; Bornhold, 1986) in the Dellwood area.

Increased carbonate productivity in the Northeast Pacific (Nayudu, 1964; Parkin and Shackleton, 1973) and in other areas such as the Panama Basin (Pedersen, 1983) during glacial maxima has been attributed to upwelling caused by intensified atmospheric and oceanic circulation. The increased productivity of carbonate associated with upwelling depresses the carbonate compensation depth which allows accumulation through reduced dissolution. Thomson and Saito (1974) noted that in the eastern equatorial Pacific, glacial maxima are accompanied by sedimentation of solution-susceptible and solution-resistant forms whereas interglacials are typified by intense solution resulting in concentration of solution-resistant forms.

#### 4.1.2 LYSOCLINE

The carbonate compensation depth (CCD) is the depth above which sediment contains calcareous tests and below which they are essentially absent because the rate of sedimentation

of  $\text{CaCO}_3$  is less than the rate of dissolution (Berger, 1976). The depth of the CCD often corresponds with the boundary between two water masses, the deeper one being more corrosive. The lysocline is defined as the depth which separates well-preserved from poorly-preserved tests and can be specific to certain organisms (e.g., foraminiferal lysocline) (Kennett, 1982). It can vary quite widely according to local oceanographic and climatic conditions.

In the Northeast Pacific at  $50^\circ\text{N}$ , Pytkowicz (1970) showed the CCD around 4000 m, Kennett (1982) at 3000 m and on Juan de Fuca ridge, Cook (1981) suggested the lysocline (which is above the CCD) may be as high as  $2100 \pm 200$  m. This is reasonable as Malott (1981) noted a decline in abundance of foraminiferan populations with depth in cores recovered between 2180 and 2633 m water depth on northern Juan de Fuca ridge. At Tuzo Wilson Seamounts, the lysocline likely occurs within the depth range in which the cores in this study were collected (1935–2415 m). This is discussed further in the section on calcium and carbonate in Chapter 5.

#### 4.2 SEDIMENT DESCRIPTION

All seven cores recovered consist of olive-green, gelatinous to sticky, homogeneous hemipelagic mud. Down-core increments in compaction and cohesiveness are evident in the longer cores but bedding is absent. The homogeneity of the cores prevented division into units. Distinct colour changes, such as those normally associated with redox boundaries in sediments, are not present probably due to the high sedimentation rate. Silt and carbonate contents vary slightly within the cores but no distinct patterns are evident. Other components include basalt chips, uncommon foraminifera and a 2 cm long section of segmented bone. Irregularly shaped blotches elongated in the plane of bedding occur indicating bioturbation.

Some cores show minor blackening, probably oxidation, usually in the bottom 20 cm of a core. The blackened portion was removed prior to sampling, which revealed that it was restricted to the outermost millimetre of the core. Evidence of disturbance during coring was visible in core 6 in the form of a "suction flame structure" in the bottom 15 cm. Brief individual core descriptions are given in Table 4.

The fine-grained, featureless nature of the muds is characteristic of hemipelagic sediments which lack the grading of turbidites and are deposited over all types of terrain (Heath *et al.*, 1974), while turbidite deposits are restricted to channels, fans and bathymetrically low areas. However, in such hemipelagic sediments, redeposited layers may be difficult or impossible to distinguish (Kelts and Arthur, 1981) but are geochemically distinct from true hemipelagic sediment. Kelts and Arthur (1981) pointed out that turbidite muds in DSDP cores contain both more carbonate and more  $C_{org}$  than interbedded hemipelagic muds. There is no evidence, either visual or geochemical, for discrete turbidite units in these cores and the relationship observed by Kelts and Arthur is probably not valid here because at very high rates of terrigenous sedimentation the preservation effect is overtaken by clastic dilution of organic input and  $C_{org}$  declines (Johnson Ibach, 1982).

Piper (1978) pointed out that turbidites may consist of ungraded massive silts and muds. Analysis of silt content can provide distinction between turbiditic and hemipelagic muds (Kelts and Arthur, 1981), but has not been attempted in this study.

**Table 4: Description of sediment cores investigated in this study.**

Core #	Depth (cm)	Description <sup>1</sup>	Features
1	0-97	Olive gray, slightly silty mud	Slightly calcareous
2	0-140	Olive to olive gray, silty mud	Slightly calcareous
3	0-20	Olive gray silty mud	Slightly calcareous
	20-30	Same as 0-20	Calcareous; segmented bone at 28-31 cm
	30-85	Only slightly silty	Slightly calcareous
4	0-40	Olive to olive gray, slightly silty watery mud	5 mm burrow at 4.5-5.0 cm; slightly calcareous
	40-70	Gradational zone to underlying more compact mud	
	70-96	Compact silty mud	Irregularly shaped blobs, elongated horizontally (bioturbation?)
5	NO	RECOVERY	
6	0-98	Very slightly silty, homogenous olive mud	Slightly calcareous; 1 cm diameter dark mottle at 30 and 63 cm; chip of slightly indurated mud at 85 cm
	98-113	Suction flame intrusion structure	
7	0-4	Gelatinous, silty dark olive gray mud	Very slightly calcareous
	4-15	Homogenous, slightly silty dark olive gray mud	Slightly calcareous
8	0-1.5	Slightly silty, watery, very dark grayish brown mud	Very slightly calcareous
	1.5-30	Slightly silty, slightly watery, dark olive gray mud	Slightly calcareous
	30-82	Compact, slightly silty dark olive gray mud	Calcareous

<sup>1</sup>Colours from Munsell soil colour chart.

#### 4.2.1 X-RADIOGRAPHY

All seven cores were X-radiographed at the facilities of Industrial Nondestructive Testing Ltd. in Vancouver. They were X-radiographed as half cores, after being split lengthwise down the middle. The X-radiographs are reproduced in Figs. 29–32.

Few details were revealed by this technique. The essentially featureless cores are also featureless on X-radiographs. Some blotches and mottled patches are visible on close inspection in cores 4 and 6, and may be evidence of bioturbation. Mottling is also common in portions of cores 1, 2 and 3. Disturbed laminae occur in core 4 between 75–80 cm. Several basalt chips are visible in core 7, one of which is almost 1 cm long. Artifacts such as holes where samples were taken prior to X-radiography (irregular white squares) ghosting of core liner end caps are evident in most cores. Widespread cracking due to drying is pervasive in cores 1, 2 and 3, especially in the upper portions where original water content was highest.

The lack of changes of the type described in section on Pleistocene sedimentation and lack of distinct boundaries on the X-radiographs suggests that none of the cores was of sufficient length to reach the Pleistocene-Holocene transition. However,  $^{14}\text{C}$  dates and geochemical changes attributed to climatic change indicate that core 3 did penetrate Pleistocene sediments.

#### 4.2.2 SMEAR-SLIDE DESCRIPTIONS

Smear-slides were prepared from the same samples that were selected for geochemical analyses. Sampling procedure and sample numbering is described in Appendix 1. The smear-slides were examined under transmitted light on a petrographic microscope using lenses with 4 and 10 power magnification. The sediment is remarkably uniform in composition both within and between cores. A summary of the components visible in smear-slides is given in Table 5. A typical smear-slide is illustrated in a transmitted light photomicrograph in Fig. 33.

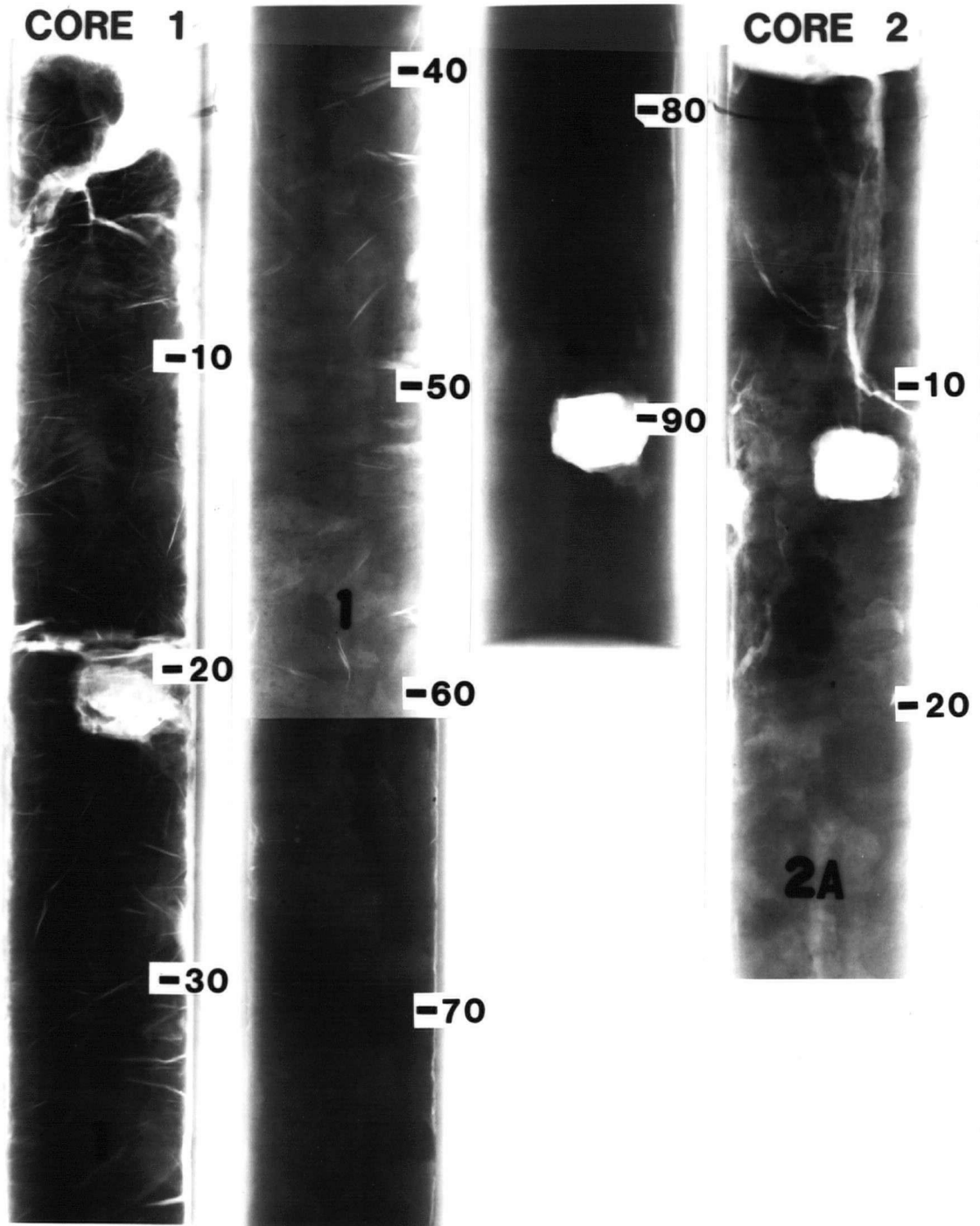


**Figure 29:** X-Radiograph of sediment cores. Depth scale at right margin of each core is in cm.

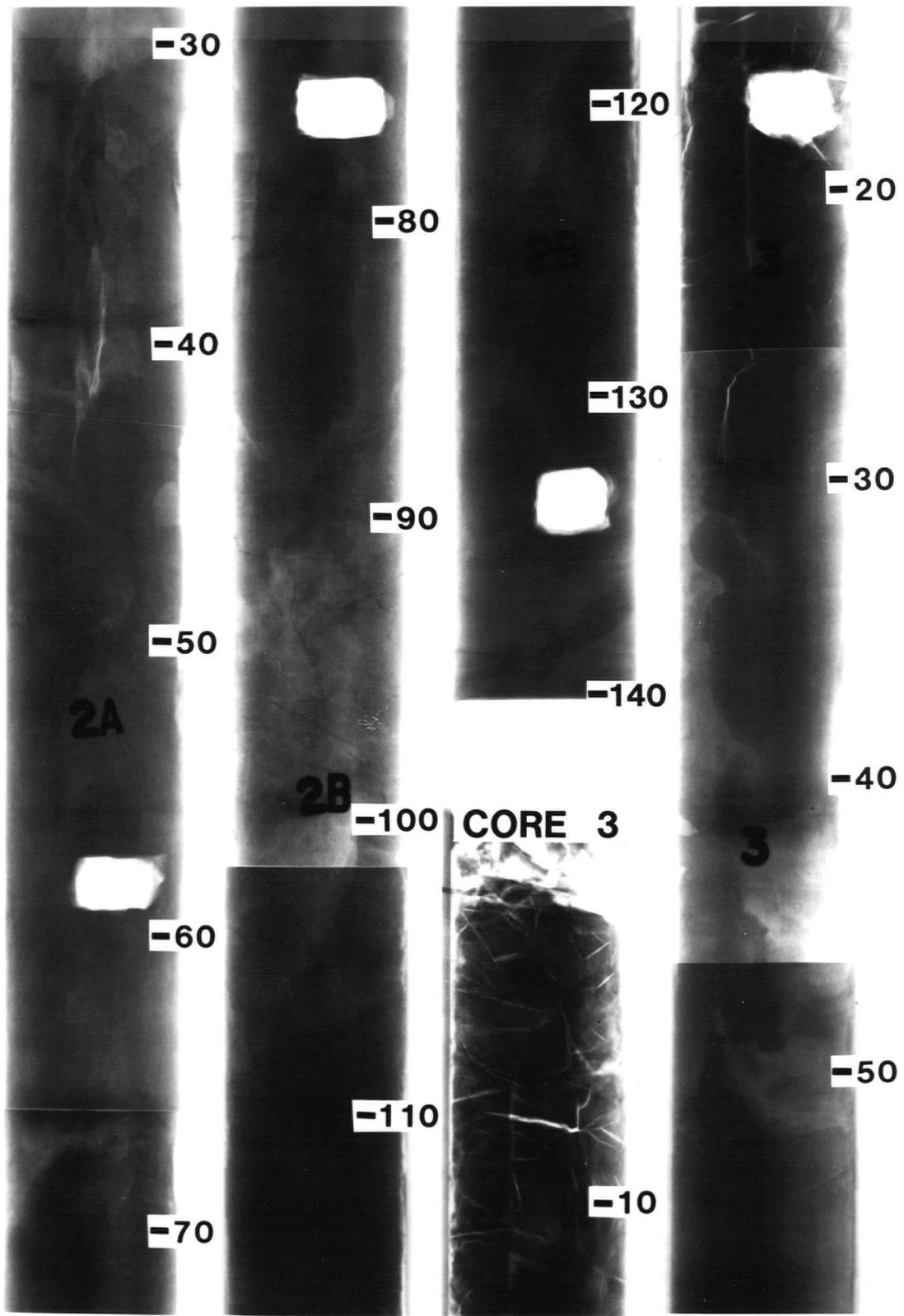


**Figure 30:** X-Radiograph of sediment cores. Depth scale at right margin of each core is in cm.

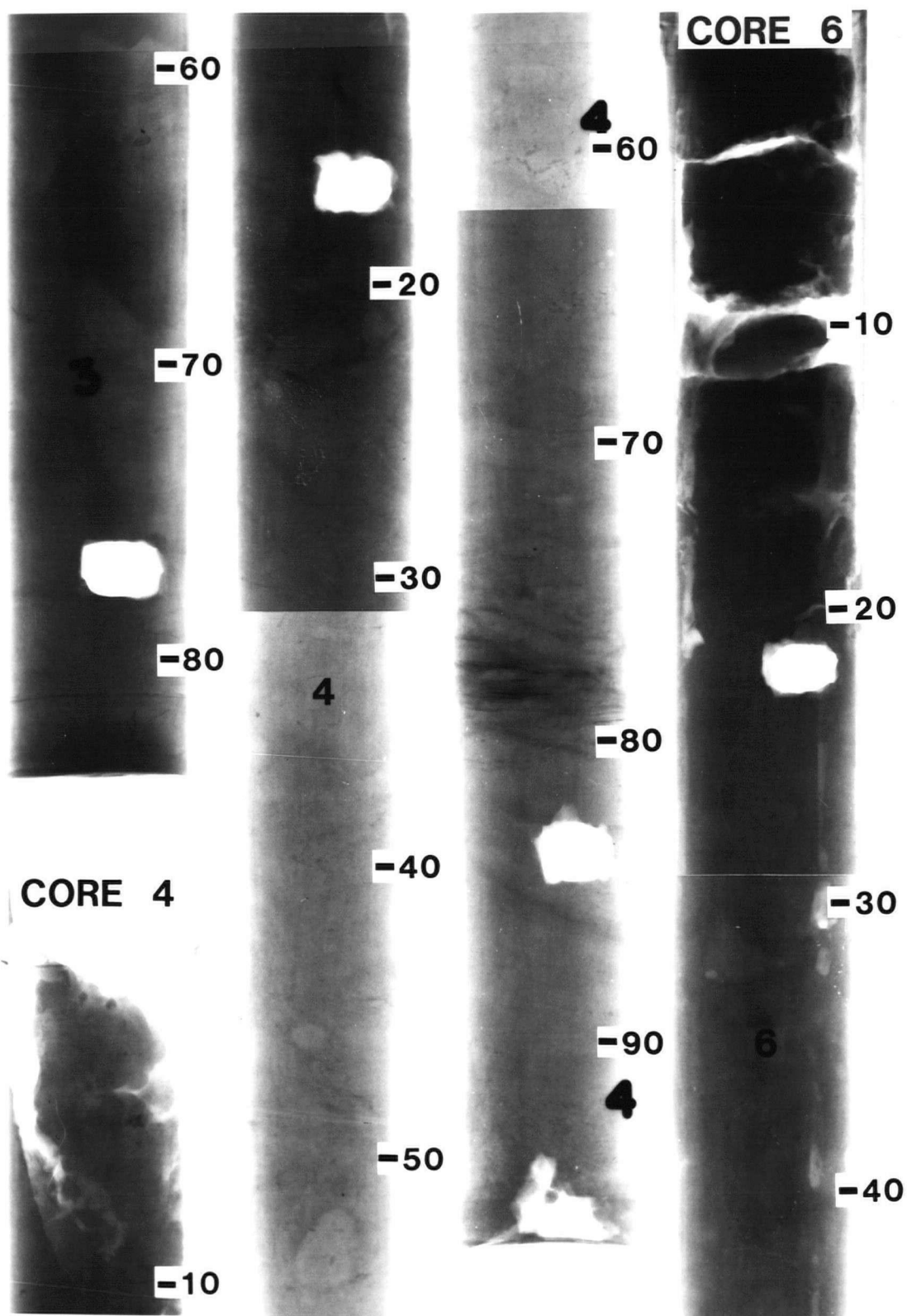


**Figure 31:** X-Radiograph of sediment cores. Depth scale at right margin of each core is in cm.

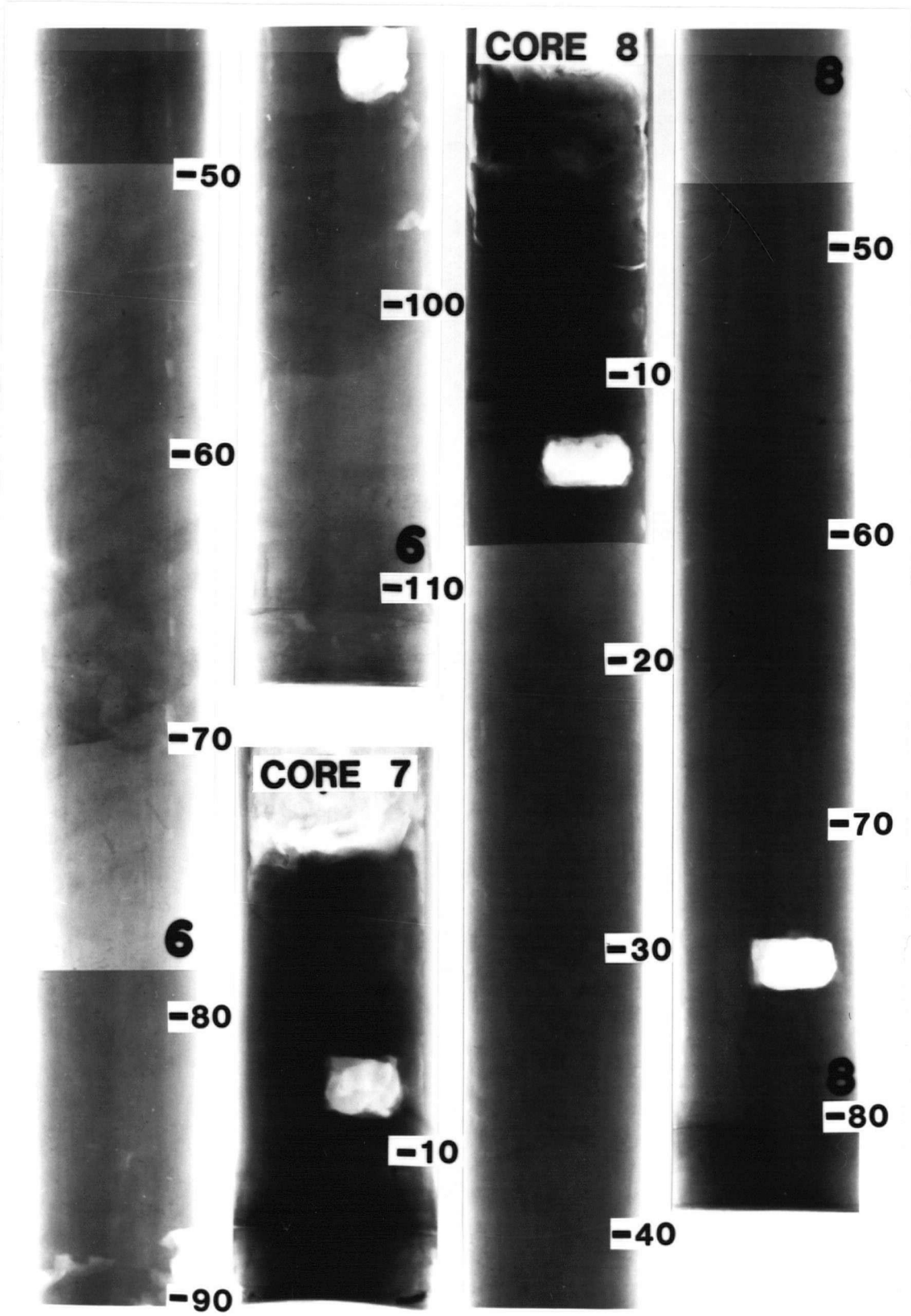


**Figure 32:** X-Radiograph of sediment cores. Depth scale at right margin of each core is in cm.

**Table 5: Components visible in smear-slides.**

Component	Content Range (%)	Comments
Quartz	25-40	Most commonly angular to subangular; rarely subrounded; Size range 0.2-<0.01 mm
Feldspar	10-15	Mostly plagioclase
Faecal Pellets/OM <sup>1</sup>	30-45	
Clay minerals	~30-40	
Chlorite	<10	
Basaltic glass	<10	As small shards; in some cases large chips (1 cm) visible in core
Opaque minerals	<5	
Diatoms	<5	Some studded with black balls (framboidal pyrite)
Foraminifera	<2	
Silicoflagellates	<5	Needles

<sup>1</sup>Organic Matter.

Clay mineral contents have not been systematically determined as part of this study but are probably similar to those found in other areas nearby. Selected samples have been analyzed by X-ray diffraction to determine mineralogical variation in two sections of core 3. This is discussed further in Chapter 5. At Dellwood Knolls the clay mineral assemblage consists of smectite (40-50%), chlorite (20-30%), illite (10-20%), lesser amounts of mixed-layer varieties, and kaolinite (<5%) (Blaise *et al.*, 1984).

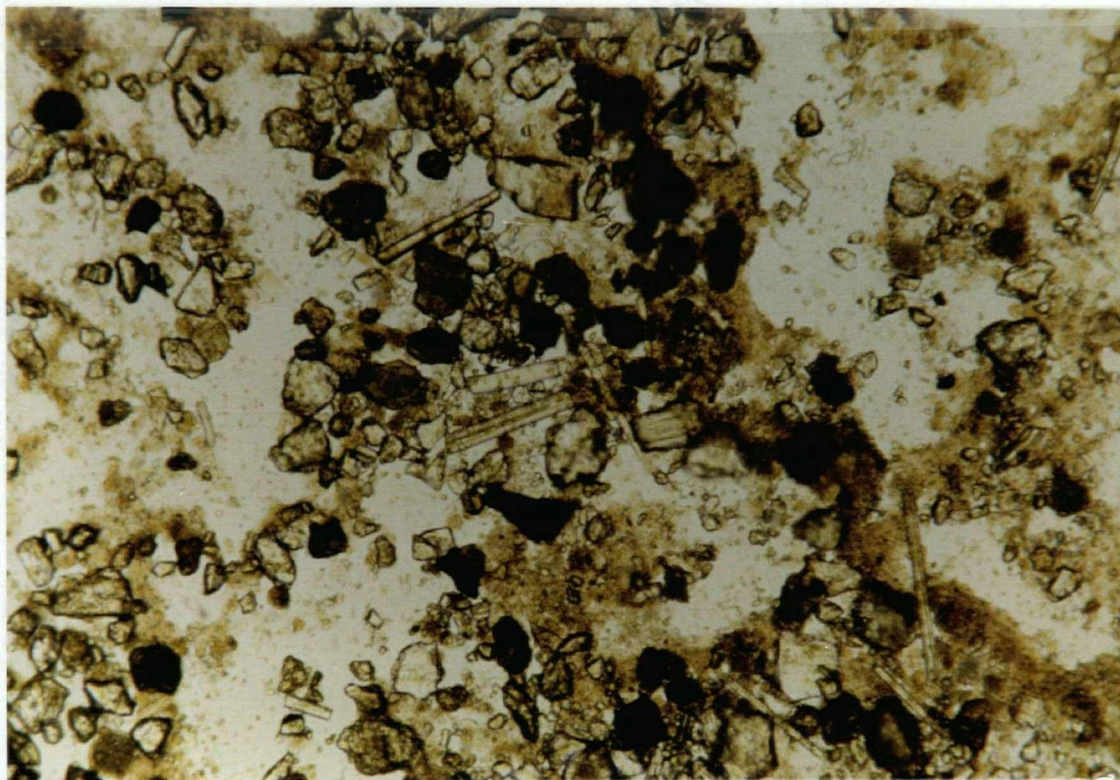


**Figure 33:** Photomicrograph of smear-slide from core 4, at depth of 10–11 cm. Note angular quartz, brown organic matter/clay and silicoflagellate needles. Scale:  = 0.1 mm.

#### 4.2.2.1 Quartz

The abundance and angularity of most of the quartz suggests intense mechanical weathering, probably during glaciation. Grains as large as 200  $\mu\text{m}$  in diameter (fine sand) have been noted in some of the cores close to the base of the slope. Most of the quartz in these cores straddles the very fine sand–silt boundary (62  $\mu\text{m}$ ) while in core 6, not unexpectedly, all the quartz is in the silt size range. Coarse ice-rafted detritus was not detected in any core.

Eolian loess deposits formed around the margin of the Laurentide and other ice sheets during the Pleistocene. Increased aridity and concomitant increased eolian transport to the oceans during the ice ages is well documented (e.g., Kolla *et al.*, 1979;

Prospero, 1981). An increase in eolian components in Pleistocene sediments has been demonstrated for the Atlantic (Parkin and Shackleton, 1973), and for the Pacific (Leinen and Heath, 1981). Katabatic winds are known to transport dust from glacial outwash areas and such winds, blowing to the west off the Cordilleran Ice Sheet, could have transported dust from glacial deposits on the Queen Charlotte Sound out to sea to the area of the Tuzo Wilson Seamounts. Although penetration well into the Pleistocene section and study of the 1–30  $\mu$  m grain size range would be required to test this hypothesis, dilution by massive input of other terrigenous sediment would likely mask such an effect at Tuzo Wilson. Eolian components have been identified by Mairs *et al.* (1985) in a core comprising turbidite-free sediments from near the Juan de Fuca ridge, but, although the core has been intensively dated, apparently no attempt has been made to study variation of the contribution of the eolian component with time.

#### 4.2.2.2 Chlorite

Chlorite in marine sediments indicates mechanical erosion and lack of chemical weathering (Kennett, 1982). At Tuzo Wilson Seamounts green chlorite, usually subangular, occurs in most samples in amounts up to 10%. Intense mechanical erosion during glaciation must have released large quantities of chlorite from continental rocks. Luternauer and Murray (1983) reported chlorite- and illite-rich glacial muds on the shelf in Queen Charlotte Sound. The muds have low  $C_{org}$  concentrations which they suggested reflects the low clay mineral content of constituent "glacial flour". It seems probable that lack of input of terrigenous organic matter during glaciation would also substantially affect the  $C_{org}$  content. These glacial muds are the most likely source of the chlorite observed at Tuzo Wilson Seamounts.

### 4.3 AGE DATES AND SEDIMENTATION RATES

#### 4.3.1 INTRODUCTION

Accelerator  $^{14}\text{C}$  age dates were obtained for two samples, 3-46 and 3-60, to bracket a suspected hydrothermal event in core 3 and to provide an estimate of sedimentation rate. The principle of radiocarbon dating by accelerator mass spectrometry has been described by Hedges and Gowlett (1984, 1986). Details of the dating technique are outlined in Appendix 1.

Sedimentation rates have been determined from cores and from seismic reflection profiles of different parts of the Juan de Fuca ridge system. As stated previously, sedimentation rates would be expected to be much higher during the Pleistocene due to accelerated erosion and transport of sediment across the shelf while eustatic sealevel was low. In the Winona Basin, estimates from seismic data indicate as much as 1.8 km of sediment may have accumulated in the past 0.5 Ma (Davis, 1981), for an average sedimentation rate of  $3.6 \text{ m ka}^{-1}$ . Davis and Riddihough (1982) give an estimate of  $4 \text{ m ka}^{-1}$ ; however, they conclude that the sedimentation rate in the Winona Basin has been increased by rapid subsidence and that during periods of non-subsidence, turbidites would pass through the basin and be deposited elsewhere. Pleistocene sedimentation rates of the same order of magnitude have been determined for the Chile Trench which also acts as a sediment sink (Thornburg and Kulm, 1983).

Sedimentation rates on the Juan de Fuca ridge are highly variable, as might be expected in such a topographically varied and tectonically active area (e.g.,  $16.5 \text{ cm ka}^{-1}$  (Pleistocene) and  $3.2 \text{ cm ka}^{-1}$  (Holocene; Malott, 1981);  $40\text{--}233 \text{ cm ka}^{-1}$  (Price, 1981);  $55\text{--}170 \text{ cm ka}^{-1}$  (McManus *et al.*, 1972); and  $670\text{--}1000 \text{ cm ka}^{-1}$  in the Pleistocene with negligible Holocene sedimentation (Davis and Lister, 1977b; Leinen, 1984)). On lower portions of the Oregon continental slope, rates of  $20\text{--}65 \text{ cm ka}^{-1}$  have been reported (Kulm and Scheidegger, 1979). Local tectonic activity, proximity to deep-sea channels, bottom

**Table 6:**  $^{14}\text{C}$  Ages and sedimentation rates for core 3.

Depth (cm)	Age (years)	Sedimentation Rate <sup>1</sup> (cm ka <sup>-1</sup> )
0 <sup>2</sup> –46.5		3.9
46.5	12,020 ± 150	
46.5–60.5		16.5
60.5	12,870 ± 160	
60.5–85.0 <sup>3</sup>		?

<sup>1</sup>Sedimentation rates determined by assuming constant sedimentation between dated samples.

<sup>2</sup>Assumes top not lost during coring.

<sup>3</sup>Bottom of core.

currents, ponding of sediment (e.g., van Andel and Komar, 1969), compaction, early lithification (e.g., Davis, 1981), and where seismic is used, inaccuracies in estimates of age and seismic velocities can all affect actual sedimentation and estimates of them. No previous determinations of Holocene sedimentation rates at Tuzo Wilson Seamounts have been made, but Bornhold (1986) estimated a rate of 20–30 cm ka<sup>-1</sup> for northernmost Juan de Fuca ridge.

#### 4.3.2 RESULTS AND DISCUSSION

The radiocarbon dates and calculated sedimentation rates are summarized in Table 6. Transported carbon, which would increase the age, is assumed to be absent because the dated samples, which bracket a geochemical event, show no unusual geochemistry. The substantial difference between the two sedimentation rates would be magnified if the rapid sedimentation that occurred between 46 and 60 cm is assumed to have continued above the 12,020 ± 150 yr date. In light of the knowledge of deglaciation and its effects on sedimentation discussed previously, such an assumption would be more reasonable than one of constant sedimentation, and is represented by the dashed line in Fig. 34.

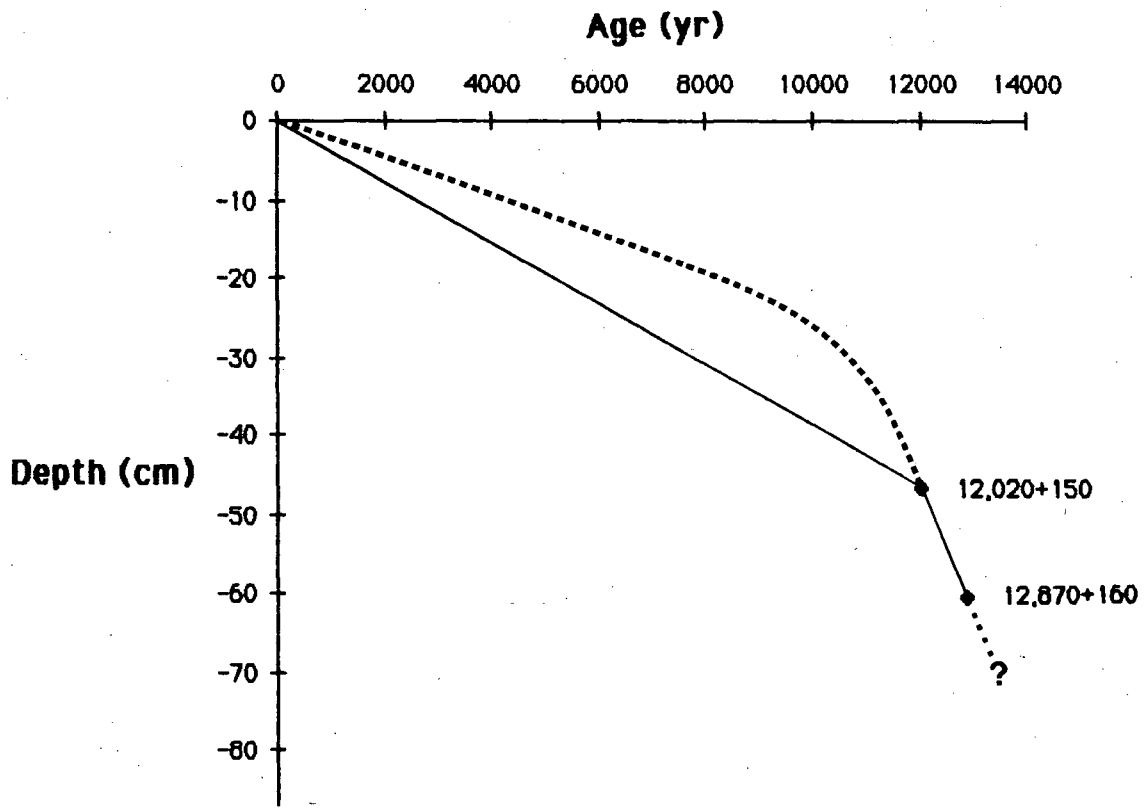


**Figure 34:** Age versus depth profile for core 3. Slopes between points represent estimated sedimentation rates. Dashed line assumes rapid sedimentation continued until around 10,000 yr BP.

The geochemical event characterized by K and Al concentrations (see Chapter 5) lower than the sediment above and below spans a short period. If a constant sedimentation rate of  $16.5 \text{ cm ka}^{-1}$  is assumed between the two dated samples, and if the possible effects of bioturbation are ignored, then the minimum duration of this event is 330 years if the top and bottom are assumed to be at 50 and 55 cm respectively (Figs. 38 and 42). X-ray diffraction (XRD) studies discussed in the next chapter show that a decline in illite relative to quartz is responsible for this geochemical change.

## 4.4 SCANNING ELECTRON MICROSCOPY

### 4.4.1 INTRODUCTION

Several samples were selected for study under the SEM to provide answers to some specific questions:

1. Are the black spheres observed in diatoms framboidal pyrite?
2. Are concentrations of heavy or resistant minerals responsible for certain geochemical anomalies? and,
3. Are there any authigenic minerals growing on the surface of the bone found in core 3, and has it suffered any alteration or dissolution?

In addition to answering these questions, a number of interesting observations were made of the character of the sediment that are not apparent at low magnification.

### 4.4.2 RESULTS AND DISCUSSION

#### 4.4.2.1 Framboidal Pyrite

Pyrite framboids were not observed clustered in diatom frustules under the SEM. However diatoms and loose framboids were observed separately. It seems likely that the black spheres observed in diatoms in smear-slides were pyrite framboids but that the ultrasonic treatment used to disaggregate the sediment shook the framboids from the frustules. Widespread formation of framboidal pyrite in Guaymas Basin sediments has been attributed to early diagenetic reaction of  $H_2S$  with the detrital iron oxide common in hemipelagic sediments (Lonsdale *et al.*, 1980). However in the oxic sediments at Tuzo Wilson Seamounts, framboidal pyrite has probably only formed in microenvironments within diatom frustules where degradation of organic matter has locally depleted oxygen. This suggests that sulphate-reducing bacteria are active in sediments at Tuzo Wilson Seamounts at depths where oxygen is no longer available.

#### 4.4.2.2 Heavy Minerals

Several minerals were detected under the SEM using its energy-dispersive X-ray emission spectrometer (EDS) system. While not strictly heavy minerals, their occurrence is interesting and they probably contribute somewhat to geochemical variations. Sample 3-30 exhibits some anomalous geochemistry (see Chapters 5 and 6) in that it has slightly elevated levels of P, Ti, Nb, Sr and Zr. This could be attributed to slightly higher levels of heavy or residual minerals from a terrigenous source. However the geochemical evidence presented in the next chapter argues for an increase in basalt detritus rather than terrigenous material. The following elements were detected in individual mineral grains (with representative minerals in parentheses): Ti-Ca-Si (sphene), Fe-Ti (ilmenite), Ca-P (apatite) and Ba-S (barite). No Zr-bearing minerals were noted although the presence of zircon is suspected. The qualitative nature of this technique and the fact that only one sample was examined for heavy minerals precludes detailed conclusions regarding the effect of these minerals on the geochemistry.

The barite occurs in an unusual form, an oblate spherule or micronodule, approximately 3.5  $\mu\text{m}$  across. Its surface appears smooth and featureless. Two such micronodules were observed in sample 3-30. Barite is often associated with hydrothermal activity (e.g., CASM, 1985; Lonsdale and Becker, 1985). Adshead *et al.* (1986) note that clay-size particles of barite are common in hydrothermal sediment in Middle Valley on Juan de Fuca ridge. They attribute their occurrence to hydrothermal plume sedimentation, and illustrate a barite particle similar to the one observed here that is about 2.5  $\mu\text{m}$  in diameter. Although there is insufficient evidence, a hydrothermal origin for these micronodules cannot be ruled out.

#### 4.4.2.3 Segmented Bone

A series of segmented bones, originally thought to be the vertebral column of a fish or burrowing organism was noted in core 3 between 28 and 31 cm. Each segment is cylindrical in shape and approximately 1.5 mm long. The cylinder is divided into two symmetrical halves along its length and separates to reveal an irregularly shaped bone housed inside. This bone is shown in Fig. 35 and a close-up of the outer surface of the housing in Fig. 36. No authigenic minerals were found growing on or in the bone structure. Interestingly an EDS analysis of the material shows that it does not contain P, and is made only of  $\text{CaCO}_3$ . This suggests that the segmented bone is not from a fish but rather from a lower animal form such as a crinoid or starfish, and is therefore more appropriately described as a calcareous exoskeleton. The intricate structure seen in Fig. 36 is characteristic of crinoids (A. Lewis, oral comm., 1986). The inclined orientation of the exoskeleton segments in the core suggests that this organism may have been transported within a turbidity current.

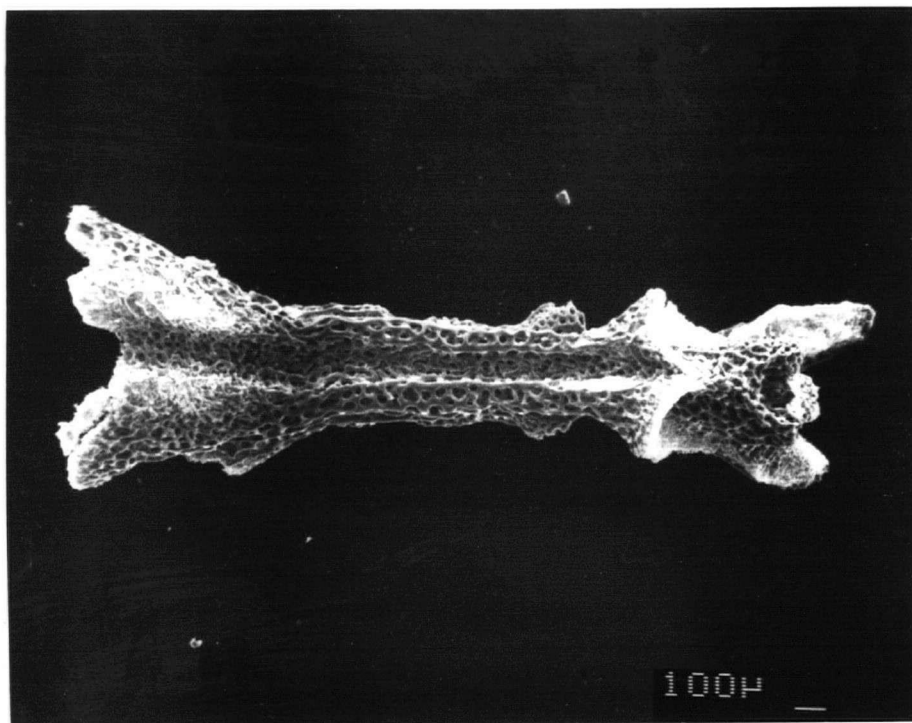


**Figure 35:** SEM photomicrograph of internal structure of bone.

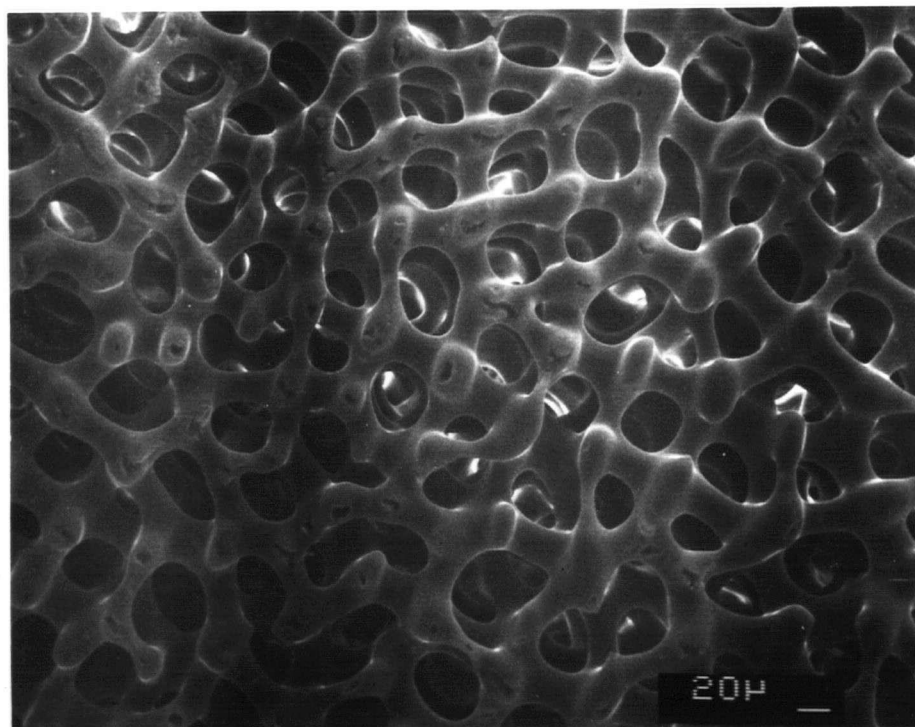


**Figure 36:** SEM photomicrograph of bone from core 3, at a depth of 28-31 cm.

## Chapter 5

### MAJOR ELEMENT AND HALOGEN DISTRIBUTION

#### 5.1 INTRODUCTION

Major elements (Si, Ti, Al, Fe, Mg, Ca, Na, K, P, and S), and halogens (I, Br, Cl) in 75 sediment samples were analyzed by X-ray fluorescence spectrometry (XRF). Total carbon ( $C_{\text{total}}$ ) and nitrogen were analyzed using a Carlo-Erba CHN Analyzer. Carbonate carbon was determined with a Coulometrics model 5010  $\text{CO}_2$  Coulometer and then subtracted from  $C_{\text{total}}$  to give organic carbon ( $C_{\text{org}}$ ).

These analyses provide insight into different aspects of sedimentation at Tuzo Wilson Seamounts. The importance of terrigenous input is emphasized by the behaviour Si, Al, K and Ti which give an indication of bulk composition and relative grain size, and by Fe and Mg which indicate the relative abundance of terrigenous minerals such as chlorite and amphibole. The distribution of Si, Fe and Mg (and Mn, discussed in Chapter 6), and  $^{14}\text{C}$  dating (Chapter 4) reveal a change in provenance in core 3 which is attributed to the climatic shift at the Pleistocene-Holocene transition.

The behaviour of Ca and carbonate provides an indication of productivity at Tuzo Wilson Seamounts and is affected by dissolution which increases with water depth.  $C_{\text{org}}$  and N are controlled by productivity, type of organic matter and conditions in the sediment. The rate of down-core decline in  $C_{\text{org}}$ , I and Br is controlled by degradation of organic matter which in these sediments is influenced principally by sedimentation rate.

Analytical procedures are described in Appendix 1. Raw analytical data are presented in Appendix 2, the program used to correct for dilution by sea salt is given in Appendix 3 and the salt-free results are listed in Appendix 4. Major elements (in weight %), trace elements and halogens (in ppm), and element ratios are listed in Appendix 4.

Sulphur was analyzed by XRF but all salt-free results are zero indicating that essentially all the sulphur in the sediments was in the form of seawater sulphate. Sulphur in pyrite framboids in diatom frustules occurs in such insignificant amounts as to be below the detection limits. As all salt-free results are zero, no plot is presented and S is omitted from further discussion. Sodium results are not discussed because they are significantly influenced by the salt correction and cannot therefore be interpreted meaningfully. Raw chlorine data used for sea-salt corrections are presented in Appendices 2 and 4 but are not plotted. Chlorine is assumed to have been present solely as chloride in seawater and is not discussed further in this chapter.

## 5.2 RESULTS AND DISCUSSION

### 5.2.1 SILICON

The distribution of Si and Al is controlled by variations in the proportions of the major lithogenous minerals such as quartz, feldspar and clays. Examination of smear-slides indicates that quartz and feldspar are abundant in these sediments, which is consistent with the importance of the terrigenous source in this area. Although some radiolaria and diatoms were noted in the smear-slides, biogenic silica is thought to be a small contributor of Si in these quartz-rich sediments.

The Si profiles in Fig. 37 indicate that all the cores have a fairly uniform content of between 26 and 29% Si. Two features in Fig. 37 are worth noting. In core 3 a sudden decrease between 20 and 24 cm is followed by an increase from 24 cm to the bottom. The decrease is associated with an apparently lower quartz content in this interval (Fig. 74), by the Si/Al ratio (Fig. 39), which decreases slightly, and by the K/Al ratio (Fig. 44), which increases abruptly. A dramatic decrease is noted for Fe, Mg and Mn (Figs. 40, 41 and 71 respectively) at this depth suggesting that the overlying sediment has a different provenance. The cause of these chemical changes is discussed later in this chapter.

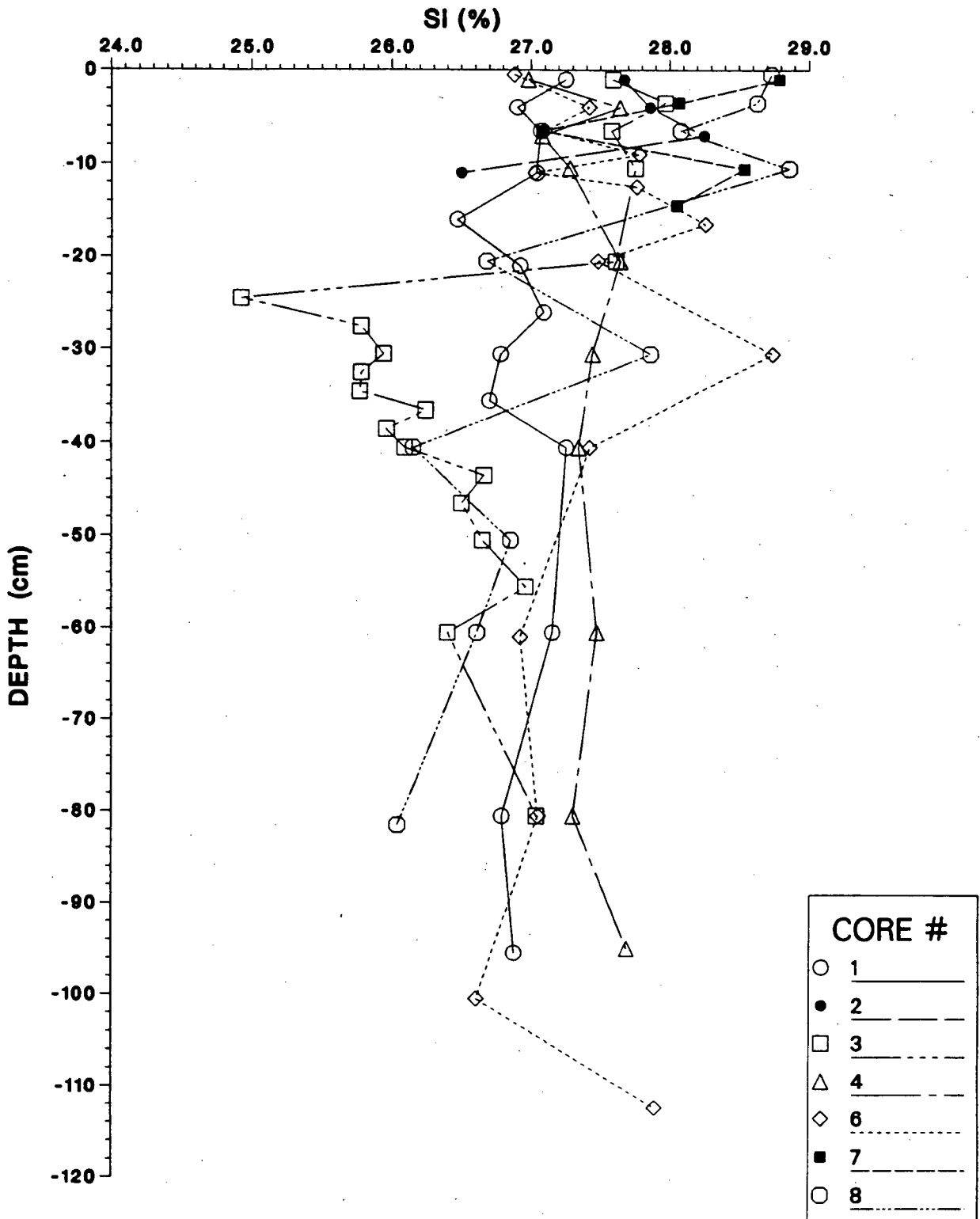


Figure 37: Si distribution (%).

### 5.2.2 ALUMINUM

The aluminum content of these sediments is probably influenced most by clay mineral and feldspar content. Al also occurs in hornblende and pyroxene, and in many of the constituent minerals of basalt. Sharp decreases in Al content occur around 50–55 cm in core 3, at the bottom of cores 6 and 7, and in core 8 at 50 cm (Fig. 38). However analytical results from the bottom two samples in core 6 must be regarded with caution due to the suction structure noted in the bottom of this core. Cores 3 and 8 are located close together and the coincident chemical change might be a result of the same event. This zone of lower Al is associated with a decrease in the K concentration (Fig. 42) and an increase in the Si/Al ratio (Fig. 39). XRD results discussed later in this chapter show that this change is caused by a decrease in the abundance of illite relative to quartz.

### 5.2.3 IRON AND MAGNESIUM

The iron (Fig. 40) and magnesium (Fig. 41) contents of these hemipelagic sediments are strongly influenced by the mineralogy of the large terrigenous component and to a lesser extent by the mafic minerals in basalt debris observed in these cores. Fe in the terrigenous component occurs in clay minerals, both within the lattices and as oxide coatings on the particles, in feldspars, hornblende, pyroxene, olivine and in resistant minerals such as magnetite and ilmenite (Chester and Aston, 1976). Mg occurs in clay minerals and in other silicates such as amphibole, chlorite, olivine and pyroxene.

In all cores Fe and Mg behave in concert which suggests strongly that variation in abundance of one mineral or mineral group is the dominant factor. The most striking example of this is in core 3 which shows a sharp increase in both Fe and Mg between 20 and 30 cm. As discussed previously, a marked change in Si and Mn in this core also occurs in this interval, strongly suggesting that a change in provenance is responsible for these chemical changes. This is discussed more fully later in this chapter.

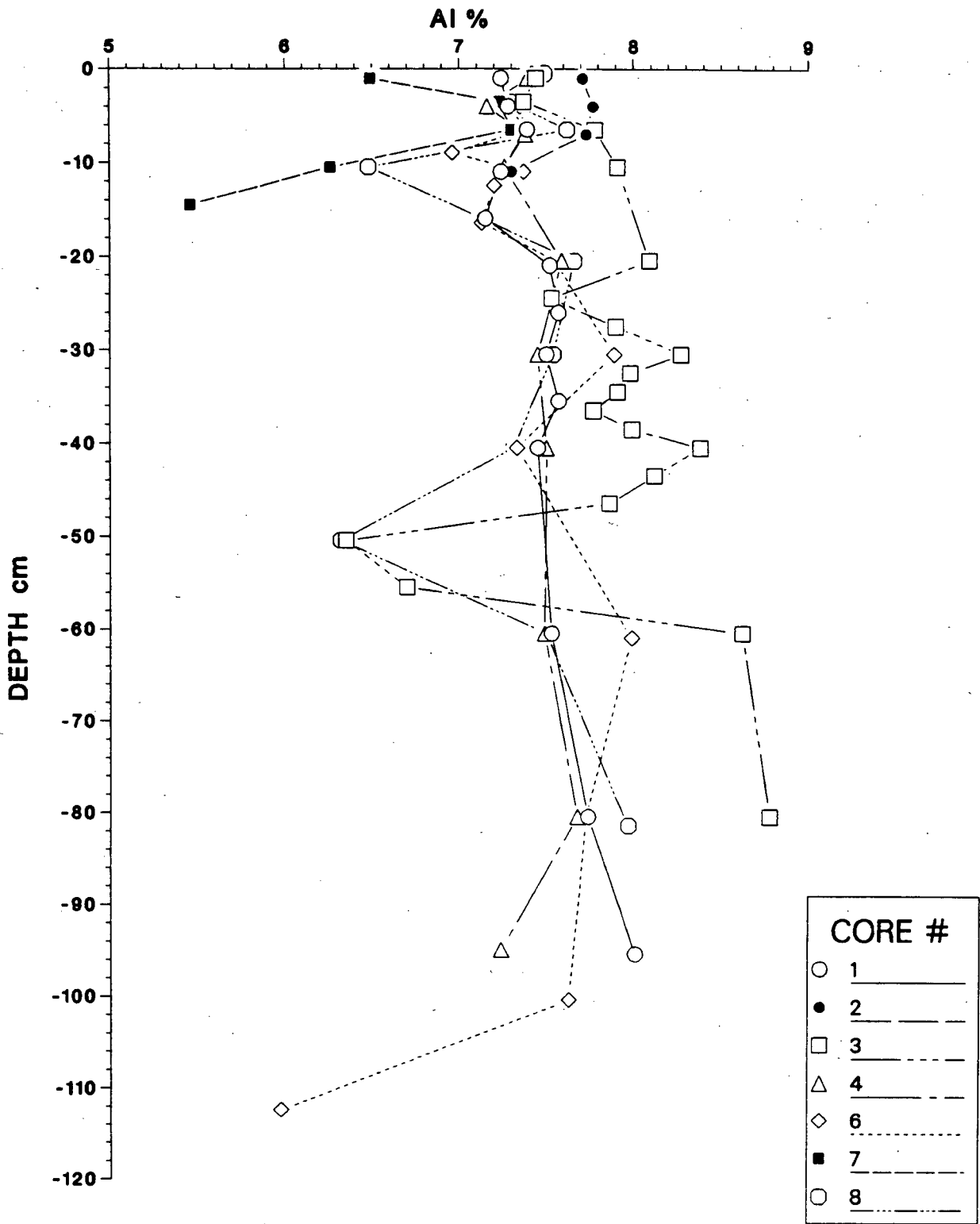


Figure 38: Al distribution (%).

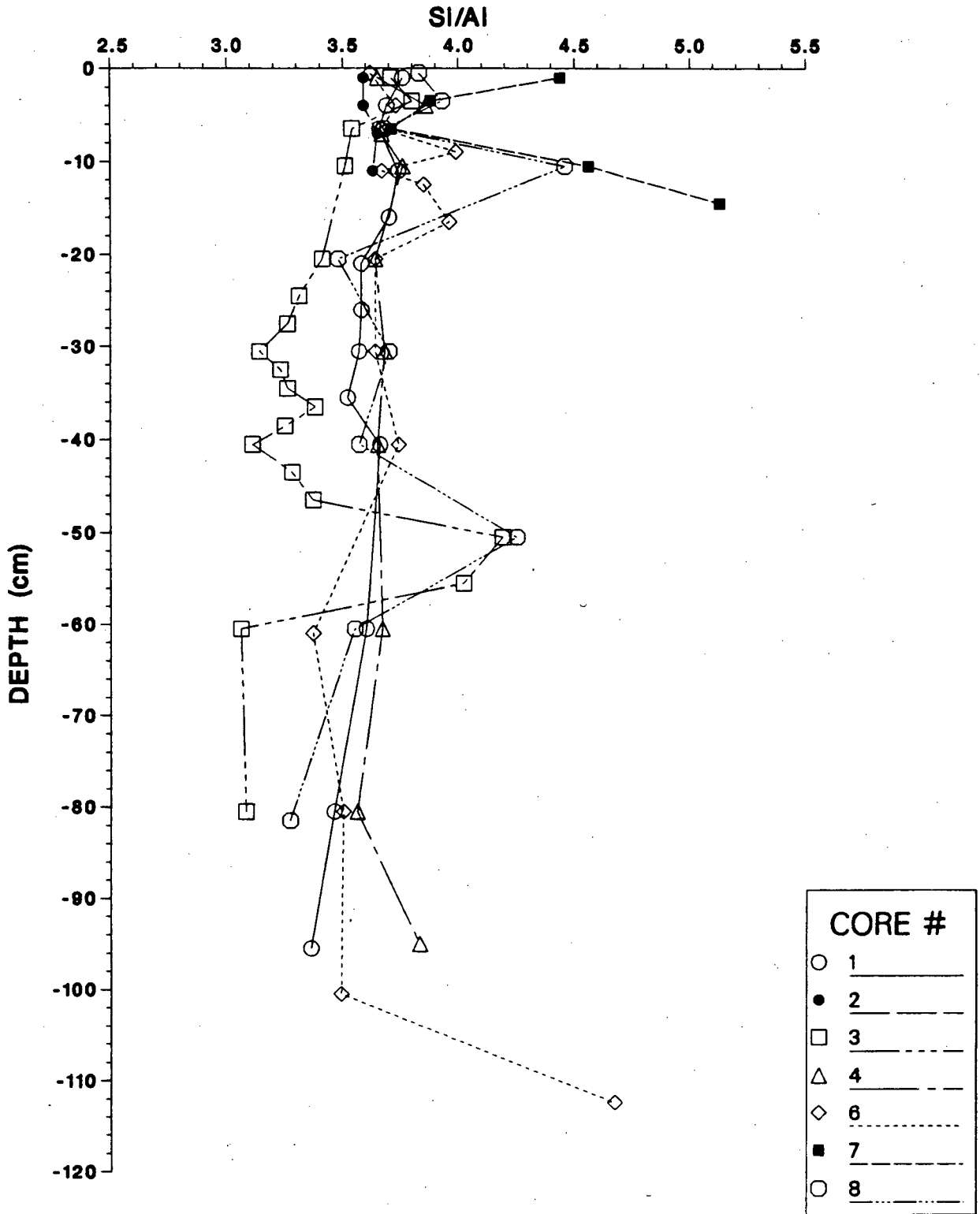


Figure 39: Si/Al ratio.

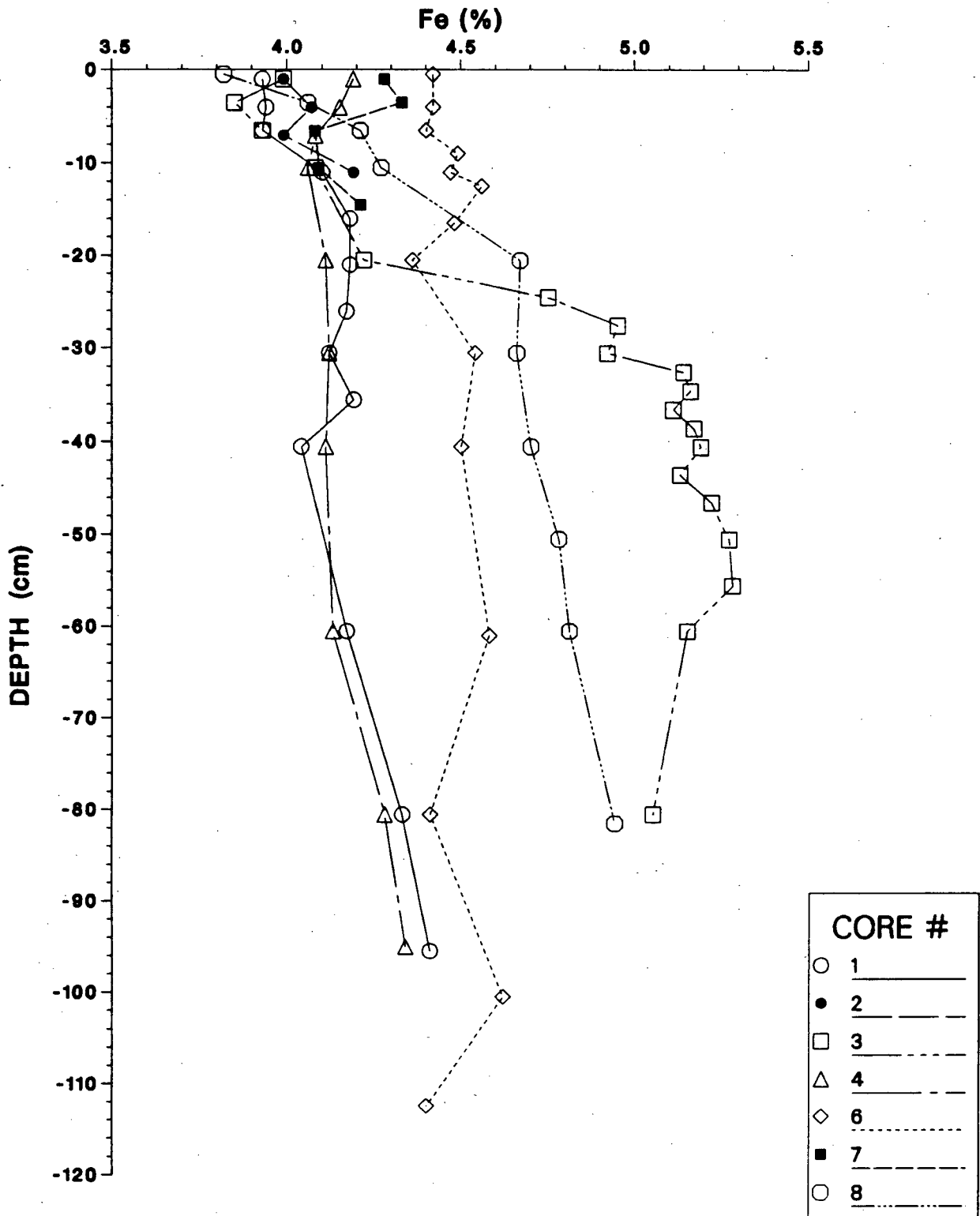


Figure 40: Fe distribution (%).

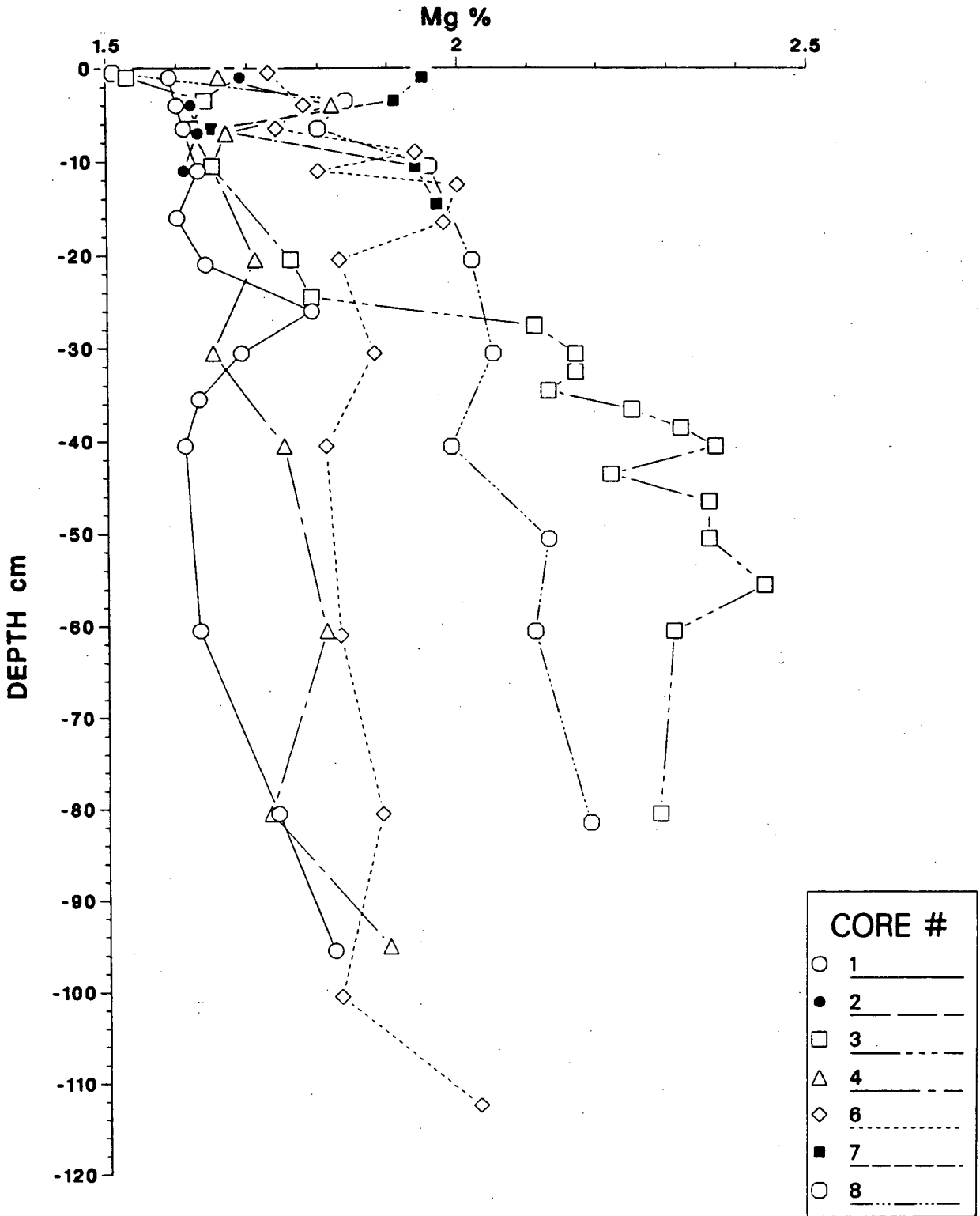


Figure 41: Mg distribution (%).

#### 5.2.4 POTASSIUM AND TITANIUM

Potassium (Fig. 42) and titanium (Fig. 43) exhibit very similar patterns. Ti occurs principally in continentally-derived resistant minerals which comprise the heavy mineral fraction of the sediment. Luternauer and Murray (1983) report concentrations of heavy mineral-rich "black sands" in central Queen Charlotte Sound, which may be a source of Ti, Zr and Fe (as magnetite). Ti content is also significantly influenced by proximity to volcanic sources (Goldberg and Arrhenius, 1958). The volcanic source for Ti at Tuzo Wilson Seamounts must be significant due to the proximity of the cores to the volcanic seamounts and because basalt glass is visible in smear-slides from all the cores and occurs as larger chips (mm size) in some of the cores.

The highest value for Ti occurs in core 3 at a depth of 30 cm in association with P, Sr and Zr enrichments (Figs. 50, 62 and 60 respectively). The anomalous increase of these four elements at 30 cm in core 3 can be most conveniently explained by a 10% increase in basalt detritus over the levels in samples just above and below. These rough calculations were performed using unpublished analyses provided by P.J. Michael. This 10% increase does not significantly alter the concentrations of other elements which remain unchanged at this depth due to the similarity of their concentrations in both basalt and sediment.

Both K and Ti, but especially Ti, exhibit a narrowing of the spread of values above 15 cm depth in almost all cores. This suggests that the upper 15 cm of sediment are being homogenized by bioturbation. This effect can also be detected in the distributions of Fe, Mg, Mn and carbonate. As noted in Chapter 3, underwater photography revealed abundant benthic fauna and burrows suggesting active bioturbation. Core 7 appears to be a notable exception to this; however the inhomogeneity it displays may be caused by the large (several mm) size basalt chips observed in this core rather than by lack of bioturbation.

Potassium occurs principally in feldspar and illite. Lower K and Al values are coincident in these sediments. The K/Al ratio (Fig. 44) does not change in core 3 at 50 and

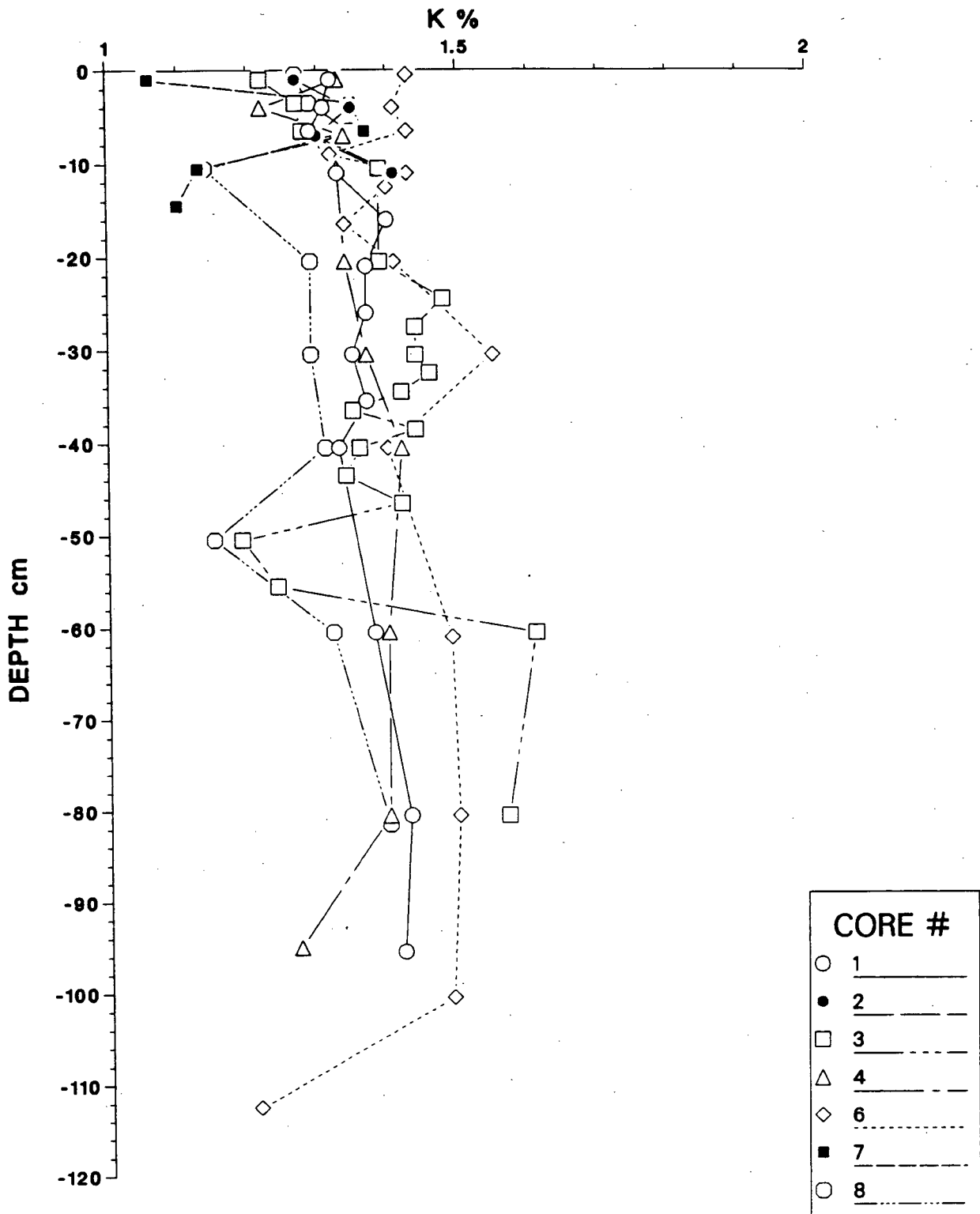


Figure 42: K distribution (%).

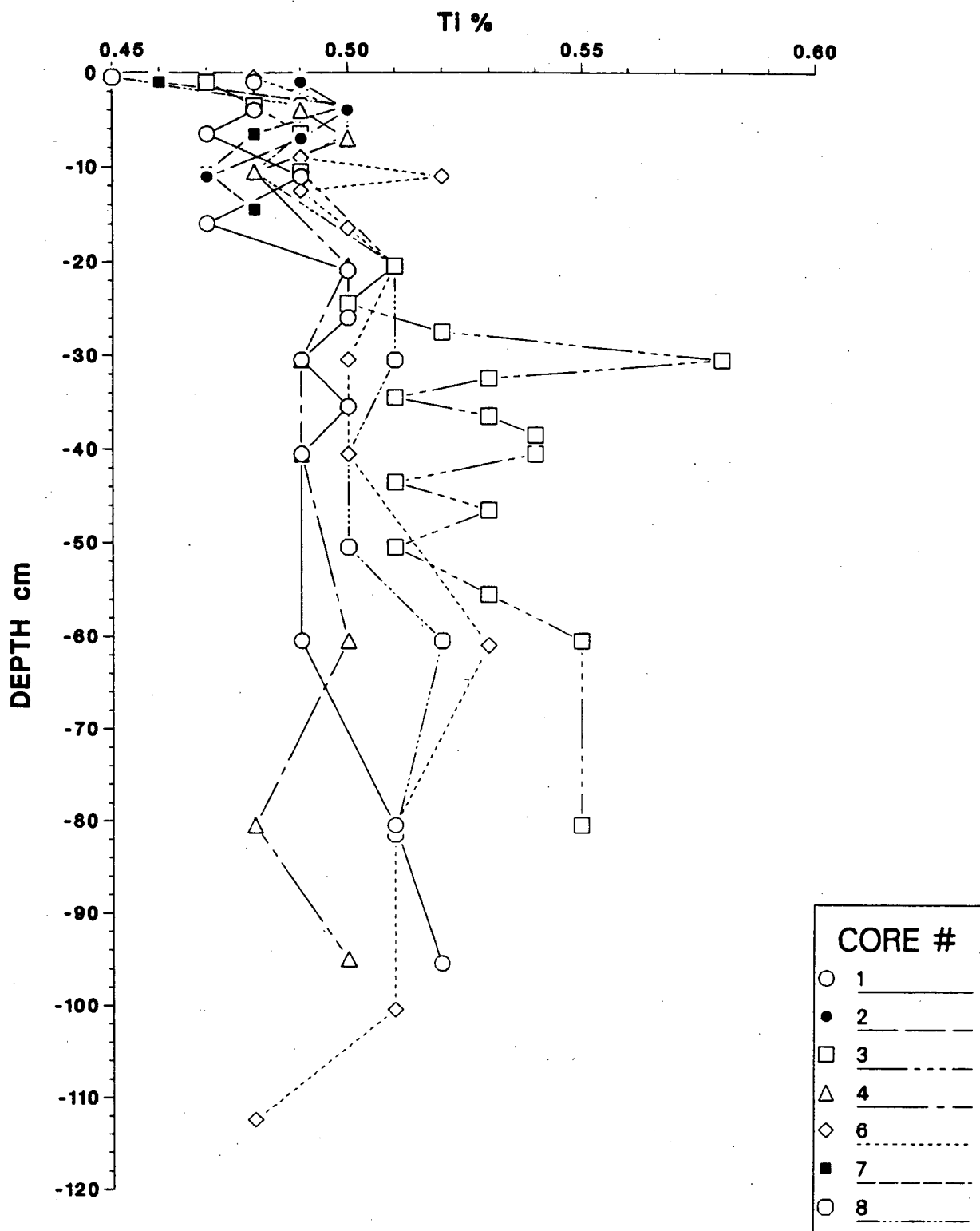


Figure 43: Ti distribution (%).

55 cm suggesting the distribution of both elements is being controlled by the same factor, probably illite content. Increases of the K/Al and Si/Al ratio below 20 and 40 cm may reflect periods of finer-grained sedimentation. K/Al is generally higher in core 6 than in any other core suggesting a finer grain size consistent with its location distant from the shelf.

#### 5.2.4.1 Mineralogy of low K-Al intervals

XRD was carried out on four samples (3–46, 50, 55, 60) to determine whether mineralogical changes could account for the low K and Al band in core 3. Accelerator  $^{14}\text{C}$  dates of  $12,020 \pm 120$  and  $12,870 \pm 160$  yr bracket this event, as discussed in Chapter 4. Sample preparation and instrument conditions are described in Appendix 1.

The XRD results are best illustrated by the quartz/illite and quartz/feldspar ratios plotted in Fig. 45. There is a clear increase of the quartz/illite ratio but no significant change in the quartz/feldspar ratio at depths of 50 and 55 cm indicating that illite decreases relative to quartz in this interval. The increase of the quartz/feldspar ratio is less dramatic than that of the quartz/illite ratio. Therefore the decrease in Al and K appears to be the result of relatively lower concentrations of illite. The same mechanism is proposed for the reduced concentrations of these elements in core 6 at 50 cm depth and at the top and bottom of core 7. The cause of these low illite intervals is not known. Thin units of coarser-grained sediment could account for changes in the quartz/illite ratio but there is no other evidence to support this.

#### 5.2.5 CALCIUM AND CARBONATE

Calcium in marine sediments occurs principally as calcium carbonate and its distribution is controlled largely by biological processes (Chester and Aston, 1976). In areas where terrigenous input is significant, such as at Tuzo Wilson, minerals such as plagioclase feldspar, amphibole and pyroxene are important contributors of Ca. The profiles for calcium and carbonate (carbonate carbon) are shown in Figs. 46 and 47 respectively. The profiles mirror

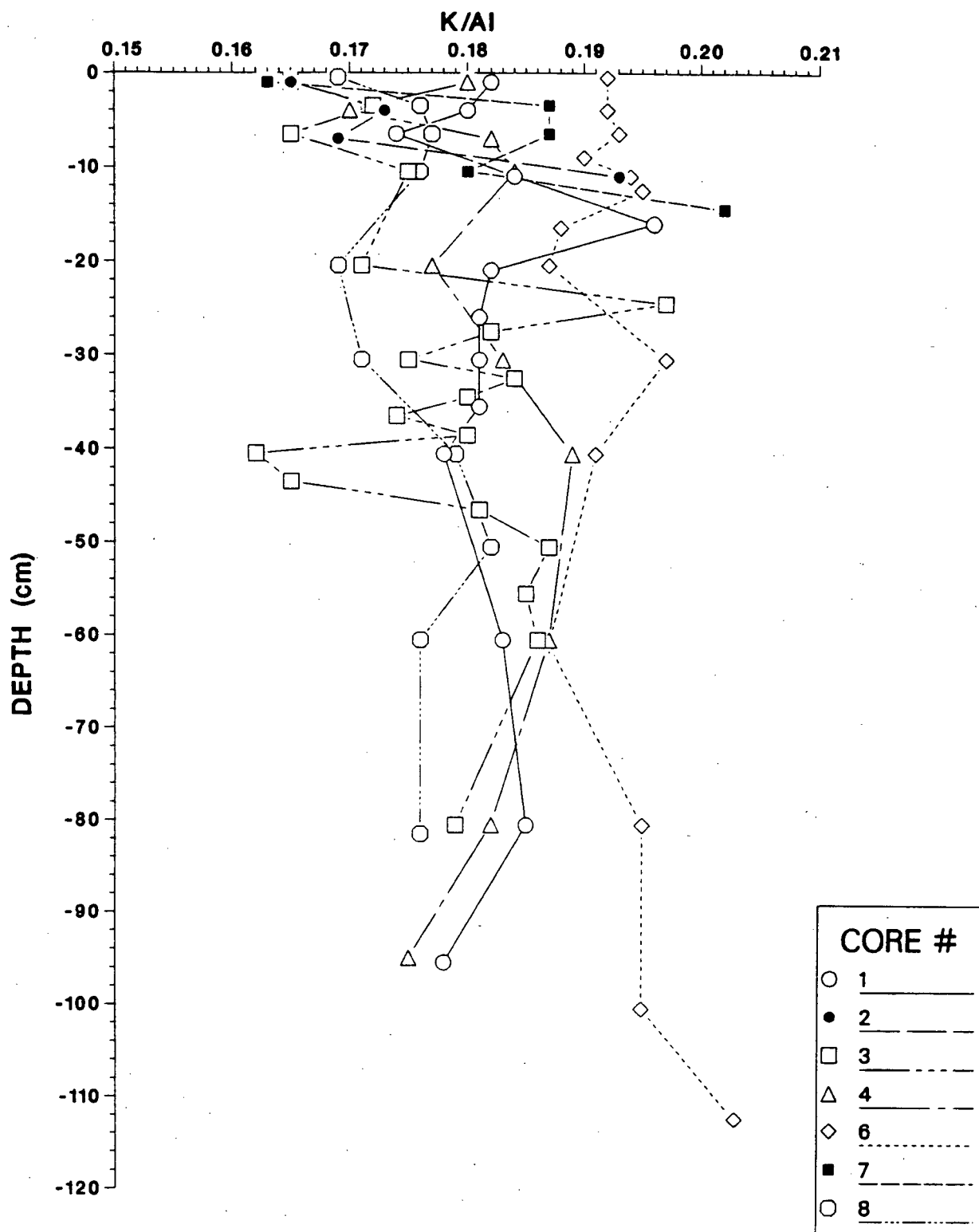
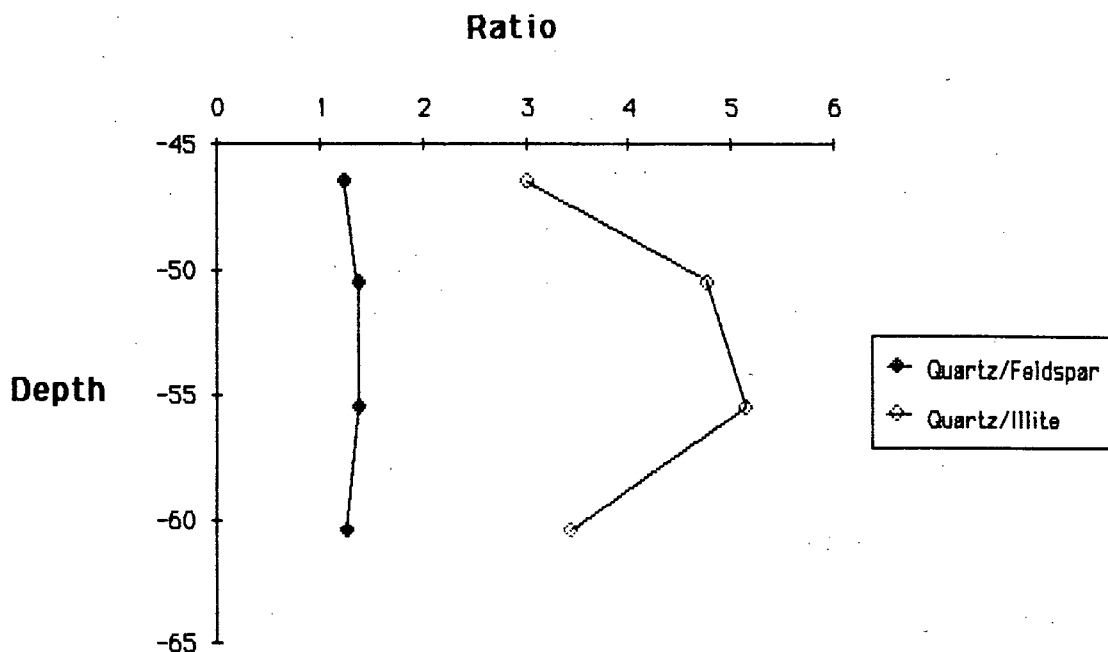


Figure 44: K/Al ratio.



**Figure 45:** Quartz/illite and quartz/feldspar XRD peak-height ratios for the  $<2\mu\text{m}$  fraction in core 3. Due to grinding, quartz represents all original size fractions.

each other indicating that calcium carbonate abundance is the principal factor controlling calcium distribution. A plot of Ca vs carbonate (Fig. 48) gives an intercept of about 0.5% Ca, which corresponds to the detrital fraction. Carbonate carbon and Si (Fig. 37) vary inversely throughout core 3. Si declines abruptly and carbonate increases between 20 and 24 cm, reaching minimum and maximum values respectively at 24 cm. Below that, Si steadily increases and Ca declines. These changes probably occurred in response to climatic change at the Pleistocene-Holocene transition which is discussed in more detail in the next chapter.

Core 6, located farthest from the continental shelf, generally has lower Ca and carbonate carbon values than the other cores. This suggests that the sediment closer to the shelf may contain some reworked carbonate from the shelf as well as that from benthic and pelagic foraminifera. Luternauer and Murray (1983) report that foraminiferan tests dominate the carbonate component at the outer shelf. Slumping of these sediments could be

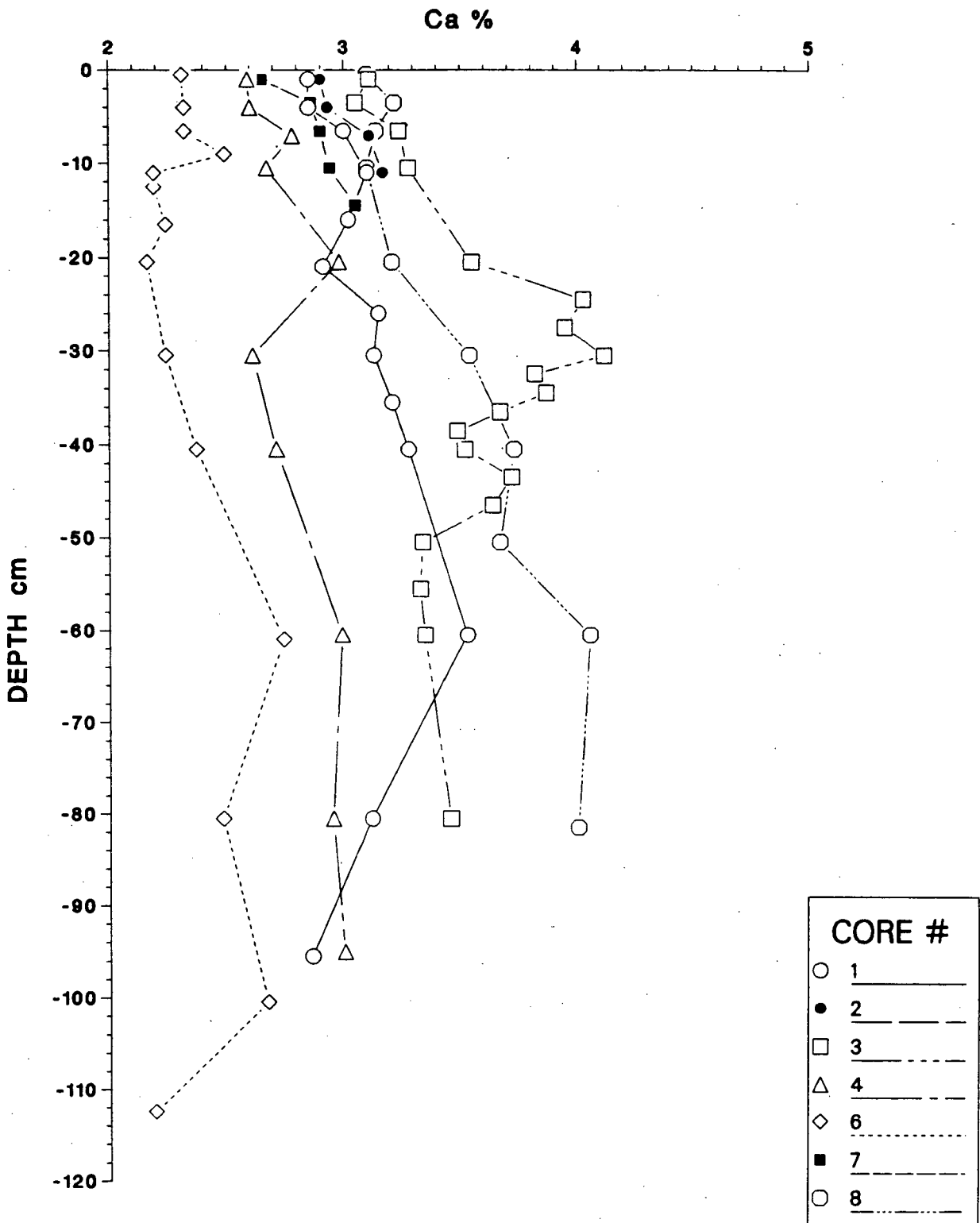


Figure 46: Ca distribution (%).

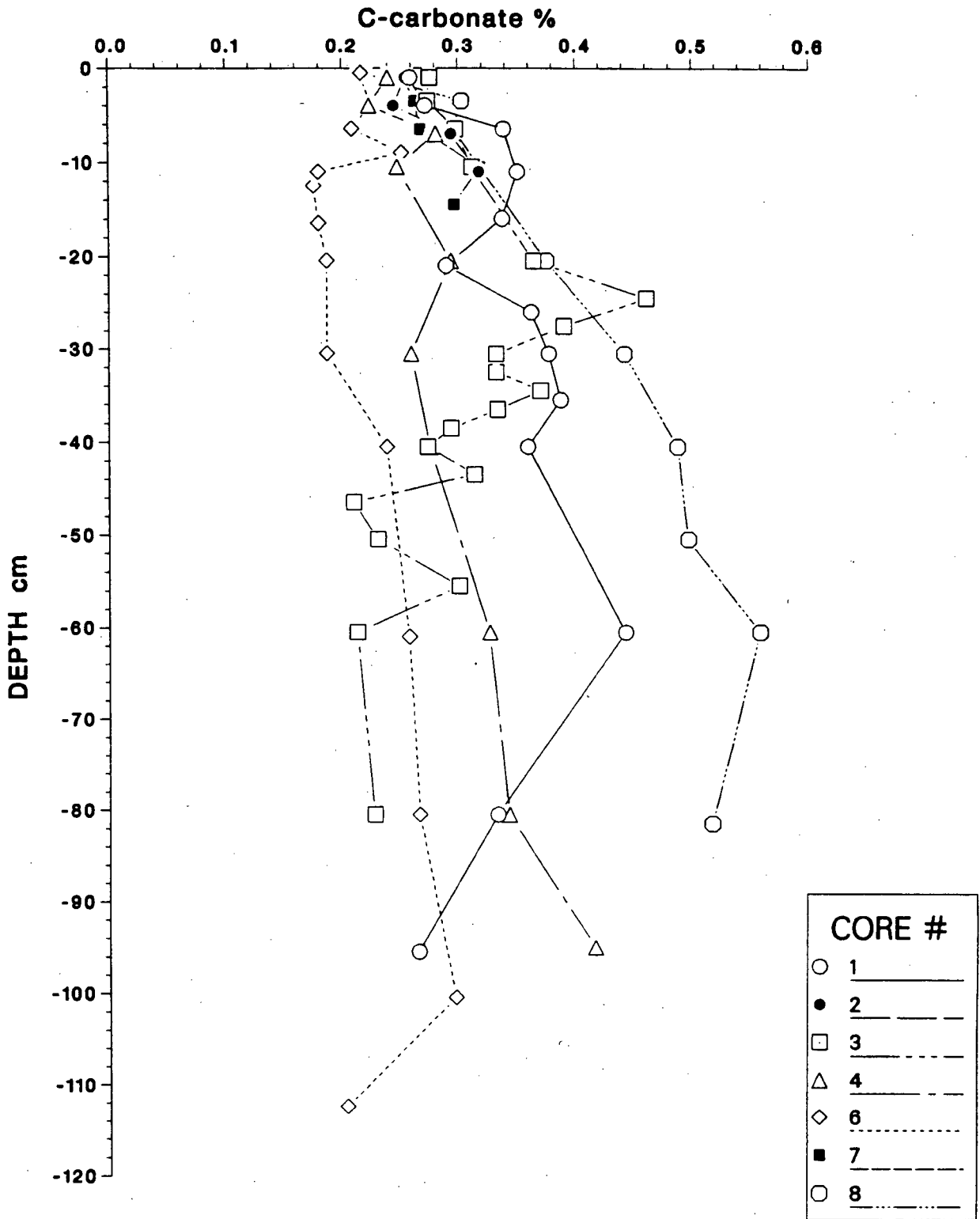
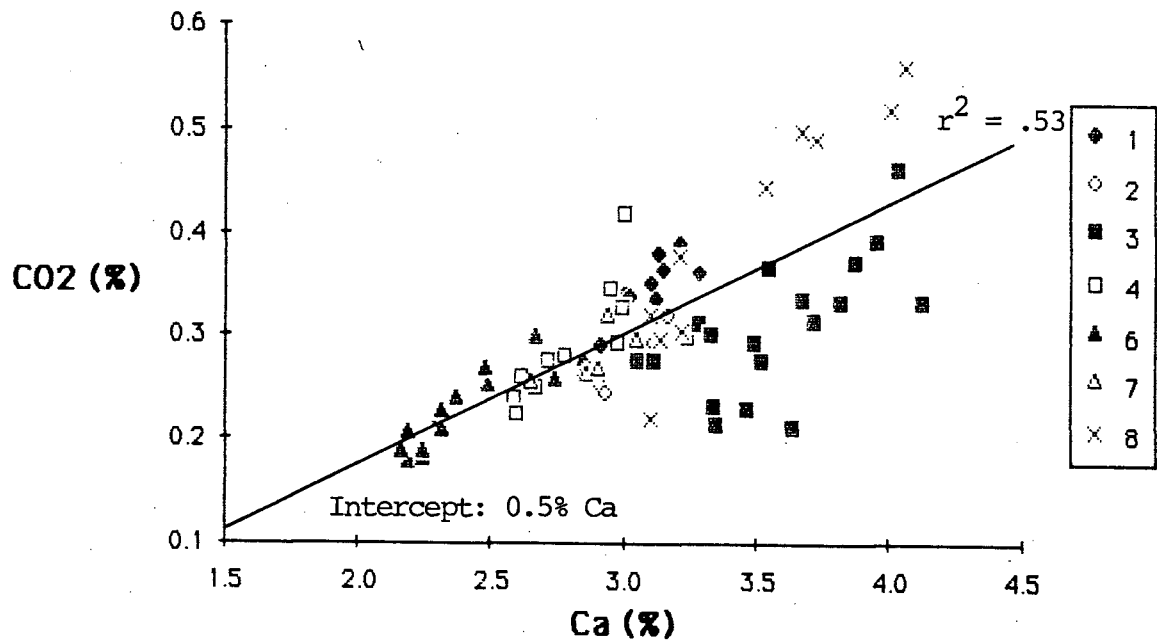


Figure 47: Carbonate carbon distribution (%).



**Figure 48:** Ca vs carbonate carbon (CO<sub>2</sub>) plot.

contributing to the carbonate content of sediments at the base of the slope near the Tuzo Wilson Seamounts.

The carbonate carbon values in core 6 can also be explained by dissolution rather than lower input. As mentioned in Chapter 4, the lysocline likely occurs within the range of these cores. The plot of depth vs CaCO<sub>3</sub> in Fig. 49 illustrates the effect of increasing dissolution with depth, assuming constant input. Core 6 was collected in the deepest water (2415 m), and lower sedimentation rates in the vicinity of this core due to its distance from the shelf would also aid dissolution by allowing longer exposure of the sediment to corrosive bottom water. Alternatively, productivity could be higher close to the shelf edge due to upwelling of nutrient-rich slope waters. This effect has been cited as a possible cause of high carbonate contents of sediments on the outer shelf near the north end of Vancouver Island by Luternauer and Murray (1983). The distribution of Ca and carbonate is likely a consequence of both higher productivity close to the shelf and dissolution in deeper water.

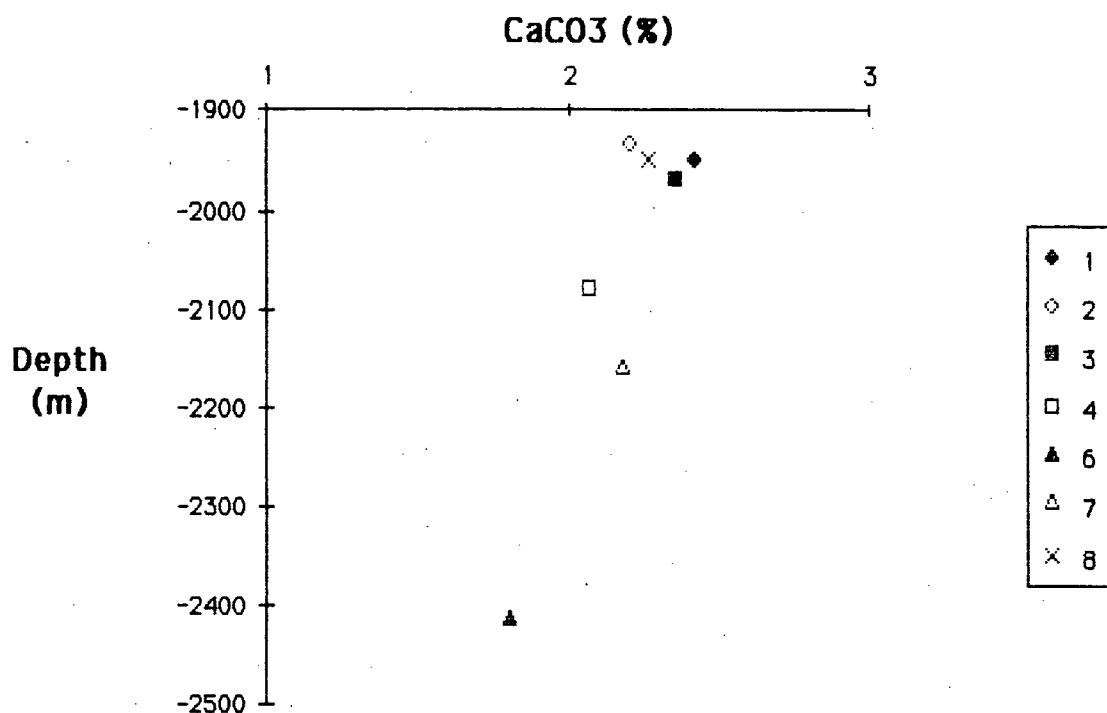


**Figure 49:** Plot of CaCO<sub>3</sub> vs depth. CaCO<sub>3</sub> calculated from average of 3 carbonate carbon values from top of each core.

### 5.2.6 PHOSPHORUS

Phosphorus values all fall within a very small range for all the cores (Fig. 50), and all values are low (mostly <0.1%). Phosphorus occurs in virtually all components of sediment (i.e. terrigenous, biogenous, authigenic and in basalt; Chester and Aston, 1976). The major host for P is biogenous phosphate; however in areas such as the Tuzo Wilson Seamounts, terrigenous input is likely to swamp this component to the point that variations are dominated by degree of terrigenous dilution rather than the actual variations in biogenic production. Basalt is also thought to be a significant source of P given that basalt glass and debris is visible in these cores. The average content of P in Tuzo Wilson Seamounts basalts is 0.37% (P.J. Michael, oral comm., 1986).

In core 3 at a depth of 30 cm, P shows an increase similar to that of Ti and several other elements (Ti, Sr and Zr). Although Ca-P (apatite) was identified by SEM-EDS (see

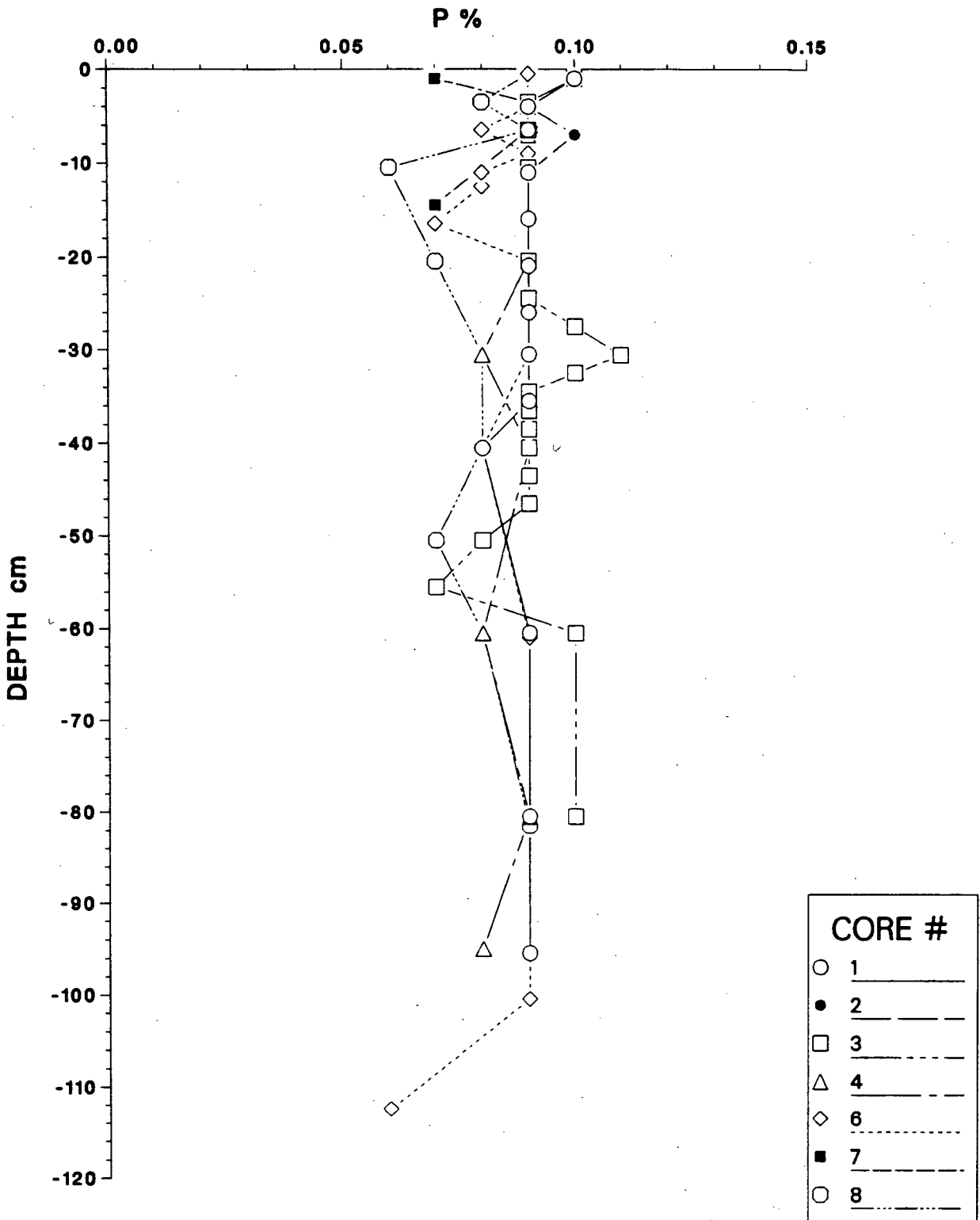


Figure 50: P distribution (%).

Chapter 4), this P increase is probably caused by a higher proportion of basalt debris in the sediment as discussed previously. SEM-EDS analysis of the segmented bones found at this depth reveals that they are composed exclusively of  $\text{CaCO}_3$  and do not therefore contribute to the P concentrations.

### 5.2.7 ORGANIC CARBON, IODINE AND BROMINE

Profiles of these elements are shown in Figs. 51, 52 and 54. Most cores show a slight decline in abundance down core. Cores 1 and 3 show the most dramatic and consistent down-core declines of  $C_{\text{Org}}$ , whereas virtually constant values are noted throughout core 8.

If a constant production rate is assumed at Tuzo Wilson Seamounts, then the distribution of  $C_{\text{Org}}$  and N implies that microbial activity has been more effective in degrading organic matter in cores 1, 3 and 4 than in the other cores, implying lower sedimentation rates, especially in core 3. The absence of such a down-core decline in cores 6 and 8 may either be due to more rapid sedimentation or may indicate the presence of refractory carbon.

Iodine and bromine in marine sediments are associated principally with the organic fraction (Price *et al.*, 1970), and consequently show good correlation with  $C_{\text{Org}}$ . In every core I decreases down-core (Fig. 52). Core 3 shows the most dramatic decrease, from 682 ppm at the surface to 18 ppm at a depth of 80 cm. Core 6 is anomalous in that I increases again from a minimum of 268 ppm at 60 cm to 462 ppm at 112 cm; however the bottom two samples in this core must be treated with caution due to the suction structure in the bottom 15 cm.

Higher iodine contents in surface sediments result from the uptake of I onto organic matter at the sediment surface (Price and Calvert, 1973) to the extent that I concentration in surface sediment is many times that in seawater ( $0.06 \text{ mg kg}^{-1}$ ; Calvert, 1976). The I incorporated into living organisms is small in comparison (Price and Calvert, 1973). As

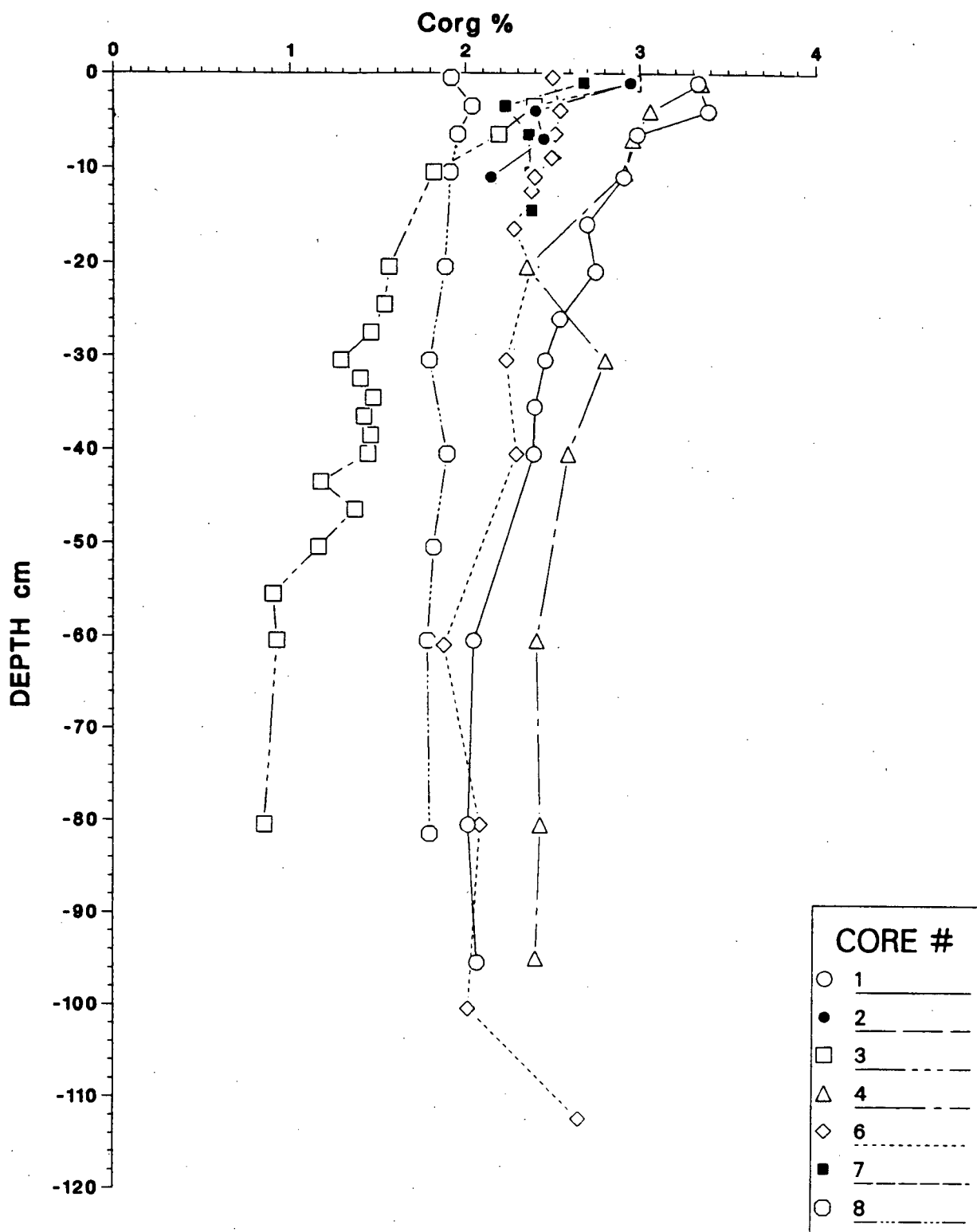


Figure 51:  $C_{org}$  distribution (%).

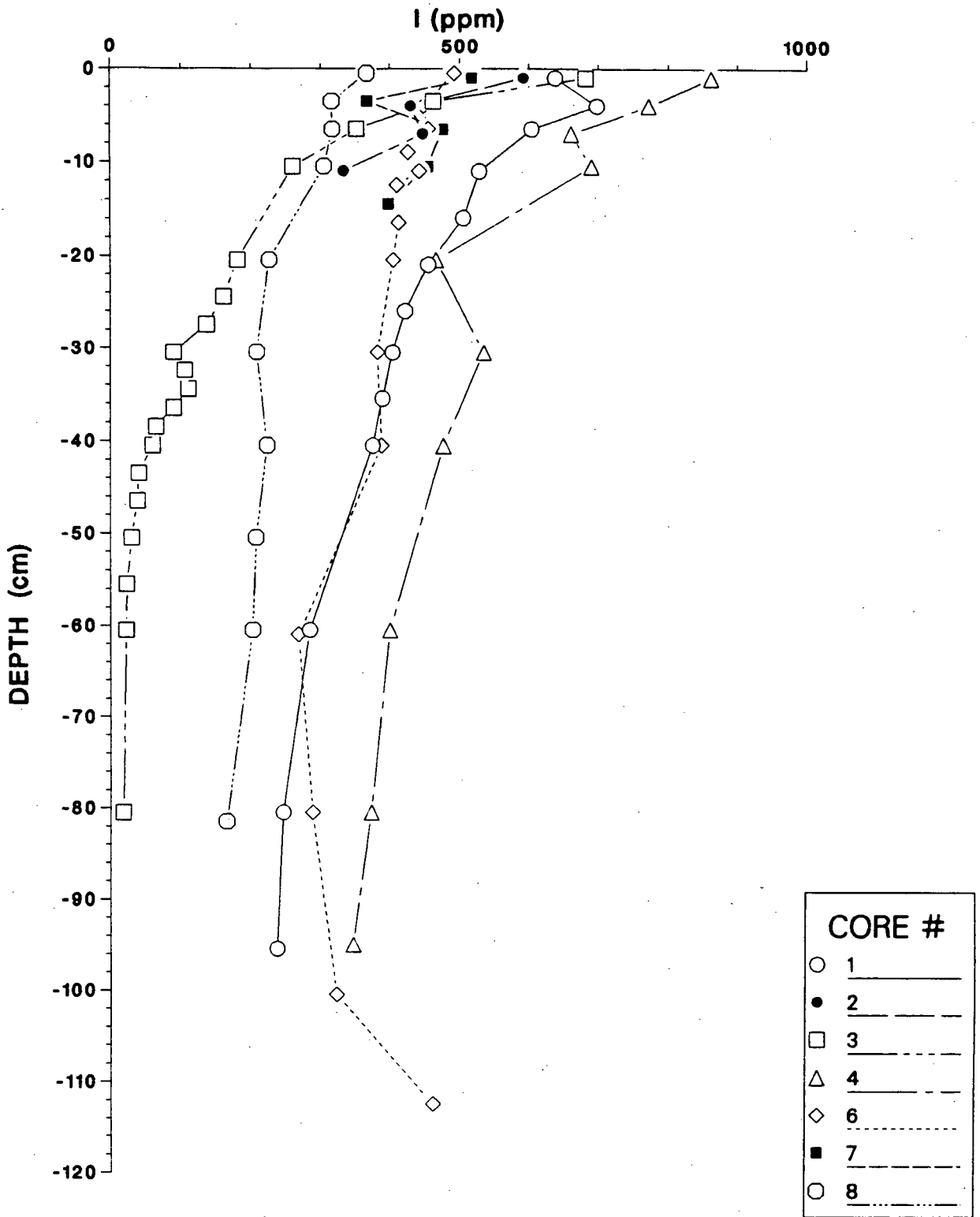


Figure 52: I distribution (ppm).

sediment undergoes burial, I is lost through degradation of marine organic matter (Ullman and Aller, 1985). This loss is evident from the down-core decline in I and  $C_{\text{Org}}$  in cores 1 and 4, and especially in core 3. The pronounced decline in core 3 implies a lower sedimentation rate. The longer residence time (lower sedimentation rate) of the upper layer of sediment allows more thorough degradation of organic matter by oxidation, bacterial activity and bioturbation. The significance of the relationship between I and  $C_{\text{Org}}$  is illustrated by the  $I/C_{\text{Org}}$  ratio (Fig. 53). The ratio declines steadily with depth in most cores, indicating a loss of I relative to  $C_{\text{Org}}$  during burial (Price *et al.*, 1970). Core 3 has a unique character (as it does for many other elements) in that its ratio decreases more markedly between 20 and 40 cm, plunging from 230 to 21 ( $\times 10^{-4}$ ). This steep decline is consistent with the interpretation of a lower sedimentation rate for this core.

The reasons for a lower sedimentation rate in core 3 are unclear; however, the core was taken on a spur extending southwest from a small submarine hill above the confluence of two channels (Fig. 2). Recent sedimentation has probably been restricted to channels resulting in a much slower sedimentation rate for core 3 than for the other cores which were collected within, or close to, submarine channels.

The distribution of Br is shown in Fig. 54. At Tuzo Wilson, Br is concentrated much less than I, with  $I/\text{Br}$  ratios averaging 3.7 for surface sediments. As pointed out by Pedersen and Price (1980), who found similar ratios in the surface sediments of the Panama Basin, this represents a substantial favouring of I over Br for incorporation into sediment (by a factor of  $4.3 \times 10^3$ ), considering that the  $I/\text{Br}$  ratio in sea water is so low ( $8.5 \times 10^{-4}$ ).

In contrast to I, which is enriched only in sediments deposited under oxidizing conditions, Br in marine sediments tends to be concentrated in both oxic and anoxic sediment facies (Calvert, 1976). In oxic sediments such as those studied here, both Br and I are lost during degradation of organic matter, but to varying degrees. Price and Calvert (1977) have shown that on the Namibian shelf the decrease in  $\text{Br}/C_{\text{Org}}$  with depth is much less than that

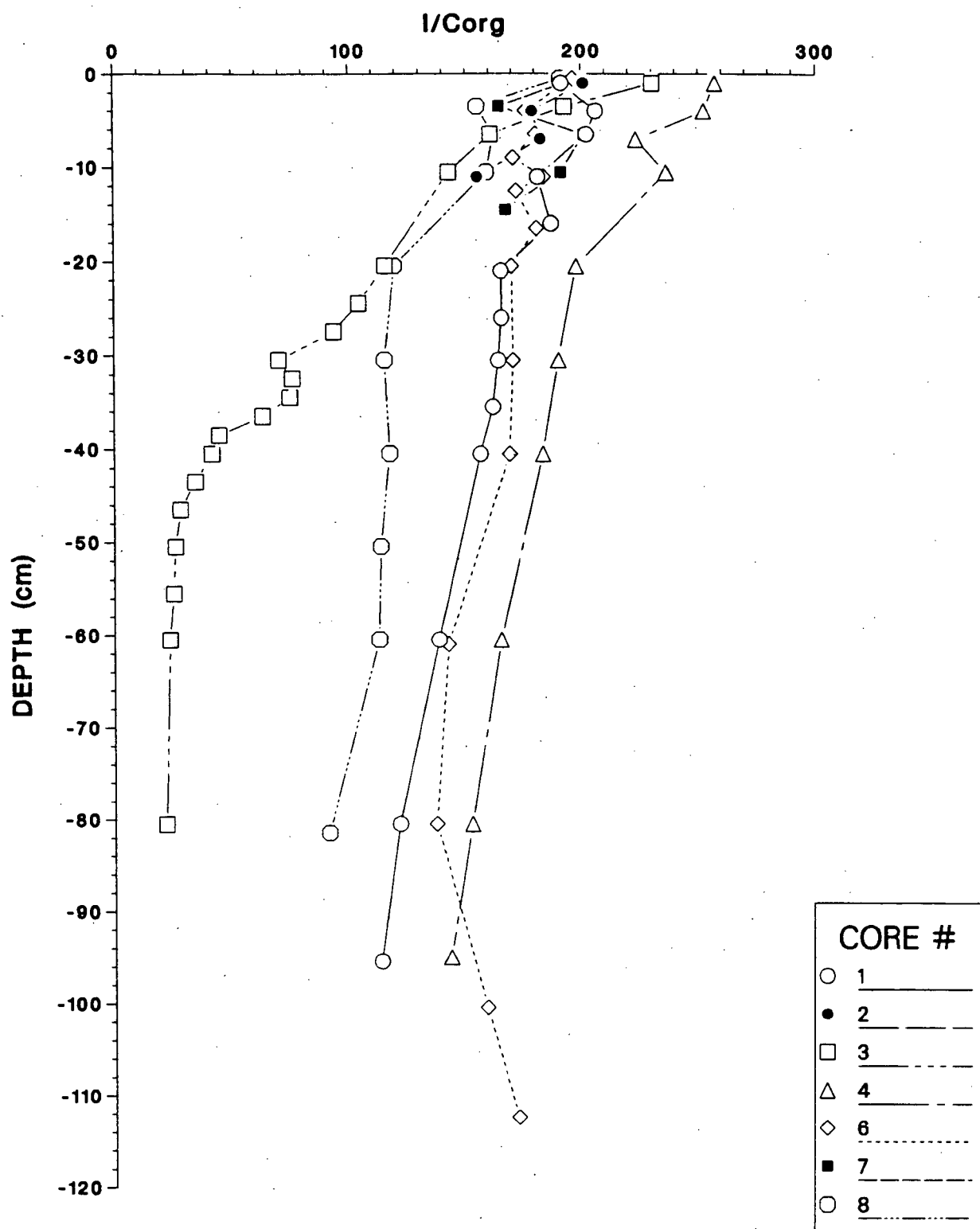


Figure 53: I/C<sub>org</sub> ratio ( $\times 10^4$ ).

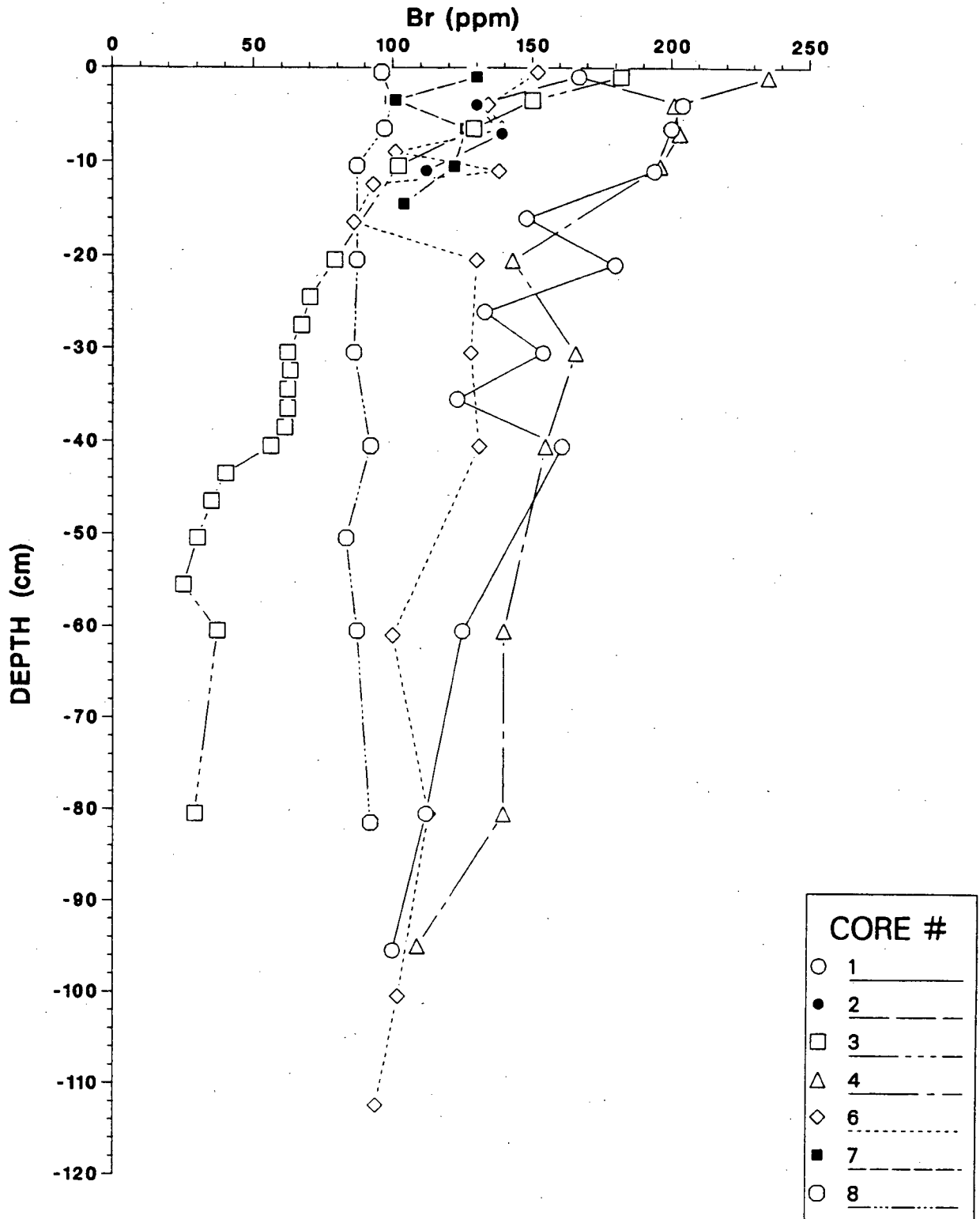


Figure 54: Br distribution (ppm, salt-free).

for  $I/C_{Org}$ . At Tuzo Wilson they decrease by factors of 2.5 and 10.7 respectively in core 3 which has the most dramatic changes (Figs. 55 and 53). The changes observed on the Namibian shelf are less dramatic for  $I/C_{Org}$  (factor of 5 decrease) but similar for  $Br/C_{Org}$  (factor of 2 decrease). Price and Calvert (1977) and Pedersen and Price (1980) accounted for the difference in behaviour of these two halogens by suggesting that Br binds more strongly to organic matter and that the binding sites may be different. This would result in an exaggeration of the relative concentrations of I and Br at the surface because the more labile I would then be more easily recycled back to the surface. Alternatively, in comparison to I, a larger proportion of the Br may be incorporated into living organisms rather than being sorbed onto organic matter. This would account for the lower Br content and lower  $Br/C_{Org}$  ratios in sediment, and the less dramatic decline in  $Br/C_{Org}$  ratios down-core.

The behaviour of Br at Tuzo Wilson Seamounts (Fig. 54), best illustrated by the  $Br/C_{Org}$  ratio (Fig. 55), is much more erratic than that of I. This may be due to the error introduced by correcting for seasalt Br in the dry sediment (Price *et al.*, 1970).

### 5.2.8 NITROGEN

The profiles of Total N (Fig. 56) and  $C_{Org}$  (Fig. 51) are very similar in appearance, as would be expected if both species were associated exclusively with organic matter. The good correlation exhibited by the  $C_{Org}$  vs Total N plot (Fig. 57) indicates that ammonia adsorbed on illite (Müller, 1977) is not a significant nitrogen-bearing species in these sediments.  $C_{Org}/N$  ratios can be used to distinguish between terrigenous and marine organic matter. Higher (terrestrial) plants contain less than 20% protein and therefore show high ( $>10$ )  $C_{Org}/N$  weight ratios whereas the average ratio for phytoplankton is close to 6 (Müller, 1977). Bornhold (1978) reported mean  $C_{Org}/N$  ratios from surficial marine sediments off northwestern Vancouver Island of 6.2.

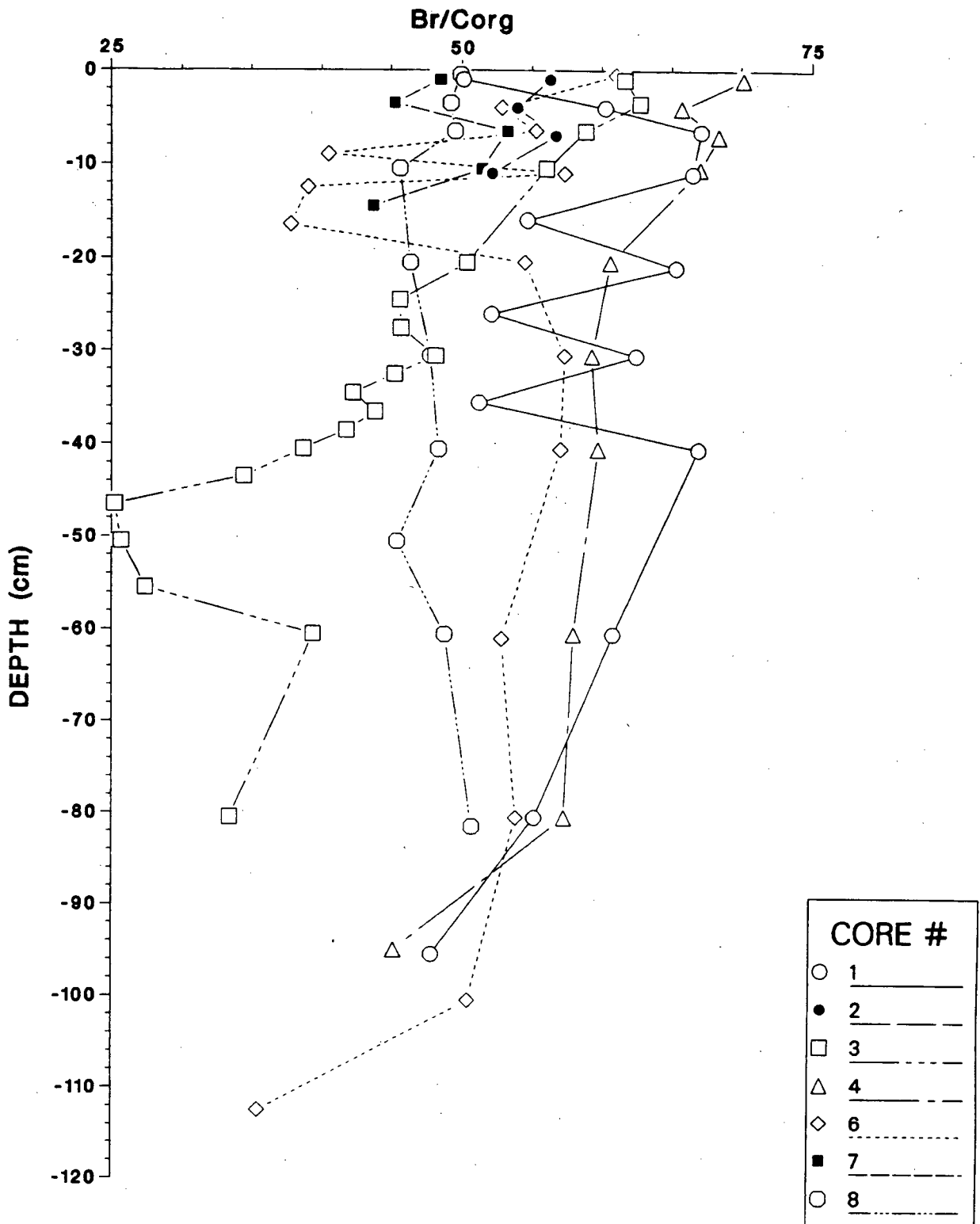


Figure 55: Br/C<sub>org</sub> ratio ( $\times 10^4$ ).

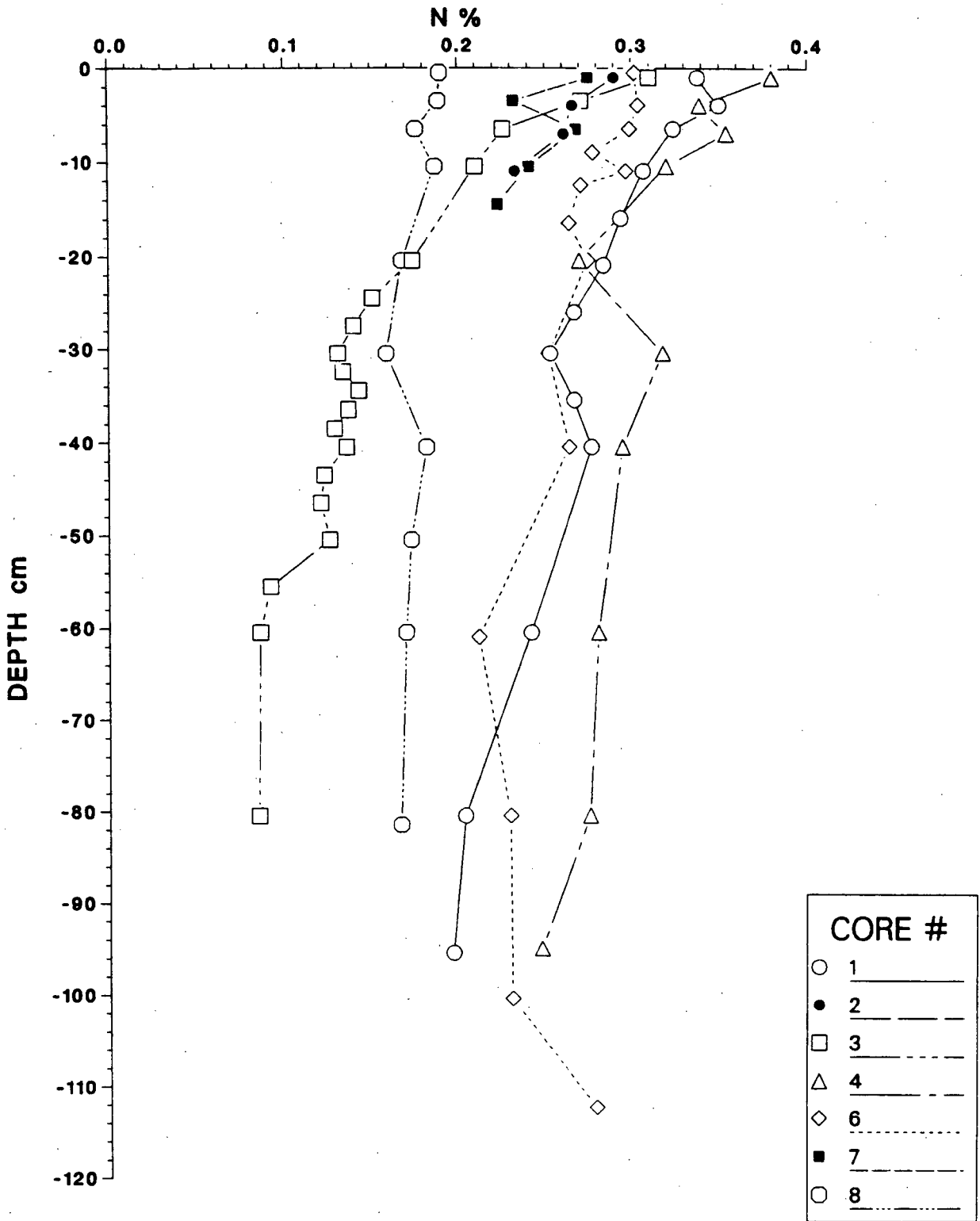


Figure 56: Total N distribution (%).

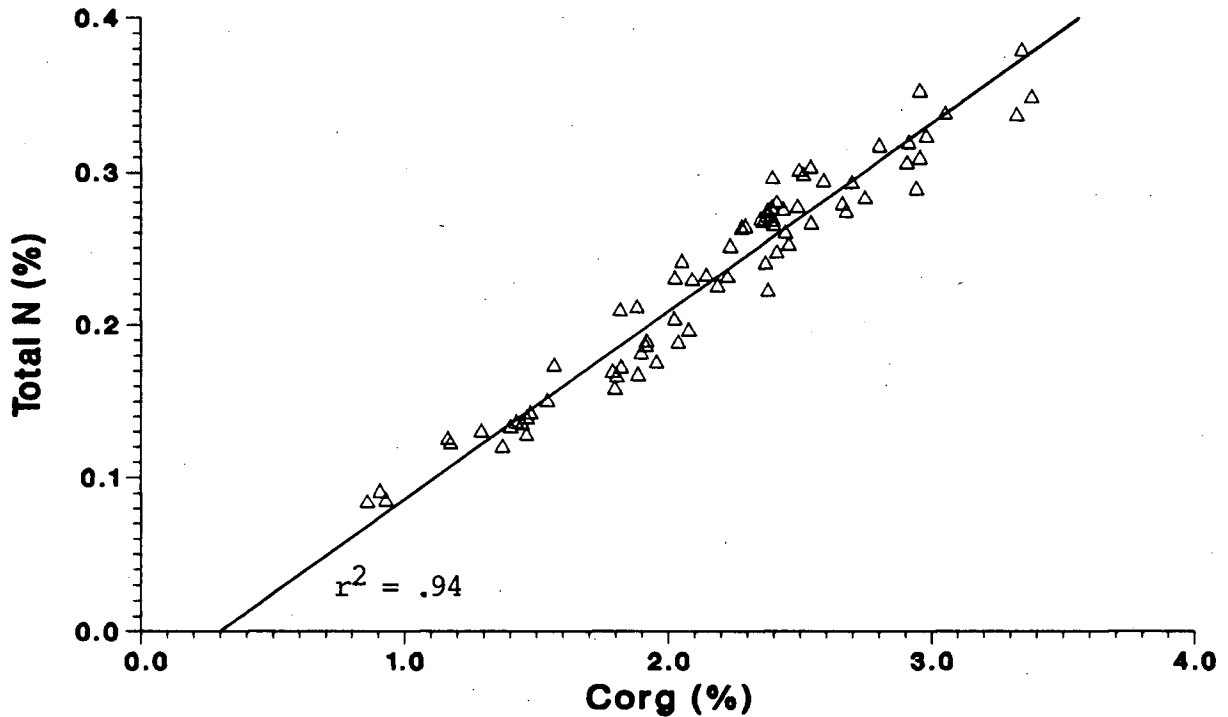


Figure 57:  $C_{Org}$  vs Total N plot.

The ratios at Tuzo Wilson Seamounts are higher (Fig. 58), ranging from 8–12 with an average of 9.6 ( $n=75$ ). Bornhold (1978) ascribed his lower ratios to lack of transport of terrigenous organic matter to the shelf and, using  $C_{Org}/N$  ratios of 5.7 and 54.0 for plankton and wood respectively, calculated that 80% of the samples contain less than 3% terrigenous plant material. The fact that most modern, terrestrially-derived sediment is trapped within deep, silled fiords (where  $C_{Org}/N$  ratios are higher) explains this. The high ratios at Tuzo Wilson Seamounts are therefore anomalous compared to the Vancouver Island shelf, as marine organic matter would be expected to dominate farther from land, depressing the ratios.

Müller and Suess (1979) demonstrated that organic matter preservation varies with sedimentation rate. N is also affected by sedimentation rate, but because it occurs principally in amino acids, which are more susceptible to degradation than most other forms of organic matter,  $C_{Org}/N$  ratios are perturbed by microbial degradation. Relative to the continental shelf, the higher ratios at Tuzo Wilson Seamounts are probably a consequence of preferential degradation of nitrogenous organic matter enhanced by a lower sedimentation rate.

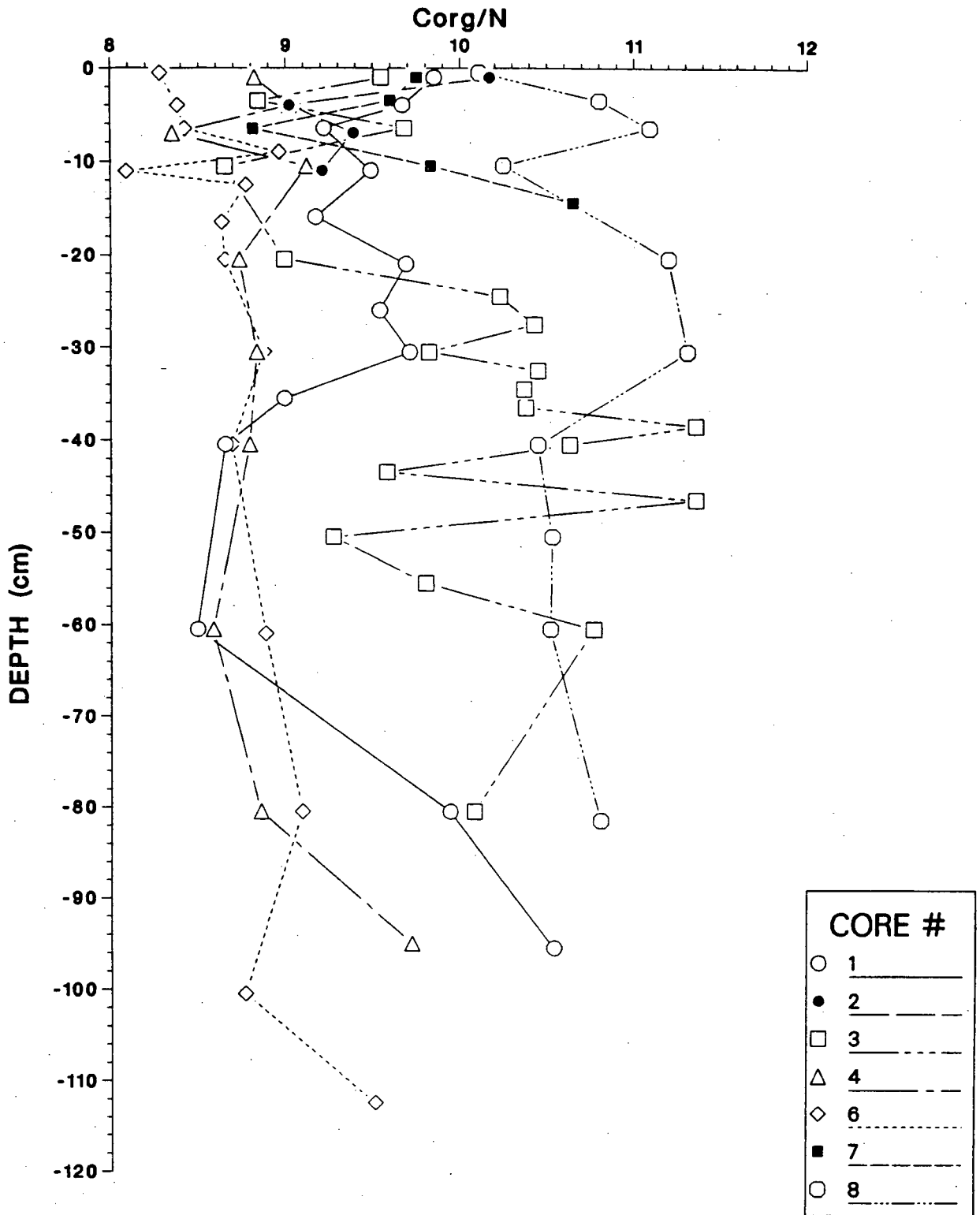


Figure 58: C<sub>org</sub>/N ratios.

## Chapter 6

### TRACE ELEMENT DISTRIBUTION AND THE EFFECT OF DEGLACIATION ON SEDIMENT

#### GEOCHEMISTRY

##### 6.1 INTRODUCTION

Trace elements (Ba, Co, Cr, Cu, Mn, Nb, Ni, Pb, Rb, Sr, V, Y, Zn, and Zr) were analyzed by XRF using the procedure outlined in Appendix 1. Their distribution provides insight into several aspects of sedimentation at Tuzo Wilson Seamounts. The geochemistry of Rb, Zr and Mn supports the climate-induced shift in provenance suggested by the change in mineralogy and by the distribution of Si, Ca, Fe and Mg. Sr correlates closely with Ca due to its substitution for Ca in  $\text{CaCO}_3$  and is therefore also susceptible to the effects of dissolution. Ba, Cu, Ni and Zn may be linked to biogenic productivity by their inverse correlation with the  $\text{C}_{\text{org}}/\text{N}$  ratio. The distribution of Mn reveals an absence of major diagenetic remobilization of oxide phases in these sediments.

Raw trace element data are presented in Appendix 2 and salt-free data in Appendix 4. Nb, Pb, and Y were analyzed but their results are not discussed here.

##### 6.2 RESULTS AND DISCUSSION

###### 6.2.1 RUBIDIUM AND ZIRCONIUM

Rb and Zr are often associated with the terrigenous fraction of marine sediments, with Rb substituting for K in feldspars and illite, and Zr occurring exclusively in the mineral zircon. Both elements occur in the basalts of the seamounts, with concentrations of 26 and 329 ppm respectively in one sample (P.J. Michael, oral comm., 1986).

The distributions of Rb and Zr in the sediments are shown in Figs. 59 and 60. No clear relationship emerges for most of the cores. At 30 cm depth in core 3, Zr increases

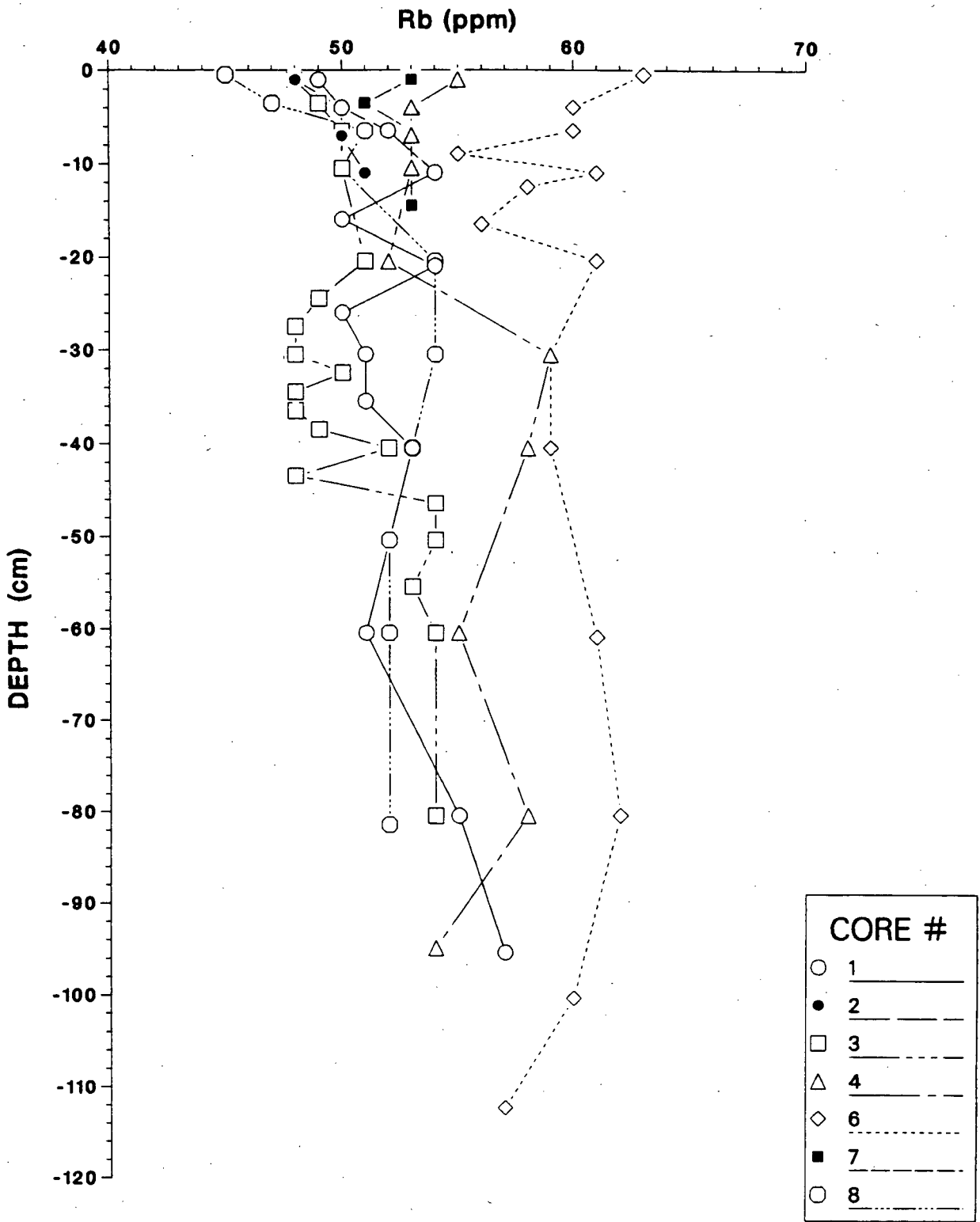


Figure 59: Rb distribution (ppm).

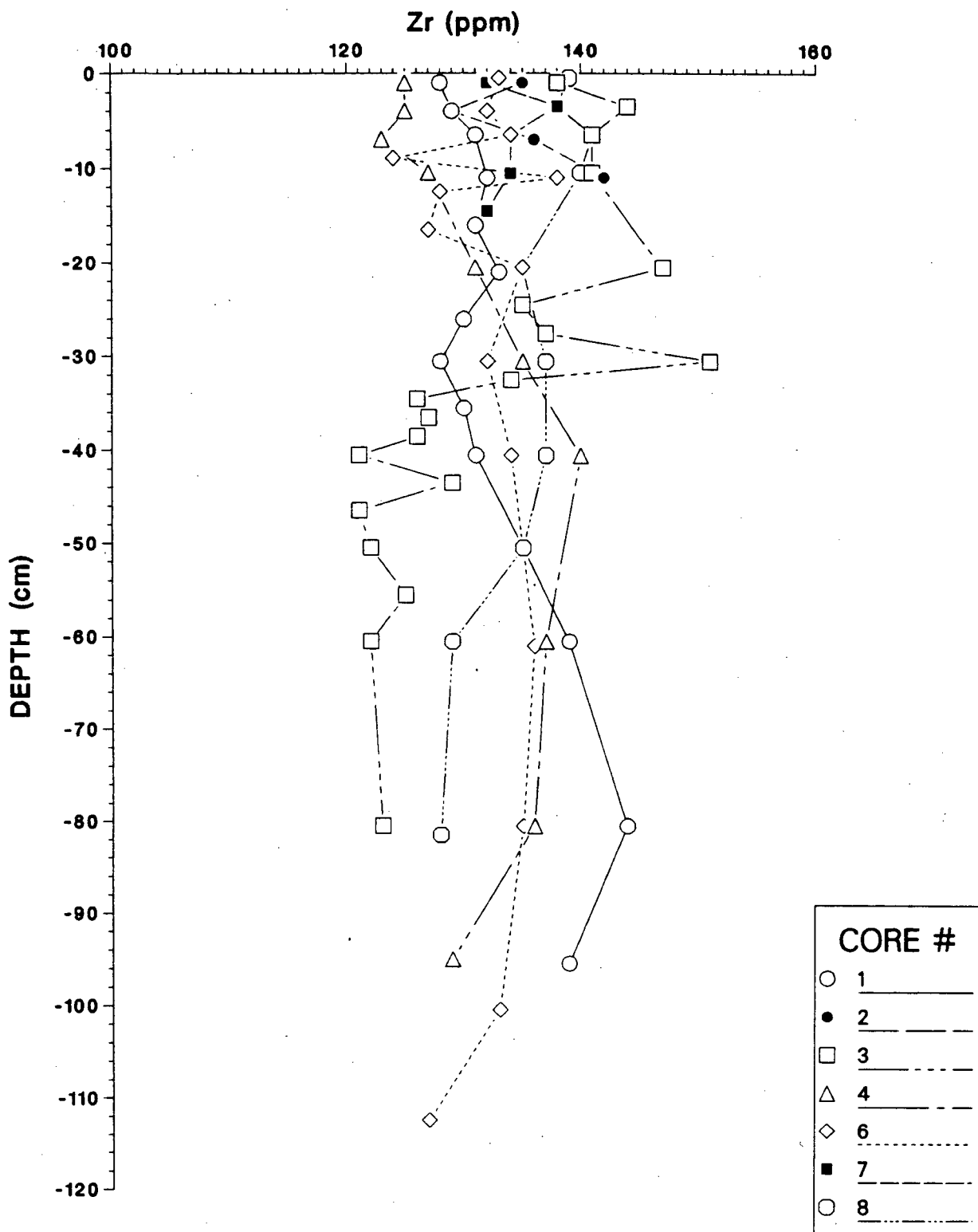


Figure 60: Zr distribution (ppm).

sharply, reducing the Rb/Zr ratio (Fig. 72). This corresponds to the Ti, P, and Sr increases discussed previously. These elements originate from several sources: continental (Zr, Ti, Sr), volcanic (all four), and biogenic (P, Sr), making distinction between the sources difficult. Basalts in the Tuzo Wilson Seamounts area have much lower Rb/Zr ratios (0.08) than the sediments so basalt debris in the sediment would reduce the ratio in the same way that Zr enrichment from terrigenous sediment would. However a 10% increase in basalt content would account for *all* the anomalies at 30 cm, arguing against a heavy mineral source which would probably enhance only Ti and Zr. In addition, the Rb/Zr ratio appears to be perturbed by Zr in basalts to the extent that the ratio is not a useful grain size indicator in these sediments.

#### 6.2.2 BARIUM AND STRONTIUM

Barium and strontium values are plotted in Figs. 61 and 62 respectively. Both Ba and Sr, as well as Rb, occur in feldspars. High Sr concentrations have been identified in the apatite phase of fish debris (Goldberg and Arrhenius, 1958). Calvert (1976) reported that the Sr distribution on the Namibian shelf is controlled by carbonate minerals, especially calcite. Sr often substitutes for Ca in minerals due to the similarity of their ionic radii (112 and 99 pm, respectively). At Tuzo Wilson Seamounts this is exemplified by their almost identical behaviour, best illustrated by a plot of Sr vs Ca (Fig. 63) which shows a linear relationship with an intercept at 220 ppm Sr corresponding to the detrital (i.e. non-carbonate) fraction. The increase of Sr at 30 cm in core 3 is attributed to basaltic debris, as discussed in the previous chapter. The segmented bone found at this depth is composed of calcium carbonate only and contains neither P nor Sr.

The depth distribution of Ba does not vary significantly (Fig. 61). Core 6 has higher Ba and Rb concentrations than the other cores, which may result from substitution of  $Ba^{2+}$  and  $Rb^{+}$  for  $K^{+}$  (ionic radii 136, 149 and 138 pm, respectively) in illite.

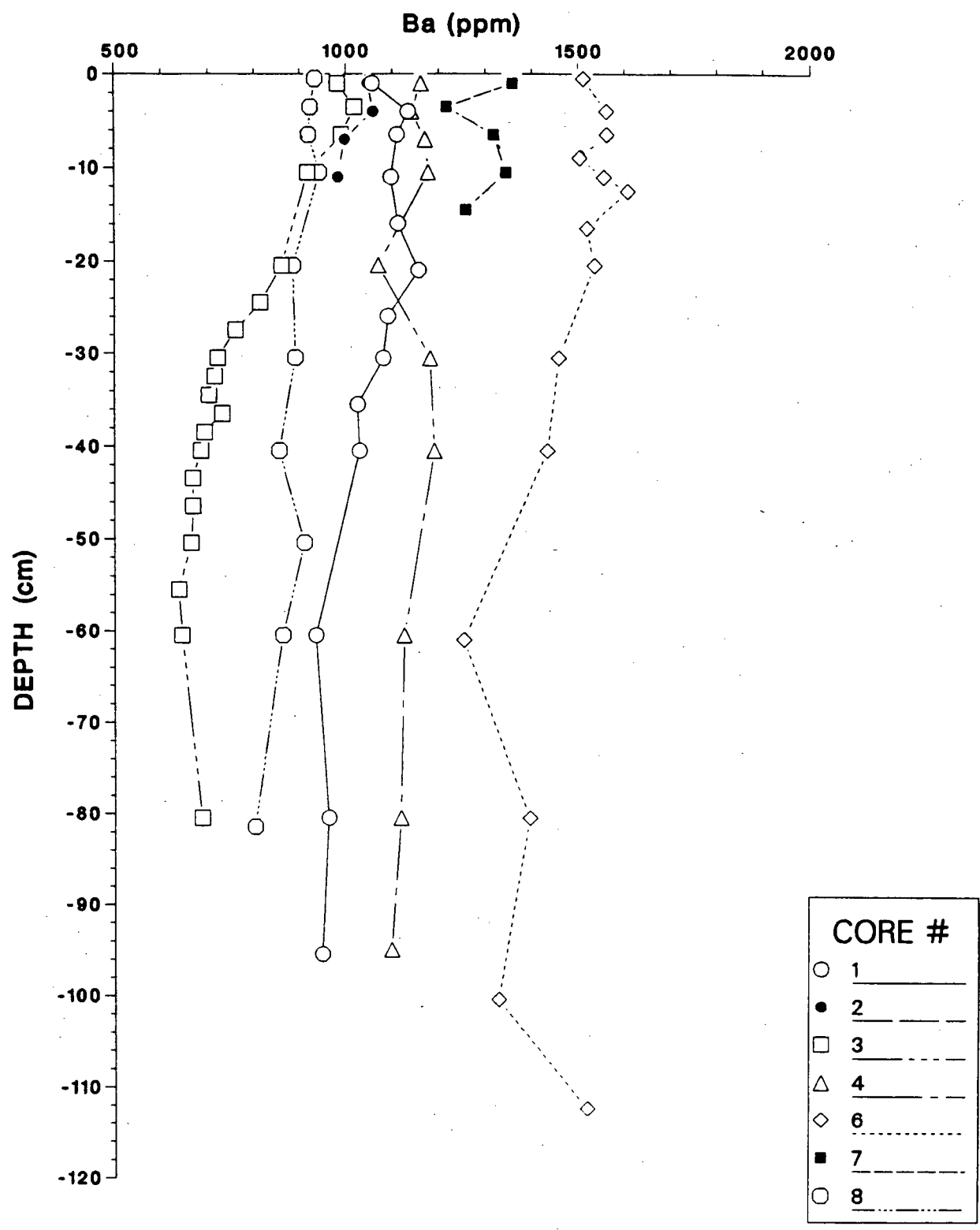


Figure 61: Ba distribution (ppm).

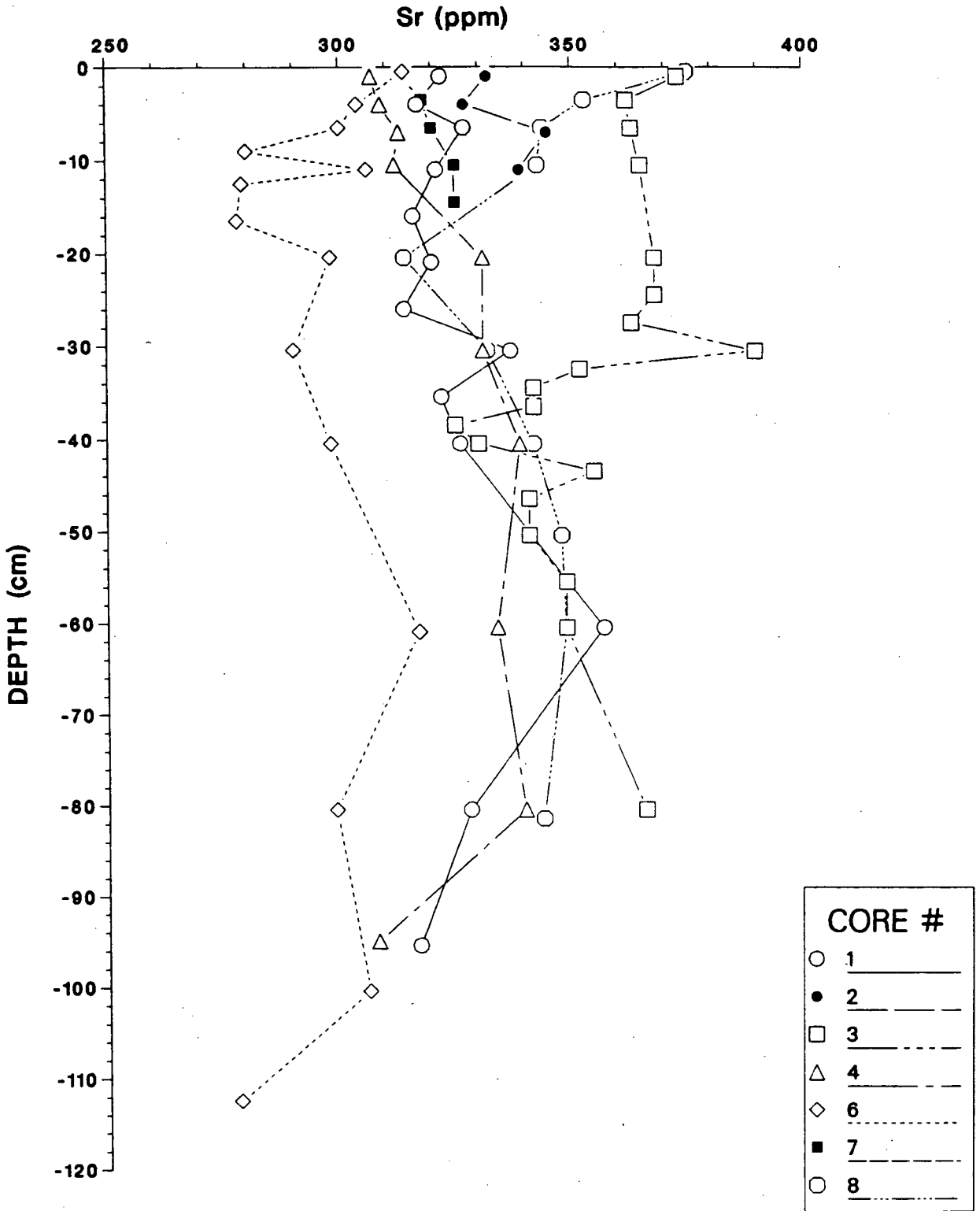


Figure 62: Sr distribution (ppm).

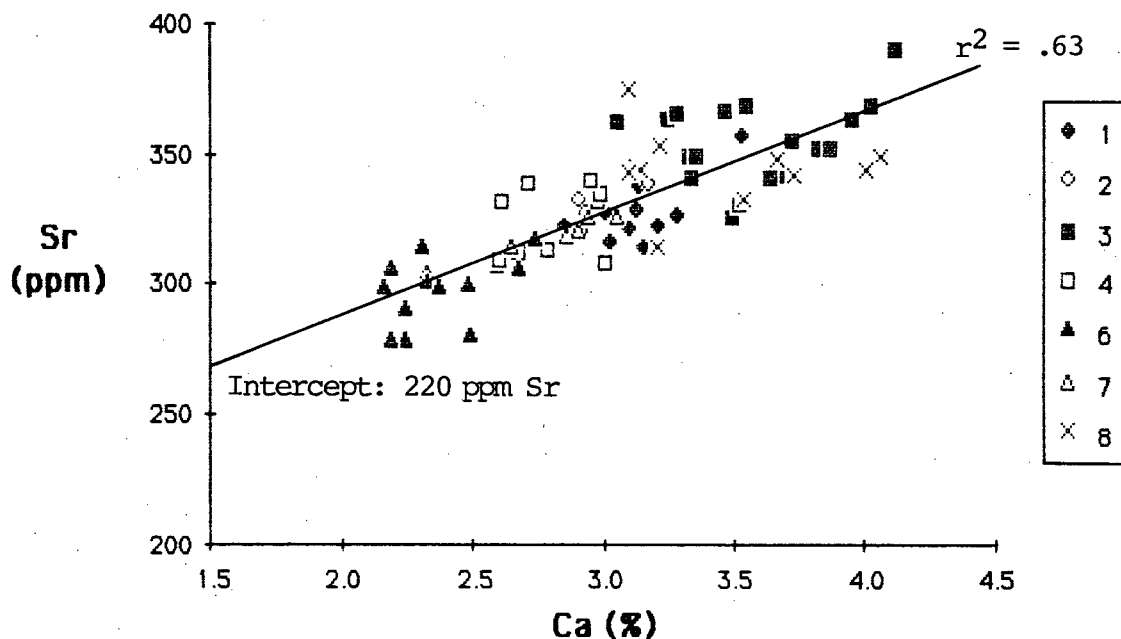


Figure 63: Sr vs Ca plot.

### 6.2.3 ZINC, VANADIUM, CHROMIUM, COBALT, NICKEL AND COPPER

The distributions of Zn and the transition metals V, Cr, Co, Ni, and Cu are shown in Figs. 64 to 69 respectively. These elements (except V and Cr) tend to be concentrated in deep-sea clays more than in terrigenous sediments (Chester and Aston, 1976). They are often adsorbed from seawater onto Mn-Fe oxyhydroxides and clay minerals, especially if these have Mn-Fe oxyhydroxide coatings. The remaining contribution is from terrigenous grains containing these elements. Data compiled by Chester and Aston (1976) from oxide-replete Pacific deep-sea clay (their values in parentheses, in ppm) indicate that the sediments at Tuzo Wilson Seamounts have similar V (130), slightly higher Cr (77) and much lower Ni (293), Co (116) and Cu (570) contents. No value is given for Zn for the Pacific, but for the Atlantic, 130 ppm is quoted, which is similar to that at Tuzo Wilson Seamounts. Average values reported by Price (1981) for Cu, Pb, Zn, Co and Ni in cores from Juan de Fuca ridge and by Bornhold *et al.* (1981) for Co, Cu, Ni and Zn from a series of cores from just west of Explorer

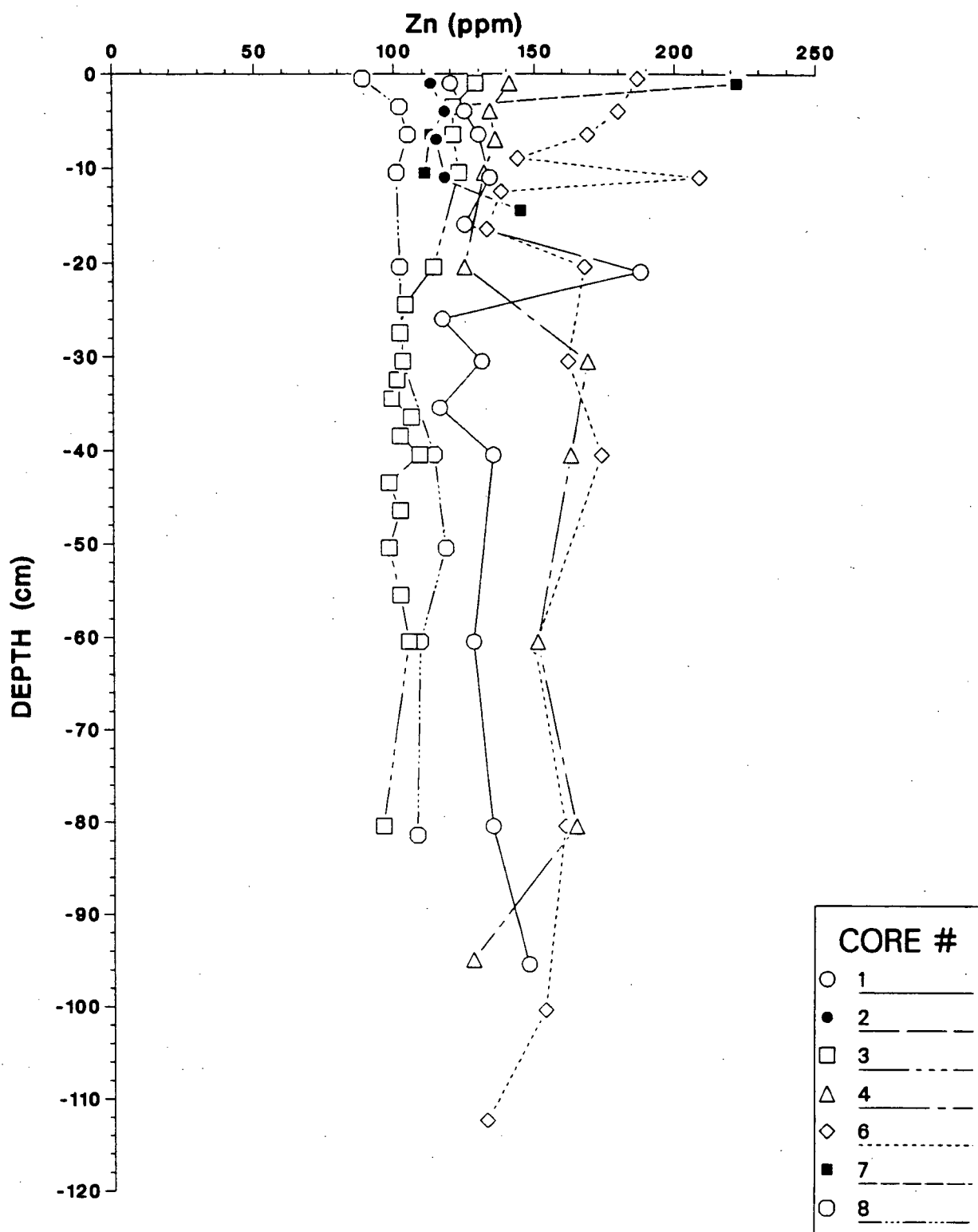


Figure 64: Zn distribution (ppm).

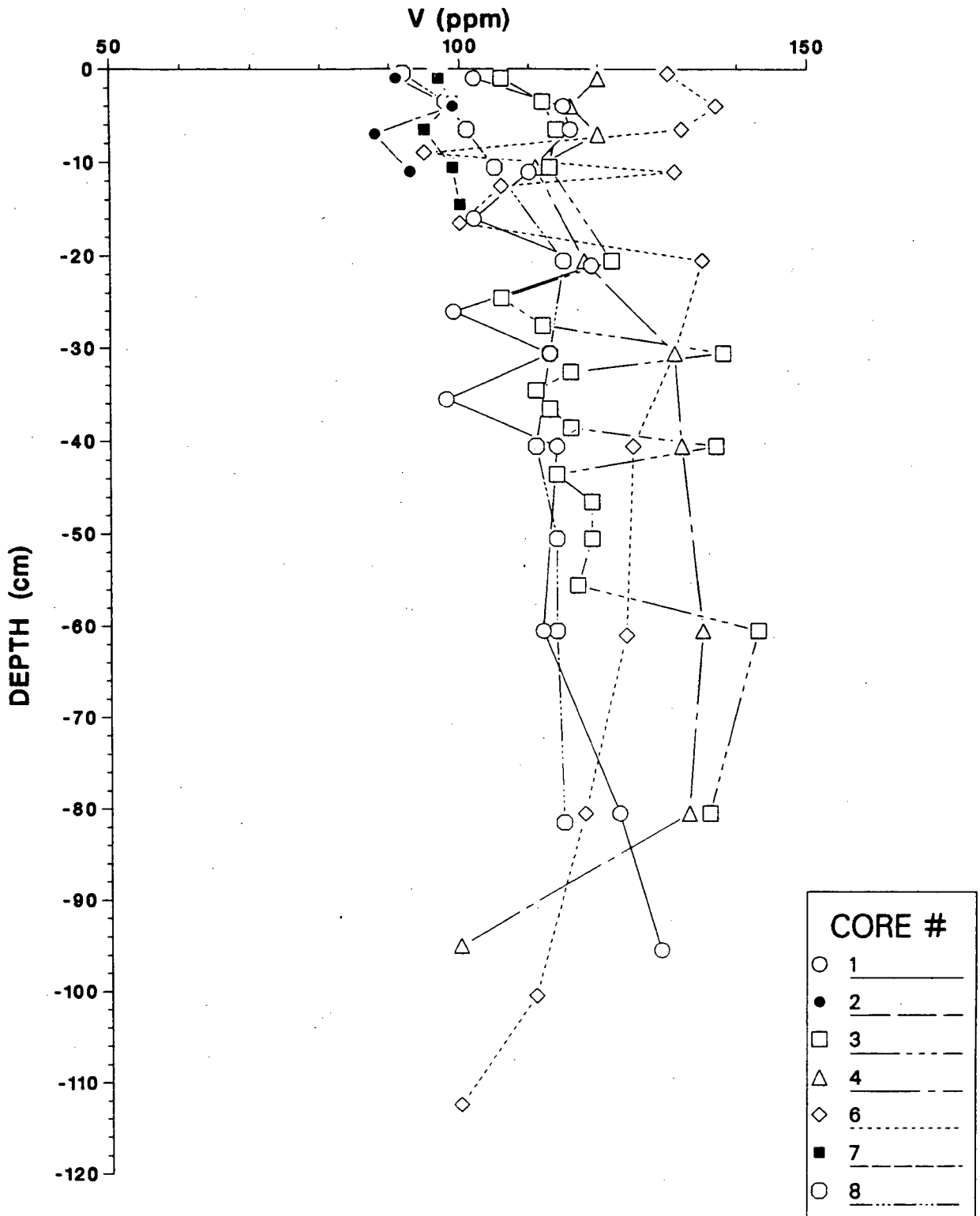


Figure 65: V distribution (ppm).

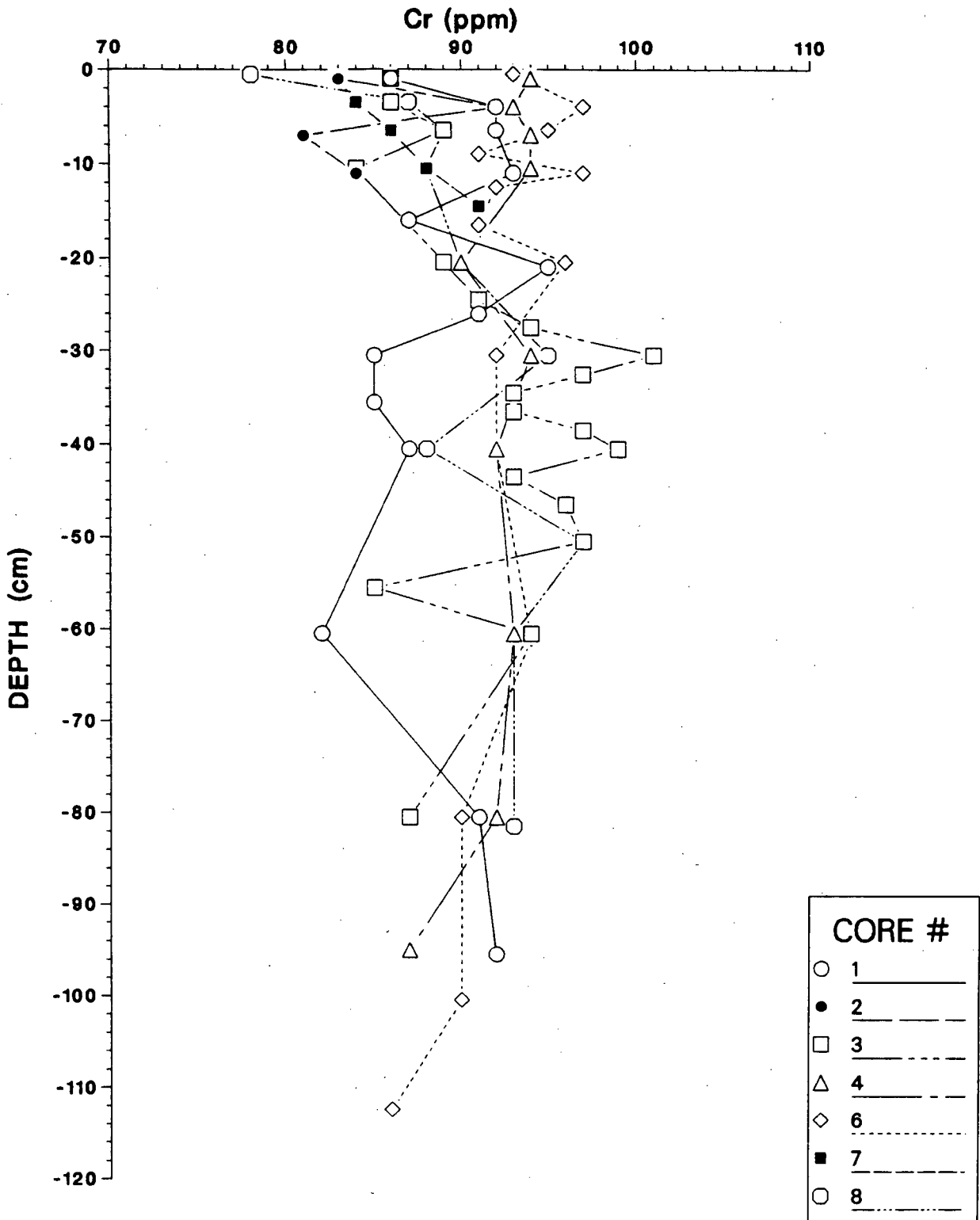


Figure 66: Cr distribution (ppm).

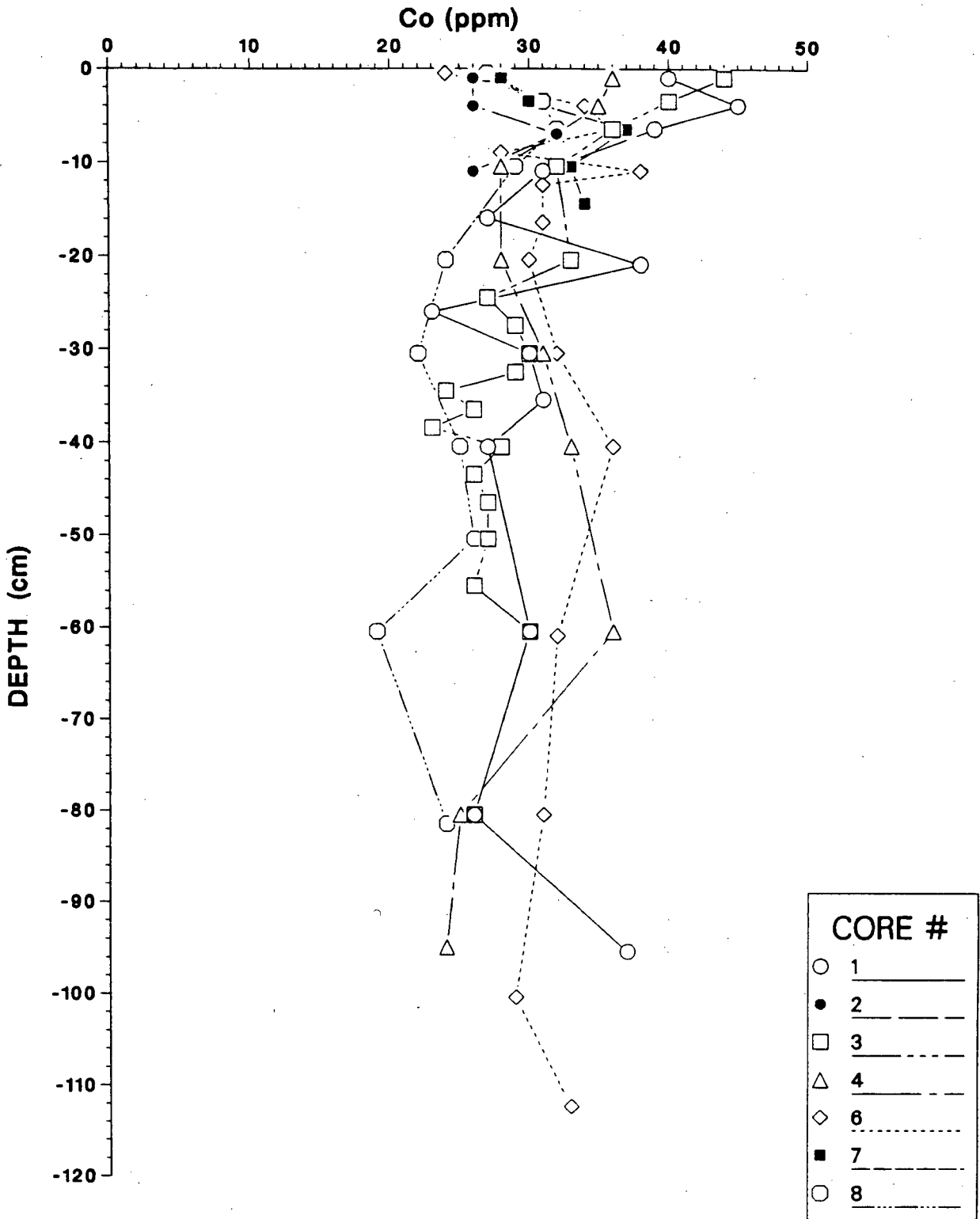


Figure 67: Co distribution (ppm).

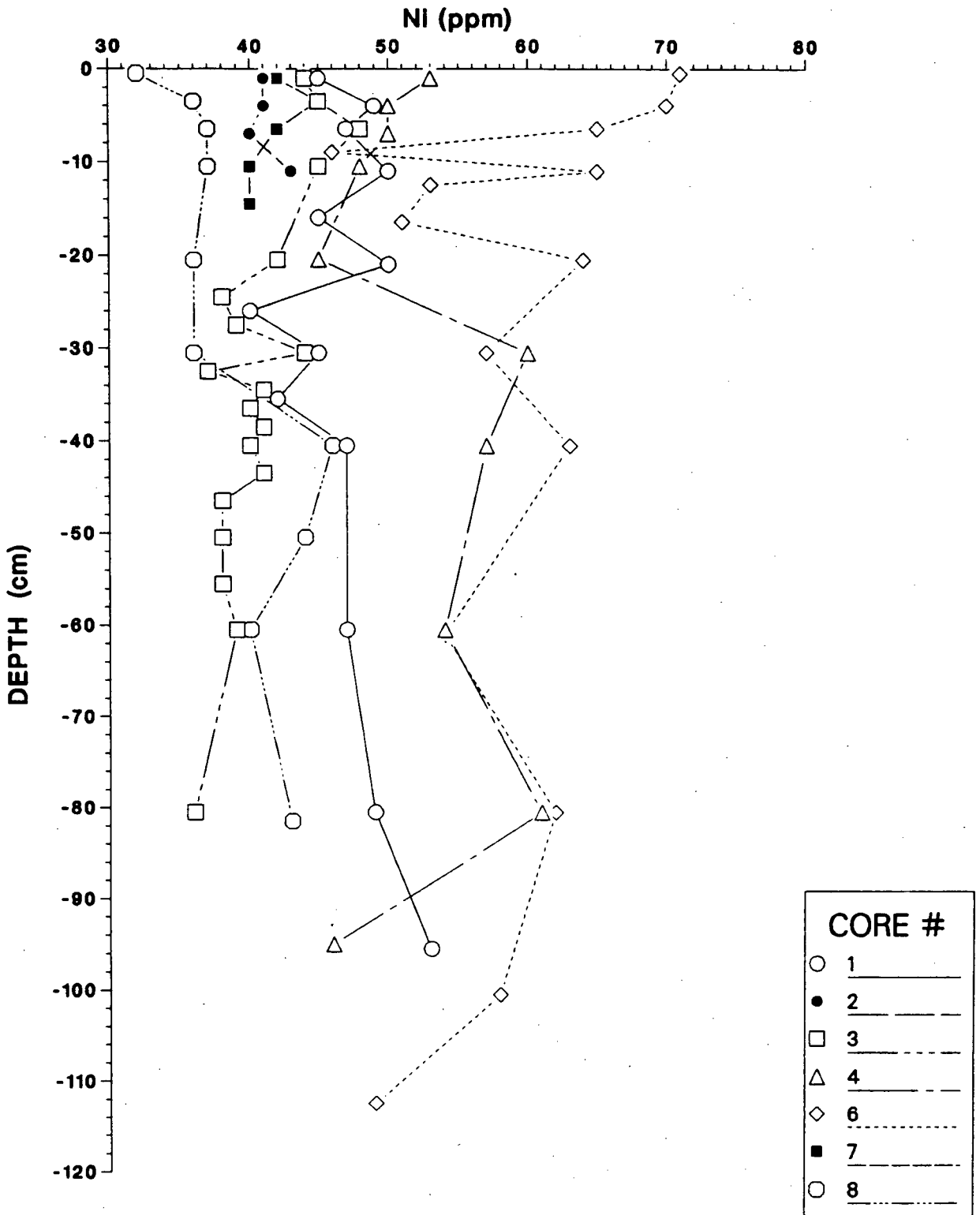


Figure 68: Ni distribution (ppm).

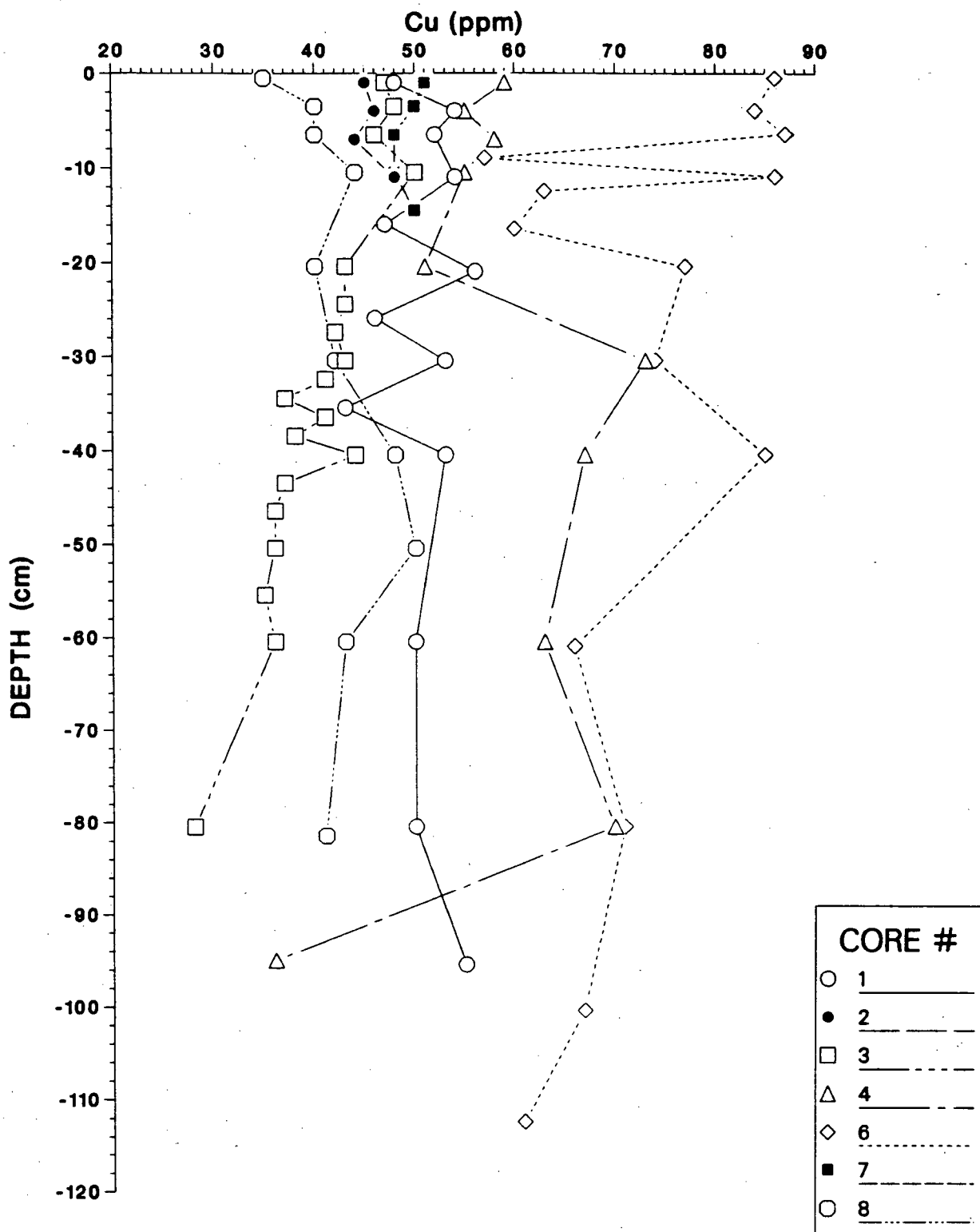


Figure 69: Cu distribution (ppm).

and Juan de Fuca ridges compare very closely with those from Tuzo Wilson Seamounts.

V and Cr values at Tuzo Wilson exhibit some similarities to each other but vary over narrow ranges. Co usually has a strong affinity for Mn-Fe oxyhydroxides (Murray, 1975); however here it exhibits little covariance with Mn and Fe suggesting that Mn- and Fe-bearing oxyhydroxides are essentially absent from these sediments.

The Ni, Cu and Zn distributions exhibit similarities and, like Ba and Rb, are higher in core 6 than in other cores. These elements occur in terrigenous mineral grains and are often associated to some extent with productivity. Cu is easily complexed with organic compounds (Goldberg and Arrhenius, 1958), and Pedersen (1979) attributed a Ni enrichment in a core from the Panama Basin to sorption of the metal from solution onto the organic phase. Plots of  $C_{Org}/N$  vs Cu, Ni, and Zn are shown in Fig. 70. Each metal exhibits an inverse relationship with the  $C_{Org}/N$  ratio. The cause of this relationship is not known. It is possible to speculate that the concentration of these metals is influenced to a certain extent by the proportion of marine organic matter. However, variations in other factors such as sedimentation rate (Pedersen *et al.*, 1986) and provenance may also be affecting metal distribution.

#### 6.2.4 MANGANESE

The participation of Mn in the oxidation-reduction cycle is a major aspect of sediment diagenesis (Murray *et al.*, 1984). Marine sediments typically have higher Mn concentrations near the surface because the element is remobilized from deeper sediments where reducing conditions prevail and is reprecipitated in the oxic layer at the surface (Lynn and Bonatti, 1965; Bender, 1971).

At Tuzo Wilson, Mn concentrations vary little with depth and are mostly around 550–700 ppm (Fig. 71). In contrast to this, cores from an area west of Explorer and Juan de Fuca ridges studied by Bornhold *et al.* (1981) have Mn contents varying from 460 to

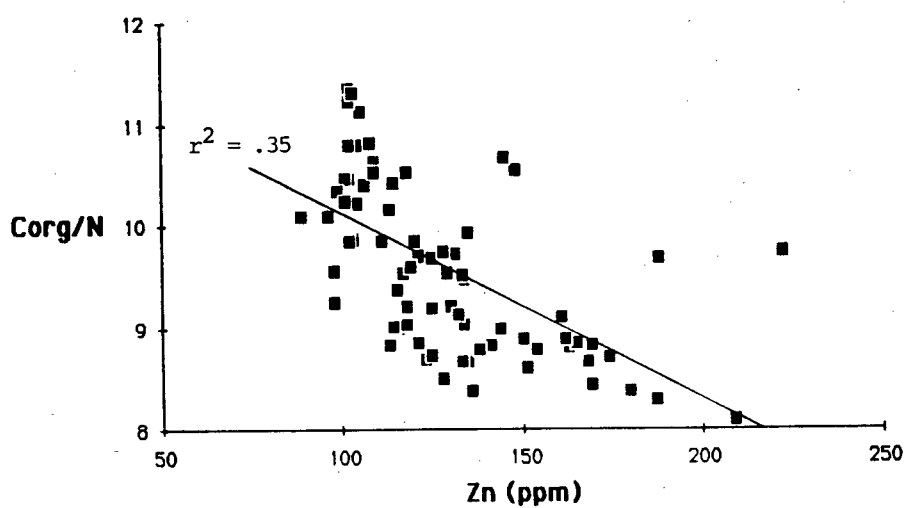
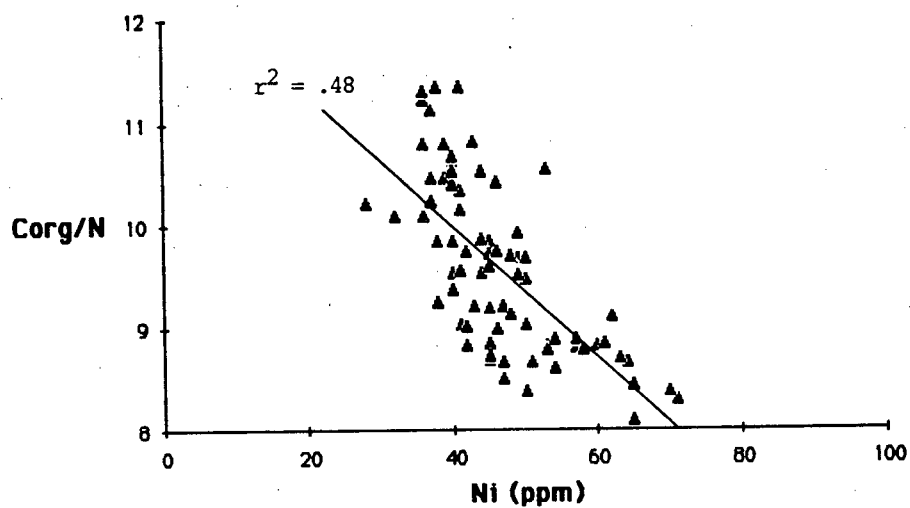
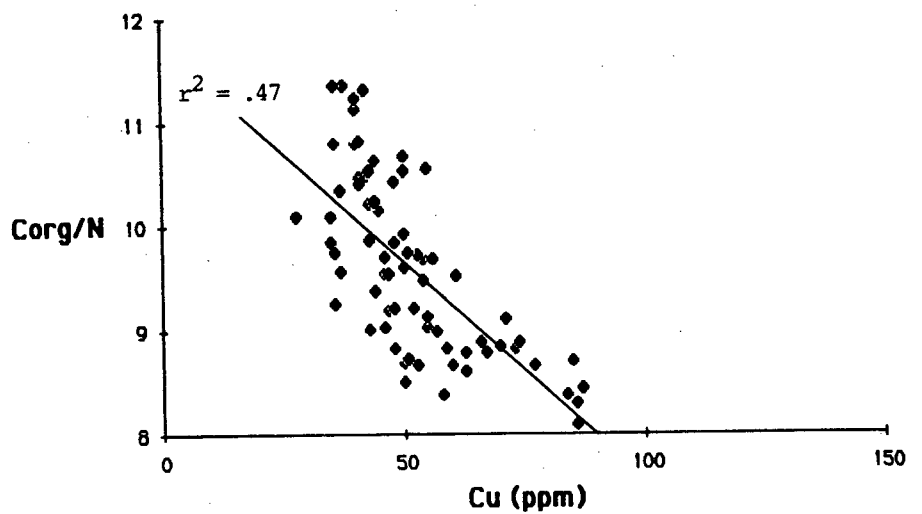


Figure 70: Plots of  $C_{org}/N$  vs Cu, Ni, and Zn.

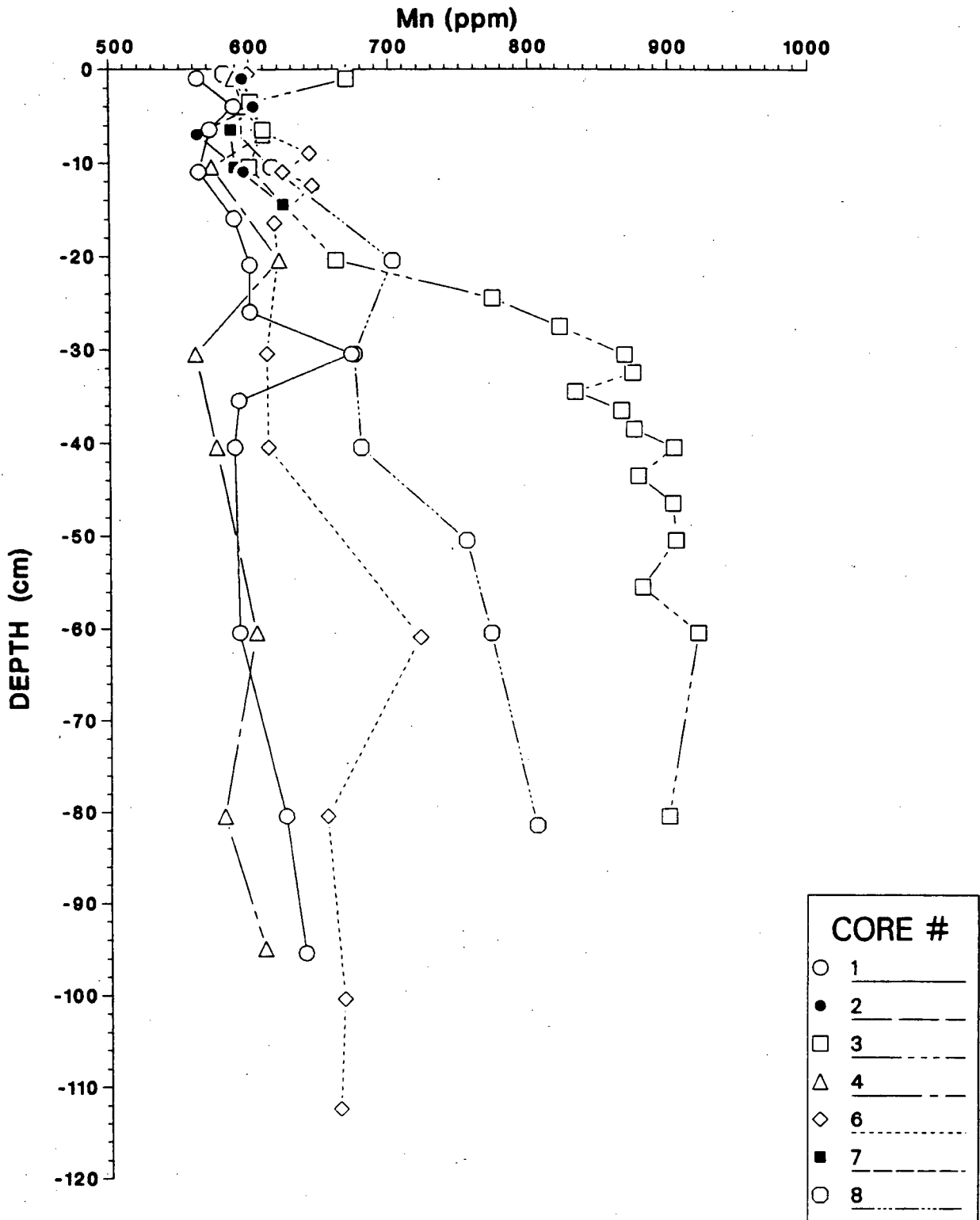


Figure 71: Mn distribution (ppm).

38,000 ppm (average 2100 ppm); some of these high values were attributed to hydrothermal activity. The relatively uniform and low values at Tuzo Wilson suggest that the hydrothermal component is absent and that diagenetic remobilization is not significant. This is supported by the lack of colour variation in the sediment.

### 6.3 THE EFFECT OF DEGLACIATION ON SEDIMENT GEOCHEMISTRY

The coincident geochemical changes of Si, Ca, Mg, Fe, and Mn in core 3 between 20 and 30 cm imply a change in provenance and depositional regime. The  $^{14}\text{C}$  dates obtained at depths of 46 and 60 cm (Fig. 34) support the contention that these changes occurred in response to climatic change and consequent rise in sealevel associated with deglaciation at the Pleistocene-Holocene transition.

The shift in the Rb/Zr ratio (Fig. 72) between 20 and 45 cm in core 3 also indicates a change in depositional conditions. The Rb/Zr ratio indicates that sedimentation during

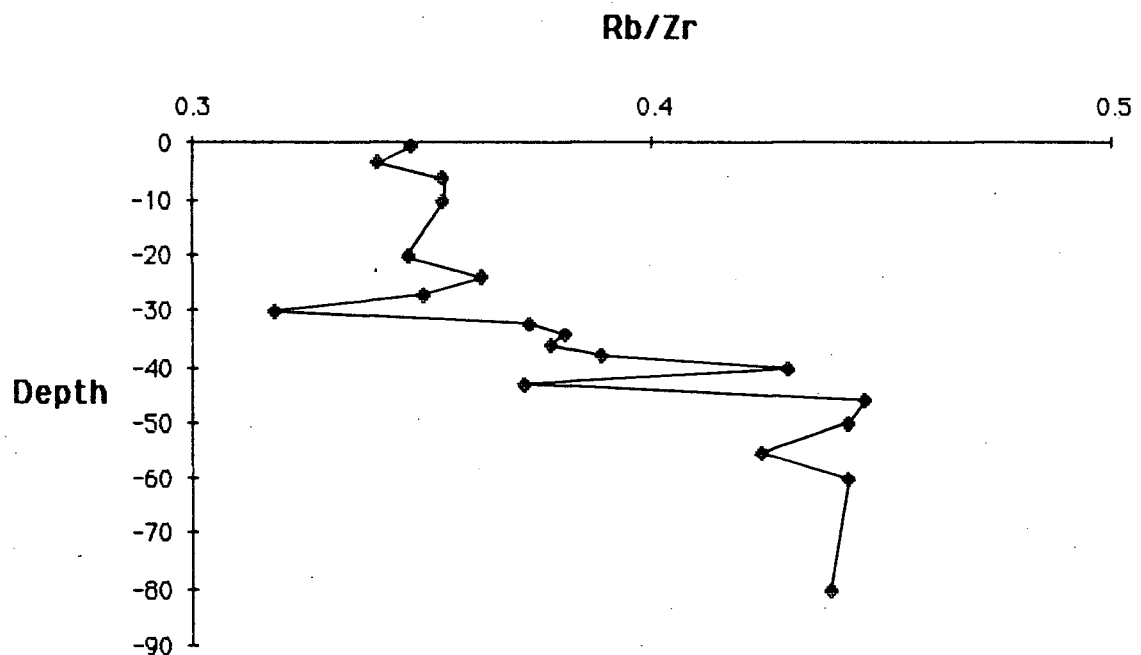


Figure 72: Rb/Zr ratio vs depth in core 3.

glaciation may have been dominated by immature sediment produced by intense glacial erosion whereas postglacial sediment has suffered some loss of Rb relative to Zr. Alternatively a change in grain size may have occurred. Zr is usually associated with coarser sediment because it occurs in the resistant mineral zircon. However, the basalt component in these sediments is significant enough to perturb the Zr distribution sufficiently to render the grain size relationship invalid. The Si/Al ratio (Fig. 39), which is also a grain size indicator, does not vary significantly in core 3, supporting this interpretation. The elevated Rb/Zr ratio therefore appears to be a result of dilution of basaltic debris by terrigenous sediment in the lower part of core 3. The low values of the Rb/Zr ratio at 30 and 43 cm depth are attributed to increased abundance of basaltic glass as discussed previously.

XRD was carried out on four samples (3–20, 24, 27, 30), as described in Appendix 1, to determine whether mineralogical changes could account for the higher Fe, Mg and Mn concentrations below 20 cm in core 3. These samples contain both chlorite and amphibole (Fig. 73). Chlorite contains both Fe and Mg and occurs in these cores in amounts up to 10% (see Chapter 4). Amphiboles also often contain both these elements. Mn is also known to occur in chlorite and amphiboles as well as in clay minerals and feldspars (Chester and Aston, 1976). If the increased abundance of these three elements is assumed to be caused solely by a change in chlorite and amphibole content, then the relative increase of Fe and Mn below 20 cm indicates that about 3% of the Fe in lattice positions is substituted by Mn.

Quartz/amphibole and quartz/chlorite peak-height ratios (Fig. 74) decrease down-core suggesting that the sediment below 20 cm is more amphibole- and chlorite-rich relative to quartz. Luternauer and Murray (1983) reported chlorite-rich glacial muds in Queen Charlotte Sound. This mineralogical change indicates that glacially-eroded sediment derived from the shelf is more abundant in the lower part of core 3.

In summary,  $^{14}\text{C}$  chronology demonstrates that core 3 penetrated the Pleistocene-Holocene transition. The abrupt geochemical and mineralogical changes in core 3 are

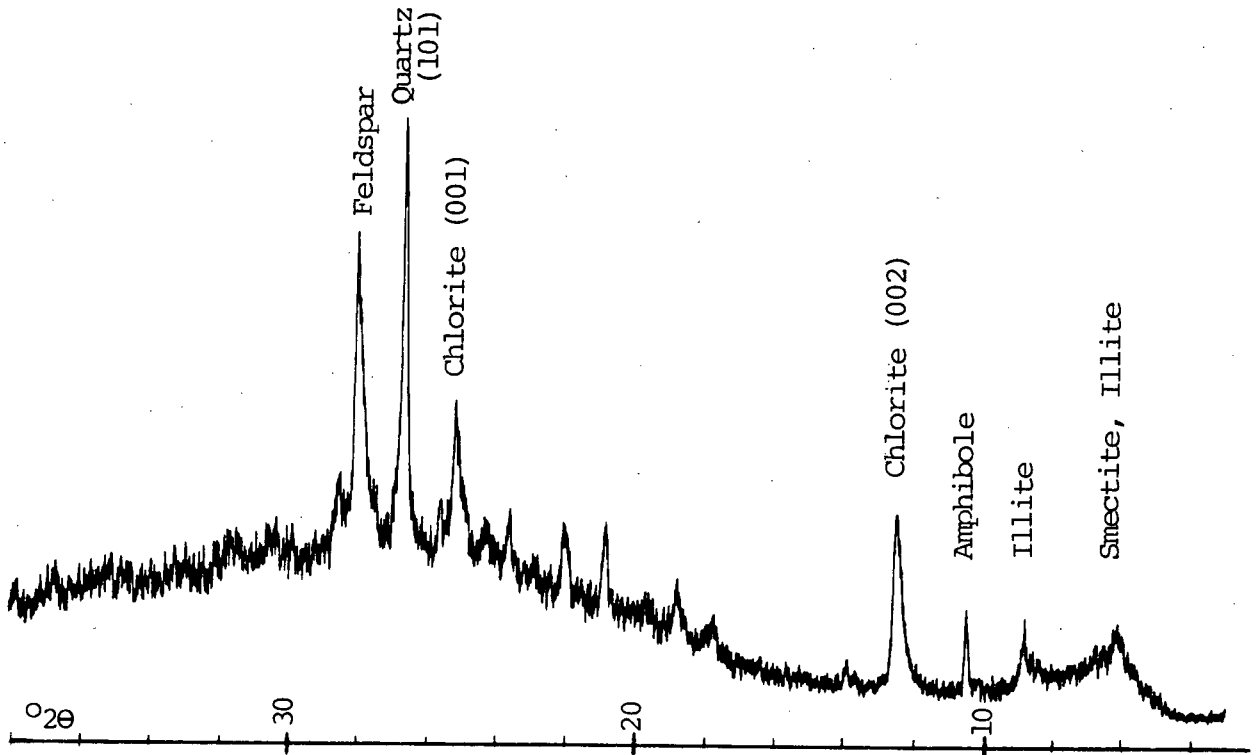


Figure 73: Diffractogram for  $<2\mu$  settled fraction of sample 3-27 showing quartz, feldspar, amphibole, chlorite and illite peaks.

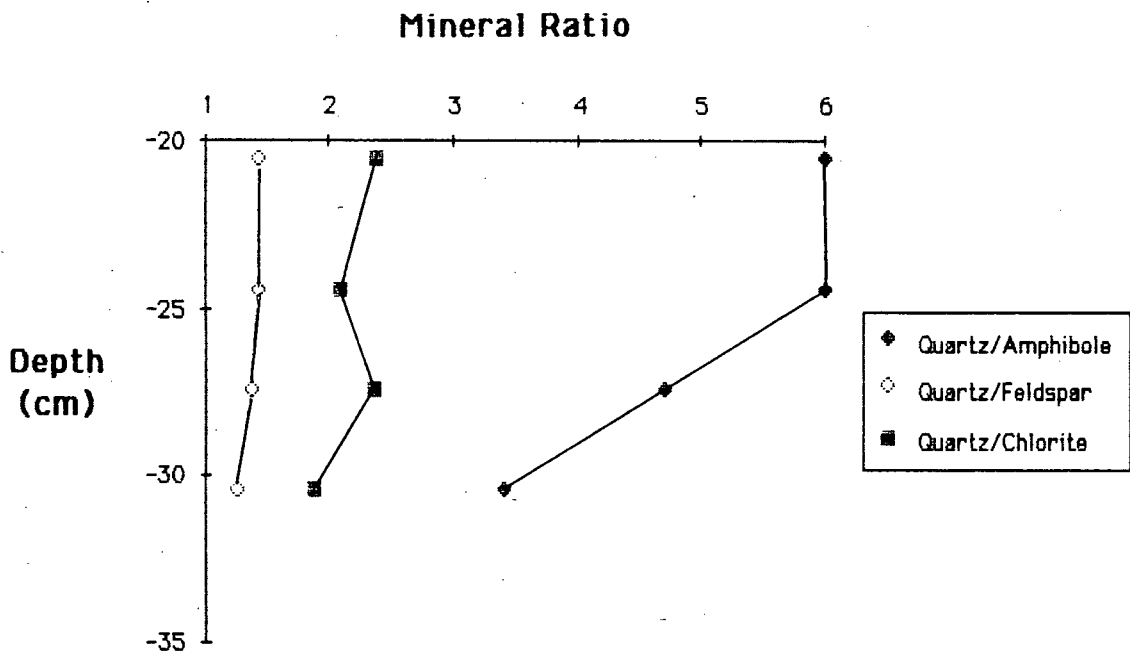


Figure 74: Quartz/feldspar, quartz/amphibole and quartz/chlorite XRD peak-height ratios for the  $<2\mu\text{m}$  fraction in core 3. Due to grinding, quartz represents all original size fractions.

probably therefore the result of a change in provenance which occurred as sealevel rose during deglaciation. The depth distribution of the  $I/C_{org}$  ratio suggests a lower Holocene sedimentation rate in core 3 explaining why climate-related geochemical changes are absent in the other cores.

## SUMMARY AND CONCLUSIONS

This study has examined the sediment geochemistry of seven short sediment cores collected along a fault scarp near the Tuzo Wilson Seamounts. Acoustic imagery and seafloor photographs have contributed to interpretation of the tectonics.

A number of conclusions arise out of this study:

1. Seafloor spreading may be occurring at Tuzo Wilson Seamounts and Dellwood Knolls simultaneously suggesting that the Queen Charlotte fault extends southeast past the Tuzo Wilson spreading segment to the Dellwood segment. This implies the existence of a separate plate, herein named the Tuzo Wilson microplate.
2. Conductivity-temperature measurements indicate that the fault scarp is a locus of hydrothermal venting.
3. Underwater camera tows did not provide any evidence of hydrothermal activity. However, frequent equipment failure, especially during tows in the scarp area, resulted in a complete lack of photographs coincident with the conductivity-temperature anomalies.
4. Sedimentation at Tuzo Wilson Seamounts in water depths of 1900–2500 m is dominated by terrigenous input due to the proximity of the seamounts to the shelf edge.
5. Sediment geochemistry does not reveal any evidence of hydrothermal activity even though the cores were located close to the scarp, probably due to the powerful diluting effect of terrigenous sedimentation.
6. Two accelerator  $^{14}\text{C}$  dates between 12,000 and 13,000 years in core 3 demonstrate that this core penetrated the Pleistocene-Holocene transition.
7. The  $^{14}\text{C}$  dates suggest that the sedimentation rate in core 3 has dropped since the Pleistocene, from about 16.5 to 3.0 cm ka $^{-1}$ , due to a combination of reduced erosion and lack of sediment transport across the shelf.
8. The unique geochemistry of many elements in core 3, supported by changes in

- mineralogy, suggests a change in provenance caused by climatic change near the Pleistocene-Holocene transition.
9. The depth distribution of  $I/C_{Org}$  ratios suggests a lower postglacial sedimentation rate in core 3 than in the other cores.
  10. Higher sedimentation rates in the other cores appear to have placed the Pleistocene-Holocene transition beyond the reach of gravity corers and explain why the geochemical and mineralogical changes in core 3 are absent in these cores.
  11.  $C_{Org}/N$  ratios indicate that organic matter is primarily of marine origin and suggest that the proportion of marine organic matter may increase with distance from the shelf. However, the ratios are higher than those found in sediments on the shelf, suggesting that the ratios have been perturbed by preferential degradation of nitrogenous organic matter in conjunction with lower sedimentation rates at Tuzo Wilson Seamounts.
  12. The distribution of the halogens I and Br is closely related to that of  $C_{Org}$ .
  13. Cu, Ni and Zn may be linked to biogenic productivity through their apparent preferential occurrence in conjunction with marine organic matter.
  14. The distribution of Mn and trace metals suggests that diagenetic remobilization of these elements is not significant.

Not all of the goals of this study have been realized, principally because the length of core recoverable was severely limited by the use of a gravity corer. Detection of accelerated diagenesis, for example, would have required much deeper penetration such as can only be obtained with a piston corer. Although this study failed to find geochemical evidence for a hydrothermal component in these sediments, the scarp is still considered to be a locus of hydrothermal activity.

The following recommendations arise out of this study:

1. Research into the tectonic setting and exploration for hydrothermal vents at Tuzo Wilson Seamounts should be continued in preparation for future submersible work.

2. An attempt should be made to determine if an extension of the Queen Charlotte fault connects the northeast ends of the Tuzo Wilson and Dellwood spreading segments, as suggested in this study.
3. The area of exploration for hydrothermal activity should be expanded to include the possibility of Oregon-type cold water vents which might occur along the base of the continental shelf, possibly in connection with the fault mentioned above (in 2).
4. A proposal should be submitted to the Ocean Drilling Program to drill a hole in the Tuzo Wilson area during the North Pacific leg in 1989. An important target is the area immediately to the south of the northeast seamount where a hole would reveal the nature of the rift valley that the seamounts occupy and the relationship between the seamounts and the underlying basement. A core extending back possibly as far as the late Tertiary, even if it consisted of intercalated lavas and sediment, would still provide useful palaeoceanographic information and a record of sedimentation during the glacial interglacial cycles of the Pleistocene. The core would also provide valuable information about the history of the growth of the seamounts, the composition of the buried flanks of the seamounts, petrologic trends, and would clarify the role of the Tuzo Wilson spreading segment in the tectonics of the Northeast Pacific.

## BIBLIOGRAPHY

- Abbey, S., 1980. Studies in "Standard Samples" for use in general analysis of silicate rocks and minerals, Part 6: 1979 edition of "usable": values, Geological Survey of Canada, Paper 80-14, 30p.
- Adshead, J.D., Bornhold, B.D., and Davis, E.E., 1986. Indurated deposits and possible plume bands in a hydrothermal mound, northeast Pacific, *In* Current Research, Part A, Geological Survey of Canada, Paper 86-1A, pp.737-748.
- Akrigg, G.P.V. and Akrigg, H.B., 1986. British Columbia place names, Sono Nis Press, Victoria, B.C., 346p.
- Anderson, R.N. and Hobart, M.A., 1976. The relation between heat flow, sediment thickness, and age in the eastern Pacific, *Journal of Geophysical Research*, v.81, pp.2968-2989.
- Au, D. and Clowes, R.M., 1982. Crustal structure from an OBS survey of the Nootka fault zone off western Canada, *Geophysical Journal of the Royal Astronomical Society*, v.68, pp.27-47.
- Ballard, R.D. and Francheteau, J., 1983. Geologic processes of the mid-ocean ridge and their relation to sulfide deposition, *Hydrothermal Processes at Seafloor Spreading Centres*, P.A. Rona, K. Boström, L. Laubier and K.L. Smith Jr., (eds.), Plenum Press, New York, pp.17-25.
- Barnard, W.D. and McManus, D.A., 1973. Planktonic foraminiferan-radiolarian stratigraphy at the Pleistocene-Holocene boundary in the Northeast Pacific, *Geological Society of America Bulletin*, v.84, pp.2097-2100.
- Barr, S.M., 1972. Geology of the northern end of Juan de Fuca ridge and adjacent continental slope, Unpublished Ph.D. Thesis, University of British Columbia, 286p.
- Barr, S.M., 1974. Structure and tectonics of the continental slope west of Vancouver Island, *Canadian Journal of Earth Sciences*, v.11, pp.1187-1199.
- Barr, S.M. and Chase, R.L., 1974. Geology of the northern end of Juan de Fuca ridge and sea-floor spreading, *Canadian Journal of Earth Sciences*, v.10, pp.1384-1406.
- Bender, M.L., 1971. Does upward diffusion supply the excess manganese in pelagic sediments?, *Journal of Geophysical Research*, v.76, pp.4212-4215.
- Benioff, H., 1962. Movements on major transcurrent faults, *In* Continental Drift, S.K. Runcorn, (ed.), Academic Press, New York, pp.103-134.
- Berger, W.H., 1976. Biogenous deep-sea sediments: production, preservation and interpretation, *In* Chemical Oceanography, Volume 5, J.P. Riley and R. Chester, (eds.), Academic Press, London, pp.265-388.
- Bertrand, W.G., 1972. A geological reconnaissance of the Dellwood seamount area, Northeast Pacific Ocean, and its relationship to plate tectonics, Unpublished M.Sc. Thesis, University of British Columbia, 151p.

- Blaise, B., Bornhold, B.D., Maillot, H., and Currie, R.G., 1984. Sedimentation near the Dellwood Knolls, northern Juan de Fuca ridge system, (abstract), EOS, Transactions of the American Geophysical Union, v.65, p.1112.
- Blaise B., Bornhold, B.D., Maillot, H., and Chamley, H., (in press). Observations sur les environnements recents au nord de la dorsale de Juan de Fuca (Pacifique Nord-Est).
- Bornhold, B.D., 1978. Carbon/nitrogen (C/N) ratios in surficial marine sediments of British Columbia, *In Current Research, Part C, Geological Survey of Canada, Paper 78-1C*, pp.108-112.
- Bornhold, B.D., 1986. Sedimentation on the Juan de Fuca ridge, (abstract), *In A Symposium on the Juan de Fuca Ridge – Programme and Abstracts, Pacific Section, Geological Association of Canada, Sidney, B.C., March 1986*, pp.28-30.
- Bornhold, B.D., Tiffin, D.L., and Currie R.G., 1981. Trace metal geochemistry of sediments, Northeast Pacific Ocean, Geological Survey of Canada, Paper 80-35, 21p.
- Bornhold, B.D. and Yorath, C.J., 1984. Surficial geology of the continental shelf, northwestern Vancouver Island, *Marine Geology*, v.57, pp.89-112.
- Brindley, G.W., 1981. X-Ray identification (with ancillary techniques) of clay minerals, *In Clays and the Resource Geologist, Mineralogical Association of Canada Short Course Handbook*, v.7, MAC, Toronto, pp.22-38.
- Bullard, E., 1975. The emergence of plate tectonics: a personal view, *In Annual Review of Earth and Planetary Sciences*, F.A. Donath, F.G. Stehli, and G.W. Wetherill, (eds.), v.3, Annual Reviews Inc., Palo Alto, California, pp.1-30.
- Calvert, S.E., 1976. The mineralogy and Geochemistry of near-shore sediments, *In Chemical Oceanography, Volume 6*, J.P. Riley and R. Chester, (eds.), Academic Press, London, pp.187-280.
- Carbotte, S.M., 1986. Geological and geophysical characteristics of the Tuzo Wilson Knolls and vicinity: triple junction tectonics in the NE Pacific, Unpublished M.Sc. Thesis, Queen's University, 274p.
- Carbotte, S.M., Dixon, J.M., Farrar, E., Davis, E.E., and Riddihough, R.P., 1986. Geological and geophysical characteristics, and geotectonic significance of the Tuzo Wilson Knolls, *In Geological Association of Canada, Program with Abstracts, Ottawa, 1986*, p.52.
- Carson, B. and Baker, E.T., 1983. Processes of offshore sediment dispersal around a submarine canyon, (abstract), EOS, Transactions of the American Geophysical Union, v.64, p. 1060.
- CASM (Canadian American Seamount Expedition), 1985. Hydrothermal vents on an axis seamount of the Juan de Fuca ridge, *Nature*, v.313, pp.212-214.
- Chase, R.L., 1977. J. Tuzo Wilson Knolls: Canadian hotspot, *Nature*, v. 266, pp.344-346.
- Chase, R.L. and Tiffin, D.L., 1972. Queen Charlotte fault-zone, British Columbia, *In Marine geology and geophysics, Section 8, 24th International Geological Congress, Montreal, 1972*, pp.17-27.

- Chase, R.L., Tiffin, D.L., and Murray, J.W., 1975. The Western Canadian continental margin, *In* Canada's Continental Margins and Offshore Petroleum Exploration, C.J. Yorath, E.R. Parker, and D.J. Glass (eds.), Canadian Society of Petroleum Geologists, Memoir 4, CSPG, Calgary, pp.701-721.
- Chester, R. and Aston, S.R., 1976. The geochemistry of deep-sea sediments, *In* Chemical Oceanography, Volume 6, J.P. Riley and R. Chester, (eds.), Academic Press, London, pp.281-390.
- Cheung, H.P.Y. and Clowes, R.M., 1981. Crustal structure from *P*- and *S*-wave analyses: ocean bottom seismometer results in the north-east Pacific, *Geophysical Journal of the Royal Astronomical Society*, v.65, pp.47-73.
- Clague, J.J., 1975. Late Quaternary sea level fluctuations, Pacific coast of Canada and adjacent areas, *In* Report of Activities, Part C, Geological Survey of Canada, Paper 75-1C, pp.17-21.
- Clague, J.J., 1978. Mid-Wisconsinian climates of the Pacific Northwest, *In* Current Research, Part B, Geological Survey of Canada, Paper 78-1B, pp.95-100.
- Clague, J.J., 1983. Glacio-isostatic effects of the Cordilleran Ice Sheet, British Columbia, Canada, *In* Shorelines and Isostasy, D.E. Smith and A.E. Dawson, (eds.), Institute of British Geographers Special Publication No. 16, Academic Press, London, pp.321-343.
- Clague, J.J., 1985. Deglaciation of the Prince Rupert - Kitimat area, British Columbia, *Canadian Journal of Earth Sciences*, v.22, pp.256-265.
- Clague, J.J., Armstrong, J.E., and Mathews, W.H., 1980. Advance of the Late Wisconsin Cordilleran ice sheet in southern British Columbia since 22,000 yr B.P., *Quaternary Research*, v.13, pp.322-326.
- Clague, J.J., Harper, J.R., Hebda, R.J., and Howes, D.E., 1982a. Late Quaternary sea levels and crustal movements, coastal British Columbia, *Canadian Journal of Earth Sciences*, v.19, pp.597-618.
- Clague, J.J., Mathews, R.W., and Warner, B.G., 1982b. Late Quaternary geology of Graham Island, Queen Charlotte Islands, British Columbia, *Canadian Journal of Earth Sciences*, v.19, pp.1786-1795.
- Clowes, R.M. and Gens-Lenartowicz, E., 1985. Upper crustal structure of southern Queen Charlotte Basin from sonobuoy refraction studies, *Canadian Journal of Earth Sciences*, v.22, pp.1696-1710.
- Clowes, R.M. and Knize, S., 1979. Crustal structure from a marine seismic survey off the west coast of Canada, *Canadian Journal of Earth Sciences*, v. 16, pp.1265-1280.
- Clowes, R.M., Thorleifson, A.J., and Lynch, S., 1981. Winona Basin, West Coast Canada: crustal structure from marine seismic studies, *Journal of Geophysical Research*, v.86, pp.225-242.
- Conolly, J.R. and Ewing, M., 1970. Ice-rafted detritus in Northwest Pacific deep-sea sediments, *In* Geological Investigations of the North Pacific, J.D. Hays, (ed.), Geological Society of America, Memoir 126, pp.219-231.

- Conway, K.W. and Luternauer, J.L., 1984. Longest core of Quaternary sediments from Queen Charlotte Sound: preliminary description and interpretation, *In Current Research, Part A, Geological Survey of Canada, Paper 84-1A*, pp.647-649.
- Conway, K.W. and Luternauer, J.L., 1985. Evidence of ice rafting and tractive transfer in cores from Queen Charlotte Sound, British Columbia, *In Current Research, Part A, Geological Survey of Canada, Paper 85-1A*, pp.703-708.
- Cook, R.A., 1981. Composition and stratigraphy of Late Quaternary sediments from the northern end of Juan de Fuca ridge, Unpublished M.Sc. Thesis, University of British Columbia, 107p.
- Corliss, J.B., Dymond, J., Gordon, L.I., Edmond, J.M., von Herzen, R.P., Ballard, R.D., Green, K., Williams, D., Bainbridge, A., Crane, K., and van Andel, T.H., 1979. Submarine Thermal springs on the Galapagos Rift, *Science*, v.203, pp.1073-1083.
- Couch, R. and Chase, R.L., 1973. Site survey of Paul Revere ridge west of northern Vancouver Island, *In L.D. Kulm, R. von Huene et al., 1973, Initial Reports of the Deep Sea Drilling Project, Volume 18, U.S. Government Printing Office, Washington*, pp.987-995.
- Cousens, B.L., 1982. Major and trace element geochemistry of basalts from the Explorer area, Northeast Pacific Ocean, Unpublished M.Sc. Thesis, University of British Columbia, 100p.
- Cousens, B.L., Chase, R.L., and Schilling, J-G., 1984. Basalt geochemistry of Explorer ridge area, Northeast Pacific Ocean, *Canadian Journal of Earth Sciences*, v.21, pp.157-170.
- Cousens, B.L., Chase, R.L., and Schilling, J-G., 1985. Geochemistry and origin of volcanic rocks from Tuzo Wilson and Bowie seamounts, Northeast Pacific Ocean, *Canadian Journal of Earth Sciences*, v.22, pp.1609-1617.
- Cox, A., (ed.), 1973. *Plate Tectonics and Geomagnetic Reversals*, W.H. Freeman, San Fransisco, 702p.
- Crane, K., 1985. The spacing of rift axis highs: dependence upon diapiric processes in the underlying asthenosphere?, *Earth and Planetary Science Letters*, v.72, pp.405-414.
- Crane, K., Aikman III, F., Embley, R., Hammond, S., Malahoff, A., and Lupton, J., 1985. The distribution of geothermal fields on the Juan de Fuca ridge, *Journal of Geophysical Research*, v.90, pp.727-744.
- Currie, R.G. and Bornhold, B.D., 1983. The magnetic susceptibility of continental-shelf sediments, west coast Vancouver Island, Canada, *Marine Geology*, v.51, pp.115-127.
- Currie, R.G. and Davis, E.E., 1986. Acoustic imagery over the northern Juan de Fuca ridge system, (abstract), *In A Symposium on the Juan de Fuca Ridge - Programme and Abstracts, Pacific Section, Geological Association of Canada, Sidney, B.C., March 1986*, pp.10-11.
- Currie, R.G., Tiffin, D.L., and Riddihough, R.P., 1980. Marine geophysical survey off the west coast of the Queen Charlotte Islands, (abstract), *EOS, Transactions of the American Geophysical Union*, v.61, p.71.

- Currie, R.G., Davis, E.E., Riddihough, R.P., and Hussong, D.M., 1984. Acoustic imagery of the Pacific-America-Explorer triple junction, (abstract), EOS, Transactions of the American Geophysical Union, v.65, p.1110.
- Davies, T.A. and Gorsline, D.S., 1976. Oceanic sediments and sedimentary processes, *In* Chemical Oceanography, Volume 5, J.P. Riley and R. Chester, (eds.), Academic Press, London, pp.1-80.
- Davis, E.E., 1981. Rapid diagenesis of marine turbidites in the Winona Basin, (abstract), EOS, Transactions of the American Geophysical Union, v.62, p.59.
- Davis, E.E., 1982. Evidence for extensive basalt flows on the sea floor, Geological Society of America Bulletin, v.93, pp.1023-1029.
- Davis, E.E. and Lister, C.R.B., 1977. Heat flow measured over the Juan de Fuca ridge: evidence for widespread hydrothermal circulation in a highly heat transportive crust, Journal of Geophysical Research, v.82, pp.4845-4860.
- Davis, E.E. and Lister, C.R.B., 1977. Tectonic structures on the Juan de Fuca ridge, Geological Society of America Bulletin v.88, pp.346-363.
- Davis, E.E. and Riddihough, R.P., 1981. Constraints on the recent history of the Queen Charlotte transform boundary as provided by the history of the Winona Basin, (abstract), EOS, Transactions of the American Geophysical Union, v.62, p.60.
- Davis, E.E. and Riddihough, R.P., 1982. The Winona Basin: structure and tectonics, Canadian Journal of Earth Sciences, v.19, pp.767-788.
- Davis, E.E. and Villinger, H., 1986. Heat flow and hydrothermal circulation: recent studies on the sedimented northern Juan de Fuca, (abstract), *In* A Symposium on the Juan de Fuca Ridge – Programme and Abstracts, Pacific Section, Geological Association of Canada, Sidney, B.C., March 1986, pp.31-32.
- Davis, E.E. and Clowes, R.M., 1986. High velocities and seismic anisotropy in Pleistocene turbidites off Western Canada, Geophysical Journal of the Royal Astronomical Society, v.84, pp.381-399.
- Davis, E.E., Lister, C.R.B., Wade, U.S., and Hyndman, R.D., 1980. Detailed heat flow measurements over the Juan de Fuca ridge system, Journal of Geophysical Research, v.85, pp.299-310.
- Davis, E.E., Currie, R.G., Sawyer, B.S., and Hussong, D.M., 1984. Juan de Fuca Ridge Atlas: SeaMARC II acoustic imagery, Earth Physics Branch, Energy Mines and Resources Canada, Open File 84-17, 21p + 164 images.
- Davis, E.E., Currie, R.G., Sawyer, B.S., and Riddihough, R.P., 1985. Juan de Fuca Ridge Atlas: SeaMARC II acoustic image mosaic (Wilson and Dellwood Knolls, 1:250,000), Earth Physics Branch, Energy Mines and Resources Canada, Open File 85-2.
- Dehler, S.A., Clowes, R.M., and Mackie, D.J., 1986. Seismic structural model of the Queen Charlotte fault zone, *In* Geological Association of Canada, Program with Abstracts, Ottawa, 1986, p.62.
- Dehlinger, P., Couch, R.W., McManus, D.A., and Gemperle, M., 1970. Northeast Pacific structure, *In* The Sea, Volume 4, A.E. Maxwell, (ed.), John Wiley and Sons, New York, pp.133-189.

- de Moustier, C. and Kleinrock, M.C., 1986. Bathymetric artifacts in Sea Beam data: how to recognize them and what causes them, *Journal of Geophysical Research*, v.91, pp.3407-3424.
- Denton, A.S., 1986. The U.B.C. Deep-tow camera system, an operating manual, Unpublished instruction manual, University of British Columbia, 25p.
- Detrick, R.S., 1986. Introduction to the seafloor mapping section, *Journal of Geophysical Research Special Section*, *Journal of Geophysical Research*, v.91, pp.3331-3333.
- Duncan, J.R., Kulm, L.D., and Griggs, G.B., 1970. Clay mineral composition Late Pleistocene and Holocene sediments of Cascadia Basin, Northeast Pacific Ocean, *Journal of Geology*, v.78, pp.213-221.
- Ellis, R.M., Spence, G.D., Clowes, R.M., Waldron, D.A., Jones, I.F., Green, A.G., Forsyth, D.A., Mair, J.A., Berry, M.J., Mereu, R.F., Kanasewich, E.R., Cumming, G.L., Hajnal, Z., Hyndman, R.D., McMechan, G.A., and Loncarevic, B.D., 1983. The Vancouver Island Seismic Project: A CO-Crust onshore-offshore study of a convergent margin, *Canadian Journal of Earth Sciences*, v.20, pp.719-741.
- Ewing, J., Ewing, M., Aitken, T., and Ludwig, W.J., 1968. North Pacific sediment layers measured by seismic profiling, *American Geophysical Union, Geophysical Monograph* 12, pp.147-173.
- Fletcher, W.K., 1981. X-Ray Fluorescence, *In Handbook of exploration geochemistry, Volume 1*, G.J.S. Govett, (ed.), Elsevier, Amsterdam, pp.167-197.
- Francheteau, J., 1983. The oceanic crust, *Scientific American*, v.249, pp.114-129.
- Freeland, H.J., Crawford, W.R., and Thomson, R.E., 1984. Currents along the Pacific Coast of Canada, *Atmosphere-Ocean*, v.22, pp.151-172.
- Gibson, W.M., 1960. Submarine topography in the Gulf of Alaska, *Geological Society of America Bulletin*, v.71, pp.1087-1108.
- Goldberg, E.D. and Arrhenius, G.O.S., 1958. Chemistry of Pacific pelagic sediments, *Geochimica et Cosmochimica Acta*, v.13, pp.153-212.
- Griggs, G.B. and Kulm, L.D., 1970. Sedimentation in Cascadia deep-sea channel, *Geological Society of America Bulletin*, v.81, pp.1361-1384.
- Griggs, G.B., Kulm, L.D., Duncan, J.R., and Fowler, G.A., 1970. Holocene faunal stratigraphy and paleoclimatic implications of deep-sea sediments in Cascadia Basin, *Palaeogeography, Palaeoclimatology and Palaeoecology*, v.7, pp.5-12.
- Grill, E.V., Chase, R.L., MacDonald, R.D., and Murray, J.W., 1981. A hydrothermal deposit from Explorer ridge in the Northeast Pacific Ocean, *Earth and Planetary Science Letters*, v. 52, pp.142-150.
- Haimila, N.E. and Proctor, R.M., 1982. Hydrocarbon potential of offshore British Columbia, *Geological Survey of Canada, Open File* 824, 28p.
- Hamilton, E.L., 1967. Marine geology of abyssal plains in Gulf of Alaska, *Journal of Geophysical Research*, v. 72, pp.4189-4213.

- Hannington, M.D., 1986. Geology, mineralogy and geochemistry of a silica-sulphate-sulfide deposit, Axial Seamount, N.E. Pacific Ocean, Unpublished Ph.D. Thesis, University of Toronto, 473p.
- Hansen, K.F., 1984. Geochemistry and mineralogy of sediments from southeast Explorer Rift (50°N; 130°W), Northeast Pacific: in search of hydrothermal activity, Unpublished M.Sc. Thesis, University of British Columbia, 281p.
- Heath, G.R., Moore Jr., T.C., and Roberts, G.L., 1974. Mineralogy of surface sediments from the Panama Basin, Eastern Equatorial Pacific, *Journal of Geology*, v.82, pp.145-160.
- Heath, G.R., Moore Jr., T.C., and Dauphin, J.P., 1976. Late Quaternary accumulation rates of opal, quartz, organic carbon, and calcium carbonate in the Cascadia Basin area, Northeast Pacific, *In Investigation of Late Quaternary Paleooceanography and Paleoclimatology*, R.M. Cline and J.D. Hays, (eds.), Geological Society of America, Memoir 145, pp.393-409.
- Hedges, R.E.M. and Gowlett, J.A.J., 1984. Accelerator radiocarbon dating, *Nature*, v.308, pp.403-404.
- Hedges, R.E.M. and Gowlett, J.A.J., 1986. Radiocarbon dating by accelerator mass spectrometry, *Scientific American*, v.254, pp.100-107.
- Heezen, B.C., 1962. The Deep-Sea Floor, *In Continental Drift*, S.K. Runcorn, (ed.), Academic Press, New York, pp.235-288.
- Heezen, B.C., Tharp, M., and Ewing, M., 1959. The Floors of the Oceans, I. The North Atlantic, Geological Society of America, Special Paper 65, 122p.
- Heezen, B.C. and Tharp, M., 1965. Tectonic fabric of Atlantic and Indian Oceans and continental drift, *In Symposium on continental drift*, P.M.S. Blackett, E.C. Bullard and S.K. Runcorn, (eds.), The Royal Society, London, pp.90-108.
- Herzer, R.H. and Bornhold, B.D., 1982. Glaciation and post-glacial history of the continental shelf off southwestern Vancouver Island, British Columbia, *Marine Geology*, v.48, pp.285-319.
- Hess, H.H., 1962. History of Ocean Basins, *In Petrologic studies: a volume in honor of A.F. Buddington; A.E.J. Engel, H.L. James, and B.F. Leonard*, (eds.), Geological Society of America, pp.599-620.
- Hess, H.H., 1965. Mid-ocean ridges and tectonics of the sea floor, *In Submarine Geology and Geophysics*, W.F. Whittard and R. Bradshaw, (eds.), Butterworth, London, pp.317-332.
- Heusser, C.J., Heusser, L.E., and Peteet, D.M., 1985. Late-Quaternary climatic change on the American North Pacific Coast, *Nature*, v.315, pp.485-487.
- Hodgson, J.H. and Milne, W.G., 1951. Direction of faulting in certain earthquakes of the North Pacific, *Bulletin of the Seismological Society of America*, v.41, pp.221-242.
- Holmes, A., 1931. Radioactivity and earth movements, Geological Society of Glasgow, *Transactions*, v.18, pp.559-606.

- Horn, D.R., Horn, B.M., and Delach, M.N., 1970. Sedimentary provinces of the North Pacific, *In Geological Investigations of the North Pacific*, J.D. Hays, (ed.), Geological Society of America, Memoir 126, pp.1-21.
- Horn, D.R., Ewing, M., Delach, M.N., and Horn, B.M., 1971. Turbidites of the Northeast Pacific, *Sedimentology*, v.16, pp.55-69.
- Horn, J.R., Bird, D.N., Ellis, R.M., and Clowes, R.M., 1981. Refraction studies across the southern Queen Charlotte fault zone, (abstract), EOS, Transactions of the American Geophysical Union, v.62, p.60.
- Horn, J.R., Clowes, R.M., Ellis, R.M., and Bird, D.N., 1984. The seismic structure across an active oceanic/continental transform fault zone, *Journal of Geophysical Research*, v.89, pp.3107-3120.
- Howell, D.G. and Normark, W.R., 1982. Sedimentology of submarine fans, *In Sandstone Depositional Environments*, P.A. Scholle and D. Spearing, (eds.), American Association of Petroleum Geologists, Tulsa, Oklahoma, pp.365-404.
- Hyndman, R.D., 1983. Juan de Fuca Plate Map: JPF-10, Geothermal Heat Flux (1:2,000,000 map), Pacific Geoscience Centre and Earth Physics Branch, Energy, Mines and Resources Canada.
- Hyndman, R.D. and Ellis, R.M., 1981a. Queen Charlotte fault zone: microearthquakes from a temporary array of land stations and ocean bottom seismographs, (abstract), EOS, Transactions of the American Geophysical Union, v.62, p.60.
- Hyndman, R.D. and Ellis, R.M., 1981b. Queen Charlotte fault zone: microearthquakes from a temporary array of land stations and ocean bottom seismographs, *Canadian Journal of Earth Sciences*, v.18, pp.776-788.
- Hyndman, R.D. and Rogers, G.C., 1981. Seismicity surveys with ocean bottom seismographs off Western Canada, *Journal of Geophysical Research*, v.86, pp.3867-3880.
- Hyndman, R.D. and Weichert, D.H., 1983. Seismicity and rates of relative motion on the plate boundaries of Western North America, *Geophysical Journal of the Royal Astronomical Society*, v.72, pp.59-82.
- Hyndman, R.D. and Weichert, D.H., 1986. Seismicity and rates of relative motion on the transform faults of the Juan de Fuca ridge system, (abstract), *In A Symposium on the Juan de Fuca Ridge - Programme and Abstracts*, Pacific Section, Geological Association of Canada, Sidney, B.C., March 1986, pp.12-13.
- Hyndman, R.D., Rogers, G.C., Bone, M.N., Lister, C.R.B., Wade, U.S., Barrett, D.L., Davis, E.E., Lewis, T., Lynch, S., and Seemann, D., 1978. Geophysical measurements in the region of the Explorer ridge off Western Canada, *Canadian Journal of Earth Sciences*, v.15, pp.1508-1525.
- Hyndman, R.D., Riddihough, R.P., and Herzer, R., 1979. The Nootka fault zone - a new plate boundary off Western Canada, *Geophysical Journal of the Royal Astronomical Society*, v.58, pp.667-683.
- Hyndman, R.D., Lewis, T., Wright, J.M., and Burgess, M., 1981. Queen Charlotte fault zone: heat flow measurements, (abstract), EOS, Transactions of the American Geophysical Union, v.62, p.60.

- Hyndman, R.D., Lewis, T., Wright, J.M., Burgess, M., Chapman, D.S., and Yamano, M., 1982. Queen Charlotte fault zone: heat flow measurements, *Canadian Journal of Earth Sciences*, v.19, pp.1657-1669.
- Isacks, B., Oliver, J., and Sykes, L.R., 1968. Seismology and the new global tectonics, *Journal of Geophysical Research*, v.73, pp.5855-5899.
- Johnson Ibach, L.E., 1982. Relationship between sedimentation rate and total organic carbon content in ancient marine sediments, *American Association of Petroleum Geologists Bulletin*, v.66, pp.170-188.
- Keen, C.E. and Hyndman, R.D., 1979. Geophysical review of the continental margins of eastern and western Canada, *Canadian Journal of Earth Sciences*, v.16, pp.712-747.
- Kelts, K. and Arthur, M.A., 1981. Turbidites after ten years of deep-sea drilling – Wringing out the mop? *In DSDP: A Decade of Progress*, J.E. Warne, R.G. Douglas, and E.L. Winterer, (eds.), Society of Economic Paleontologists and Mineralogists, Special Publication No. 32, SEPM, Tulsa, Oklahoma, pp.91-127.
- Kennett, J.P., 1982. *Marine Geology*, Prentice-Hall, Englewood Cliffs, N.J., 813p.
- Kolla, V., Biscaye, P.E., and Hanley, A.F., 1979. Distribution of quartz in Late Quaternary Atlantic sediments in relation to climate, *Quaternary Research*, v.11, pp.261-277.
- Kulm, L.D. and Scheidegger, K.F., 1979. Quaternary sedimentation on the tectonically active Oregon continental slope, *In Geology of Continental Slopes*, L.J. Doyle and O.H. Pilkey, (eds.), Society of Economic Paleontologists and Mineralogists, Special Publication No. 27, SEPM, Tulsa, Oklahoma, pp.247-263.
- Kulm, L.D., von Huene, R., *et al.*, 1973. Site 177, *In Kulm, L.D., von Huene, R., et al.*, Initial Reports of the Deep Sea Drilling Project, Volume 18, U.S. Government Printing Office, Washington, pp.233-285.
- Leinen, M., 1984. Rates of hydrothermal sedimentation on the Juan de Fuca ridge, (abstract), *EOS, Transactions of the American Geophysical Union*, v.65, p.1112.
- Leinen, M. and Heath, G.R., 1981. Sedimentary indicators of atmospheric activity in the northern hemisphere during the Cenozoic, *Palaeogeography, Palaeoclimatology and Palaeoecology*, v.36, pp.1-21.
- Lewis, D.W., 1984. *Practical sedimentology*, Van Nostrand Reinhold, New York, 229p.
- Lister, C.R.B., 1970. Heat flow on the Juan de Fuca ridge, *Journal of Geophysical Research*, v.75, pp.2648-2654.
- Lister, C.R.B., 1972. On the thermal balance of a mid-ocean ridge, *Geophysical Journal of the Royal Astronomical Society*, v.26, pp.515-535.
- Lonsdale, P., 1977. Deep-tow observations at the mounds abyssal hydrothermal field, Galapagos rift, *Earth and Planetary Science Letters*, v.36, pp.92-110.
- Lonsdale, P. and Becker, K., 1985. Hydrothermal plumes, hot springs, and conductive heat flow in the Southern Trough of Guaymas Basin, *Earth and Planetary Science Letters*, v.73, pp.211-225.

- Lonsdale, P.F., Bischoff, J.L., Burns, V.M., Kastner, M., and Sweeney, R.E., 1980. A high-temperature hydrothermal deposit on the seabed at a Gulf of California spreading centre, *Earth and Planetary Science Letters*, v.49, pp.8-20.
- Luternauer, J.L., 1972. Patterns of sedimentation in Queen Charlotte Sound, British Columbia, Unpublished Ph.D. Thesis, University of British Columbia, 203p.
- Luternauer, J.L. and Murray, J.W., 1983. Late Quaternary morphologic development and sedimentation, central British Columbia continental shelf, Geological Survey of Canada, Paper 83-21, 38p.
- Lynn, D.C. and Bonatti, E., 1965. Mobility of manganese in diagenesis of deep-sea sediments, *Marine Geology*, v.3, pp.457-474.
- Macdonald, K.C., 1982. Mid-ocean ridges: fine scale tectonic, volcanic and hydrothermal processes within the plate boundary zone, *Annual Review of Earth and Planetary Sciences*, F.A. Donath, F.G. Stehli, and G.W. Wetherill, (eds.), v.10, pp.155-190.
- Mairs, H., Leinen, M., Oakman, M.R., Jenkins, J., and Kadko, D., 1985. A 600 ky record of hydrothermal sedimentation in the vicinity of the Juan de Fuca ridge, (abstract), *EOS, Transactions of the American Geophysical Union*, v.66, p.930.
- Malacek, S.T. and Clowes, R.M., 1978. Crustal structure near Explorer ridge from a marine deep seismic sounding survey, *Journal of Geophysical Research*, v.83, pp.5899-5912.
- Malahoff, A., Hammond, S.R., Embley, R.W., Currie, R.G., Davis, E.E., Riddihough, R.P., and Sawyer, B.S., 1984. Juan de Fuca Ridge Atlas, Preliminary SEABEAM Bathymetry Sheet 102 O/6,7 (1:50,000 map), Earth Physics Branch, Energy Mines and Resources Canada, Open File 84-6.
- Malott, M.L., 1981. Distribution of foraminifera in cores from Juan de Fuca ridge, North East Pacific, Unpublished M.Sc. Thesis, University of British Columbia, 136p.
- Mammerickx, J. and Taylor, I.L., 1971. Bathymetry of the *Pioneer* survey area north of 45°N Lat., *Scripps Institution of Oceanography, Special Chart No. 1*.
- Mason, R.G., 1958. A magnetic survey off the west coast of the United States between latitudes 32° and 36°N. and longitudes 121° and 128°W., *Geophysical Journal of the Royal Astronomical Society*, v.1, pp.320-329.
- Mason, R.G. and Raff, A.D., 1961. Magnetic survey off the west coast of the United States, 32°N. latitude to 42°N. latitude, *Geological Society of America Bulletin*, v.72, pp.1259-1266.
- Mathewes, R.W. and Clague, J.J., 1982. Stratigraphic relationships and paleoecology of a late-glacial peat bed from the Queen Charlotte Islands, British Columbia, *Canadian Journal of Earth Sciences*, v.19, pp.1185-1195.
- Mathewes, R.W., Vogel, J.S., Southon, J.R., and Nelson, D.E., 1985. Accelerator radiocarbon date confirms early deglaciation of Queen Charlotte Islands, *Canadian Journal of Earth Sciences*, v.22, pp.790-791.
- Mathews, W.H., Fyles, J.G., and Nasmith, H.W., 1970. Postglacial crustal movements in southwestern British Columbia and adjacent Washington state, *Canadian Journal of Earth Sciences*, v.7, pp.690-702.

- McKenzie, D.P. and Morgan, W.J., 1969. The evolution of triple junctions, *Nature*, v.224, pp.125-133.
- McKenzie, D.P. and Parker, R.L., 1967. The North Pacific: An example of tectonics on a sphere, *Nature*, v.216, pp.1276-1280.
- McManus, D.A., 1967. Physiography of Cobb and Gorda Rises, Northeast Pacific Ocean, *Geological Society of America Bulletin*, v.78, pp.527-546.
- McManus, D.A., Holmes, M.L., Carson, B., and Barr, S.M., 1972. Late Quaternary tectonics, northern end of Juan de Fuca ridge (Northeast Pacific), *Marine Geology*, v.12, pp.141-164.
- Menard, H.W., 1964. *Marine Geology of the Pacific*, McGraw-Hill, New York, 271p.
- Menard, H.W. and Atwater, T., 1969. Origin of fracture zone topography, *Nature*, v.222, pp.1037-1040.
- Michael, P.J. and Chase, R.L., 1985. Trace element and Sr-isotope variations in basalts from the Explorer, Dellwood and Tuzo Wilson Spreading segments and seamounts, Northeast Pacific, (abstract), EOS, Transactions of the American Geophysical Union, v.66, p.926.
- Michael, P.J., Chase, R.L., Shea, G.T., and Massey, N., 1986. Chemistry of basalts from north of the Sovanco fracture zone, Northeast Pacific Ocean, (abstract), *In A Symposium on the Juan de Fuca Ridge – Programme and Abstracts, Pacific Section, Geological Association of Canada, Sidney, B.C., March 1986*, pp.26-27.
- Milne, W.G., Rogers, G.C., Riddihough, R.P., McMechan, G.A., and Hyndman, R.D., 1978. Seismicity of Western Canada, *Canadian Journal of Earth Sciences*, v.15, pp. 1170-1193.
- Minster, J.B., Jordan, T.H., Molnar, P. and Haines, E., 1974. Numerical modelling of instantaneous plate tectonics, *Geophysical Journal of the Royal Astronomical Society*, v.36, pp.541-576.
- Minster, J.B. and Jordan, T.H., 1978. Present-day plate motions, *Journal of Geophysical Research*, v.83, pp.5331-5354.
- Moen, A.D., 1971. Symposium on tectonism in the Pacific Northwest, (abstract), EOS, Transactions of the American Geophysical Union, v.52, pp.628-645.
- Morgan, W.J., 1968. Rises, trenches, great faults and crustal blocks, *Journal of Geophysical Research*, v.73, pp.1959-1982.
- Morgan, J.P. and Parmentier, E.M., 1984. Lithospheric stress near a ridge-transform intersection, *Geophysical Research Letters*, v.11, pp.113-116.
- Müller, P.J., 1977. C/N ratios in Pacific deep-sea sediments: Effects of inorganic ammonium and organic nitrogen compounds sorbed by clays, *Geochimica et Cosmochimica Acta*, v.41, pp.765-776.
- Müller, P.J. and Suess, E., 1979. Productivity, sedimentation rate, and sedimentary organic matter in the oceans – I. Organic carbon preservation, *Deep-Sea Research*, v.26A, pp.1347-1362.

- Murray, J.W., 1975. The interaction of cobalt with hydrous manganese dioxide, *Geochimica et Cosmochimica Acta*, v.39, pp.635-647.
- Murray, J.W., Balistrieri, L.S., and Paul, B., 1984. The oxidation state of manganese in marine sediments and ferromanganese nodules, *Geochimica et Cosmochimica Acta*, v.48, pp.1237-1247.
- Nayudu, Y.R., 1964. Carbonate deposits and paleoclimatic implications in the Northeast Pacific Ocean, *Science*, v.146, pp.515-517.
- Nelson, D.E., Vogel, J.S., Southon, J.R., and Brown, T.A., 1986. Accelerator radiocarbon dating at Simon Fraser University, *Radiocarbon*, v.28(2A), pp.215-222.
- Nelson, H., 1976. Late Pleistocene and Holocene depositional trends, processes, and history of Astoria deep-sea fan, Northeast Pacific, *Marine Geology*, v.20, pp.129-173.
- Nelson, C.H. and Kulm, L.D., 1973. Submarine fans and deep-sea channels, *In Turbidites and Deep-Water Sedimentation* (short course lecture notes), Pacific Section, Society of Economic Paleontologists and Mineralogists, PS-SEPM, Los Angeles, pp.39-78.
- Norrish, K. and Hutton, J.T., 1969. An accurate X-ray spectrographic method for the analysis of a wide range of geological samples, *Geochimica et Cosmochimica Acta*, v.33, pp.431-453.
- Parkin, D.W. and Shackleton, N.J., 1973. Trade wind and temperature correlations down a deep-sea core off the Saharan Coast, *Nature*, v.245, pp.455-456.
- Pedersen, T.F., 1979. The geochemistry of sediments of the Panama Basin, Eastern Equatorial Pacific, Unpublished Ph.D. Thesis, University of Edinburgh, 235p.
- Pedersen, T.F., 1983. Increased productivity in the eastern equatorial Pacific during the last glacial maximum (19,000 to 14,000 yr B.P.), *Geology*, v.11, pp.16-19.
- Pedersen, T.F. and Price, N.B., 1980. The geochemistry of iodine and bromine in sediments of the Panama Basin, *Journal of Marine Research*, v.38, pp.397-411.
- Pedersen, T.F., Vogel, J.S., and Southon, J.R., 1986. Copper and manganese in hemipelagic sediments at 21°N, East Pacific Rise: Diagenetic contrasts, *Geochimica et Cosmochimica Acta*, v.50, (in press).
- Pilkey, O.H., Locker, S.D., and Cleary, W.J., 1980. Comparison of sand-layer geometry on flat floors of 10 modern depositional basins, *American Association of Petroleum Geologists Bulletin*, v.64, pp.841-856.
- Piper, D.J.W., 1978. Turbidite muds and silts on deepsea fans and abyssal plains, *In Sedimentation in Submarine Canyons, Fans and Trenches*, D.J. Stanley and G. Kelling, (eds.), Dowden, Hutchinson and Ross Inc., Stroudsburg, Penn., pp.163-176.
- Piper, D.Z., Veeh, H.H., Bertrand, W.G., and Chase, R.L., 1975. An iron-rich deposit from the Northeast Pacific, *Earth and Planetary Science Letters*, v.26, pp.114-120.
- Prospero, J.M., 1981. Eolian transport to the world ocean, *In The Sea, Volume 7 (The Oceanic Lithosphere)*, C. Emiliani, (ed.), John Wiley and Sons, New York, pp.801-874.

- Price, M.G., 1981. A study of sediments from the Juan de Fuca ridge, Northeast Pacific Ocean: with special reference to hydrothermal and diagenetic components, Unpublished M.Sc. Thesis, University of British Columbia, 141p.
- Price, N.B. and Calvert, S.E., 1973. The geochemistry of iodine in oxidised and reduced Recent marine sediments, *Geochimica et Cosmochimica Acta*, v.37, pp.2149-2158.
- Price, N.B. and Calvert, S.E., 1977. The contrasting geochemical behaviours of iodine and bromine in recent sediments from the Namibian shelf, *Geochimica et Cosmochimica Acta*, v.41, pp.1769-1775.
- Price, N.B., Calvert, S.E., and Jones, P.G.W., 1970. The distribution of iodine and bromine in the sediments of the southwestern Barents Sea, *Journal of Marine Research*, v.28, pp.22-34.
- Pytkowicz, R.M., 1970. On the carbonate compensation depth in the Pacific Ocean, *Geochimica et Cosmochimica Acta*, v.34, pp.836-839.
- Raff, A.D. and Mason, R.G., 1961. Magnetic survey off the West Coast of North America, 40°N. Lat to 52°N. Lat., *Geological Society of America Bulletin*, v.72, pp.1267-1270.
- Riddihough, R.P., 1977. A model for recent plate interactions off Canada's West Coast, *Canadian Journal of Earth Sciences*, v.14, pp.384-396.
- Riddihough, R.P., 1979. Gravity and structure of an active margin – British Columbia and Washington, *Canadian Journal of Earth Sciences*, v.16, pp.350-363.
- Riddihough, R.P., 1981. Gravity modelling across the Queen Charlotte fault zone, (abstract), EOS, *Transactions of the American Geophysical Union*, v.62, p.60.
- Riddihough, R.P., 1982a. Contemporary movements and tectonics on Canada's West Coast: a discussion, *Tectonophysics*, v.86, pp.319-341.
- Riddihough, R.P., 1982b. Contemporary vertical movements and tectonics on Canada's West Coast, (abstract), EOS, *Transactions of the American Geophysical Union*, v.63, p.173.
- Riddihough, R.P., 1982c. One hundred million years of plate tectonics in Western Canada, *Geoscience Canada*, v.9, pp.28-34.
- Riddihough, R.P., 1984. Recent movements of the Juan de Fuca plate system, *Journal of Geophysical Research*, v.89, pp.6980-6994.
- Riddihough, R.P. and Hyndman, R.D., 1976. Canada's active western margin – The case for subduction, *Geoscience Canada*, v.3, pp.269-278.
- Riddihough, R.P. and Seemann, D.A., 1982. Juan de Fuca Plate Map: JPF-8, Gravity Anomaly (1:2,000,000 map), Pacific Geoscience Centre and Earth Physics Branch, Energy, Mines and Resources Canada.
- Riddihough, R.P., Currie, R.G., and Hyndman, R.D., 1980. The Dellwood Knolls and their role in triple junction tectonics off northern Vancouver Island, *Canadian Journal of Earth Sciences*, v.17, pp.577-593.

- Riddihough, R.P., Beck, M.E., Chase, R.L., Davis, E.E., Hyndman, R.D., Johnson, S.H., and Rogers, G.C., 1983. Geodynamics of the Juan de Fuca plate, *In* Geodynamics of the Eastern Pacific Region, Caribbean and Scotia Arcs, R. Cabré, (ed.), Geodynamics Series, v.9, American Geophysical Union, Washington, D.C., and Geological Society of America, Boulder, Colorado, pp.5-21.
- Rogers, G.C., 1979. Earthquake fault plane solutions near Vancouver Island, *Canadian Journal of Earth Sciences*, v.16, pp.523-531.
- St. Amand, P., 1957. Geological and geophysical synthesis of the tectonics of portions of British Columbia, the Yukon Territory, and Alaska, *Geological Society of America Bulletin*, v.68, pp.1343-1370.
- Sclater, J.G., Crowe, J., and Anderson, R.N., 1976. On the reliability of oceanic heat flow averages, *Journal of Geophysical Research*, v.81, pp.2997-3006.
- Scott, S.D., 1986. Seafloor polymetallic sulfides: Scientific curiosities or mines of the future?, *Proceedings of NATO Advanced Research Workshop on "Marine Minerals: Resource Assessment Strategies"*, P. Teleki *et al.*, (eds.), D. Reidel Publishing Company, (in press).
- Seemann, D.A., 1982. Bathymetry off the coast of British Columbia (1:1,000,000 map), Earth Physics Branch, Energy Mines and Resources Canada, Open File 82-25.
- Seemann, D.A., 1983. Deep sea channels off the West Coast of Canada, (abstract), *EOS, Transactions of the American Geophysical Union*, v.64, p.729.
- Seyfried Jr., W.E., Berndt, M.E., and Janecky, D.R., 1986. Chloride depletions and enrichments in seafloor hydrothermal fluids: constraints from experimental basalt alteration studies, *Geochimica et Cosmochimica Acta*, v.50, pp.469-475.
- Shouldice, D.H., 1971. Geology of the Western Canadian continental shelf, *Bulletin of Canadian Petroleum Geology*, v.19, pp.405-436.
- Shouldice, D.H., 1973. Western Canadian continental shelf, *In* The Future Petroleum provinces of Canada – Their Geology and Potential, R.G. McCrossan, (ed.), Canadian Society of Petroleum Geologists, Memoir 1, CSPG, Calgary, pp.7-35.
- Silver, E.A., von Huene, R., and Crouch, J.K., 1974. Tectonic significance of the Kodiak-Bowie seamount chain, Northeastern Pacific, *Geology*, v.2, pp.147-150.
- Simoneit, B.R.T. and Lonsdale, P.F., 1982. Hydrothermal petroleum in mineralized mounds at the seabed of the Guaymas Basin, *Nature*, v.295, pp.198-202.
- Srivastava, S.P., 1973. Interpretation of gravity and magnetic measurements across the continental margin of British Columbia, Canada, *Canadian Journal of Earth Sciences*, v.10, pp.1664-1677.
- Srivastava, S.P., Barrett, D.L., Keen, C.E., Manchester, K.S., Shih, K.G., Tiffin, D.L., Chase, R.L., Thomlinson, A.G., Davis, E.E., and Lister, C.R.B., 1971. Preliminary analysis of geophysical measurements north of Juan de Fuca ridge, *Canadian Journal of Earth Sciences*, v.8, pp.1265-1281.
- Stacey, R.A., 1974. Structure of Queen Charlotte Basin, *In* Canada's Continental Margins and Offshore Petroleum Exploration, C.J. Yorath, E.R. Parker, and D.J. Glass (eds.), Canadian Society of Petroleum Geologists, Memoir 4, CSPG, Calgary, pp.723-741.

- Sutherland Brown, A. and Yorath, C.J., 1985. Lithoprobe profile across southern Vancouver Island: geology and tectonics, *In* Field Guides to Geology and Mineral Deposits in the Southern Canadian Cordillera, D. Tempelman-Kluit, (ed.), Geological Society of America, Cordilleran Section Meeting, Vancouver, B.C., May, 1985, pp.8-1 – 8-23.
- Thomson, R.E., 1981. Oceanography of the British Columbia Coast, Canadian Special Publication of Fisheries and Aquatic Sciences 56, Department of Fisheries and Oceans, Ottawa, 291p.
- Thomson, R.E. and Emery, W.J., 1986. The Haida Current, *Journal of Geophysical Research*, v.91, pp.845-861.
- Thompson, P.R. and Saito, T., 1974. Pacific Pleistocene sediments: planktonic foraminifera dissolution cycles and geochronology, *Geology*, v.2, pp.333-335.
- Thornburg, T.M. and Kulm, L.D., 1983. Depositional environments and sedimentary processes in Chile Trench, (abstract), *American Association of Petroleum Geologists Bulletin*, v.67, pp.557-558.
- Tiffin, D.L., 1972. Geological and geophysical studies of the Pacific continental margin, and Beaufort Sea, Report of Activities, Part A, Geological Survey of Canada, Paper 72-1A, pp.19-20.
- Tiffin, D.L., 1973. Marine geophysical activities on the Pacific margin, Report of Activities, Part A, Geological Survey of Canada, Paper 73-1A, p.121.
- Tiffin, D.L., 1974. Marine geophysical and geological studies on the Pacific margin, Report of Activities, Part A, Geological Survey of Canada, Paper 74-1A, p.127.
- Tiffin, D.L., Cameron, B.E.B., and Murray, J.W., 1972. Tectonics and depositional history of the continental margin off Vancouver Island, British Columbia, *Canadian Journal of Earth Sciences*, v.9, pp.280-296.
- Tiffin, D.L. and Currie, R.G., 1977. Natural Resource Map No 19410-E (Magnetic Anomaly), Canadian Hydrographic Service, Department of Fisheries and the Environment, Ottawa.
- Tiffin, D.L., Bornhold, B.D., Yorath, C.J., Herzer, R.H., and Taylor, G.C., 1978. Bottom sediments – Vicinity of Juan de Fuca and Explorer ridges, Northeast Pacific Ocean, Current Research, Part A, Geological Survey of Canada, Paper 78-1A, pp.533-537.
- Tobin, D.G. and Sykes, L.R., 1968. Seismicity and tectonics of the Northeast Pacific Ocean, *Journal of Geophysical Research*, v.73, pp.3821-3845.
- Turner, D.L., Jarrard, R.D., and Forbes, R.B., 1980. Geochronology and origin of the Pratt-Welker Seamount Chain, Gulf of Alaska: A new pole of rotation for the Pacific plate, *Journal of Geophysical Research*, v.85, pp.6547-6556.
- Ullman, W.J. and Aller, R.C., 1985. The geochemistry of iodine in near-shore carbonate sediments, *Geochimica et Cosmochimica Acta*, v.49, pp.967-978.
- van Andel, T.H. and Komar, P.D., 1969. Ponged sediments of the mid-Atlantic ridge between 22° and 23° north latitude, *Geological Society of America Bulletin*, v.80, pp.1163-1190.

- Verhoef, J., 1985. The sedimentation pattern around the Atlantis-Meteor seamount complex: a model study, *Earth and Planetary Science Letters*, v.73, pp.117-128.
- Villinger, H. and Davis, E.E., 1984. Heat flow and bottom water temperature measurements from the rift valley of the northern Juan de Fuca ridge, (abstract), *EOS, Transactions of the American Geophysical Union*, v.65, p.1111.
- Vine, F.J., 1966. Spreading of the ocean floor: new evidence, *Science*, v.154, pp.1405-1415.
- Vine, F.J., 1966. The continental drift debate, *Nature*, v.266, pp.19-22.
- Vine, F.J. and Matthews, D.H., 1963. Magnetic anomalies over ocean ridges, *Nature*, v.199, pp.947-949.
- Vine, F.J. and Wilson, J.T., 1965. Magnetic anomalies over a young oceanic ridge off Vancouver Island, *Science*, v.150, pp.485-489.
- Vogel, J.S., Southon, J.R., Nelson, D.E., and Brown, T.A., 1984. Performance of catalytically condensed carbon for use in accelerator mass spectrometry, *In Proceedings of the Third International Conference on Accelerator Mass Spectrometry*, W. Wölfli, H.A. Polach and H.H. Andersen, (eds.), *Nuclear Instruments and Methods*, v.B5, pp.289-293.
- von Huene, R., Larson, E., and Crouch, J., 1973. Preliminary study of ice-rafted erratics as indicators of glacial advances in the Gulf of Alaska, *In Kulm, L.D., von Huene, R., et al., 1973, Initial Reports of the Deep Sea Drilling Project, Volume 18, U.S. Government Printing Office, Washington, pp.835-842.*
- von Huene, R., Shor Jr., G.G., and Wageman, J., 1979. Continental margins of the eastern Gulf of Alaska and boundaries of tectonic plates, *In Geological and Geophysical Investigations of Continental Margins*, J.S. Watkins, L. Montadert, and P.W. Dickerson, (eds.), *American Association of Petroleum Geologists, Memoir 29, AAPG, Tulsa, Oklahoma, pp.273-290.*
- von Huene, R., Crouch, J., and Larson, E., 1976. Glacial advance in the Gulf of Alaska area implied by ice-rafted material, *In Investigation of Late Quaternary Paleooceanography and Paleoclimatology*, R.M. Cline and J.D. Hays, (eds.), *Geological Society of America, Memoir 145, pp.411-422.*
- von Stackelberg, U., von Rad, U., and Zobel, B., 1979. Asymmetric sedimentation around Great Meteor Seamount (North Atlantic), *Marine Geology*, v.33, pp.117-132.
- Walker, R.G., 1984. Shelf and shallow marine sands, *In Facies Models (2nd ed.)*, R.G. Walker, (ed.), *Geological Association of Canada, Reprint Series 1, GAC, St. John's, Newfoundland, pp.141-170.*
- Warner, B.G., Mathewes, R.W., and Clague, J.J., 1982. Ice-free conditions on the Queen Charlotte Islands, British Columbia, at the height of Late Wisconsin glaciation, *Science*, v.218, pp.675-677.
- Wilson, J.T., 1965a. A new class of faults and their bearing on continental drift, *Nature*, v.207, pp.343-347.
- Wilson, J.T., 1965b. Transform faults, oceanic ridges, and magnetic anomalies southwest of Vancouver Island, *Science*, v.150, pp.482-485.

- Yorath, C.J., Bornhold, B.D., and Thomson, R.E., 1979. Oscillation ripples on the Northeast Pacific continental shelf, *Marine Geology*, v.31, pp.45-58.
- Yorath, C.J. and Chase, R.L., 1981. Tectonic history of the Queen Charlotte Islands and adjacent areas – a model, *Canadian Journal of Earth Sciences*, v.18, pp.1717-1739.
- Yorath, C.J. and Hyndman, R.D., 1983. Subsidence and thermal history of Queen Charlotte Basin, *Canadian Journal of Earth Sciences*, v.20, pp.135-159.
- Young, I.F., 1981. Structure of the western margin of the Queen Charlotte Basin, British Columbia, Unpublished M.Sc. Thesis, University of British Columbia, 380p.
- Young, I.F. and Chase, R.L., 1977. Marine geological-geophysical study: southwestern Hecate Strait, British Columbia, Report of Activities, Part A, Geological Survey of Canada, Paper 77-1A, pp.315-318.

APPENDIX 1 – SAMPLING AND ANALYTICAL PROCEDURES

## 6.1 CORING AND SAMPLING PROCEDURES

All cores were taken with a steel gravity corer lined with clear butyrate tubing with a 60 mm internal diameter. Sediment was retained in the core barrel during the ascent from the seafloor to the ship's afterdeck by a spring-loaded plug at the top end and a stainless steel sphincter at the bottom. This arrangement was not always successful in retaining the core as occasionally lumps of mud were observed dropping from the mouth of the corer as it was pulled from the water. Loss of the soupy core top due to the sudden impact of the corer with the seafloor is suspected in all seven cores. Verification of absence of core top using  $^{210}\text{Pb}$  dating has not been attempted in this study.

Once on deck the corer liner was laid horizontally and the liner carefully removed from the core barrel. Seawater filling the top portion of the liner was carefully decanted to avoid disturbance of the uppermost portion of the core. Plastic caps were placed on both ends and thoroughly taped with black PVC electrical tape to prevent oxidation and shrinkage due to drying. In some cases the core liner was shortened by cutting with a hacksaw prior to attachment of the top cap. The liners were carefully labelled as to top and core number and immediately placed in 4°C storage in the ship to retard bacterial degradation. The liners were kept vertical during storage and during all subsequent movements until splitting and sampling when they were laid horizontally.

The cores were split in half in Ottawa in the Energy, Mines and Resources Sedimentology laboratory under the direction of J.D. Adshead of the Geological Survey of Canada. The cores were removed from cold storage (4°C) for splitting one at a time. The liners were cut by feeding them through a specially-designed guide attached to a radial arm power saw. Some of the cores (1-3) were split by pulling apart the two halves of the liners, separating the sediment inside at the same time. The others (4, 6-8) were split by drawing nylon monofilament fishing line through them after the liners had been cut.

Sampling was carried out in Vancouver after the half cores had been brought from Ottawa by air. The archival half of each core remains in cold storage in Ottawa. Sample bags were labelled and the sampling area prepared in advance to minimize the duration of exposure to air and room temperature. The flat interior surface of cores 4 and 6-8 was meticulously scraped to remove any material that may have been smeared along the core by drawing the fishline through. This was not necessary for the split cores (1-3).

The half cores were disgorged from their plastic liners onto a strip of plastic film. The semicylindrical outer surface of the core was then scraped to remove any material displaced by smearing along the interior of the liner during coring. Some cores were slightly blackened on the outside due to oxidation during storage. This was limited to the very outermost film (<1 mm thick) of core and was easily removed by the scraping process described above.

The cores were then sliced into 1 cm slabs and placed into Ziplock sample bags according to the depth of the top of the 1 cm sample. For example, the 1 cm thick slab sampled in core 2 from a depth of 44 to 45 cm is designated as sample number "2-44". Ease of sampling varied from core to core, but cores 1-3 had suffered some drying and other mistreatment prior to being returned to Vancouver, which made separation of the 1 cm slices more difficult. This drying is evident from cracks visible in the X-radiographs of cores 1-3 as pointed out previously. Air was excluded as much as possible from the sample bags to discourage oxidation and bacterial activity. The samples were then frozen for long term storage.

Samples at the following depths in each core (where applicable) were separated initially from the main batch for analysis: 0-1, 3-4, 6-7, 10-11, 20-21, 30-31, 40-41, 60-61, 80-81, 100-101, 130-131 cm. A separate sample from each of the above intervals was collected and stored in a glass vial. These samples were stored at 4°C and reserved for later smear slide and SEM examination of components such as faecal pellets which would suffer damage if frozen. A complete listing of the samples from each core is given in Appendix 4.

Selected samples were heated in an oven at 50°C until dry (about 48 hours), and were then ground in a tungsten carbide disc mill. Powdered sample yield was variable and in some cases less than 6 g. Low-yield samples were generally from the upper portions of cores which were less compacted and had higher water contents. These low-yield samples were combined in equal portions (4 g + 4 g dry weight) with the 1 cm thick sample interval immediately below and are numbered as combined samples (e.g., 6-10,11 for core 6, with 1 cm thick samples taken from 10 and 11 cm depths combined into one sample).

## 6.2 ANALYTICAL PROCEDURES

### 6.2.1 <sup>14</sup>C DATING

Two samples, 3-46 and 3-60, from depths of 46-47 and 60-61 cm in core 3, were selected for bulk <sup>14</sup>C dating. Lack of benthic foraminifera in the sediment prevented the more specific dating of foraminiferal carbonate. <sup>14</sup>C/<sup>12</sup>C ratios were measured by tandem Van de Graaf accelerator mass spectrometry at the Tandem Laboratory, McMaster University. The samples were prepared by iron catalyst graphitization (Vogel *et al.*, 1984) for introduction to the accelerator ion source, and <sup>14</sup>C/<sup>12</sup>C ratios were then measured as described by Nelson *et al.* (1986).

### 6.2.2 SCANNING ELECTRON MICROSCOPY

Small portions of the original samples were removed prior to drying and grinding of the remainder for geochemical analyses and stored in glass vials at 4°C. The samples selected for examination were 1-10 (for diatoms), 3-30 and 4-10 (for heavy minerals), and a special portion of core 3 containing the bone, from depth of 28-31 cm. Several pieces of bone were picked out of the sediment by hand under a binocular microscope. Some were cleaned ultrasonically in water, and others gently rinsed in water prior to mounting on a carbon stub. Suspensions were made of the other samples by ultrasonically agitating a small plastic vial containing water and a minute amount of mud. Coarse and fine fractions were

pipetted off separately. Small drops from each fraction were then placed on carbon stubs and allowed to evaporate. The suspension samples and the mounted bone sample were sputter-coated with carbon prior to examination under a Semco Nanolab 7 SEM.

### 6.2.3 X-RAY DIFFRACTION

XRD was performed on a series of eight samples (3–20, 24, 27, 30, 46, 50, 55, 60), all from core 3. Separate runs were made on oriented mounts prepared by three different techniques, bulk sample,  $<2 \mu\text{m}$  settled, and glycolated  $<2 \mu\text{m}$  settled.

Bulk samples were prepared by mixing 50 mg of dried, ground sample in 5 mL of water and agitating for 5 minutes. 1 mL of the resultant slurry was pipetted off, placed on glass discs and allowed to evaporate overnight leaving a coating of sediment on the disc.

Settled samples were prepared by mixing 1 g of dry, powdered sediment with 5 ml of "Calgon" dispersant (sodium hexametaphosphate) mixed at a concentration of  $50 \text{ g L}^{-1}$  as recommended by Lewis (1984). This solution was agitated for 5 minutes and decanted into a 1 L settling cylinder to which was added an additional 15 mL of dispersant and made up to 1 L with water. The suspension was mixed and allowed to stand for 8.5 hours whereupon 40 mL was pipetted off from a depth of 10 cm according to the method outlined by Lewis (1984). This suspension was then centrifuged at 3000 RPM for 10 minutes, the supernatant liquid decanted off, and the tube topped up with water. This was centrifuged again for 5 minutes and the supernatant liquid decanted leaving only 2 mL in the bottom of the centrifuge tube. This was agitated and 1 mL pipetted off and placed on a glass disc. The samples were analyzed on the XRD after evaporation overnight.

Glycolation was carried out on the  $<2 \mu\text{m}$  samples by placing the slides in a vacuum dessicator which contained a tray of ethylene glycol. The samples were left in the dessicator overnight and run through the XRD immediately upon removal.

The samples used for XRD analysis had all been previously ground as unground portions were not available. Grindley (1981) advised against such a practice especially where quartz is present because of damage suffered by the clay minerals during grinding. Despite this, satisfactory results were obtained.

A Philips PW 1729 X-Ray Diffractometer with accompanying PW 1710 control unit was used. The samples were scanned over a range of  $3\text{--}38^\circ 2\theta$  using Cu K $\alpha$  radiation at 40 kV and 20 mA, with a scan speed of  $0.01^\circ 2\theta \text{ sec}^{-1}$  and a chart scale of  $10 \text{ mm } ^\circ 2\theta^{-1}$ .

#### 6.2.4 MAJOR ELEMENTS

Fused glass discs for XRF analysis of major elements were prepared using a technique similar to that described by Norrish and Hutton (1969). The discs were formed by heating 0.4000 g of sample and 3.6000 g of Flux 105 in a platinum crucible at  $1100^\circ\text{C}$  for 20 minutes. The crucible was allowed to cool to room temperature and weight loss was made up with Flux 100. The sample was then refused by heating over a Bunsen burner, poured into an aluminum mould and immediately pressed into a disc with a plunger. Lanthanum in the Flux 105 readily absorbs X-rays so that any variation in the mass absorption of the sample is small in comparison. The weight loss on fusion is made up using Flux 100 which does not contain La in order to maintain a constant heavy absorber/element ratio.

Analyses were carried out on a Philips PW 1450 automated X-ray fluorescence (XRF) spectrometer in the Department of Oceanography. The principles of XRF analysis are described by Fletcher (1981). International rock standards were used for calibration and for drift tests on each run. Values used for these standards are those published by Abbey (1980). Agreement with the established standards after calibration was generally excellent.

Determination of carbon ( $C_{\text{total}}$ ) and nitrogen was performed using a Carlo-Erba CHN (carbon-hydrogen-nitrogen) Analyzer. Dry powdered sample was weighed into minute tin containers. Sample weights ranged from 10–50  $\mu\text{g}$ . Twenty-three samples were analyzed in

each run, of which usually two were blanks and five were standards. Acetanilide ( $\text{CH}_3\text{CONHC}_6\text{H}_5$ ) was used as the standard. The samples are automatically released into the analyzer every ten minutes. They fall into a vertical combustion tube which is maintained at  $1030^\circ\text{C}$  and flushed with a constant flow of helium. A brief surge of oxygen causes combustion. The combustion gases are passed over copper at  $650^\circ\text{C}$  to remove oxygen and reduce nitrogen oxides to nitrogen. The gases then pass through a chromatographic column and are separated into  $\text{N}_2$ ,  $\text{CO}_2$  and  $\text{H}_2\text{O}$ , measured by a thermal conductivity detector and then integrated.

Carbonate carbon was determined with a Coulometrics model 5010  $\text{CO}_2$  coulometer. An accurately weighed amount of dry powdered sample (30–70 mg) is acidified with HCl in a closed system. The  $\text{CO}_2$  produced by reaction of the acid with carbonate in the sample is flushed into a solution containing ethanolamine and a colourimetric indicator through which a light source passes. The  $\text{CO}_2$  is absorbed by the ethanolamine causing the indicator to fade. This is detected by a photocell and a current is applied to titrate the solution. The total amount of current required for titration is integrated and converted to micrograms of carbonate carbon. Pure  $\text{CaCO}_3$  is used as a standard for calibration.

#### 6.2.5 MINOR ELEMENTS AND HALOGENS

Pellets for analysis of minor elements and halogens by XRF were formed by pressing 6.00 g of dry, powdered sample with finely powdered boric acid ( $\text{H}_3\text{BO}_3$ ) as the medium in a 10 tonne hydraulic press. Analysis was then performed with an automated XRF spectrometer using the same procedure described above for major elements. Synthetic standards embracing a wide range of concentrations were used for calibration. Analysis of I and Br standards yielded values in very close agreement with the calculated concentrations. Such close agreement was not obtained for Cl suggesting that some factor such as mass absorption was affecting the results. The effect of Cl concentration on salt corrections was discussed in the section in Chapter 5 on Na distribution.

The sediment samples were dried at 50°C to avoid loss of I and Br, as recommended by Price and Calvert (1973).

APPENDIX 2 — RAW XRF, CHN AND COULOMETER DATA

## Raw Data - Major Elements (%)

Sample #	depth	S102	TiO2	Al2O3	Fe2O3	MgO	CaO	Na	K2O	P2O5	Cl	S	N	C:tot	CO2
1-0,1	-1.0	56.08	0.77	13.15	5.41	2.77	3.89	2.95	1.58	0.21	2.13	0.03	0.325	3.449	0.249
1-3,4	-4.0	55.64	0.78	13.30	5.44	2.77	3.90	2.85	1.57	0.21	1.88	0.03	0.338	3.533	0.263
1-6	-6.5	55.69	0.76	13.43	5.40	2.80	4.10	2.87	1.54	0.20	2.15	0.04	0.311	3.194	0.326
1-10,11	-11.0	55.68	0.78	13.16	5.64	2.83	4.23	2.84	1.59	0.19	2.10	0.06	0.295	3.137	0.338
1-15,16	-16.0	54.51	0.76	12.99	5.75	2.78	4.13	2.67	1.67	0.19	2.11	0.06	0.283	2.921	0.325
1-20,21	-21.0	55.46	0.80	13.68	5.76	2.85	3.98	2.89	1.64	0.19	2.08	0.06	0.273	2.925	0.279
1-25,26	-26.0	55.86	0.80	13.79	5.75	3.08	4.30	2.66	1.64	0.20	2.03	0.06	0.257	2.801	0.350
1-30	-30.5	55.20	0.79	13.64	5.67	2.92	4.28	2.79	1.62	0.19	2.05	0.07	0.244	2.733	0.364
1-35	-35.5	55.02	0.81	13.78	5.77	2.83	4.38	2.75	1.64	0.20	2.07	0.07	0.257	2.683	0.373
1-40	-40.5	56.08	0.79	13.53	5.55	2.81	4.47	2.83	1.59	0.18	2.13	0.06	0.266	2.648	0.346
1-60	-60.5	56.02	0.79	13.72	5.75	2.82	4.82	2.76	1.65	0.19	2.01	0.08	0.233	2.407	0.428
1-80	-80.5	55.19	0.82	14.07	5.96	3.01	4.26	2.88	1.71	0.20	2.09	0.08	0.196	2.269	0.321
1-95	-95.5	55.18	0.83	14.51	6.05	3.15	3.90	3.01	1.70	0.19	2.27	0.07	0.189	2.248	0.255
2-0,1	-1.0	56.68	0.78	13.95	5.46	2.94	3.95	2.81	1.52	0.21	2.38	0.03	0.277	3.062	0.244
2-3,4	-4.0	57.15	0.80	14.07	5.58	2.83	3.99	2.88	1.61	0.20	2.31	0.03	0.255	2.535	0.235
2-6,7	-7.0	58.01	0.79	14.02	5.47	2.85	4.24	2.84	1.56	0.21	2.25	0.04	0.250	2.630	0.282
2-10,11	-11.0	54.55	0.75	13.26	5.76	2.80	4.32	2.85	1.68	0.20	2.12	0.04	0.224	2.370	0.306
3-0,1	-1.0	56.83	0.75	13.53	5.49	2.67	4.25	3.08	1.47	0.21	2.10	0.03	0.298	3.111	0.265
3-3	-3.5	57.74	0.77	13.43	5.31	2.84	4.17	2.94	1.52	0.19	1.97	0.03	0.261	2.572	0.264
3-6	-6.5	57.18	0.79	14.25	5.44	2.80	4.44	2.79	1.54	0.20	1.74	0.03	0.219	2.410	0.289
3-10	-10.5	57.68	0.79	14.52	5.67	2.83	4.50	2.73	1.66	0.20	1.62	0.03	0.204	2.068	0.303
3-20	-20.5	57.34	0.82	14.83	5.85	3.02	4.86	2.79	1.66	0.20	1.66	0.03	0.169	1.874	0.354
3-24	-24.5	51.72	0.81	13.80	6.59	3.07	5.51	2.73	1.77	0.20	1.70	0.03	0.146	1.942	0.448
3-27	-27.5	53.52	0.84	14.48	6.87	3.58	5.40	2.82	1.72	0.23	1.68	0.03	0.136	1.798	0.379
3-30	-30.5	54.11	0.94	15.22	6.86	3.66	5.66	2.79	1.73	0.25	1.43	0.03	0.128	1.581	0.324
3-32	-32.5	53.44	0.85	14.60	7.12	3.68	5.22	2.89	1.75	0.22	1.75	0.03	0.130	1.680	0.322
3-34	-34.5	53.42	0.83	14.48	7.14	3.62	5.29	2.87	1.70	0.19	1.75	0.03	0.138	1.790	0.359
3-36	-36.5	54.50	0.85	14.24	7.09	3.81	5.03	2.85	1.62	0.19	1.66	0.04	0.133	1.705	0.324
3-38	-38.5	53.96	0.87	14.67	7.18	3.91	4.78	2.80	1.72	0.21	1.61	0.04	0.125	1.705	0.285
3-40	-40.5	54.21	0.87	15.37	7.21	3.99	4.82	2.81	1.63	0.20	1.64	0.04	0.132	1.669	0.266
3-43	-43.5	55.39	0.82	14.90	7.12	3.75	5.10	2.92	1.61	0.20	1.64	0.08	0.119	1.445	0.305
3-46	-46.5	54.97	0.85	14.40	7.23	3.99	4.98	2.87	1.70	0.20	1.72	0.05	0.117	1.532	0.203
3-50	-50.5	55.45	0.83	11.67	7.33	3.98	4.59	2.85	1.43	0.17	1.56	0.04	0.122	1.355	0.224
3-55	-55.5	56.19	0.86	12.33	7.35	4.10	4.57	2.80	1.49	0.16	1.47	0.03	0.090	1.175	0.293
3-60	-60.5	55.15	0.89	15.90	7.19	3.89	4.61	2.77	1.92	0.22	1.34	0.04	0.084	1.113	0.208
3-80	-80.5	56.51	0.89	16.19	7.05	3.85	4.76	2.80	1.88	0.22	1.33	0.05	0.083	1.059	0.222

## Raw Data - Major Elements (%)

Sample #	depth	S102	T102	Al2O3	Fe2O3	MgO	CaO	Na	K2O	P2O5	Cl	S	N	C:tot	CO2
4-0,1	-1.0	54.79	0.78	13.25	5.69	2.92	3.52	3.14	1.59	0.21	2.84	0.04	0.360	3.403	0.228
4-3,4	-4.0	56.06	0.77	12.82	5.62	3.18	3.53	3.26	1.46	0.20	2.91	0.04	0.321	3.107	0.212
4-6,7	-7.0	55.01	0.79	13.24	5.53	2.94	3.77	3.14	1.60	0.20	2.83	0.04	0.336	3.074	0.267
4-10	-10.5	55.12	0.76	12.95	5.48	2.93	3.61	3.31	1.59	0.20	3.10	0.05	0.302	2.987	0.234
4-20	-20.5	56.42	0.80	13.67	5.60	2.99	4.05	3.13	1.60	0.20	2.57	0.06	0.257	2.524	0.280
4-30	-30.5	55.68	0.78	13.35	5.58	2.91	3.55	3.16	1.63	0.18	2.87	0.07	0.301	2.905	0.246
4-40	-40.5	55.60	0.77	13.46	5.58	3.06	3.68	3.16	1.69	0.19	2.77	0.06	0.280	2.724	0.262
4-60	-60.5	56.22	0.79	13.54	5.65	3.14	4.07	2.98	1.67	0.18	2.43	0.08	0.269	2.621	0.313
4-80	-80.5	56.01	0.76	13.90	5.86	3.00	4.02	2.83	1.67	0.19	2.31	0.09	0.264	2.666	0.330
4-94,95	-95.0	56.59	0.79	13.06	5.93	3.29	4.08	2.79	1.52	0.17	2.51	0.06	0.237	2.703	0.399
6-0	-0.5	54.90	0.77	13.38	6.03	3.02	3.16	2.88	1.70	0.19	2.53	0.08	0.288	2.592	0.207
6-3,4	-4.0	55.90	0.80	13.23	6.02	3.11	3.17	3.00	1.68	0.19	2.63	0.08	0.289	2.636	0.214
6-6	-6.5	55.13	0.79	13.25	5.98	3.04	3.16	3.04	1.70	0.18	2.74	0.08	0.284	2.590	0.199
6-8,9	-9.0	56.41	0.77	12.48	6.09	3.36	3.38	2.97	1.58	0.19	2.84	0.07	0.264	2.604	0.239
6-10,11	-11.0	55.04	0.82	13.25	6.08	3.13	2.99	3.09	1.70	0.18	2.69	0.08	0.282	2.453	0.171
6-12	-12.5	56.32	0.78	12.90	6.18	3.46	2.99	3.10	1.67	0.17	2.89	0.07	0.257	2.422	0.167
6-16	-16.5	57.46	0.79	12.80	6.09	3.42	3.05	3.06	1.60	0.15	2.78	0.07	0.251	2.337	0.171
6-20	-20.5	55.82	0.80	13.54	5.92	3.19	2.95	3.11	1.68	0.19	2.83	0.08	0.261	2.434	0.177
6-30	-30.5	58.33	0.79	14.13	6.16	3.28	3.05	3.09	1.84	0.20	2.87	0.09	0.239	2.298	0.177
6-40	-40.5	55.80	0.80	13.16	6.12	3.15	3.23	3.06	1.67	0.17	2.73	0.11	0.251	2.408	0.227
6-60,61	-61.0	55.20	0.85	14.46	6.27	3.16	3.74	2.95	1.78	0.20	2.33	0.09	0.203	2.050	0.247
6-80	-80.5	55.32	0.82	13.95	6.02	3.27	3.38	2.90	1.79	0.20	2.46	0.08	0.220	2.255	0.255
6-100	-100.5	54.43	0.82	13.78	6.31	3.18	3.64	2.89	1.77	0.19	2.46	0.09	0.221	2.222	0.285
6-112	-112.5	56.29	0.75	10.63	5.93	3.52	2.98	3.22	1.45	0.14	3.18	0.05	0.264	2.702	0.192
7-0,1	-1.0	58.10	0.73	11.56	5.77	3.40	3.58	3.19	1.28	0.15	3.17	0.03	0.259	2.763	0.239
7-3	-3.5	57.23	0.79	13.01	5.90	3.31	3.89	3.13	1.61	0.19	2.63	0.03	0.221	2.371	0.250
7-6	-6.5	55.14	0.76	13.13	5.55	2.90	3.93	3.15	1.63	0.20	2.70	0.03	0.255	2.502	0.255
7-10	-10.5	58.05	0.75	11.25	5.56	3.36	3.99	3.17	1.36	0.17	2.75	0.03	0.229	2.555	0.303
7-14	-14.5	56.99	0.76	9.80	5.72	3.41	4.13	3.17	1.33	0.15	2.81	0.03	0.212	2.540	0.282
8-0	-0.5	58.98	0.72	13.58	5.24	2.65	4.22	3.09	1.52	0.19	2.26	0.03	0.182	2.050	0.210
8-3	-3.5	58.79	0.79	13.22	5.57	3.17	4.39	3.02	1.54	0.18	2.25	0.03	0.181	2.246	0.291
8-6	-6.5	57.63	0.78	13.81	5.77	3.11	4.28	3.01	1.61	0.19	2.29	0.04	0.169	2.158	0.284
8-10	-10.5	59.22	0.76	11.73	5.86	3.37	4.22	2.95	1.37	0.13	2.29	0.03	0.179	2.141	0.306
8-20	-20.5	54.66	0.82	13.86	6.39	3.47	4.36	2.97	1.55	0.16	2.38	0.04	0.161	2.164	0.360
8-30	-30.5	57.42	0.82	13.71	6.41	3.50	4.82	2.77	1.54	0.18	2.06	0.04	0.153	2.157	0.426
8-40	-40.5	53.94	0.81	13.32	6.48	3.40	5.08	2.77	1.57	0.17	2.01	0.06	0.175	2.300	0.471
8-50	-50.5	55.50	0.81	11.53	6.60	3.62	5.01	2.71	1.38	0.15	1.91	0.05	0.167	2.240	0.481
8-60	-60.5	54.95	0.83	13.68	6.63	3.60	5.53	2.73	1.58	0.18	1.96	0.06	0.164	2.265	0.540
8-81	-81.5	54.08	0.83	14.62	6.86	3.71	5.49	2.54	1.68	0.19	1.65	0.07	0.162	2.254	0.503

## Raw Data - Trace Elements and Halogens (ppm)

Sample #	Ba	Co	Cr	Cu	Mn	Nb	Ni	Pb	Rb	Sr	V	Y	Zn	Zr	I	Br
1-0.1	1016.	38.	83.	46.	541.	9.	43.	14.	47.	318.	110.	16.	115.	123.	613.	234.
1-3,4	1095.	43.	89.	52.	569.	8.	47.	16.	48.	314.	124.	16.	121.	125.	674.	262.
1-6	1067.	37.	88.	50.	550.	9.	45.	8.	50.	323.	124.	17.	125.	126.	580.	267.
1-10,11	1055.	30.	89.	52.	542.	9.	48.	9.	52.	317.	118.	17.	129.	127.	508.	259.
1-15,16	1069.	26.	84.	45.	566.	10.	43.	14.	48.	313.	111.	16.	120.	126.	486.	215.
1-20,21	1112.	37.	91.	54.	577.	10.	48.	6.	52.	316.	128.	19.	181.	128.	438.	245.
1-25,26	1050.	22.	88.	44.	578.	8.	39.	10.	48.	311.	108.	17.	113.	125.	406.	198.
1-30	1040.	29.	82.	51.	648.	8.	43.	13.	49.	333.	121.	17.	126.	123.	389.	219.
1-35	986.	30.	82.	41.	570.	10.	40.	14.	49.	318.	106.	16.	112.	125.	374.	190.
1-40	989.	26.	84.	51.	566.	8.	45.	11.	51.	322.	121.	16.	130.	126.	360.	228.
1-60	900.	29.	79.	48.	570.	9.	45.	13.	49.	352.	119.	17.	123.	134.	274.	190.
1-80	925.	25.	88.	48.	601.	9.	47.	12.	53.	324.	129.	19.	130.	139.	237.	180.
1-95	909.	35.	88.	53.	613.	9.	51.	15.	55.	313.	135.	20.	142.	133.	227.	174.
2-0.1	1003.	25.	79.	43.	569.	9.	39.	16.	46.	327.	99.	16.	108.	129.	566.	241.
2-3,4	1014.	25.	88.	44.	578.	9.	39.	14.	48.	323.	107.	18.	113.	124.	412.	204.
2-6,7	957.	31.	78.	42.	540.	10.	38.	13.	48.	340.	96.	17.	110.	130.	429.	211.
2-10,11	945.	25.	81.	46.	573.	9.	41.	11.	49.	335.	101.	18.	113.	137.	320.	181.
3-0.1	944.	42.	83.	45.	644.	9.	42.	14.	46.	367.	113.	16.	124.	133.	656.	248.
3-3	982.	39.	83.	46.	579.	9.	43.	10.	47.	357.	120.	17.	117.	139.	445.	213.
3-6	960.	35.	86.	45.	591.	9.	46.	12.	48.	359.	122.	17.	117.	137.	341.	185.
3-10	890.	31.	82.	49.	582.	8.	44.	19.	49.	361.	120.	19.	119.	137.	252.	155.
3-20	834.	32.	86.	42.	642.	9.	41.	14.	49.	364.	128.	18.	111.	143.	176.	134.
3-24	788.	26.	88.	42.	750.	11.	37.	11.	47.	364.	112.	18.	101.	131.	156.	127.
3-27	737.	28.	91.	41.	798.	12.	38.	11.	47.	359.	117.	19.	99.	133.	133.	123.
3-30	702.	29.	98.	42.	846.	14.	43.	16.	47.	386.	143.	18.	100.	147.	88.	110.
3-32	692.	28.	94.	40.	847.	10.	36.	9.	48.	348.	121.	19.	98.	130.	103.	122.
3-34	680.	23.	90.	36.	807.	10.	40.	9.	46.	338.	116.	18.	96.	122.	107.	121.
3-36	709.	25.	90.	40.	841.	9.	39.	9.	47.	339.	118.	20.	103.	123.	87.	118.
3-38	673.	22.	94.	37.	850.	8.	40.	10.	48.	322.	121.	18.	99.	122.	63.	115.
3-40	665.	27.	96.	43.	878.	8.	39.	12.	50.	327.	141.	19.	106.	117.	58.	111.
3-43	648.	25.	90.	36.	853.	9.	40.	11.	47.	351.	118.	20.	95.	125.	39.	96.
3-46	647.	26.	93.	35.	876.	9.	37.	15.	52.	337.	123.	19.	99.	117.	37.	93.
3-50	645.	26.	94.	35.	880.	10.	37.	12.	52.	338.	123.	17.	95.	119.	29.	83.
3-55	620.	25.	83.	34.	858.	9.	37.	13.	52.	346.	121.	19.	99.	122.	22.	75.
3-60	628.	29.	92.	35.	900.	9.	38.	11.	53.	346.	147.	17.	102.	119.	21.	82.
3-80	670.	25.	85.	27.	879.	9.	35.	10.	53.	363.	141.	18.	94.	120.	18.	74.

## Raw Data - Trace Elements and Halogens (ppm)

Sample #	Ba	Co	Cr	Cu	Mn	Nb	Ni	Pb	Rb	Sr	V	Y	Zn	Zr	I	Br
4-0,1	1101.	34.	89.	56.	559.	9.	50.	14.	52.	303.	127.	17.	134.	119.	817.	321.
4-3,4	1081.	33.	88.	52.	564.	9.	47.	15.	50.	305.	123.	16.	127.	118.	731.	291.
4-6,7	1110.	30.	89.	55.	579.	9.	47.	15.	50.	309.	127.	15.	129.	117.	627.	290.
4-10	1111.	26.	89.	52.	541.	9.	45.	14.	50.	307.	118.	15.	125.	120.	651.	292.
4-20	1019.	27.	86.	49.	592.	9.	43.	14.	50.	326.	125.	16.	119.	125.	444.	225.
4-30	1119.	29.	89.	69.	532.	8.	57.	8.	56.	326.	138.	19.	160.	128.	506.	257.
4-40	1129.	31.	87.	64.	547.	8.	54.	13.	55.	333.	139.	17.	155.	133.	452.	243.
4-60	1074.	34.	89.	60.	577.	8.	52.	14.	53.	329.	142.	18.	144.	131.	382.	218.
4-80	1070.	24.	88.	67.	557.	7.	58.	19.	56.	335.	140.	18.	158.	130.	357.	214.
4-94,95	1047.	23.	83.	34.	582.	10.	44.	11.	52.	304.	108.	19.	122.	123.	331.	191.
6-0	1441.	23.	89.	82.	571.	8.	68.	14.	60.	310.	141.	18.	178.	127.	469.	233.
6-3,4	1486.	32.	92.	80.	574.	7.	67.	15.	57.	300.	148.	17.	171.	126.	427.	219.
6-6	1484.	34.	90.	83.	577.	8.	62.	12.	57.	296.	143.	19.	161.	127.	432.	227.
6-8,9	1426.	27.	86.	54.	610.	10.	44.	17.	52.	277.	107.	16.	137.	118.	404.	194.
6-10,11	1480.	36.	92.	82.	593.	8.	62.	16.	58.	302.	142.	18.	199.	131.	420.	224.
6-12	1523.	29.	87.	60.	611.	10.	50.	13.	55.	276.	119.	18.	131.	121.	388.	188.
6-16	1443.	29.	86.	57.	587.	10.	48.	6.	53.	275.	112.	17.	126.	121.	392.	178.
6-20	1457.	28.	91.	73.	588.	8.	61.	10.	58.	294.	146.	17.	159.	128.	384.	221.
6-30	1383.	30.	87.	70.	580.	7.	54.	9.	56.	287.	141.	17.	154.	125.	362.	221.
6-40	1363.	34.	87.	81.	583.	8.	60.	6.	56.	294.	135.	18.	165.	127.	369.	219.
6-60,61	1200.	31.	90.	63.	691.	8.	52.	11.	58.	313.	133.	18.	144.	130.	257.	176.
6-80	1334.	30.	86.	68.	626.	9.	59.	11.	59.	296.	129.	18.	154.	129.	275.	193.
6-100	1270.	28.	86.	64.	637.	10.	55.	16.	57.	302.	121.	19.	147.	127.	309.	183.
6-112	1434.	31.	81.	57.	626.	9.	46.	17.	54.	275.	111.	16.	125.	120.	435.	199.
7-0,1	1281.	26.	78.	48.	560.	10.	40.	21.	50.	309.	107.	15.	209.	124.	487.	232.
7-3	1158.	29.	80.	48.	575.	10.	43.	14.	49.	314.	108.	17.	113.	131.	349.	187.
7-6	1253.	35.	82.	46.	558.	10.	40.	16.	50.	315.	105.	16.	107.	127.	452.	213.
7-10	1278.	31.	84.	46.	560.	10.	38.	18.	50.	320.	109.	17.	105.	127.	431.	211.
7-14	1194.	32.	86.	47.	592.	10.	38.	21.	50.	320.	109.	18.	138.	125.	378.	196.
8-0	895.	26.	75.	34.	558.	9.	31.	16.	43.	369.	99.	15.	85.	133.	352.	170.
8-3	885.	30.	83.	38.	578.	10.	35.	16.	45.	348.	105.	16.	98.	132.	303.	174.
8-6	881.	31.	85.	38.	564.	10.	35.	12.	49.	339.	107.	17.	101.	135.	304.	172.
8-10	904.	28.	84.	42.	590.	10.	35.	13.	48.	338.	111.	17.	97.	134.	292.	163.
8-20	847.	23.	86.	38.	673.	9.	34.	7.	52.	310.	120.	17.	98.	129.	216.	166.
8-30	857.	21.	91.	40.	650.	10.	35.	17.	52.	328.	119.	18.	99.	132.	200.	154.
8-40	824.	24.	85.	46.	655.	10.	44.	12.	51.	338.	117.	19.	110.	132.	215.	158.
8-50	877.	25.	94.	48.	729.	10.	42.	13.	50.	344.	121.	20.	114.	130.	200.	146.
8-60	831.	18.	90.	41.	745.	10.	39.	11.	50.	345.	120.	18.	105.	124.	195.	152.
8-81	777.	23.	90.	40.	782.	9.	42.	12.	50.	340.	121.	17.	105.	124.	160.	146.

### APPENDIX 3 — SALT-CORRECTION PROGRAM

The results obtained by XRF, CHN and coulometer were entered onto computer files and processed through a Fortran program to provide elemental (rather than oxide) data on a salt-free basis. Carbonate carbon was subtracted from  $C_{\text{total}}$  to give  $C_{\text{org}}$ . The raw data can be found in Appendix 2, and the computer program used to process them in Appendix 4. The salt correction was applied using chlorine values determined with the other halogens (bromine and iodine) by XRF and assumes that the Cl is entirely of seawater origin. In addition other elements that occur in significant quantities in seawater had individual correction applied (Na, Mg, Ca, K, S, the minor element Sr, and the halogen Br). Details of these corrections appear in the program that follows and are explained by the comment lines therein. The original program was written by Brian Cousens of the Department of Oceanography but has been extensively modified by this author to suit the needs of the research described herein.

```

C          ** SEASALT **
C          A sea salt correction program with element ratios.
C
C          REAL EL(100,25), S(100), CL(100), FACTOR(9), NIT(100),
C          . CARBON(100), CO2(100), SIAL(100),
C          . FEAL(100), TIAL(100), MGAL(100), KAL(100), MNAL(100),
C          . CRAL(100), ZRAL(100), FENI(100), MNFE(100), NICO(100),
C          . IC(100), BRC(100), CN(100)
C          INTEGER SAMPLE, P, PAGES
C          REAL*8 SAM(100), DEPTH(100), TITLE(5)
C
C          Data factors are for conversion of oxides to elements.
C          DATA FACTOR/ .467, .599, .529, .699, .603, .715, .742,
C          .830, .436/
C
C          CALL FTNCMD('DEFAULT 3=*MSINK*:')
C          To run: $R *FTN SCARDS=SEASALT
C          $R -LOAD 4=majorsinputfile 5=minorsinputfile
C          6=outputfile
C
C          Program asks user how many samples and title of job.
C          WRITE(3,100)
C          READ(3,101) SAMPLE
C          WRITE(3,105)
C          READ(3,106) (TITLE(N),N=1,5)
100  FORMAT('&How many samples (3 digits)? ')
101  FORMAT(I3)
105  FORMAT('&Title of this job? ')
106  FORMAT(5A8)
C
C          DO 301 J=1,SAMPLE
C          Program reads in raw data from major element input file in
C          specified Fortran format in the following order: Sample #,
C          Depth, SiO2, TiO2, Al2O3, Fe2O3, MgO, CaO, Na, K2O, P2O5,
C          Cl, S, Total C, and Carbonate C.
C          READ(4,110) SAM(J), DEPTH(J), (EL(J,N),N=1,9), CL(J),
C          S(J), NIT(J), CARBON(J), CO2(J)
110  FORMAT(A8,A8,3X,4(F5.2,1X),1X,7(F5.2,1X),1X,3(F5.3,1X))
C          Program reads in raw data from minor element input file
C          in specified Fortran format in the following order: Ba,
C          Co, Cr, Cu, Mn, Nb, Ni, Pb, Rb, Sr, V, Y, Zn, Zr, I, Br.
C          READ(5,112) (EL(J,N),N=10,25)
112  FORMAT(17X,F5.0,2X,3(F4.0,2X),F5.0,1X,11(F4.0,2X))
C          Ba and Mn are F5.0's
C
C          Convert major element oxides to elements.
C          DO 305 N=1,9
C          Exclude Na as this was analyzed on with minors and is
C          reported as an element not an oxide.
C          IF(N.EQ.7) GO TO 305
C          EL(J,N)=EL(J,N)*FACTOR(N)
305  CONTINUE
C          correction of V for Ba LB interference during
C          XRF analysis.
C          EL(J,20)=EL(J,20)-0.012*EL(J,10)
C          Salt correction for Na in seawater.
C          EL(J,7)=EL(J,7)-0.556*CL(J)
C          Salt correction for Mg in seawater.
C          EL(J,5)=EL(J,5)-0.067*CL(J)

```

```

C      Salt correction for Ca in seawater.
      EL(J,6)=EL(J,6)-0.021*CL(J)
C      Salt correction for K in seawater.
      EL(J,8)=EL(J,8)-0.020*CL(J)
C      Salt correction for S in seawater.
      S(J)=S(J)-0.0465*CL(J)
C      Salt correction for Sr in seawater.
      EL(J,19)=EL(J,19)-4.13*CL(J)
C      Salt correction for Br in seawater.
      EL(J,25)=EL(J,25)-34.6*CL(J)
C
C      Chloride salt correction applied to all elements.
      DO 400 N=1,25
        EL(J,N)=EL(J,N)*100/(100-1.82*CL(J))
        IF(EL(J,N).LT.0) EL(J,N)=0.00
300  CONTINUE
      NIT(J)=NIT(J)*100/(100-1.82*CL(J))
      S(J)=S(J)*100/(100-1.82*CL(J))
      IF(S(J).LT.0) S(J)=0.00
C      Total C data converted to Corg prior to salt correction.
      CARBON(J)=CARBON(J)-CO2(J)
      CARBON(J)=CARBON(J)*100/(100-1.82*CL(J))
      CO2(J)=CO2(J)*100/(100-1.82*CL(J))
C
C      Calculation of element ratios.
C      Add in other ratios or replace existing ones to
C      a maximum of 16.
      SIAL(J)=EL(J,1)/EL(J,3)
      FEAL(J)=EL(J,4)/EL(J,3)
      TIAL(J)=EL(J,2)/EL(J,3)
      MGAL(J)=EL(J,5)/EL(J,3)
      KAL(J)=EL(J,8)/EL(J,3)
      MNAL(J)=EL(J,14)/EL(J,3)
      CRAL(J)=EL(J,12)/EL(J,3)
      ZRAL(J)=EL(J,23)/EL(J,3)
      FENI(J)=EL(J,4)/EL(J,16)
      MNFE(J)=EL(J,14)/EL(J,4)
      NICO(J)=EL(J,16)/EL(J,11)
      IC(J)=EL(J,24)/CARBON(J)
      BRC(J)=EL(J,25)/CARBON(J)
      CN(J)=CARBON(J)/NIT(J)
301  CONTINUE
C
C      Major element salt-free data written to output file.
      P=0
      PAGES=SAMPLE/27+1
      DO 310 L=1,PAGES
        WRITE(6,909)
        WRITE(6,910) TITLE, SAMPLE
        WRITE(6,912)
        DO 315 M=1,27
          J=27*P+M
          IF(J.GT.SAMPLE) GO TO 80
          WRITE(6,915) SAM(J), DEPTH(J), (EL(J,N),N=1,9),
            S(J), NIT(J), CARBON(J), CO2(J), CL(J)
315  CONTINUE
        P=P+1
310  CONTINUE
C
C      Minor element and halogen data written to output file.

```

```

80  P=0
    DO 320 L=1,PAGES
      WRITE(6,919)
      WRITE(6,920) TITLE, SAMPLE
      WRITE(6,922)
      DO 325 M=1,27
        J=27*P+M
        IF(J.GT.SAMPLE) GO TO 83
        WRITE(6,925) SAM(J), DEPTH(J), (EL(J,N),N=10,25)
325  CONTINUE
      P=P+1
320  CONTINUE
C
C  Ratios written to output file.
83  P=0
    DO 330 L=1,PAGES
      WRITE(6,929)
      WRITE(6,930) TITLE, SAMPLE
      WRITE(6,932)
      DO 335 M=1,27
        J=27*P+M
        IF(J.GT.SAMPLE) GO TO 86
        WRITE(6,935) SAM(J),DEPTH(J),SIAL(J),FEAL(J),TIAL(J),
          MGAL(J),KAL(J),MNAL(J),CRAL(J),ZRAL(J),FENI(J),
          MNFE(J),NICO(J),IC(J),BRC(J),CN(J)
335  CONTINUE
      P=P+1
330  CONTINUE
C
C  Output formats designed to give labelled columns of data.
909  FORMAT('1')
910  FORMAT('-',.25X,'Salt-corrected Major Element
      Concentrations: ', 5A8,1X, '(,I3,' samples)')
C
912  FORMAT('O',.2X,'Sample',.4X,'Depth',.5X,'Si',.5X,'Ti',.5X,'Al',
      .5X,'Fe',.5X,'Mg',.5X,'Ca',.5X,'Na',.5X,'K',.6X,'P',.6X,'S',
      .7X,'N',.6X,'Corg',.4X,'CO2',.8X,'[C1]')
915  FORMAT('O',.2X,A8,A8,2X,10(F5.2,2X),.1X,3(F5.3,3X),3X,F5.2)
C
919  FORMAT('1')
920  FORMAT('-',.25X,'Salt-corrected Trace Element
      Concentrations: ', 5A8,1X, '(,I3,' samples)')
C
922  FORMAT('O',.2X,'Sample',.4X,'Depth',.6X,
      .5X,'Ba',.5X,'Co',.4X,'Cr',.4X,'Cu',.4X,'Mn',.4X,'Nb',.4X,
      .5X,'Ni',.4X,'Pb',.4X,'Rb',.4X,'Sr',.4X,'V',.6X,'Y',.4X,'Zn',.4X,
      .5X,'Zr',.6X,'I',.5X,'Br')
925  FORMAT('O',.2X,A8,A8,3X,14F6.0,2X,2F6.0)
C
929  FORMAT('1')
930  FORMAT('-',.35X,'Element Ratios: ',
      5A8,20X, '(,I3,' samples)')
932  FORMAT('O',.2X,'Sample',.4X,'Depth',.5X,'Si/Al',.2X,'Fe/Al',
      .2X,'Ti/Al',.2X,'Mg/Al',.3X,'K/Al',.2X,'Mn/Al',.2X,'Cr/Al',
      .2X,'Zr/Al',.2X,'Fe/Ni',.2X,'Mn/Fe',.2X,'Ni/Co',.2X,
      .1X,'I/Corg',.1X,'Br/Corg',.1X,'Corg/N')
935  FORMAT('O',.2X,A8,A8,2X,F7.2,4(F7.3),3(F7.2),F7.3,F7.1,
      F7.2,1X,F7.1,2(F7.2))
86  STOP
    END

```

APPENDIX 4 — SALT-CORRECTED XRF, CHN AND COULOMETER DATA

## Salt-corrected Major Element Concentrations: Tuzo Wilson - Core 1

( 13 samples)

Sample	Depth	Si	Ti	Al	Fe	Mg	Ca	Na	K	P	S	N	Corg	CO2	[C1]
1-0,1	-1.0	27.25	0.48	7.24	3.93	1.59	2.85	1.84	1.32	0.10	0.0	0.338	3.329	0.259	2.13
1-3,4	-4.0	26.90	0.48	7.28	3.94	1.60	2.85	1.87	1.31	0.09	0.0	0.350	3.386	0.272	1.88
1-6	-6.5	27.07	0.47	7.39	3.93	1.61	3.00	1.74	1.29	0.09	0.0	0.324	2.985	0.339	2.15
1-10,11	-11.0	27.04	0.49	7.24	4.10	1.63	3.10	1.74	1.33	0.09	0.0	0.307	2.910	0.351	2.10
1-15,16	-16.0	26.47	0.47	7.15	4.18	1.60	3.02	1.56	1.40	0.09	0.0	0.294	2.700	0.338	2.11
1-20,21	-21.0	26.92	0.50	7.52	4.18	1.64	2.91	1.80	1.37	0.09	0.0	0.284	2.750	0.290	2.08
1-25,26	-26.0	27.09	0.50	7.57	4.17	1.79	3.15	1.59	1.37	0.09	0.0	0.267	2.545	0.363	2.03
1-30	-30.5	26.78	0.49	7.50	4.12	1.69	3.13	1.71	1.35	0.09	0.0	0.253	2.461	0.378	2.05
1-35	-35.5	26.70	0.50	7.57	4.19	1.63	3.21	1.66	1.37	0.09	0.0	0.267	2.400	0.388	2.07
1-40	-40.5	27.25	0.49	7.45	4.04	1.61	3.28	1.71	1.33	0.08	0.0	0.277	2.395	0.360	2.13
1-60	-60.5	27.15	0.49	7.53	4.17	1.63	3.53	1.70	1.38	0.09	0.0	0.242	2.054	0.444	2.01
1-80	-80.5	26.79	0.51	7.74	4.33	1.74	3.12	1.79	1.43	0.09	0.0	0.204	2.025	0.334	2.09
1-95	-95.5	26.88	0.52	8.01	4.41	1.82	2.86	1.82	1.42	0.09	0.0	0.197	2.079	0.266	2.27

## Salt-corrected Trace Element Concentrations: Tuzo Wilson - Core 1

( 13 samples)

Sample	Depth	Ba	Co	Cr	Cu	Mn	Nb	Ni	Pb	Rb	Sr	V	Y	Zn	Zr	I	Br
1-0,1	-1.0	1057.	40.	86.	48.	563.	9.	45.	15.	49.	322.	102.	17.	120.	128.	638.	167.
1-3,4	-4.0	1134.	45.	92.	54.	589.	8.	49.	17.	50.	317.	115.	17.	125.	129.	698.	204.
1-6	-6.5	1110.	39.	92.	52.	572.	9.	47.	8.	52.	327.	116.	18.	130.	131.	604.	200.
1-10,11	-11.0	1097.	31.	93.	54.	564.	9.	50.	9.	54.	321.	110.	18.	134.	132.	528.	194.
1-15,16	-16.0	1112.	27.	87.	47.	589.	10.	45.	15.	50.	316.	102.	17.	125.	131.	505.	148.
1-20,21	-21.0	1156.	38.	95.	56.	600.	10.	50.	6.	54.	320.	119.	20.	188.	133.	455.	180.
1-25,26	-26.0	1090.	23.	91.	46.	600.	8.	40.	10.	50.	314.	99.	18.	117.	130.	422.	133.
1-30	-30.5	1080.	30.	85.	53.	673.	8.	45.	14.	51.	337.	113.	18.	131.	128.	404.	154.
1-35	-35.5	1025.	31.	85.	43.	592.	10.	42.	15.	51.	322.	98.	17.	116.	130.	389.	123.
1-40	-40.5	1029.	27.	87.	53.	589.	8.	47.	11.	53.	326.	114.	17.	135.	131.	375.	161.
1-60	-60.5	934.	30.	82.	50.	592.	9.	47.	13.	51.	357.	112.	18.	128.	139.	284.	125.
1-80	-80.5	962.	26.	91.	50.	625.	9.	49.	12.	55.	328.	123.	20.	135.	144.	246.	112.
1-95	-95.5	948.	37.	92.	55.	639.	9.	53.	16.	57.	317.	129.	21.	148.	139.	237.	100.

## Element Ratios: Tuzo Wilson - Core 1

( 13 samples)

Sample	Depth	Si/Al	Fe/Al	Ti/Al	Mg/Al	K/Al	Mn/Al	Cr/Al	Zr/Al	Fe/Ni	Mn/Fe	Ni/Co	I/Corg	Br/Corg	Corg/N
1-0,1	-1.0	3.76	0.544	0.066	0.220	0.182	77.77	11.93	17.68	0.088	143.1	1.13	191.6	50.09	9.85
1-3,4	-4.0	3.69	0.540	0.066	0.220	0.180	80.87	12.65	17.77	0.081	149.6	1.09	206.1	60.23	9.67
1-6	-6.5	3.66	0.531	0.064	0.217	0.174	77.42	12.39	17.74	0.084	145.7	1.22	202.2	67.16	9.22
1-10,11	-11.0	3.74	0.566	0.067	0.225	0.184	77.86	12.78	18.24	0.082	137.5	1.60	181.5	66.57	9.49
1-15,16	-16.0	3.70	0.585	0.066	0.223	0.196	82.37	12.22	18.34	0.093	140.8	1.65	187.2	54.70	9.17
1-20,21	-21.0	3.58	0.556	0.066	0.218	0.182	79.73	12.57	17.69	0.084	143.3	1.30	165.5	65.39	9.69
1-25,26	-26.0	3.58	0.551	0.066	0.236	0.181	79.23	12.06	17.14	0.103	143.8	1.77	165.6	52.13	9.54
1-30	-30.5	3.57	0.549	0.066	0.225	0.181	89.81	11.36	17.05	0.092	163.5	1.48	164.2	62.50	9.71
1-35	-35.5	3.52	0.553	0.067	0.215	0.181	78.19	11.25	17.15	0.101	141.3	1.33	161.9	51.25	8.99
1-40	-40.5	3.66	0.542	0.066	0.217	0.178	79.08	11.74	17.60	0.086	145.9	1.73	156.4	67.03	8.65
1-60	-60.5	3.60	0.554	0.065	0.216	0.183	78.54	10.88	18.46	0.089	141.8	1.55	138.5	60.87	8.49
1-80	-80.5	3.46	0.560	0.066	0.225	0.185	80.75	11.82	18.68	0.089	144.3	1.88	121.7	55.28	9.94
1-95	-95.5	3.36	0.551	0.065	0.228	0.178	79.86	11.46	17.33	0.083	145.0	1.46	113.9	47.90	10.54

## Salt-corrected Major Element Concentrations: Tuzo Wilson - Core 2

( 4 samples)

Sample	Depth	Si	Ti	Al	Fe	Mg	Ca	Na	K	P	S	N	Corg	CO2	[C1]
2-0,1	-1.0	27.67	0.49	7.71	3.99	1.69	2.90	1.55	1.27	0.10	0.0	0.290	2.946	0.255	2.38
2-3,4	-4.0	27.86	0.50	7.77	4.07	1.62	2.93	1.67	1.35	0.09	0.0	0.266	2.401	0.245	2.31
2-6,7	-7.0	28.25	0.49	7.73	3.99	1.63	3.11	1.66	1.30	0.10	0.0	0.261	2.448	0.294	2.25
2-10,11	-11.0	26.50	0.47	7.30	4.19	1.61	3.17	1.74	1.41	0.09	0.0	0.233	2.147	0.318	2.12

## Salt-corrected Trace Element Concentrations: Tuzo Wilson - Core 2

( 4 samples)

Sample	Depth	Ba	Co	Cr	Cu	Mn	Nb	Ni	Pb	Rb	Sr	V	Y	Zn	Zr	I	Br
2-0,1	-1.0	1048.	26.	83.	45.	595.	9.	41.	17.	48.	332.	91.	17.	113.	135.	592.	166.
2-3,4	-4.0	1059.	26.	92.	46.	603.	9.	41.	15.	50.	327.	99.	19.	118.	129.	430.	130.
2-6,7	-7.0	998.	32.	81.	44.	563.	10.	40.	14.	50.	345.	88.	18.	115.	136.	447.	139.
2-10,11	-11.0	983.	26.	84.	48.	596.	9.	43.	11.	51.	339.	93.	19.	118.	142.	333.	112.

Element Ratios: Tuzo Wilson - Core 2

( 4 samples)

Sample	Depth	Si/Al	Fe/Al	Ti/Al	Mg/Al	K/Al	Mn/Al	Cr/Al	Zr/Al	Fe/Ni	Mn/Fe	Ni/Co	I/Corg	Br/Corg	Corg/N
2-0,1	-1.0	3.59	0.517	0.063	0.219	0.165	77.10	10.71	17.48	0.098	149.1	1.56	200.9	56.30	10.17
2-3,4	-4.0	3.59	0.524	0.064	0.208	0.173	77.66	11.82	16.66	0.100	148.2	1.56	179.1	53.95	9.02
2-6,7	-7.0	3.65	0.516	0.064	0.211	0.169	72.81	10.52	17.53	0.101	141.2	1.23	182.7	56.71	9.39
2-10,11	-11.0	3.63	0.574	0.064	0.220	0.193	81.69	11.55	19.53	0.098	142.3	1.64	155.0	52.16	9.21

## Salt-corrected Major Element Concentrations: Tuzo Wilson - Core 3

( 19 samples)

Sample	Depth	Si	Ti	Al	Fe	Mg	Ca	Na	K	P	S	N	Corg	CO2	[Cl]
3-0,1	-1.0	27.59	0.47	7.44	3.99	1.53	3.11	1.99	1.22	0.10	0.0	0.310	2.959	0.276	2.10
3-3	-3.5	27.97	0.48	7.37	3.85	1.64	3.05	1.91	1.27	0.09	0.0	0.271	2.394	0.274	1.97
3-6	-6.5	27.58	0.49	7.78	3.93	1.62	3.24	1.88	1.28	0.09	0.0	0.226	2.190	0.298	1.74
3-10	-10.5	27.75	0.49	7.91	4.08	1.65	3.28	1.88	1.39	0.09	0.0	0.210	1.819	0.312	1.62
3-20	-20.5	27.61	0.51	8.09	4.22	1.76	3.55	1.93	1.39	0.09	0.0	0.174	1.567	0.365	1.66
3-24	-24.5	24.92	0.50	7.53	4.75	1.79	4.03	1.84	1.48	0.09	0.0	0.151	1.542	0.462	1.70
3-27	-27.5	25.78	0.52	7.90	4.95	2.11	3.95	1.95	1.44	0.10	0.0	0.140	1.464	0.391	1.68
3-30	-30.5	25.94	0.58	8.27	4.92	2.17	4.12	2.05	1.44	0.11	0.0	0.131	1.291	0.333	1.43
3-32	-32.5	25.78	0.53	7.98	5.14	2.17	3.82	1.98	1.46	0.10	0.0	0.134	1.403	0.333	1.75
3-34	-34.5	25.77	0.51	7.91	5.16	2.13	3.87	1.96	1.42	0.09	0.0	0.143	1.478	0.371	1.75
3-36	-36.5	26.24	0.53	7.77	5.11	2.25	3.67	1.99	1.35	0.09	0.0	0.137	1.424	0.334	1.66
3-38	-38.5	25.96	0.54	7.99	5.17	2.32	3.49	1.96	1.44	0.09	0.0	0.129	1.463	0.294	1.61
3-40	-40.5	26.09	0.54	8.38	5.19	2.37	3.52	1.96	1.36	0.09	0.0	0.136	1.446	0.274	1.64
3-43	-43.5	26.66	0.51	8.12	5.13	2.22	3.72	2.07	1.34	0.09	0.00	0.123	1.175	0.314	1.64
3-46	-46.5	26.50	0.53	7.86	5.22	2.36	3.64	1.98	1.42	0.09	0.0	0.121	1.372	0.210	1.72
3-50	-50.5	26.65	0.51	6.35	5.27	2.36	3.34	2.04	1.19	0.08	0.0	0.126	1.164	0.231	1.56
3-55	-55.5	26.96	0.53	6.70	5.28	2.44	3.33	2.04	1.24	0.07	0.0	0.092	0.906	0.301	1.47
3-60	-60.5	26.40	0.55	8.62	5.15	2.31	3.35	2.08	1.61	0.10	0.0	0.086	0.928	0.213	1.34
3-80	-80.5	27.04	0.55	8.78	5.05	2.29	3.46	2.11	1.57	0.10	0.0	0.085	0.858	0.228	1.33

## Salt-corrected Trace Element Concentrations: Tuzo Wilson - Core 3

( 19 samples)

Sample	Depth	Ba	Co	Cr	Cu	Mn	Nb	Ni	Pb	Rb	Sr	V	Y	Zn	Zr	I	Br
3-0,1	-1.0	982.	44.	86.	47.	670.	9.	44.	15.	48.	373.	106.	17.	129.	138.	682.	182.
3-3	-3.5	1019.	40.	86.	48.	601.	9.	45.	10.	49.	362.	112.	18.	121.	144.	462.	150.
3-6	-6.5	991.	36.	89.	46.	610.	9.	48.	12.	50.	363.	114.	18.	121.	141.	352.	129.
3-10	-10.5	917.	32.	84.	50.	600.	8.	45.	20.	50.	365.	113.	20.	123.	141.	260.	102.
3-20	-20.5	860.	33.	89.	43.	662.	9.	42.	14.	51.	368.	122.	19.	114.	147.	181.	79.
3-24	-24.5	813.	27.	91.	43.	774.	11.	38.	11.	49.	368.	106.	19.	104.	135.	161.	70.
3-27	-27.5	760.	29.	94.	42.	823.	12.	39.	11.	48.	363.	112.	20.	102.	137.	137.	67.
3-30	-30.5	721.	30.	101.	43.	869.	14.	44.	16.	48.	390.	138.	18.	103.	151.	90.	62.
3-32	-32.5	715.	29.	97.	41.	875.	10.	37.	9.	50.	352.	116.	20.	101.	134.	106.	63.
3-34	-34.5	702.	24.	93.	37.	834.	10.	41.	9.	48.	342.	111.	19.	99.	126.	111.	62.
3-36	-36.5	731.	26.	93.	41.	867.	9.	40.	9.	48.	342.	113.	21.	106.	127.	90.	62.
3-38	-38.5	693.	23.	97.	38.	876.	8.	41.	10.	49.	325.	116.	19.	102.	126.	65.	61.
3-40	-40.5	685.	28.	99.	44.	905.	8.	40.	12.	52.	330.	137.	20.	109.	121.	60.	56.
3-43	-43.5	668.	26.	93.	37.	879.	9.	41.	11.	48.	355.	114.	21.	98.	129.	40.	40.
3-46	-46.5	668.	27.	96.	36.	904.	9.	38.	15.	54.	341.	119.	20.	102.	121.	38.	35.
3-50	-50.5	664.	27.	97.	36.	906.	10.	38.	12.	54.	341.	119.	17.	98.	122.	30.	30.
3-55	-55.5	637.	26.	85.	35.	882.	9.	38.	13.	53.	349.	117.	20.	102.	125.	23.	25.
3-60	-60.5	644.	30.	94.	36.	922.	9.	39.	11.	54.	349.	143.	17.	105.	122.	22.	37.
3-80	-80.5	687.	26.	87.	28.	901.	9.	36.	10.	54.	366.	136.	18.	96.	123.	18.	29.

## Element Ratios: Tuzo Wilson - Core 3

( 19 samples )

Sample	Depth	Si/Al	Fe/Al	Ti/Al	Mg/Al	K/Al	Mn/Al	Cr/Al	Zr/Al	Fe/Ni	Mn/Fe	Ni/Co	I/Corg	Br/Corg	Corg/N
3-0,1	-1.0	3.71	0.536	0.063	0.205	0.165	89.98	11.60	18.58	0.091	167.8	1.00	230.5	61.61	9.55
3-3	-3.5	3.80	0.522	0.065	0.222	0.172	81.50	11.68	19.57	0.086	156.0	1.10	192.8	62.75	8.84
3-6	-6.5	3.54	0.504	0.063	0.209	0.165	78.40	11.41	18.17	0.083	155.4	1.31	160.8	58.84	9.68
3-10	-10.5	3.51	0.516	0.062	0.208	0.175	75.77	10.68	17.84	0.090	146.8	1.42	142.8	56.06	8.65
3-20	-20.5	3.41	0.521	0.063	0.218	0.171	81.83	10.96	18.23	0.100	157.0	1.28	115.8	50.37	8.99
3-24	-24.5	3.31	0.631	0.066	0.238	0.197	102.74	12.05	17.94	0.124	162.8	1.42	104.4	45.64	10.23
3-27	-27.5	3.26	0.627	0.066	0.267	0.182	104.18	11.88	17.36	0.126	166.2	1.36	93.7	45.72	10.43
3-30	-30.5	3.14	0.596	0.070	0.262	0.175	105.08	12.17	18.26	0.112	176.4	1.48	70.0	48.15	9.82
3-32	-32.5	3.23	0.644	0.066	0.272	0.184	109.67	12.17	16.83	0.138	170.2	1.29	75.8	45.25	10.45
3-34	-34.5	3.26	0.652	0.065	0.270	0.180	105.35	11.75	15.93	0.125	161.7	1.74	74.8	42.24	10.37
3-36	-36.5	3.38	0.658	0.068	0.290	0.174	111.64	11.95	16.33	0.127	169.7	1.56	63.0	43.86	10.38
3-38	-38.5	3.25	0.647	0.067	0.290	0.180	109.53	12.11	15.72	0.125	169.4	1.82	44.4	41.76	11.36
3-40	-40.5	3.11	0.620	0.064	0.282	0.162	107.99	11.81	14.39	0.129	174.2	1.44	41.3	38.67	10.63
3-43	-43.5	3.28	0.631	0.062	0.273	0.165	108.22	11.42	15.86	0.124	171.4	1.60	34.2	34.44	9.58
3-46	-46.5	3.37	0.663	0.067	0.301	0.181	115.00	12.21	15.36	0.137	173.3	1.42	27.8	25.20	11.36
3-50	-50.5	4.19	0.830	0.081	0.372	0.187	142.55	15.23	19.28	0.138	171.8	1.42	25.6	25.66	9.27
3-55	-55.5	4.02	0.788	0.079	0.364	0.185	131.54	12.73	18.70	0.139	167.0	1.48	24.9	27.37	9.80
3-60	-60.5	3.06	0.598	0.063	0.268	0.186	107.00	10.94	14.15	0.132	179.1	1.31	23.2	39.38	10.77
3-80	-80.5	3.08	0.575	0.062	0.261	0.179	102.63	9.92	14.01	0.141	178.4	1.40	21.5	33.43	10.08

## Salt-corrected Major Element Concentrations: Tuzo Wilson - Core 4

( 10 samples)

Sample	Depth	Si	Ti	Al	Fe	Mg	Ca	Na	K	P	S	N	Corg	CO2	[C]
4-0,1	-1.0	26.98	0.49	7.39	4.19	1.66	2.59	1.65	1.33	0.10	0.0	0.380	3.348	0.240	2.84
4-3,4	-4.0	27.64	0.49	7.16	4.15	1.82	2.60	1.73	1.22	0.09	0.0	0.339	3.057	0.224	2.91
4-6,7	-7.0	27.08	0.50	7.38	4.08	1.67	2.78	1.65	1.34	0.09	0.0	0.354	2.959	0.281	2.83
4-10	-10.5	27.28	0.48	7.26	4.06	1.65	2.67	1.68	1.33	0.09	0.0	0.320	2.918	0.248	3.10
4-20	-20.5	27.64	0.50	7.59	4.11	1.71	2.98	1.78	1.34	0.09	0.0	0.270	2.354	0.294	2.57
4-30	-30.5	27.44	0.49	7.45	4.12	1.65	2.61	1.65	1.37	0.08	0.0	0.318	2.806	0.260	2.87
4-40	-40.5	27.34	0.49	7.50	4.11	1.75	2.71	1.71	1.42	0.09	0.0	0.295	2.593	0.276	2.77
4-60	-60.5	27.47	0.50	7.49	4.13	1.81	2.99	1.70	1.40	0.08	0.0	0.281	2.415	0.327	2.43
4-80	-80.5	27.30	0.48	7.68	4.28	1.73	2.95	1.61	1.40	0.09	0.0	0.276	2.439	0.344	2.31
4-94,95	-95.0	27.69	0.50	7.24	4.34	1.90	3.00	1.46	1.27	0.08	0.0	0.248	2.414	0.418	2.51

## Salt-corrected Trace Element Concentrations: Tuzo Wilson - Core 4

( 10 samples)

Sample	Depth	Ba	Co	Cr	Cu	Mn	Nb	Ni	Pb	Rb	Sr	V	Y	Zn	Zr	I	Br
4-0,1	-1.0	1161.	36.	94.	59.	589.	9.	53.	15.	55.	307.	120.	18.	141.	125.	862.	235.
4-3,4	-4.0	1141.	35.	93.	55.	596.	10.	50.	16.	53.	309.	116.	17.	134.	125.	772.	201.
4-6,7	-7.0	1170.	32.	94.	58.	610.	9.	50.	16.	53.	313.	120.	16.	136.	123.	661.	203.
4-10	-10.5	1177.	28.	94.	55.	573.	10.	48.	15.	53.	312.	111.	16.	132.	127.	690.	196.
4-20	-20.5	1069.	28.	90.	51.	621.	9.	45.	15.	52.	331.	118.	17.	125.	131.	466.	143.
4-30	-30.5	1181.	31.	94.	73.	561.	8.	60.	8.	59.	331.	131.	20.	169.	135.	534.	166.
4-40	-40.5	1189.	33.	92.	67.	576.	8.	57.	14.	58.	339.	132.	18.	163.	140.	476.	155.
4-60	-60.5	1124.	36.	93.	63.	604.	8.	54.	15.	55.	334.	135.	19.	151.	137.	400.	140.
4-80	-80.5	1117.	25.	92.	70.	581.	7.	61.	20.	58.	340.	133.	19.	165.	136.	373.	140.
4-94,95	-95.0	1097.	24.	87.	36.	610.	10.	46.	12.	54.	308.	100.	20.	128.	129.	347.	109.

## Element Ratios: Tuzo Wilson - Core 4

( 10 samples)

Sample	Depth	Si/Al	Fe/Al	Ti/Al	Mg/Al	K/Al	Mn/Al	Cr/Al	Zr/Al	Fe/Ni	Mn/Fe	Ni/Co	I/Corg	Br/Corg	Corg/N
4-0,1	-1.0	3.65	0.567	0.067	0.224	0.180	79.75	12.70	16.98	0.080	140.5	1.47	257.3	70.15	8.82
4-3,4	-4.0	3.86	0.579	0.068	0.254	0.170	83.16	12.98	17.40	0.084	143.6	1.42	252.5	65.74	9.02
4-6,7	-7.0	3.67	0.552	0.068	0.226	0.182	82.67	12.71	16.70	0.082	149.8	1.57	223.4	68.43	8.35
4-10	-10.5	3.76	0.559	0.066	0.228	0.184	78.97	12.99	17.52	0.085	141.2	1.73	236.5	67.11	9.12
4-20	-20.5	3.64	0.541	0.066	0.226	0.177	81.86	11.89	17.29	0.091	151.2	1.59	197.9	60.64	8.73
4-30	-30.5	3.68	0.552	0.066	0.221	0.183	75.33	12.60	18.12	0.068	136.4	1.97	190.3	59.31	8.83
4-40	-40.5	3.65	0.548	0.065	0.233	0.189	76.82	12.22	18.68	0.072	140.2	1.74	183.6	59.77	8.79
4-60	-60.5	3.67	0.551	0.066	0.242	0.187	80.56	12.43	18.29	0.076	146.1	1.53	165.5	58.03	8.58
4-80	-80.5	3.56	0.557	0.062	0.225	0.182	75.75	11.97	17.68	0.071	136.0	2.42	152.8	57.39	8.85
4-94,95	-95.0	3.83	0.600	0.068	0.263	0.175	84.24	12.01	17.80	0.094	140.4	1.91	143.7	45.21	9.72

## Salt-corrected Major Element Concentrations: Tuzo Wilson - Core 6

( 14 samples)

Sample	Depth	Si	Ti	Al	Fe	Mg	Ca	Na	K	P	S	N	Corg	CO2	[C1]
6-0	-0.5	26.88	0.48	7.42	4.42	1.73	2.31	1.54	1.43	0.09	0.0	0.302	2.500	0.217	2.53
6-3,4	-4.0	27.42	0.50	7.35	4.42	1.78	2.32	1.62	1.41	0.09	0.0	0.304	2.544	0.225	2.63
6-6	-6.5	27.10	0.50	7.38	4.40	1.74	2.32	1.60	1.43	0.08	0.0	0.299	2.516	0.209	2.74
6-8,9	-9.0	27.78	0.49	6.96	4.49	1.94	2.49	1.47	1.32	0.09	0.0	0.278	2.494	0.252	2.84
6-10,11	-11.0	27.03	0.52	7.37	4.47	1.80	2.19	1.68	1.43	0.08	0.0	0.297	2.399	0.180	2.69
6-12	-12.5	27.76	0.49	7.20	4.56	2.00	2.19	1.58	1.40	0.08	0.0	0.271	2.380	0.176	2.89
6-16	-16.5	28.26	0.50	7.13	4.48	1.98	2.24	1.60	1.34	0.07	0.0	0.264	2.281	0.180	2.78
6-20	-20.5	27.48	0.51	7.55	4.36	1.83	2.16	1.62	1.41	0.09	0.0	0.275	2.380	0.187	2.83
6-30	-30.5	28.74	0.50	7.89	4.54	1.88	2.24	1.58	1.55	0.09	0.0	0.252	2.238	0.187	2.87
6-40	-40.5	27.42	0.50	7.33	4.50	1.81	2.37	1.62	1.40	0.08	0.0	0.264	2.295	0.239	2.73
6-60,61	-61.0	26.92	0.53	7.99	4.58	1.83	2.74	1.73	1.49	0.09	0.0	0.212	1.883	0.258	2.33
6-80	-80.5	27.05	0.51	7.73	4.41	1.89	2.48	1.60	1.50	0.09	0.0	0.230	2.094	0.267	2.46
6-100	-100.5	26.61	0.51	7.63	4.62	1.83	2.67	1.59	1.49	0.09	0.0	0.231	2.028	0.298	2.46
6-112	-112.5	27.90	0.48	5.97	4.40	2.03	2.19	1.54	1.21	0.06	0.0	0.280	2.664	0.204	3.18

## Salt-corrected Trace Element Concentrations: Tuzo Wilson - Core 6

( 14 samples)

Sample	Depth	Ba	Co	Cr	Cu	Mn	Nb	Ni	Pb	Rb	Sr	V	Y	Zn	Zr	I	Br
6-0	-0.5	1511.	24.	93.	86.	599.	8.	71.	15.	63.	314.	130.	19.	187.	133.	492.	152.
6-3,4	-4.0	1561.	34.	97.	84.	603.	7.	70.	16.	60.	304.	137.	18.	180.	132.	448.	134.
6-6	-6.5	1562.	36.	95.	87.	607.	8.	65.	13.	60.	300.	132.	20.	169.	134.	455.	139.
6-8,9	-9.0	1504.	28.	91.	57.	643.	11.	46.	18.	55.	280.	95.	17.	144.	124.	426.	101.
6-10,11	-11.0	1556.	38.	97.	86.	624.	8.	65.	17.	61.	306.	131.	19.	209.	138.	442.	138.
6-12	-12.5	1608.	31.	92.	63.	645.	11.	53.	14.	58.	279.	106.	19.	138.	128.	410.	93.
6-16	-16.5	1520.	31.	91.	60.	618.	11.	51.	6.	56.	278.	100.	18.	133.	127.	413.	86.
6-20	-20.5	1536.	30.	96.	77.	620.	8.	64.	11.	61.	298.	135.	18.	168.	135.	405.	130.
6-30	-30.5	1459.	32.	92.	74.	612.	7.	57.	9.	59.	290.	131.	18.	162.	132.	382.	128.
6-40	-40.5	1434.	36.	92.	85.	613.	8.	63.	6.	59.	298.	125.	19.	174.	134.	388.	131.
6-60,61	-61.0	1253.	32.	94.	66.	722.	8.	54.	11.	61.	317.	124.	19.	150.	136.	268.	100.
6-80	-80.5	1397.	31.	90.	71.	655.	9.	62.	12.	62.	299.	118.	19.	161.	135.	288.	113.
6-100	-100.5	1330.	29.	90.	67.	667.	10.	58.	17.	60.	306.	111.	20.	154.	133.	323.	102.
6-112	-112.5	1522.	33.	86.	61.	664.	10.	49.	18.	57.	278.	100.	17.	133.	127.	462.	94.

## Element Ratios: Tuzo Wilson - Core 6

( 14 samples)

Sample	Depth	Si/Al	Fe/Al	Ti/Al	Mg/Al	K/Al	Mn/Al	Cr/Al	Zr/Al	Fe/Ni	Mn/Fe	Ni/Co	I/Corg	Br/Corg	Corg/N
6-0	-0.5	3.62	0.596	0.065	0.233	0.192	80.67	12.57	17.94	0.062	135.5	2.96	196.6	60.99	8.28
6-3,4	-4.0	3.73	0.601	0.068	0.243	0.192	82.02	13.15	18.00	0.063	136.4	2.09	176.3	52.85	8.38
6-6	-6.5	3.67	0.596	0.068	0.235	0.193	82.32	12.84	18.12	0.067	138.0	1.82	180.7	55.29	8.42
6-8,9	-9.0	3.99	0.645	0.070	0.278	0.190	92.40	13.03	17.87	0.097	143.3	1.63	170.8	40.48	8.96
6-10,11	-11.0	3.67	0.606	0.070	0.244	0.194	84.60	13.13	18.69	0.069	139.5	1.72	184.0	57.37	8.09
6-12	-12.5	3.85	0.633	0.068	0.277	0.195	89.54	12.75	17.73	0.086	141.4	1.72	172.1	39.03	8.77
6-16	-16.5	3.96	0.629	0.070	0.277	0.188	86.69	12.70	17.87	0.089	137.9	1.66	181.0	37.77	8.63
6-20	-20.5	3.64	0.578	0.067	0.242	0.187	82.09	12.70	17.87	0.068	142.1	2.18	170.1	54.53	8.65
6-30	-30.5	3.64	0.576	0.063	0.239	0.197	77.59	11.64	16.72	0.080	134.7	1.80	170.7	57.38	8.87
6-40	-40.5	3.74	0.614	0.069	0.247	0.191	83.74	12.50	18.24	0.071	136.3	1.76	169.2	57.10	8.69
6-60,61	-61.0	3.37	0.573	0.067	0.229	0.187	90.33	11.77	16.99	0.084	157.7	1.68	142.5	52.90	8.88
6-80	-80.5	3.50	0.570	0.067	0.245	0.195	84.83	11.65	17.48	0.071	148.8	1.97	137.5	53.94	9.09
6-100	-100.5	3.49	0.605	0.067	0.240	0.195	87.38	11.80	17.42	0.080	144.4	1.96	159.5	50.53	8.76
6-112	-112.5	4.67	0.737	0.080	0.340	0.203	111.32	14.40	21.34	0.090	151.0	1.48	173.3	35.45	9.51

## Salt-corrected Major Element Concentrations: Tuzo Wilson - Core 7

( 5 samples)

Sample	Depth	Si	Ti	Al	Fe	Mg	Ca	Na	K	P	S	N	Corg	CO2	[C1]
7-0,1	-1.0	28.79	0.46	6.49	4.28	1.95	2.65	1.51	1.06	0.07	0.0	0.275	2.679	0.254	3.17
7-3	-3.5	28.07	0.50	7.23	4.33	1.91	2.86	1.75	1.35	0.09	0.0	0.232	2.228	0.263	2.63
7-6	-6.5	27.08	0.48	7.30	4.08	1.65	2.90	1.73	1.37	0.09	0.0	0.268	2.363	0.268	2.70
7-10	-10.5	28.54	0.47	6.26	4.09	1.94	2.94	1.73	1.13	0.08	0.0	0.241	2.371	0.319	2.75
7-14	-14.5	28.05	0.48	5.46	4.21	1.97	3.05	1.69	1.10	0.07	0.0	0.223	2.380	0.297	2.81

## Salt-corrected Trace Element Concentrations: Tuzo Wilson - Core 7

( 5 samples)

Sample	Depth	Ba	Co	Cr	Cu	Mn	Nb	Ni	Pb	Rb	Sr	V	Y	Zn	Zr	I	Br
7-0,1	-1.0	1359.	28.	83.	51.	594.	11.	42.	22.	53.	314.	97.	16.	222.	132.	517.	130.
7-3	-3.5	1216.	30.	84.	50.	604.	11.	45.	15.	51.	318.	99.	18.	119.	138.	367.	101.
7-6	-6.5	1318.	37.	86.	48.	587.	11.	42.	17.	53.	320.	95.	17.	113.	134.	475.	126.
7-10	-10.5	1345.	33.	88.	48.	590.	11.	40.	19.	53.	325.	99.	18.	111.	134.	454.	122.
7-14	-14.5	1258.	34.	91.	50.	624.	11.	40.	22.	53.	325.	100.	19.	145.	132.	398.	104.

Element Ratios: Tuzo Wilson - Core 7

( 5 samples)

Sample	Depth	Si/Al	Fe/Al	Ti/Al	Mg/Al	K/Al	Mn/Al	Cr/Al	Zr/Al	Fe/Ni	Mn/Fe	Ni/Co	I/Corg	Br/Corg	Corg/N
7-0,1	-1.0	4.44	0.660	0.072	0.301	0.163	91.57	12.76	20.28	0.101	138.8	1.54	192.9	48.46	9.75
7-3	-3.5	3.88	0.599	0.069	0.264	0.187	83.55	11.62	19.03	0.096	139.4	1.48	164.5	45.26	9.60
7-6	-6.5	3.71	0.559	0.066	0.226	0.187	80.34	11.81	18.28	0.097	143.8	1.14	201.2	53.22	8.81
7-10	-10.5	4.56	0.653	0.075	0.309	0.180	94.10	14.11	21.34	0.102	144.1	1.23	191.4	51.44	9.83
7-14	-14.5	5.13	0.771	0.088	0.360	0.202	114.19	16.59	24.11	0.105	148.1	1.19	167.4	43.74	10.65

## Salt-corrected Major Element Concentrations: Tuzo Wilson - Core 8

( 10 samples)

Sample	Depth	Si	Ti	Al	Fe	Mg	Ca	Na	K	P	S	N	Corg	CO2	[C1]
8-0	-0.5	28.73	0.45	7.49	3.82	1.51	3.10	1.91	1.27	0.09	0.0	0.190	1.919	0.219	2.26
8-3	-3.5	28.63	0.49	7.29	4.06	1.84	3.22	1.84	1.29	0.08	0.0	0.189	2.038	0.303	2.25
8-6	-6.5	28.08	0.49	7.62	4.21	1.80	3.14	1.81	1.35	0.09	0.0	0.176	1.956	0.296	2.29
8-10	-10.5	28.86	0.48	6.48	4.27	1.96	3.10	1.75	1.14	0.06	0.0	0.187	1.915	0.319	2.29
8-20	-20.5	26.68	0.51	7.66	4.67	2.02	3.21	1.72	1.29	0.07	0.0	0.168	1.886	0.376	2.38
8-30	-30.5	27.86	0.51	7.54	4.66	2.05	3.54	1.69	1.29	0.08	0.0	0.159	1.798	0.443	2.06
8-40	-40.5	26.15	0.50	7.31	4.70	1.99	3.73	1.72	1.31	0.08	0.0	0.182	1.898	0.489	2.01
8-50	-50.5	26.85	0.50	6.32	4.78	2.13	3.67	1.71	1.15	0.07	0.0	0.173	1.822	0.498	1.91
8-60	-60.5	26.61	0.52	7.50	4.81	2.11	4.06	1.70	1.32	0.08	0.0	0.170	1.789	0.560	1.96
8-81	-81.5	26.04	0.51	7.97	4.94	2.19	4.01	1.67	1.40	0.09	0.0	0.167	1.805	0.519	1.65

## Salt-corrected Trace Element Concentrations: Tuzo Wilson - Core 8

( 10 samples)

Sample	Depth	Ba	Co	Cr	Cu	Mn	Nb	Ni	Pb	Rb	Sr	V	Y	Zn	Zr	I	Br
8-0	-0.5	933.	27.	78.	35.	582.	9.	32.	17.	45.	375.	92.	16.	89.	139.	367.	96.
8-3	-3.5	923.	31.	87.	40.	603.	10.	36.	17.	47.	353.	98.	17.	102.	138.	316.	100.
8-6	-6.5	919.	32.	89.	40.	589.	10.	37.	13.	51.	344.	101.	18.	105.	141.	317.	97.
8-10	-10.5	943.	29.	88.	44.	616.	10.	37.	14.	50.	343.	105.	18.	101.	140.	305.	87.
8-20	-20.5	885.	24.	90.	40.	703.	9.	36.	7.	54.	314.	115.	18.	102.	135.	226.	87.
8-30	-30.5	890.	22.	95.	42.	675.	10.	36.	18.	54.	332.	113.	19.	103.	137.	208.	86.
8-40	-40.5	855.	25.	88.	48.	680.	10.	46.	12.	53.	342.	111.	20.	114.	137.	223.	92.
8-50	-50.5	909.	26.	97.	50.	755.	10.	44.	13.	52.	348.	114.	21.	118.	135.	207.	83.
8-60	-60.5	862.	19.	93.	43.	773.	10.	40.	11.	52.	349.	114.	19.	109.	129.	202.	87.
8-81	-81.5	801.	24.	93.	41.	806.	9.	43.	12.	52.	344.	115.	18.	108.	128.	165.	92.

## Element Ratios: Tuzo Wilson - Core 8

( 10 samples)

Sample	Depth	Si/Al	Fe/Al	Ti/Al	Mg/Al	K/Al	Mn/Al	Cr/Al	Zr/Al	Fe/Ni	Mn/Fe	Ni/Co	I/Corg	Br/Corg	Corg/N
8-0	-0.5	3.83	0.510	0.060	0.201	0.169	77.67	10.44	18.51	0.118	152.3	1.19	191.3	49.89	10.11
8-3	-3.5	3.93	0.557	0.068	0.252	0.176	82.65	11.87	18.87	0.111	148.5	1.17	155.0	49.18	10.80
8-6	-6.5	3.68	0.552	0.064	0.236	0.177	77.20	11.64	18.48	0.115	139.8	1.13	162.2	49.50	11.09
8-10	-10.5	4.46	0.660	0.073	0.303	0.176	95.08	13.54	21.59	0.117	144.0	1.25	159.1	45.65	10.25
8-20	-20.5	3.48	0.609	0.067	0.264	0.169	91.79	11.73	17.59	0.131	150.7	1.48	119.7	46.37	11.20
8-30	-30.5	3.70	0.618	0.068	0.272	0.171	89.62	12.55	18.20	0.128	145.1	1.67	115.5	47.79	11.31
8-40	-40.5	3.57	0.643	0.069	0.272	0.179	92.96	12.06	18.73	0.103	144.6	1.83	117.6	48.36	10.45
8-50	-50.5	4.25	0.756	0.080	0.337	0.182	119.52	15.41	21.31	0.110	158.0	1.68	113.7	45.43	10.53
8-60	-60.5	3.55	0.640	0.069	0.282	0.176	102.95	12.44	17.13	0.119	160.8	2.17	113.0	48.80	10.52
8-81	-81.5	3.27	0.620	0.064	0.275	0.176	101.11	11.64	16.03	0.114	163.1	1.83	91.4	50.78	10.81